

AN ABSTRACT OF THE DISSERTATION OF

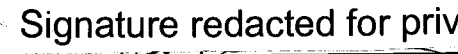
Erica Ann Hoffa Smithwick for the degree of Doctor of Philosophy in Forest Science presented on October, 19 2001.

Title: Potential Carbon Storage at the Landscape Scale in the Pacific Northwest, U.S.A.

Abstract approved:


Signature redacted for privacy.

Mark E. Harmon


Signature redacted for privacy.

Warren B. Cohen

Estimates of potential carbon (C) storage can be used to constrain predictions of future carbon sequestration and to understand the degree to which disturbances, both natural and anthropogenic, affect C storage. An upper bound on C storage in the Pacific Northwest (PNW) of the United States was estimated using field data from old-growth forests, which are near steady-state conditions and have been relatively undisturbed for long periods of time. The sites were located across a broad, biogeographical gradient in western Washington and Oregon, allowing comparison of potential carbon storage given a wide range of climate, soils, and vegetation conditions. Total ecosystem carbon (TEC) ranged from 195 Mg C ha⁻¹ in eastern Oregon to 1127 Mg C ha⁻¹ at the Oregon coast. A simple, area-weighted average of TEC to a soil depth of 1 m was 671 Mg C ha⁻¹. Compared to estimates of current C storage, up to 338 Mg C ha⁻¹ could be stored in addition to current stores in this region. A new model called MAXCARB was developed to predict potential carbon storage over a large area (approximately 10⁵ ha), in part to better understand the role of disturbances on potential carbon storage. MAXCARB

simulates the effects of climate, soils, or vegetation on potential carbon storage at steady state, for a range of natural and anthropogenic disturbance regimes. Initial results indicate that as the average interval between disturbance events increased, the steady-state C stores at the landscape scale increased. Predictions were well correlated to observed C stores in the PNW. Spatial interactions affect C flux processes at multiple levels of spatial interactions. Using another model, STANDCARB, the relative effect of edge-induced, tree mortality (mainly due to wind), and light limitations, on C dynamics were assessed for several artificial forest landscapes. Emergent behaviors resulting from the interaction of these processes were present at all levels of spatial interaction (stand and landscape). However, the magnitude of the emergent behaviors depended on the spatial structure of the landscape and the level of spatial interaction that was considered. When wind-mortality was high (8 times above natural mortality rates), the dynamics of C processes in fragmented landscapes was not captured using an additive approach. The spatial arrangement of patches on the landscape led to emergent behaviors for one case. However, in many cases, emergent behaviors were not significant or could be accounted for with traditional modeling methods.

©Copyright by Erica Ann Hoffa Smithwick
October 19, 2001
All Rights Reserved

Potential Carbon Storage at the Landscape Scale in the
Pacific Northwest, U.S.A.

by
Erica Ann Hoffa Smithwick

A DISSERTATION

submitted to

Oregon State University

in partial fulfillment of
the requirement for the
degree of

Doctor of Philosophy

Presented October 19, 2001
Commencement June 2002

ACKNOWLEDGMENTS

I am deeply thankful to my major advisor, Mark Harmon, for the constancy of his support and encouragement, and for all the hours spent in deep discussions. His expectations that I think “out of the box” scientifically will remain a constant challenge and source of inspiration. I would also like to thank the rest of my committee. Particularly, I would like to thank Warren Cohen, my co-major advisor, for his support, especially for his contribution to remote sensing work that, while not included in the dissertation, has been part of my intellectual stimulation at OSU. I would also like to thank Julia Jones, for her enthusiasm and curiosity, and David Turner for joining my committee at late notice. Finally, I would like to thank Barbara Bond, who served on my committee for most of my time at OSU and whose dedication to her work has partially inspired my own. I am indebted to the following sources of funding for this work: the NASA-LCLUC (Land-Cover, Land-Use Change Program), an H.J. Andrews Long Term Ecological Research Grant (DEB-9632921), a National Science Foundation Fellowship in Landscape Ecology through Oregon State University, and the Richardson Endowment to the College of Forestry, Oregon State University.

A special thanks goes to Jimm Domingo, whose collaboration on the design of the MAXCARB model, as well as his programming skill, was invaluable. Moreover, his positive attitude and jovial spirit made it a joy to work with him (“pea-brain” and all). I would also like to thank Gody Spycher for his assistance in the design of computer code to analyze the old-growth data.

I may never have embarked upon such an intellectual voyage, and surely never would have seen it to completion, were it not for the support and inspiration I received from family and friends. The inspiration took many forms: the companionship on long runs in the forest, bike rides in the Corvallis countryside, easy evenings doing yoga, and good food and pleasant company during warm summer nights and cool winter evenings. To my many friends who contributed to these experiences, I am indebted. They kept me healthy in mind, body, and soul and gave me a perspective on life I will cherish. I would especially like to acknowledge the inspiration of my father, whose dissertation endeavor many years earlier, is surely the reason I am writing this today. Any successes in the writing of this work can only be attributed to the father, while any failures can only be attributed to the daughter.

To Penny, Pebbles, Petey, and Ashley, I am in awe of your unswerving love and humor. Thank you for keeping me laughing, and reminding me that a day in the forest, or out in the sun on the back porch, is better than any day by the computer. To Pearce, I am more thankful than I can express. You have suffered through many drafts, and made many sacrifices, always wearing a smile, to make this dissertation come real for me. I am deeply thankful for your benevolence, your consult, your friendship, and your love.

CONTRIBUTION OF AUTHORS

Dr. Mark Harmon was involved in the design, analysis and writing of each manuscript. Suzanne Remillard was responsible for the soil data. She also assisted in the writing of the methods section of the first manuscript and in the understory vegetation calculations. Dr. Steve Acker provided the data sets necessary to develop some allometric equations, and provided consultation on the data collection in the permanent plots. Jerry Franklin established the permanent plot network. James Domingo added modifications to the STANDCARB model in the second manuscript. In the third manuscript, he assisted in the conceptual design of the MAXCARB model and wrote the computer code.

TABLE OF CONTENTS

	<u>Page</u>
CHAPTER 1: INTRODUCTION.....	1
CHAPTER 2: POTENTIAL UPPER BOUNDS OF CARBON STORES IN FORESTS OF THE PACIFIC NORTHWEST.....	5
Abstract.....	6
Introduction.....	8
Methods.....	11
Site Description.....	11
Above- and Belowground Tree C.....	19
Understory C.....	22
Coarse Woody Debris C.....	23
Fine Woody Debris C.....	24
Organic Horizon C.....	24
Mineral Soil C.....	24
Epiphytes.....	26
Results.....	26
Discussion.....	36
Confidence in Site Estimates.....	36
Role of Disturbance.....	37
Regional Implications.....	38
Comparison with Global Studies.....	40
Why Does Old-growth in the PNW Store So Much C?.....	42
C Sequestration and Economic Implications.....	43
Conclusions.....	44
Acknowledgments.....	45
References.....	46

TABLE OF CONTENTS (Continued)

	<u>Page</u>
CHAPTER 3: A MODEL TO PREDICT POTENTIAL C STORAGE AS A FUNCTION OF DISTURBANCE REGIMES AND CLIMATE....	52
Abstract.....	53
Introduction.....	54
Model Description.....	57
Overview.....	57
General Approach.....	62
STEADY-STATE Module.....	64
Description.....	64
Calculations.....	66
CLIMATE Module.....	67
Description.....	67
Calculations.....	67
DISTURBANCE Module.....	70
Description.....	70
Calculations.....	72
Disturbance Event Transfers.....	75
Age-dependent Rate Functions.....	76
Simulation Experiments.....	77
Results.....	81
Simulating Natural Disturbance Regimes.....	81
Simulating Regulated Disturbance Regimes.....	86
Calibration with STANDCARB.....	88
Comparison with Observed Old-growth Forest Data at the H.J. Andrews.....	93
Sensitivity Analysis.....	95
Comparison with Observed Old-growth Forest Data in the PNW.....	95
Discussion.....	106

TABLE OF CONTENTS (Continued)

	<u>Page</u>
Conclusions.....	113
Acknowledgments.....	114
References.....	115
CHAPTER 4: EXAMINING MULTISCALE EFFECTS OF LIGHT LIMITATIONS AND EDGE-INDUCED MORTALITY ON CARBON STORES IN FOREST LANDSCAPES.....	120
Abstract.....	121
Introduction.....	122
Methods.....	128
Model Description.....	128
Modeling Light Processes.....	130
Modeling Wind Mortality.....	132
Model Parameterization and Calibration.....	134
Model Simulation Experiments.....	138
Stand Scale.....	140
Landscape Scale.....	143
Results.....	146
Cell-to-Cell Patterns in Carbon Stores.....	146
Cell-to-Cell Emergent Behaviors.....	151
Cell-to-Cell * Process Patterns in Species Dynamics.....	153
Cell-to-Cell * Process Emergent Behaviors.....	157
Cell-to-Cell * Age Patterns in Carbon Stores.....	157
Cell-to-Cell * Age Emergent Behaviors.....	159
Patch-to-Patch Patterns Across Edge Zones.....	159
Live Stores.....	162
Dead Stores.....	166
Total Stores.....	170
Patch-to-Patch Emergent Behaviors.....	173
Patch-to-Patch * Process Emergent Behaviors.....	173
Patch-to-Patch * Structure Emergent Behaviors.....	176

TABLE OF CONTENTS (Continued)

	<u>Page</u>
Discussion.....	176
Conclusions.....	186
Acknowledgments.....	188
References.....	189
CHAPTER 5: CONCLUSIONS AND FUTURE DIRECTIONS.....	192
Conclusions.....	193
Future Directions.....	195
BIBLIOGRAPHY.....	201
APPENDICES.....	217

LIST OF FIGURES

<u>Figure</u>	<u>Page</u>
2.1. Locations of sites used to measure old-growth biomass in the PNW within each of the physiographic provinces.....	13
2.2. Boxplot of mean stand Total Ecosystem Carbon (TEC) by province.....	27
2.3. Average percentage of TEC in measured C pools for stands in the Oregon Cascades province.....	32
2.4. Boxplots describing C storage estimates from the literature for (a) live (b) detrital and (c) SOC pools, compared to the average C storage among provinces in the PNW (this study).....	41
3.1. Overall conceptual structure of MAXCARB, showing the DISTURBANCE, STEADY-STATE, and CLIMATE Modules and their interactions.....	59
3.2. Flowchart of the calculations used in the MAXCARB model, showing the relationship between the DISTURBANCE, STEADY-STATE, and CLIMATE Modules.....	60
3.3. Cascade of calculations used in the STEADY-STATE Module to calculate landscape-average, steady-state mass.....	65
3.4. Flowchart of the calculations used in the DISTURBANCE Module.....	71
3.5. Conceptual representation of the age-class structure for regulated and natural disturbance regimes.....	73
3.6. Examples of dynamic rate functions used in the DISTURBANCE Module: (a) branch respiration (b) coarse root pruning.....	78
3.7. Example of dynamic rate function for foliage mass used in the DISTURBANCE Module.....	79
3.8. Comparison of fire flux (loss) between a 200-year and 50-year natural disturbance (fire) regime.....	82

LIST OF FIGURES (Continued)

<u>Figure</u>	<u>Page</u>
3.9. Comparison of total mass through time for a 200-year and a 50-year natural disturbance (fire) regime.....	83
3.10. Comparison of the respiration flux (loss) of total carbon between a 200-year and a 50-year natural disturbance (fire) regime.....	84
3.11. Landscape-average rates of burn loss calculated in the DISTURBANCE Module for live, dead, and stable pools.....	85
3.12. Effect of rotation interval on landscape-average steady-state carbon stores, expressed as a percent of maximum total stores.....	87
3.13. Comparison of MAXCARB and STANDCARB steady-state carbon stores for all live pools.....	89
3.14. Comparison of MAXCARB and STANDCARB steady-state carbon stores for all dead pools.....	90
3.15. Comparison of MAXCARB and STANDCARB steady-state carbon stores for all stable pools.....	91
3.16. Comparison of steady-state carbon stores in live, dead, and stable pools between STANDCARB, MAXCARB, and old-growth forest data (H.J. Andrews, Oregon Cascades).....	94
3.17. Results of a sensitivity test on the rates in the DISTURBANCE Module showing the effect of changing tree mortality rates $\pm 10\%$ on total carbon stores.....	96
3.18. Results of a sensitivity test on the rates in the DISTURBANCE Module showing the effect of changing allocation ratios $\pm 10\%$ on total carbon stores.....	97
3.19. Results of a sensitivity test on the rates in the DISTURBANCE Module showing the effect of changing respiration rates $\pm 10\%$ on total carbon stores.....	98

LIST OF FIGURES (Continued)

<u>Figure</u>	<u>Page</u>
3.20. Predicted (MAXCARB) vs. observed (old-growth forest data) steady-state carbon stores.....	99
3.21. Temporal variation in (a) monthly minimum and (b) monthly maximum temperature for the five ecoregions represented by old-growth forest data	102
3.22. Temporal variation in (a) monthly precipitation and (b) monthly radiation for the five ecoregions represented by old-growth forest data.....	103
3.23. Linear regression between mean annual precipitation of observed (old-growth forest sites) and the difference between predicted (MAXCARB) and observed carbon stores at steady-state.....	105
4.1. Conceptual structure of carbon pools and vegetation layers for STANDCARB 2.0.....	129
4.2. Arrangement of cells in STANDCARB, representing the spatial structure used to calculate light limitations and wind mortality ...	131
4.3. Graphical representation of elevated mortality rates across an edge.....	135
4.4. Artificial landscape cutting patterns used to drive the model.....	139
4.5. Example of the zones used to calculate carbon stores within Landscape AD.....	145
4.6. Total (live+dead+stable) carbon stores in Landscape OG as a function of processes included in the simulations.....	147
4.7. Old-growth carbon stores in live, dead, and total carbon pools as a function of simulations with either no light limitations or wind mortality, or simulations with wind mortality set to $k=8$	150
4.8. Emergent behaviors due to interactions at the cell-to-cell level.....	152

LIST OF FIGURES (Continued)

<u>Figure</u>	<u>Page</u>
4.9. Effect of increasing k values on the number of upper trees for PSME (Douglas-fir, <i>Pseudotsuga menziesii</i>) and TSHE (western hemlock, <i>Tsuga heterophylla</i>) for simulations with only wind mortality included.....	154
4.10. The trend in (a) total dead and (b) total live carbon through time for simulations with only wind mortality included (k set to 3 or 8), only light-limitations included, or neither included (None) for Landscape OG.....	155
4.11. Effect of increasing k values on the number of upper trees for PSME (Douglas-fir, <i>Pseudotsuga menziesii</i>) and TSHE (western hemlock, <i>Tsuga heterophylla</i>) for simulations with both light and wind mortality limitations included.....	156
4.12. Emergent behaviors due to the cell-to-cell * process interactions...	158
4.13. The trend in (a) total live and (b) total dead carbon through time for simulations with only wind mortality included (k set to 3 or 8), only light-limitations included, or neither included (None) for Landscape Y (young).....	160
4.14. Emergent behaviors due to the cell-to-cell * age interactions.....	161
4.15. Live carbon by zone for different light and wind simulations for (a) foliage and (b) fine root pools in Landscape AD.....	163
4.16. Live carbon by zone for different light and wind simulations for (a) heartwood and (b) sapwood pools in Landscape AD.....	164
4.17. Live carbon by zone for different light and wind simulations for (a) branch and (b) coarse root pools in Landscape AD.....	165
4.18. Dead carbon by zone for different light and wind simulations for (a) foliage and (b) fine root pools in Landscape AD.....	167
4.19. Dead carbon by zone for different light and wind simulations for (a) sapwood and (b) heartwood pools in Landscape AD.....	168
4.20. Dead carbon by zone for different light and wind simulations for (a) branch and (b) coarse root pools in Landscape AD.....	169

LIST OF FIGURES (Continued)

<u>Figure</u>	<u>Page</u>
4.21. Effect of light limitations and wind mortality on (a) total live and (b) total dead carbon, by zone, in Landscape AD.....	171
4.22. Effect of light limitations and wind mortality on (a) total stable and (b) total (live+dead+stable) carbon, by zone, in Landscape AD.....	172
4.23. Emergent behaviors due to patch-to-patch interactions.....	174
4.24. Emergent behaviors due to patch-to-patch * process interactions....	175
4.25. Emergent behaviors due to patch-to-patch * structure interactions...	177
4.26. Results of a simple mixing model showing the potential errors caused by edge-induced, emergent behaviors for increasing patch widths.....	184

LIST OF TABLES

<u>Table</u>	<u>Page</u>
2.1. Stand characteristics of the five study provinces in the PNW.....	14
2.2. Average C pools for 43 old-growth stands in the PNW.....	28
2.3. The relative amounts of understory, above- and below-ground tree, detrital, and soil carbon in the five provinces as a percent of Total Ecosystem Carbon (TEC).....	34
3.1. Constants in the DISTURBANCE Module after calibration with STANDCARB.....	92
3.2. Site parameter values used in the CLIMATE Module of MAXCARB to predict total carbon stores at steady-state for multiple sites in the Pacific Northwest, U.S.A.....	101
4.1. Calibration of modeled carbon pools in STANDCARB v.2.0 to old-growth forest pools	136
4.2. Description of methodology used to test for emergent behaviors at various levels of spatial interaction.....	142
4.3. The effect of Neighbor functions (wind and/or light) on average carbon stores for different landscape cutting patterns.....	148

LIST OF APPENDICES

<u>Appendix</u>	<u>Page</u>
A. Species names, foliage biomass equations, and global comparison of old-growth forest data from Chapter 2.....	218
B. Abbreviations used in descriptions of the MAXCARB model.....	230
C. The calculations in the DISTURBANCE Module of MAXCARB.....	232
D. The calculations in the STEADY-STATE Module of MAXCARB.....	266
E. The calculations in the CLIMATE Module of MAXCARB	276

LIST OF APPENDIX FIGURES

<u>Figure</u>	<u>Page</u>
C.1. Foliage mass as a function of age.....	236
C.2. Branch to bole ratio as a function of age.....	237
C.3. Coarse root to bole ratio as a function of age.....	237
C.4. The rate of heartwood formation as a function of age.....	238
C.5. The rate of heart-rot formation as a function of age.....	239
C.6. The rate of sapwood respiration as a function of age.....	240
C.7. The rate of heart-rot respiration as a function of age.....	240
C.8. The rate of branch respiration as a function of age.....	241
C.9. The rate of coarse root respiration as a function of age.....	241
C.10. The rate of foliage turnover as a function of age.....	242
C.11. The rate of fine root turnover as a function of age.....	243
C.12. The rate of branch pruning as a function of age.....	244
C.13. The rate of coarse root pruning as a function of age.....	244
C.14. The mortality rate of trees as a function of age.....	245
C.15. The decay rate of dead foliage inputs as a function of age.....	246
C.16. The decay rate of dead sapwood inputs as a function of age.....	247
C.17. The decay rate of dead heartwood inputs as a function of age.....	247
C.18. The decay rate dead branch inputs as a function of age.....	248
C.19. The decay rate of dead coarse root inputs as a function of age.....	248
C.20. The decay rate dead fine root inputs as a function of age.....	249

LIST OF APPENDIX TABLES

<u>Table</u>	<u>Page</u>
A.1. Scientific and common names of observed tree species and their abbreviations	219
A.2. Source of equations used to calculate foliage biomass.....	220
A.3. Comparison with estimates from the literature for vegetation, detritus, and soil carbon stores in ecosystems around the globe.....	222
B.1. Abbreviations used in the MAXCARB module equations.....	231
C.1. The age-dependent functions used by the DISTURBANCE Module.....	234
C.2. Equations for landscape-average rate-constants in the DISTURBANCE Module.....	262

**Potential Carbon Storage at the Landscape Scale in the
Pacific Northwest, U.S.A.**

CHAPTER 1

INTRODUCTION

Erica A. H. Smithwick

In recent decades, there has been increased interest in quantifying the carbon (C) cycle due to evidence of increasing carbon dioxide (CO₂) in the atmosphere, attributed to industrialization and the associated release of CO₂ from fossil fuels (Baes et al. 1977). This increase in atmospheric CO₂, among other greenhouse gases such as methane (CH₄), nitrous oxide (N₂O), and water vapor (H₂O), is presumed to be the basis of current and future climate change (Baird 1999; Hansen et al. 2000; Schimel et al. 2000; Levitus et al. 2001). Nations are now urged to ameliorate climate change that exceeds natural variability by stabilizing greenhouse gas concentrations in the atmosphere according to Article 2 of the United Nations Framework Convention on Climate Change (Watson et al. 1997).

To mitigate C increases in the atmosphere, a full accounting of the C cycle is necessary. Carbon is exchanged between the atmosphere, the oceans, the terrestrial biosphere, and, over long time periods, sedimentary rocks. To understand the C cycle, one must understand the exchanges and stores of C among these global reservoirs. Thus, a "C budget" refers to the balance of C in the atmosphere, terrestrial biosphere, sediments, rocks, and oceans after accounting for the fluxes in and out of the reservoirs (or "pools"), and the exchanges between pools. Since C is assumed to be relatively stable in sediments and rocks, fluxes are typically estimated for the atmosphere, terrestrial biosphere, and oceans. Sources of C reflect the net release of C from one pool to another, while sinks of carbon reflect the net absorption of C in one pool relative to another. At a global scale, between 1989 and 1998, global emissions from fossil fuel burning and cement

production averaged $6.3 \pm 0.6 \text{ Gt C yr}^{-1}$. After subtracting C uptake in the ocean ($2.3 \pm 0.8 \text{ Gt C yr}^{-1}$) and the atmosphere ($3.3 \pm 0.2 \text{ Gt C yr}^{-1}$), there remained a net terrestrial uptake of $0.7 \pm 1.0 \text{ Gt C yr}^{-1}$. Additionally, $1.6 \pm 0.8 \text{ Gt C yr}^{-1}$ was released from land-use change, resulting in a residual C sink of $2.3 \pm 1.3 \text{ Gt C yr}^{-1}$ (Watson et al. 2000). Recent research has indicated that this “missing” C sink may be due to either the regrowth of Northern Hemisphere temperate forests, enhanced growth caused by CO_2 fertilization and nitrogen deposition, and/or climate warming that has resulted in a lengthening in the growing season at high-latitudes. Despite these advances in our understanding, there is still considerable uncertainty about the constraints to further increases in atmospheric C at a global scale. To constrain global C budgets more precisely, current scientific research on the terrestrial C cycle is focused on locating C sources and sinks regionally, and understanding the local ecosystem-level stores of C and other nutrients as well as their responses to anthropogenic and natural stresses. Towards this end, the spatial and temporal variability of the sources and sinks of C must be better understood at broad and fine scales.

One of the major uncertainties in the terrestrial C cycle is the role of disturbances, both natural and anthropogenic, on future C storage. It is difficult to explicitly model the effects of disturbance on the global C cycle because the resolution of global models is too large to detect most individual disturbance events, even though disturbance effects may be embedded within estimates of broad-scale processes. Conversely, studies at fine scales, while providing information on specific disturbance events, are also not appropriate for

understanding the role of disturbances because the resolution is too small to detect the effects of overarching disturbance regimes. The landscape-scale provides a tractable link between fine-scale measures of disturbance events and the C storage implications at broad-scales. The landscape-scale is also an appropriate scale to study the impact of disturbances because it is possible to observe both disturbance events as well as the spatial and temporal pattern of disturbance regimes.

In this dissertation, I present field-based estimates of the upper bounds of C storage across a broad, biogeoclimatic gradient in western Oregon and Washington (Chapter 2). I demonstrate that this region has the potential to store more C than is currently stored. This is of interest to ecosystem scientists as it elucidates the variation in the upper bounds of C storage across a gradient of substrate, vegetation, and climate. I then present a new model that places an upper bound on C storage at the landscape scale and predicts potential C storage in response to disturbance regimes and climate (Chapter 3). The novelty of this research lies in the development of a methodology to directly determine the effect of regulated and natural disturbance regimes on steady-state C storage. This research is of interest to global C modelers as it provides a tool to study C storage at a tractable spatial scale, yielding results on the effects of disturbance processes that may be appropriate for inclusion in global models. Finally, I present a heuristic modeling exercise that determines whether emergent behaviors result from spatial pattern-process interactions at several spatial scales (Chapter 4). The importance of this research is that it helps in scaling information between stand and landscape scales, assessing common assumptions of spatial homogeneity in ecosystem modeling.

CHAPTER 2

POTENTIAL UPPER BOUNDS OF CARBON STORES IN FORESTS OF THE PACIFIC NORTHWEST

Erica A. H. Smithwick, Mark E. Harmon, Suzanne M. Remillard, Steve A. Acker,
and Jerry F. Franklin

Submitted to *Ecological Applications*,
Ecological Society of America, Ithaca, NY
Accepted August 05, 2001

Abstract

Placing an upper bound to carbon (C) storage in forest ecosystems helps to constrain predictions on the amount of C that forest management strategies could sequester and the degree to which natural and anthropogenic disturbances change C storage. The potential, upper bound to C storage is difficult to approximate in the field because it requires studying old-growth forests, of which few remain. In this paper, we put an upper bound (or limit) on C storage in the Pacific Northwest (PNW) of the United States using field data from old-growth forests, which are near steady-state conditions. Specifically, the goals of this study were: (1) to approximate the upper bounds of C storage in the PNW by estimating total ecosystem carbon (TEC) stores of 43 old-growth forest stands in 5 distinct biogeoclimatic provinces, and (2) to compare these TEC storage estimates with those from other biomes, globally. Finally, we suggest that the upper bounds of C storage in forests of the PNW are higher than current estimates of C stores, presumably due to a combination of natural and anthropogenic disturbances, which indicates a potentially substantial and economically significant role of C sequestration in the region. Results showed that coastal Oregon stands stored, on average, $1127 \text{ Mg C ha}^{-1}$ (1006 to $1245 \text{ Mg C ha}^{-1}$, $n=8$), which was the highest for the study area, while stands in eastern Oregon stored the least, 195 Mg C ha^{-1} (158 to 252 Mg C ha^{-1} , $n=4$). In general, Oregon coastal stands (average = $1127 \text{ Mg C ha}^{-1}$, range = 1006 to $1245 \text{ Mg C ha}^{-1}$, $n=8$) stored slightly more than Washington coastal stands (average = 820 Mg C ha^{-1} , range = 767 to 993 Mg C ha^{-1} , $n=7$). Similarly, stands in the Oregon Cascades (average = 829 Mg C ha^{-1} , range = 445 to

1097 Mg C ha⁻¹, n=14) stored more, on average, than the Washington Cascades (average = 754 Mg C ha⁻¹, range = 463 to 1050 Mg C ha⁻¹, n=10). A simple, area-weighted average TEC storage to 1 m soil depth (TEC₁₀₀) for the PNW was 671 Mg C ha⁻¹. When soil was included only to 50 cm (TEC₅₀), the area-weighted average was 640 Mg C ha⁻¹. Subtracting estimates of current forest C storage (obtained from the literature) from the potential, upper bound of C storage in this study, a maximum of 338 Mg C ha⁻¹ (TEC₁₀₀) could be stored in PNW forests in addition to current stores.

Introduction

Managing forests to enhance carbon sequestration is one means of reducing CO₂ concentrations in the atmosphere to mitigate potential threats from global climate change (Vitousek 1991; Brown 1996). The magnitude and duration of carbon (C) sequestration over the long term can be constrained by knowing the upper bounds (or limit) of C storage, relative to current C storage. The use of “baseline” studies in science has been heralded as a way to bound scientific understanding. For example, Bender et al. (2000) conclude that scientists “...need to have baseline studies from relatively un-impacted regions of the earth to discern mechanisms and magnitudes of modern human impacts, and, importantly, examine factors that influenced carbon and nutrient dynamics in pre-industrial environments.” We suggest that setting an upper bound to carbon sequestration potential is equally necessary to constrain estimates of uncertain C sequestration predictions, and ideally to inform scientists and managers of the limits of the system. Once the upper bounds of C storage are identified over broad biogeoclimatic gradients, C sequestration, and its economic implications, can be assessed most effectively.

One way to measure past changes in carbon storage from the terrestrial biosphere to the atmosphere is to measure the change in C stores in terrestrial ecosystems between two points in time. This has been called the ‘difference’ approach (Turner et al. 2000a). It has been used to measure changes in forest inventory data over time (Kauppi et al. 1992, Krankina and Dixon 1994) and to estimate the change in landscape C stores over time using multi-date remote

sensing imagery (Cohen et al. 1996). Similarly, the difference approach can be used to constrain potential carbon sequestration by subtracting current C storage from the upper bounds.

However, while there is significant information on current C stores, it is difficult to constrain the magnitude and duration of C sequestration potential because few stands exist in which the upper bounds of carbon storage can be measured directly. Most forests never reach their upper bound of C storage due to the combined effects of anthropogenic and/or natural disturbances that cause a reduction in C storage from their potential. While old-growth forests maintain higher levels of C storage than are found earlier in succession (Odum 1969; Janisch and Harmon 2002; Franklin et al., in press), managed forests in temperate regions may contain as little as 30 % of the living tree biomass and 70 % of the soil C found in old-growth forests (Cooper 1983). Disturbances of old-growth temperate forests may reduce C storage for at least 250 years and with continual harvesting, C storage may be reduced indefinitely (Harmon et al. 1990).

Due to the lack of field data to estimate the upper bounds of C sequestration potential, models are used to predict future C sequestration. However, many ecosystem models rely on current, rather than potential, estimates of C densities (C storage on an area basis) to initiate and validate model simulations, such as from remote sensing. Current C density estimates may reflect integrated ecosystem responses to past degradation and/or disturbance processes. For example, Brown et al. (1991) suggest that current C densities in the tropics reflect historical degradation by selective logging and other forms of human disturbance. Regrowth

in these and other secondary forests may have a larger role in explaining the “missing” C sink than previously thought (Houghton et al. 1998).

It is also difficult to estimate C sequestration potential since most field studies do not account for all manageable pools of C. By including Total Ecosystem Carbon (TEC), we provide sufficient data from which managers will be able to make accurate predictions about how much carbon can be sequestered in the future. We additionally calculate TEC to a depth of 100 cm (TEC₁₀₀) and to a depth of 50 cm (TEC₅₀), since the latter may be more amenable for C sequestration activities in the short term. We present TEC values to 100 cm unless otherwise specified to fully account for the upper bounds of these ecosystems.

In this paper we: (1) approximate the upper bounds of C storage in the Pacific Northwest (PNW) region of the United States by estimating TEC of 43 old-growth forest stands in 5 biogeoclimatic zones, and (2) compare these TEC storage estimates to those from other regions, globally. These old-growth forests are at or near steady-state (inputs \approx outputs) based on recent studies (Turner and Long 1975; Long and Turner 1975; DeBell and Franklin, 1987; Acker et al., in press; Franklin et al. in press). The stands have not experienced catastrophic disturbances for 150 to 1200 years, and are therefore appropriate locations to determine the upper bounds of C storage in the absence of human or natural disturbances. Certainly, the stands have had minor gap-phase disturbances such as single-tree mortality events from wind or disease. However, these are endogenous disturbances (Bormann and Likens 1979), resulting in an oscillation of steady-state conditions around a mean. In this paper, we are concerned with an estimate of the long-term, upper bound of C

storage. We recognize, however, that at shorter temporal scales and smaller spatial scales, steady state conditions may not occur.

Previously, Grier and Logan (1977) showed that late-successional *Pseudotsuga menziesii* forests of the western Cascades of Oregon had greater stores of biomass than had been measured by other studies in the region (Turner and Long 1975, Fujimori et al. 1976). This study extends the work of Grier and Logan (1977) by examining trends in a complete inventory of all the significant C pools along a wide biogeoclimatic gradient, not just the Oregon Cascades, providing estimates of the upper bounds of C storage as well as its variability between biogeoclimatic regions.

Methods

Site Description

Sampling was conducted in 43 stands at 7 sites in western Oregon and Washington. The sites are located within 5 of the general physiographic provinces described by Franklin and Dyrness (1988). Assuming the sites are representative (**Table 2.1** and Franklin and Dyrness (1988)), we designated each site to a respective province: Oregon Coast (ORCOAST), Washington Coast (WACOAST), Oregon Cascades (ORCASC), Washington Cascades (WACASC), or Eastern Oregon (OREAST). ORCOAST was represented by 8 stands at Cascade Head Experimental Forest; WACOAST was represented by 7 stands on the Olympic Peninsula; ORCASC was represented by 14 stands at the H.J. Andrews

Experimental Forest; WACASC was represented by 10 stands at Mt. Rainer National Park and Wind River Experimental Forest (T.T. Munger Research Natural Area); and OREAST was represented by 4 stands at Metolius Research Natural Area and Pringle Falls Research Natural Area (**Figure 2.1** and **Table 2.1**).

All sites were part of a permanent plot network designed to observe and monitor changes in composition, structure, and functions of forest ecosystems over long time periods (see Acker et al. 1998 for a complete description of the history and characteristics of the network). The 43 old-growth sites used in this study are located on lands managed by either the United States Forest Service (USFS) or the National Park Service and are maintained by the H.J. Andrews Experimental Forest Long-Term Ecological Research program (LTER) and The Cascade Center for Ecosystem Management (a cooperative effort between Oregon State University, the Pacific Northwest Research Station of the USFS, and the Willamette National Forest). Data from the network is stored in the Forest Science Data Bank of the Department of Forest Science at Oregon State University.

The youngest stands in our study were at Cascade Head, in the ORCOAST. Their average age is 150 years, having developed after a catastrophic crown fire, the Nestucca Burn, in the late 1840s (Harcombe 1986; Acker et al., in press). Stands at the Olympic Peninsula have not had a stand-replacing disturbance for 230 to 280 years, while the remaining stands have not had a catastrophic disturbance for 450 to 1200 years (**Table 2.1**).

In the PNW, there is a strong east-west gradient in precipitation and temperature. Climate is generally mild and moist in the coastal sites, with cooler

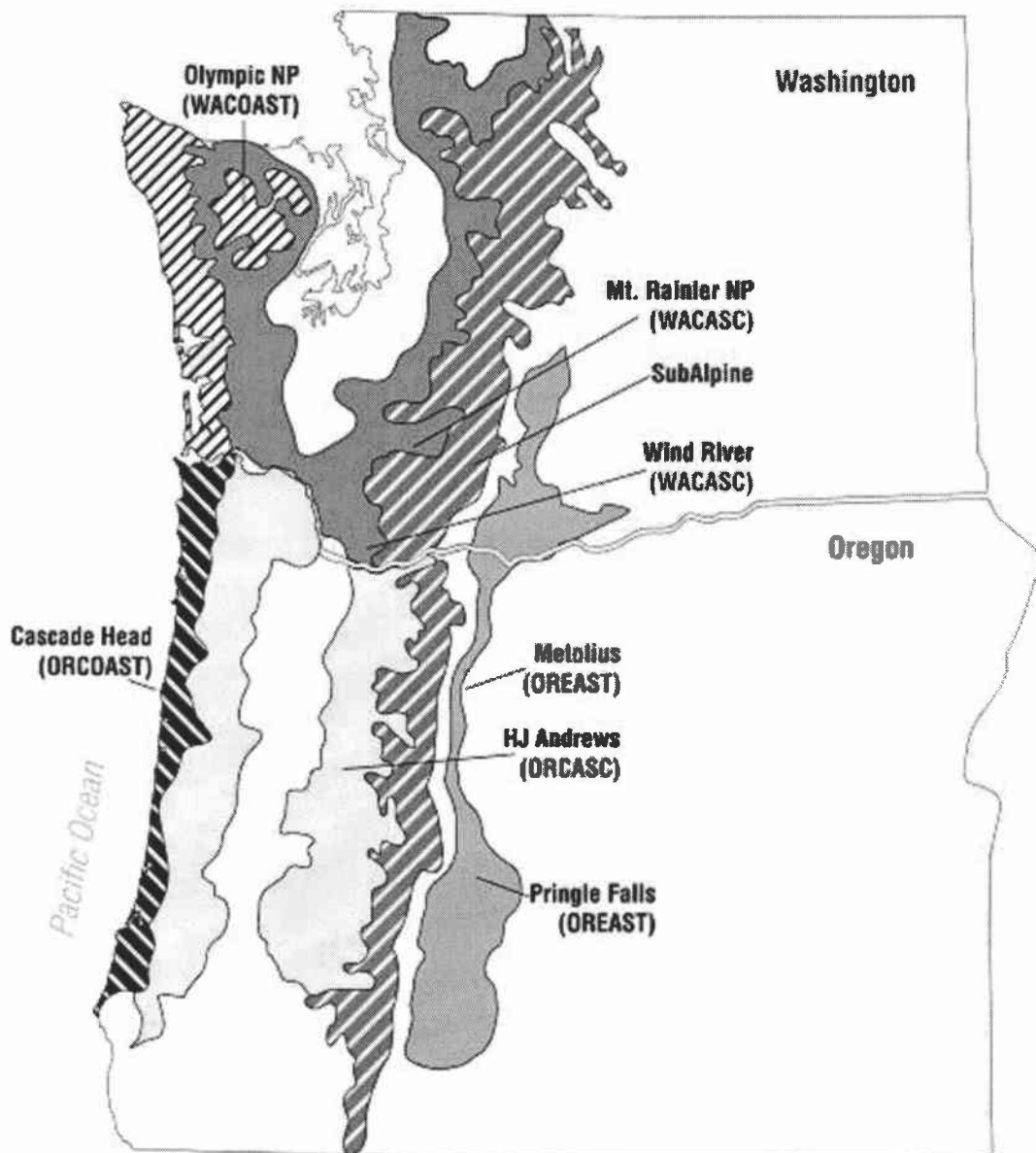


Figure 2.1. Locations of sites used to measure old-growth biomass in the PNW within each of the physiographic provinces.

Table 2.1. Stand characteristics of the five study provinces in the PNW.

Site	Stand Name (if applicable)	Stand Abbrev.	Size (ha)	Lat. N (°)	Long. W (°)	Elev. (m)	Age ¹ (yrs)	Temp. (°C)	Ppt. ² (mm)	#soil pits ³	# plots	Habitat Type ⁴	Dominant Species ⁴
OREGON CASCADES (ORCASC)													
H.J. Andrews		RS01	1.0	44.202	122.257	510	460	11.4	1719	2	16	PSME/HODI	PSME, ACMA
		RS02	1.0	44.217	122.243	520	460	10.9	1868	2	16	TSHE/BENE	PSME, TSHE
		RS03	1.0	44.260	122.159	950	460	7.8	2202	2	16	TSHE-ABAM/ RHMA-LIBO	PSME, THPL
		RS07	0.3	44.213	122.148	490	460	5.8	2260	2	1	TSHE/OXOR	PSME, TSHE
		RS10	0.3	44.213	122.217	610	450	10.1	2003	2	1	TSHE/RHMA /GASH	PSME, TSHE
		RS12	0.3	44.227	122.122	1020	460	7.0	2332	2	1	ABAM/VAAL/ COCA	PSME, TSHE
		RS15	0.3	44.212	122.236	720	460	8.9	1906	2	1	TSHE/POMU	PSME, TSHE
		RS16	0.3	44.214	122.241	670	460	10.3	1869	2	1	TSHE/CACH	PSME, PILA
		RS20	1.0	44.222	122.249	700	450	10.4	1859	1	16	PSME/HODI	PSME, PILA

Table 2.1. (Continued)

	RS22	1.0	44.274	122.140	1290	450	3.8	2282	2	16	ABAM/VAME/ XETE	ABPR, PSME
	RS23	1.0	44.227	122.123	1020	450	7.1	1240	2	16	ABAM/VAAL/ COCA	TSHE, PSME
	RS27	1.0	44.254	122.175	790	450	8.5	2118	2	24	TSHE-ABAM/ RHMA-LIBO	PSME, TSHE
	RS29	1.0	44.231	122.146	800	450	8.0	2264	2	16	TSHE-ACCI/ POMU	PSME, THPL
	RS31	1.0	44.262	122.181	900	450	8.1	2101	2	16	TSHE-ABAM/ RHMA-LIBO	PSME, THPL

OREGON COAST (ORCOAST)

Cascade Head

	CH01	0.4	45.046	123.897	305	150	8.3	2658	2	4	TSHE/OXOR	TSHE, PISI
	CH03	0.4	45.044	123.901	280	150	8.6	2660	2	4	TSHE/OXOR	TSHE, PISI
	CH04	0.4	45.065	123.941	259	150	9.0	2554	2	4	TSHE/OXOR	TSHE, PISI
	CH05	0.4	45.065	123.942	259	150	9.0	2552	2	4	TSHE/OXOR	TSHE, PISI
	CH07	0.4	45.063	123.939	244	150	8.7	2559	2	4	TSHE/OXOR	TSHE, PISI

Table 2.1. (Continued)

	CH08	0.4	45.065	123.944	271	150	9.0	2549	2	4	TSHE/OXOR	TSHE, PISI
	CH10	0.4	45.062	123.990	396	150	7.9	2417	2	4	TSHE/OXOR	TSHE, PISI
	CH12	0.4	45.049	123.898	280	150	8.5	2651	3	4	TSHE/OXOR	TSHE, PISI

EASTERN OREGON (OREAST)

Metolius RNA	MRNA	4.5	44.488	121.631	933	300	8.1	355	4	72	PIPO/PUTR	PIPO
Pringle Falls RNA	PF27	1.0	43.707	121.609	1353	400	5.7	545	2	16	PIPO	PIPO, PICO
	PF28	1.0	43.709	121.603	1372	400	5.	539	2	16	PIPO	PIPO, PICO
	PF29	1.0	43.706	121.613	1353	500	5.8	549	2	16	PIPO	PIPO, PICO

WASHINGTON CASCADES (WACASC)

Mt. Rainier NP

White River (R.)	AB08	1.0	46.919	121.538	1050	500	7.3	2076	2	16	ABAM/BENE	TSHE, THPL
Nisqually R.	AE10	1.0	46.768	121.742	1430	300	4.1	2812	1	16	ABAM/ERMO	ABAM, CHNO
Nisqually R.	AG05	1.0	46.748	121.803	950	700	6.1	2421	2	16	ABAM/GASH	ABAM, THPL

Table 2.1. (Continued)

Nisqually R.	AV06	1.0	46.777	121.783	1060	750	6.0	2658	2	16	ABAM/VAAL	ABAM, TSHE
Nisqually R.	TO04	1.0	46.741	121.887	640	750	8.8	2166	2	16	TSHE/OPHO	TSHE, PSME
Ohanapeccosh R.	AO03	1.0	46.827	121.546	853	1000	6.6	2257	1	16	ABAM/OPHO	ABAM, TSHE
Ohanapeccosh R.	AV02	1.0	46.823	121.551	841	1000	5.4	2249	1	16	ABAM/VAAL	ABAM, TSHE
Carbon R.	AV14	1.0	46.960	121.843	1080	1200	3.9	2500	2	16	ABAM/VAAL	ABAM, TSHE
Carbon R.	TO11	1.0	46.995	121.880	610	550	8.1	2112	2	16	TSHE/OPHO	PSME, TSHE

Wind River

T.T. Munger RNA	MUNA	4.5	45.828	121.969	411	470	7.8	2496	8	21	TSHE/BENE	PSME, TSHE
-----------------	------	-----	--------	---------	-----	-----	-----	------	---	----	-----------	------------

WASHINGTON COAST (WACOAST)

Olympic Peninsula

S. Fork Hoh R.	HR01	1.0	47.779	123.908	244	280	8.2	3669	2	16	TSHE/OXOR	TSHE, PISI
S. Fork Hoh R.	HR02	1.0	47.779	123.908	244	280	8.2	3669	2	16	TSHE/OXOR	TSHE, PISI
S. Fork Hoh R.	HR02	1.0	47.779	123.908	250	280	8.2	3669	2	16	TSHE/OXOR	TSHE, PISI
S. Fork Hoh R.	HR 04	1.0	47.779	123.908	250	280	8.2	3669	2	16	TSHE/OXOR	TSHE, PISI

Table 2.1. (Continued)

Quinault RNA	HS02	1.0	47.429	123.873	122	230	8.9	2899	2	16	TSHE/OXOR	TSHE
Quinault RNA	HS03	1.0	47.430	123.873	122	230	8.9	2893	2	16	TSHE/OXOR	TSHE, PISI
Twin Creeks RNA	HS04	1.0	47.834	123.990	152	230	8.9	3026	2	16	TSHE/OXOR	TSHE, PISI

¹ Ages determined from tree cores (unpublished data, S. A. Acker and M. E. Harmon); Mt. Rainier ages determined from age-class maps (Franklin et al. 1988)

...² Precipitation data was from PRISM (Precipitation-elevation Regressions on Independent Slopes Model; Daly et al. 1994), and temperature data was from the POTT (POTential Temperature) model (Dodson and Marks 1997); Methods to calculate the values for each stand are described by Remillard (1999)

³ Soil pit data from Brown and Parsons (1972) was used for stands RS01 – RS16

..⁴ Abbreviations from Garrison et al. (1976); See **Appendix A** for tree species names

temperatures at high elevations, and lower precipitation east of the mountains. For example, mean annual temperature ranges from 11.4 °C at a low elevation stand in H.J. Andrews to 3.8 °C at Pringle Falls. Mean annual precipitation ranges from 3669 mm at the South Fork of the Hoh River, Olympic Peninsula, to 355 mm at Metolius RNA. Sites within the Oregon and Washington coastal provinces are represented by *Tsuga heterophylla*-*Picea sitchensis* habitats, while higher elevation sites are represented by *P. menziesii*-*Thuja heterophylla* habitats. East of the Cascades, *Pinus ponderosa* habitats predominate.

At each site, between 3 and 14 stands were sampled. Each stand was composed of 1 to 72 (median = 16) plots (**Table 2.1**). In addition to aboveground measurements within the stand, soil C was estimated from soil pits located just outside the measured area of the stand. The C pools (Mg C ha⁻¹) that were measured are described below. A biomass:C ratio of 2:1 was used for all calculations except for soil organic carbon estimates, where C density values were calculated directly. Unless otherwise described, TEC for each stand was calculated as an average of the plots on a per hectare basis. TEC for each province (e.g., ORCASC, ORCOAST, etc.) was calculated as the average of the stands in that province.

Above- and Belowground Tree C

Estimation of above and belowground tree C included the following pools: stem wood, stem bark, live and dead branches, foliage, live and dead coarse roots, and fine roots. In each stand, the diameters of all trees (>5 cm diameter at breast

height (DBH)) were measured. The biomass of stem wood, stem bark, and live and dead attached branches, were calculated by applying species-specific allometric equations from BIOPAK (Means et al. 1994). In some cases, species-specific equations were not available so we made substitutions with equations for similar species. We tested the effect of these substitutions by switching equations within and between families of tree species (while maintaining the observed distribution of DBH). In general, within-family conifer substitutions accounted for very small variations in biomass (e.g., 2.7 %, *Abies amabilis* for *Abies procera*). Between family conifer substitutions were more significant (e.g., 19 %, *T. heterophylla* for *A. amabilis*) but were rare. Hardwoods only occupied 1.3 % of the stems in the region so we assumed that uncertainty in these equations was not significant.

Foliage carbon stores were calculated from leaf area index (LAI, $\text{m}^2 \text{m}^{-2}$) using species-specific leaf area (SLA, g cm^{-2}) estimates found in the literature (**Appendix A**). We obtained estimates of LAI by calculating sapwood area (SA, cm^2), or sapwood thickness, from DBH using species-specific biomass equations (**Appendix A**). Predicting LAI from SA is preferable to prediction of LAI directly from DBH, as the latter overestimates LAI and leaf mass for mature and old-growth forests (Marshall and Waring 1986; Turner et al. 2000b). We derived species-specific allometric equations to predict SA from DBH for *P. sitchensis*, *Pinus contorta* and *Pinus ponderosa* using data from the permanent plots and published data from western softwoods (Lassen and Okkonen 1969). We applied appropriate substitution equations when species-specific allometric equations were lacking (**Appendix A**).

Fine-root biomass was not directly measured due to time constraints and due to its spatial and temporal variability. Instead, we assumed that fine root biomass is approximately 2% of total aboveground biomass (Table 7 in Grier and Logan 1977). Since approximately 1.6 times more fine root biomass is present in dry sites than wet sites (Table 3 in Santantonio and Hermann (1985)), we assumed that approximately 3 % of above-ground biomass ($2 \% * 1.6$) is allocated belowground in OREAST, where precipitation is limited (Gholz 1980). This is in general agreement with current understanding about tree physiology that, in water or nutrient limited sites, more NPP is allocated to fine roots (Waring and Running 1998).

We estimated live, coarse-root biomass (>10 mm diameter) for each tree from equations for *P. menziesii* in Santantonio et al. (1977) and corrected the values for different tree species using species-specific green densities (U.S. Forest Products Laboratory 1974). Dead, coarse-root biomass was estimated by assuming that it is the same proportion of coarse woody debris (logs + snags) as the proportion of live coarse root biomass is to aboveground tree biomass. For example, at stand RS01 (H.J. Andrews), live coarse root biomass is 29 % of aboveground tree biomass (live and dead branches, foliage, stem bole, stem bark). Therefore, we assumed that dead, coarse-root biomass was 29 % of coarse woody debris (29 % of 44.9) or 13.1 Mg C ha⁻¹. In this calculation, we assumed that the ratio of above- and below-ground decomposition rates does not diverge through time. We tested this assumption by calculating dead, coarse-root biomass with differing decay rates and comparing the ratio of roots to boles through time. We

would need to double the decay rates of dead, coarse-roots to see a 10 % decrease in the ratio of roots to boles. Given the range of decay rates for this region reported by Chen et al. (2001), we would not expect this to be the case. Thus, we have confidence that this assumption is appropriate.

Alternatively, to improve confidence in our estimates, we calculated coarse- and fine-root biomass with a regression equation developed by Cairns et al. (1997), which predicts total root biomass from aboveground biomass. We then calculated fine-root biomass as a ratio of fine roots to total roots (Figure 4 in Cairns et al. 1997). We compared the fine, and live, coarse-root biomass estimates from these two methods. Since the methods used in Santantonio et al. (1977) allow for the separation of live and dead, coarse-roots, we present these root estimates in the final TEC calculations.

Understory C

To determine understory C, dimensional measurements including cover and/or basal diameters were taken within each stand. Small tree (<5 cm) and shrub diameters, as well as shrub and herb cover, were measured along 4 transects within the stand. Transects were either 25 m or 50 m in length, depending on stand size.

The percent of shrub and herb cover was measured using line transects. Herb cover classes were noted for each species in 0.2 by 0.5 m micro-plots placed at systematic intervals of approximately 1 m. Diameters of shrub and small tree stems were tallied in a 1-m-wide belt transect by species and basal diameter classes (i.e., diameter at ground). Allometric biomass equations for total aboveground

biomass (BAT) were selected using BIOPAK (Means et al. 1994) by assembling the appropriate combination of equations describing components of biomass. For shrubs, if we could not predict BAT by one equation, we used a combination of equations, (e.g., entire aboveground = live branch + total stem + total foliage). We assigned a substitute equation for shrub and herb species whose biomass equations could not be found, or whose basal areas or cover values were outside of the range for which the species-specific equations were developed. Total biomass per stand was calculated by summing the biomass per species on each transect and then averaging the biomass per transect for each stand.

Coarse Woody Debris C

Coarse woody debris (CWD) included standing and fallen detrital biomass (≥ 10 cm diameter; ≥ 1 m in length). For each fallen tree, we measured the length, end diameter, and middle diameter. For each snag, we measured the height and end diameters. In addition to these dimensions, we recorded the species and decay class of each piece. The decay class is an index of the stage of decay of the log or snag, indicating its physical and biological characteristics, density, and nutrient content (Harmon and Sexton 1996). We converted the data to volumes and then to biomass using wood densities specific to its decay-class and species (Harmon and Sexton 1996).

Fine Woody Debris C

Downed, fine woody debris biomass (1 cm to 10 cm diameter) was estimated by harvesting downed branches and twigs in five, 1-m² micro-plots placed evenly along the transects used to sample herbs, shrubs, and small trees. The fresh weight of dead branches was determined on a portable electronic scale (Harmon and Sexton 1996) and sub-samples were weighed in the field and later oven dried to determine a dry:wet weight correction factor.

Organic Horizon C

This pool included the forest floor and buried rotten wood. A 5-cm diameter corer was used to collect samples of the O horizon at 5 locations along each transect that was used to sample fine woody debris. We separated the samples into fine, litter-derived material and coarse, wood-derived material based on color and texture. Each core sample was oven-dried (55 °C), weighed and analyzed for LOI (loss on ignition) to determine ash-free mass, which was used to calculate the proportion of organic matter in the sample. Organic matter was converted to C using a 2:1 ratio of ash-free biomass to C.

Mineral Soil C

Mineral soil organic C (SOC, Mg C ha⁻¹) estimates for these stands were reported by Remillard (1999), and detailed methods are described therein; we will

describe the methods briefly here. On the perimeter of each stand, one to three 1-m³ soil pits were used for a total of 79 soil pits. Pits were located to best represent the stand in terms of slope, aspect, vegetation-density and cover. The number of soil pits per stand ranged from one to eight, depending on soil heterogeneity. At each pit, soil samples were collected from three mineral soil layers (0- to 20-cm, 20- to 50-cm, and 50- to 100-cm).

SOC was calculated on a layer basis:

$$\text{SOC} = C * D * S * L * 100$$

Where C is the organic C concentration (g C kg⁻¹) of the C-bearing fraction; D is the bulk density (g cm⁻³) of this fraction; S is the C-bearing fraction as a proportion of total sample volume; L is the layer depth (cm); and 100 is the conversion factor (10⁸ cm⁻² ha⁻¹ 10⁻⁶ Mg g⁻¹) to yield the desired units (Mg C ha⁻¹).

To obtain the organic C concentration, samples were sieved and hand-sorted into the following components: <2 mm C-bearing soil fraction, 2- to 4-mm C-bearing soil fraction, > 4-mm C-bearing soil fraction, >2 mm rock (non-C bearing), and >2-mm buried wood, roots, and charcoal. The C-bearing fraction >2 mm were either hardened soil aggregates or soft, weathered rocks, which have been shown to be nutrient-rich and an important component of C stores (Ugolini et al. 1996; Corti et al. 1998; Cromack et al. 1999). Buried wood, roots, and charcoal accounted for <3 % of the sample mass and were disregarded in mineral SOC estimates. Sub-samples (50 to 100g) of the <2-mm, 2- to 4-mm, and >4-mm C-bearing fractions were analyzed for total C and N concentration using a LECO CSN 2000 analyzer by the Central Analytical Laboratory, Oregon State University, Corvallis. A mass-

weighted C concentration was computed for each size class by knowing the total C concentration (g C kg^{-1}) and the oven-dry mass of the material. Bulk density was determined for each soil layer with a core sampler for non-rocky soils or by excavating a known volume of soil for rocky soils. In addition to these 79 soil pits, data from Brown and Parsons (1972) for 8 soil pits (0-100 cm depth) in the H.J. Andrews, ORCASC, were also used (Table 2.1).

Epiphytes

We did not include epiphytes in our estimate of TEC. Epiphytes may account for only 0.06% of aboveground tree biomass (e.g., 17.8 kg of 29,174 kg in Pike et al. 1977), or perhaps even less (0.003%; Harmon et al., In review), indicating that the exclusion of this pool does not lead to significant underestimates of total C stores.

Results

There was significant variation of TEC_{100} averages between provinces (Figure 2.2) and among the stands (Table 2.2). ORCOAST stands stored, on average, $1127 \text{ Mg C ha}^{-1}$ (1006 to $1245 \text{ Mg C ha}^{-1}$, $n=8$), which was the highest for the study area, while stands in OREAST stored the least, 195 Mg C ha^{-1} (158 to 252 Mg C ha^{-1} , $n=4$). In general, ORCOAST stands (average= $1127 \text{ Mg C ha}^{-1}$, range= 1006 to $1245 \text{ Mg C ha}^{-1}$, $n=8$) stored slightly more than WACOAST stands (average = 820 Mg C ha^{-1} , range = 767 to 993 Mg C ha^{-1} , $n=7$). Similarly,

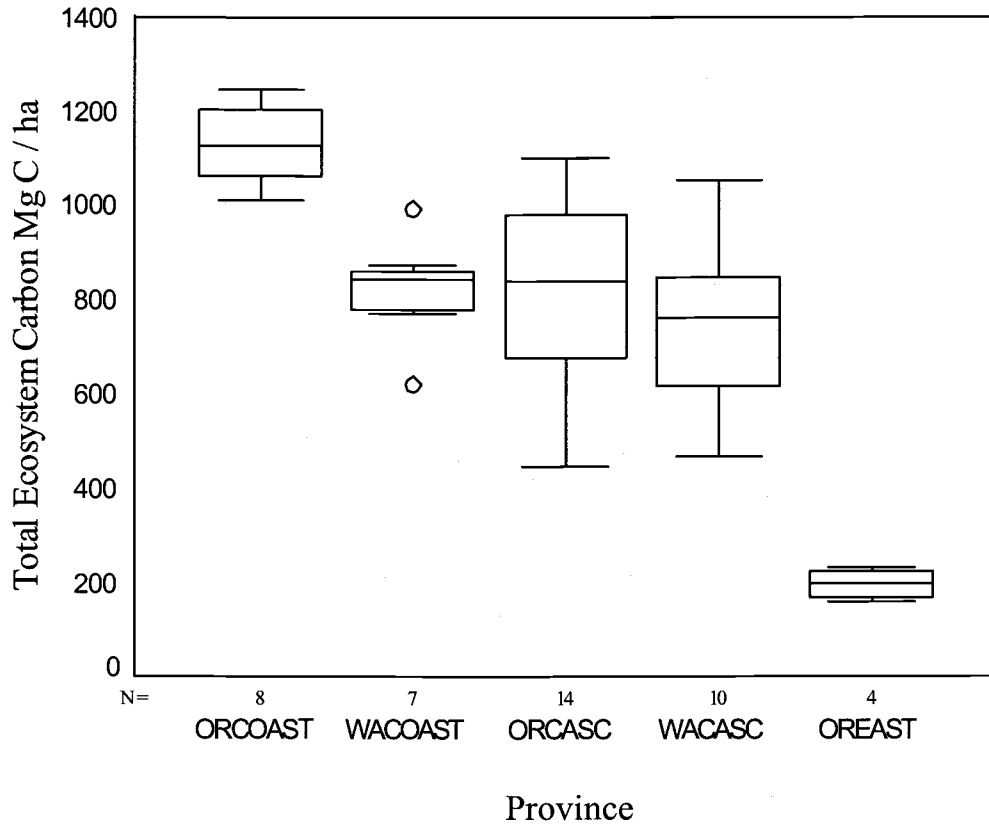


Figure 2.2. Boxplot of mean stand Total Ecosystem Carbon (TEC) by province.

Table 2.2. Average C pools for 43 old-growth stands in the PNW. Units are Mg C ha⁻¹.

Stand	Live branch	Dead branch	Foliage	Stem bark	Stem wood	Fine roots	Live coarse roots	Dead coarse roots	Fine woody debris	Forest floor	Rotten wood	Logs	Snags	Soil	Shrubs	Herbs	Total
ORCASC																	
RS01	18.0	4.0	4.2	57.4	208.5	5.8	85.0	13.1	9.5	13.3	0.0	20.8	24.1	122.5 ^a	1.0	nm ^b	587.4
RS02	28.6	4.9	4.7	55.5	230.8	6.5	93.6	19.7	16.4	22.5	0.0	45.0	23.4	122.5 ^a	0.6	nm	674.8
RS03	42.1	7.1	5.4	60.1	309.3	8.5	136.0	34.2	29.2	18.3	15.9	60.6	45.9	122.5 ^a	2.2	nm	897.3
RS07	37.1	6.3	4.2	71.0	299.8	8.4	106.9	15.3	13.1	13.0	17.1	38.9	21.1	122.5 ^a	0.2	nm	775.0
RS10	22.4	5.3	5.1	57.8	227.1	6.4	69.1	9.3	13.9	16.1	10.5	35.6	7.1	122.5 ^a	1.6	nm	609.9
RS12	66.2	11.0	4.9	98.0	441.7	12.4	152.8	24.2	7.0	31.3	25.2	32.3	66.1	122.5 ^a	1.5	nm	1097.3
RS15	42.3	6.9	4.4	98.9	380.0	10.6	141.4	32.2	11.0	7.5	0.0	33.9	87.3	122.5 ^a	0.1	nm	978.9
RS16	28.9	5.1	4.0	86.9	306.3	8.6	115.9	14.6	8.3	22.9	0.0	18.5	35.8	122.5 ^a	2.2	nm	780.5
RS20	16.9	4.0	4.4	50.3	186.5	5.2	71.4	5.9	13.8	21.3	0.0	12.4	9.4	41.9	0.1	0.4	443.8
RS22	31.0	5.2	8.9	53.0	244.2	6.8	93.9	46.0	33.3	28.5	22.2	69.0	98.5	179.2	0.5	0.3	920.4
RS23	52.5	8.6	4.3	43.9	262.6	7.4	99.0	25.5	5.1	18.5	26.0	36.6	59.1	102.8	1.7	0.3	753.9
RS27	54.8	9.4	5.9	108.1	452.4	12.6	189.8	17.9	12.6	23.3	11.2	54.3	5.1	121.8	0.5	0.3	1079.8
RS29	45.2	7.2	4.4	91.4	413.9	11.2	198.3	20.5	9.7	6.4	29.8	49.5	8.5	146.5	0.6	0.4	1043.4
RS31	45.4	7.5	5.9	88.3	364.7	10.2	157.0	27.4	8.6	19.5	0.0	75.9	13.4	143.2	1.7	0.2	969.0

Table 2.2. (Continued)

ORCOAST																	
CH01	77.5	12.5	6.3	22.0	291.9	8.2	102.8	22.2	18.1	16.9	54.9	53.5	35.0	472.3	2.3	0.1	1196.4
CH03	60.6	9.6	5.8	22.3	389.1	9.7	148.7	21.8	15.2	21.4	0.0	45.0	26.5	346.7	0.8	0.3	1123.5
CH04	55.9	9.4	6.9	26.4	416.3	10.3	153.0	21.4	11.2	27.7	24.5	40.0	32.0	407.4	2.6	0.2	1245.2
CH05	56.1	8.8	6.7	26.5	448.5	10.9	170.0	18.3	18.1	16.7	23.8	45.0	14.0	339.2	0.8	0.3	1203.8
CH07	69.1	11.3	6.8	24.1	338.9	9.0	119.1	16.1	17.4	30.5	25.7	40.0	21.0	275.4	1.0	0.1	1005.7
CH08	73.1	11.8	6.9	21.7	285.5	8.0	94.4	18.6	20.0	40.3	4.4	54.0	24.5	377.2	2.0	0.1	1042.4
CH10	51.8	7.7	5.6	21.1	400.0	9.7	155.5	16.3	16.8	13.8	3.4	34.5	16.5	326.3	0.8	0.4	1080.4
CH12	67.7	10.9	5.8	20.7	317.1	8.4	115.7	26.3	18.4	13.1	37.6	69.4	26.5	380.1	0.9	0.3	1118.9
OREAST																	
MRNA	13.9	1.6	0.5	15.6	53.0	2.5	24.9	8.6	6.9	14.9	0.0	14.3	14.8	58.7	1.0	0.3	231.6
PF27	11.2	1.0	0.4	11.7	44.0	2.1	20.1	5.3	8.5	6.1	0.0	8.9	9.0	29.2	0.0	0.0	157.5
PF28	13.0	1.3	0.4	14.4	49.6	2.4	22.7	4.3	10.1	8.6	0.0	9.3	5.6	32.1	0.1	0.0	173.7
PF29	17.6	1.6	0.8	17.7	71.7	3.3	36.1	5.5	8.2	10.1	0.0	8.8	7.9	27.0	0.2	0.0	216.5
WACASC																	
AB08	42.5	7.1	12.5	25.4	197.2	5.7	94.1	21.0	11.2	11.3	61.1	57.4	6.3	59.9	0.5	0.2	613.3
AE10	37.1	11.2	9.2	34.1	271.2	7.3	99.1	11.8	24.1	11.2	21.2	25.6	17.8	262.6	1.2	0.0	844.9
AG05	33.0	7.5	9.1	47.1	266.8	7.3	99.2	20.2	10.0	9.0	41.8	53.1	20.8	54.7	0.6	0.1	680.2
AO03	60.6	12.6	11.4	47.7	380.2	10.2	147.0	28.6	10.5	17.5	27.5	55.3	44.3	95.9	0.3	0.2	949.6

Table 2.2. (Continued)

AV02	58.4	11.8	9.1	35.4	284.9	8.0	96.2	27.8	10.4	26.9	45.9	84.9	30.4	109.3	1.8	0.1	841.1
AV06	24.1	5.1	8.6	24.0	147.9	4.2	48.2	12.9	6.0	28.3	18.1	32.1	24.0	78.1	1.5	0.3	463.1
AV14	53.7	11.9	8.7	30.8	295.1	8.0	121.7	9.8	15.0	6.5	37.3	20.2	12.2	204.8	1.4	0.2	837.2
MUNA	41.1	7.2	4.8	49.3	248.5	7.0	31.8	3.8	9.4	33.3	17.1	16.6	24.9	116.6	1.4	0.8	613.5
TO04	43.4	7.1	4.4	39.7	266.1	7.2	100.1	9.2	5.8	30.8	25.1	4.6	28.5	75.6	0.5	0.3	648.5
TO11	55.0	8.7	5.1	68.1	419.8	11.1	159.6	36.1	20.9	16.3	13.9	85.6	40.3	109.0	0.2	0.4	1050.1
WACOAST																	
HR01	39.7	5.6	6.1	13.5	240.2	6.1	95.3	26.3	5.4	6.7	21.5	73.1	11.0	216.5	nm	nm	767.0
HR02	51.0	5.8	8.6	17.6	389.5	9.4	161.5	26.5	17.2	8.2	15.8	66.4	11.3	204.2	nm	nm	993.0
HR03	31.2	3.4	5.4	9.9	236.9	5.7	99.5	22.6	13.2	8.8	12.1	53.0	12.0	109.0	nm	nm	622.8
HR04	59.5	7.8	6.9	14.5	332.7	8.4	137.1	18.6	5.6	10.3	0.0	44.8	12.5	131.6	nm	nm	790.3
HS02	61.7	9.5	5.9	14.5	237.3	6.6	89.3	23.8	7.7	10.1	0.0	74.7	13.1	288.5	0.2	0.4	843.3
HS03	50.8	7.5	7.4	14.5	266.6	6.9	100.6	18.7	9.2	18.4	19.3	50.5	14.0	264.6	0.3	0.4	849.7
HS04	53.9	8.2	6.6	24.7	289.6	7.7	116.3	35.0	6.0	23.0	30.7	87.0	28.4	153.3	0.8	0.5	871.6

^a Values are average from other reported values in the field

^b nm = not measured

ORCASC stands (average = 829 Mg C ha⁻¹, range = 445 to 1097 Mg C ha⁻¹, n=14) stored more, on average, than the WACASC (average = 754 Mg C ha⁻¹, range = 463 to 1050 Mg C ha⁻¹, n=10). The lowest C density among the 43 stands was at Pringle Falls, OREAST (PF27), where only 158 Mg C ha⁻¹ was stored, while the highest C density was at stand CH04 at Cascade Head, ORCOAST, with 1245 Mg C ha⁻¹.

Almost all C pools were consistent between provinces in their percent of TEC (calculated from **Table 2.2**; **Figure 2.3**). The live branch pool averaged 5.9 % (± 0.4 %) of TEC₁₀₀ for all provinces (n = 5). The dead branch and foliage pool averaged 0.9 % (± 0.1 %) and 0.7 % (± 0.1 %), respectively. Stem wood averaged 33.8 % (± 1.7 %) while stem bark averaged 5.1 % (± 1.4 %) of TEC₁₀₀. The fine-root pool averaged 1.0 % (± 0.1 %) of TEC₁₀₀ for all provinces while live and dead coarse roots averaged 13.4 % (± 0.5 %) and 2.6 % (± 0.2 %), respectively. The standard deviation of fine-root biomass could be much larger or smaller since fine-root biomass was calculated simply as a ratio to above-ground biomass and therefore represents the variability of the latter numbers. Fine woody debris averaged 2.0 % (± 0.6 %), forest floor averaged 2.7 % (± 0.6 %), and rotten wood averaged 1.8 % (± 0.7 %). The log pool averaged 5.6 % (± 0.6 %) and the snag pool averaged 3.3 % (± 0.6 %). Of all ecosystem C pools, stem wood was the most significant component, ranging from 28.0 % of TEC₁₀₀ in OREAST stands to 37.0 % in the Cascades (**Figure 2.3**).

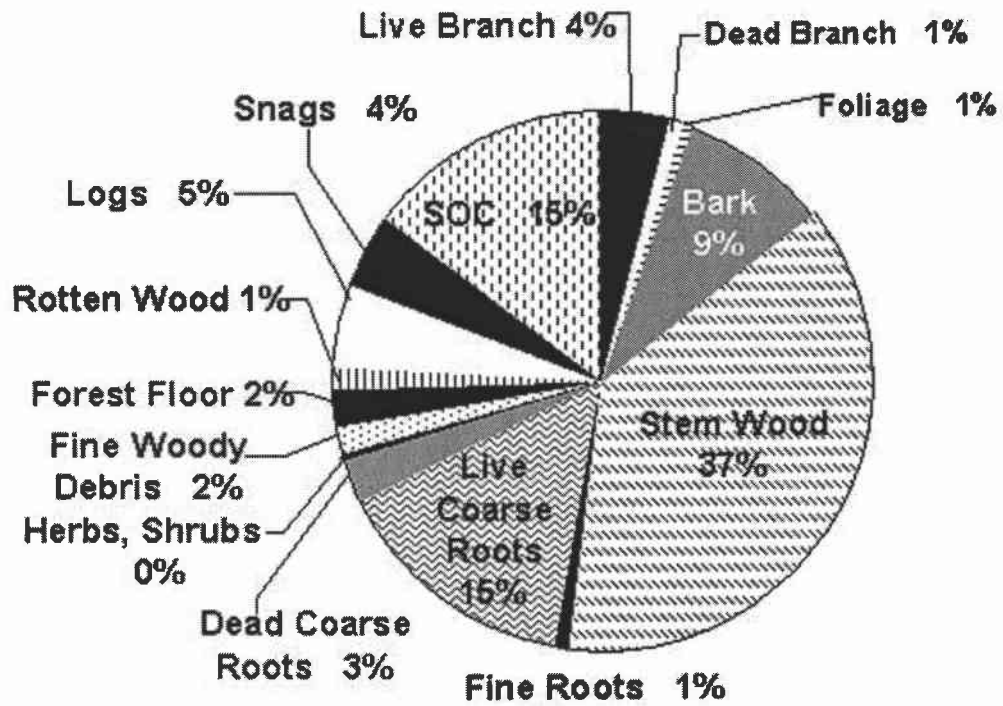


Figure 2.3. Average percentage of TEC in measured C pools for stands in the Oregon Cascades province (rounded to the nearest whole number); other provinces were similar (see text).

Average SOC values varied widely between provinces (**Table 2.3**), highlighting the large biogeoclimatic variability in the PNW. The percent of SOC₁₀₀ relative to TEC₁₀₀ ranged from 15.0 % in the Washington Cascades to 32.0 % in the Oregon Coast, with a mean of 21.1 % (Standard Error (SE) = 3.3 %). ORCOAST stands stored ten times the SOC that is stored in OREAST (365.5 versus 36.7 Mg C ha⁻¹). ORCOAST stands stored, on average, 130 Mg C ha⁻¹ more SOC than stands at WACOAST and about 3 times as much as was found in the stands in the Oregon and Washington Cascades. As a percent of TEC₅₀, SOC₅₀ was, in general, a smaller proportion of total C, ranging from 11.4 % in the WACASC to 24.5 % in ORCOAST (average = 16.5 %, SE = 2.4 Mg C ha⁻¹).

In each of the 5 provinces, total tree C, total detrital C, and total understory C were consistent percentages of TEC, respectively (**Table 2.3**). Understory biomass was very small in all provinces (average = 0.1 %, SE = 0.02 %). Above-ground tree C (live and dead branches, foliage, stem wood and bark), was the largest component of TEC₁₀₀ and TEC₅₀. Above-ground tree C was between 41 % and 52 % of TEC₁₀₀ (average = 46 %, SE = 2.1 %) and 45 % to 54 % of TEC₅₀ (average = 49 %, SE = 1.7 %). Below-ground tree C (fine roots, live and dead coarse roots) ranged from 14.4 % (ORCOAST) to 18.4 % (ORCASC) of TEC₁₀₀ (average = 17.0 %, SE = 0.71 %) and from 16.0 % (ORCOAST) to 19.0 % (WACOAST) of TEC₅₀ (average = 17.9 %, SE = 0.6 %). ORCOAST had the lowest percent of total tree C. This is because soil C represents a larger proportion of TEC at ORCOAST relative to the other provinces (**Table 2.3**).

Table 2.3. The relative amounts of understory, above- and below-ground tree, detrital, and soil carbon in the five provinces (ORCASC = Oregon Cascades, ORCOAST = Oregon Coast, OREAST = Eastern Oregon, WACASC = Washington Cascades, WACOAST = Washington Coast) as a percent of Total Ecosystem Carbon (TEC). Percent values outside of parentheses (%₁₀₀) represent calculations with TEC₁₀₀^a; values inside parentheses (%₅₀) represent calculations with TEC₅₀^b.

Province	<u>TEC₁₀₀</u> ^a	<u>TEC₅₀</u> ^b	<u>Understory</u> ^c		<u>Above-ground Tree</u> ^d		<u>Below-ground Tree</u> ^e		<u>Detrital</u> ^f		<u>SOC₁₀₀</u>		<u>SOC₅₀</u>	
	Mg C ha ⁻¹	Mg C ha ⁻¹	Mg C ha ⁻¹	% ₁₀₀ (% ₅₀)	Mg C ha ⁻¹	% ₁₀₀ (% ₅₀)	Mg C ha ⁻¹	% ₁₀₀ (% ₅₀)	Mg C ha ⁻¹	% ₁₀₀ (% ₅₀)	Mg C ha ⁻¹	Mg C ha ⁻¹	% ₁₀₀ (% ₅₀)	% ₁₀₀ (% ₅₀)
ORCASC	829.4	805.7	1.1	0.13 (0.14)	431.7	52.0 (53.6)	152.6	18.4 (18.9)	121.4	14.6 (15.1)	122.5	98.8	14.8 (12.3)	
ORCOAST	1127.0	1009.0	1.6	0.14 (0.16)	464.7	41.2 (46.1)	161.8	14.4 (16.0)	133.5	11.8 (13.2)	365.5	247.5	32.4 (24.5)	
OREAST	194.8	187.0	0.4	0.21 (0.21)	85.3	43.9 (45.6)	34.5	17.7 (18.4)	37.9	19.5 (20.3)	36.7	28.9	18.8 (15.5)	
WASCASC	754.2	719.3	1.2	0.16 (0.17)	380.2	50.4 (52.9)	125.4	16.6 (17.4)	130.7	17.3 (18.2)	116.6	81.7	15.5 (11.4)	
WACOAST	819.7	767.7	0.4	0.05 (0.01)	363.5	44.3 (47.4)	146.0	17.8 (19.0)	114.4	14.0 (14.9)	195.4	143.0	23.8 (18.6)	

^a Understory + Tree + Soil Organic Carbon from 0-100cm (SOC₁₀₀)

^b Understory + Tree + Soil Organic Carbon from 0-50cm (SOC₅₀)

^c Shrubs + herbs

^d Live and dead branch, foliage, stem bark, stem wood

^e Fine roots, live and dead coarse roots

^f Fine woody debris, forest floor, rotten wood, logs, snags (excluding dead coarse roots, dead branches)

Detrital carbon (fine woody debris, dead coarse roots, dead branches, forest floor, rotten wood, logs, snags) ranged from 14.5 % in the ORCOAST to 23.2 % of TEC in the OREAST (mean = 19 %, SE = 1.5 %) for TEC_{100} and from 13.2 % (ORCOAST) to 20.3 % (OREAST) for TEC_{50} (mean = 16.3 %, SE = 1.3 %).

Stands in eastern Oregon had much less detritus C ($45.2 \text{ Mg C ha}^{-1}$) compared to coastal and Cascades stands (145.7 to $163.9 \text{ Mg C ha}^{-1}$), even though the percent relative to TEC was the greatest. Among detrital pools, however, there was significant variation between provinces (**Table 2.2**). ORCOAST had 46 % more fine woody debris and forest floor C than WACOAST and 39 % more snag C. However, WACOAST had 35 % more C in the form of logs than ORCOAST. ORCASC and WACASC stands had a similar distribution of C in their detrital pools, although the WACASC stands had >60 % more rotten wood than ORCASC.

The percentage of root C relative to TEC differs depending on the method used to estimate root C. When using the regression equation developed by Cairns et al. (1997), TRCD averaged 13.4 % of TEC. When using the Santantonio et al. (1977) equations, and adjusting for species density, roots averaged 17.0 % of TEC. Root to shoot ratios (R:S) were the same for the ORCOAST and ORCASC regardless of which method was used. Both methods showed higher R:S for stands in OREAST, where more resources are stored belowground.

Discussion

Confidence in Site Estimates

As a proportion of TEC, estimation errors of the foliage pool are not significant. Foliage C is only 0.7 %, on average, of TEC in these old-growth forests and, therefore, even gross estimation errors would not significantly affect TEC. Indeed, we would have to increase the foliage pool 18 times to increase TEC by 10 %. Similarly, we would have to increase shrub C 100 times to increase TEC by 10 %. Nonetheless, prediction of foliage and understory C is critical for estimation of productivity and further species-specific equations need to be developed for this purpose.

Because of the effort required to directly measure coarse- and fine-root C, we used published allometric relationships instead. Review of the available root literature is complicated because measurements often reflect limited spatial and temporal domains, making comparisons difficult, and because different authors use dissimilar definitions of fine- and coarse-roots. Dead coarse-root biomass averaged 2.6 % of TEC. We would need to increase dead, coarse-root C by five times to change TEC by 10 %. We would have to increase fine-root C eleven times to increase TEC by 10 %. Therefore, although our estimates of these pools are rough, we have confidence that small changes in these pools will not affect TEC significantly. In contrast, live, coarse-root C is \approx 13.4 % of TEC. Therefore, we would need to increase this pool only 1.5 times to see a 10 % increase in TEC.

Estimation errors in the stem wood pool have the potential to provide the greatest uncertainty in TEC since this pool represents the largest proportion of TEC (34 %, on average). Yet, these are the pools about which we have the most confidence since over 14,000 trees were measured for stem wood volume and since the allometric equations used to calculate biomass are well documented and validated (see BIOPAK, Means et al. 1994).

In addition, by including coarse soil aggregates and estimating SOC to a depth of 1 m, the soil C estimates used in this study represent an improvement on previous regional estimates of C storage in the PNW. Remillard (1999) found that 39 to 66 % of SOC in soil pits was below 20-cm and up to 44 % of SOC was found in C-bearing material >2-mm. Therefore, reducing the degree that these C pools are underestimated results in more reliable estimates of the upper bounds of C storage in this region.

Role of Disturbance

Our estimates of the upper bounds of C storage simply place a limit on C storage for the region, based on the unrealistic assumption that all forests eventually reach old-growth conditions. Instead, natural disturbances such as fire, windstorms, landslides, as well as land conversion and management create a mosaic of age classes on a landscape (Bormann and Likens 1979). In theory, some old-growth stands persist due to the stochastic nature of disturbance processes (Johnson and Van Wagner 1985), but natural and managed landscapes will store less C than landscapes covered completely by old-growth forests because of the

high proportion of younger forests, which store less C than old-growth forests (Harmon et al. 1990). Despite these caveats, the theoretical construct of a completely old-growth landscape is useful as a neutral model (Gardner et al. 1987) in which one predicts the pattern (of C storage) in the absence of a process (Turner 1989) (e.g., human or natural disturbances). Such models could be used to distinguish systematically the effects of different management strategies on C storage. By bounding estimates of C sequestration potential, managers can determine the efficacy of different sequestration strategies relative to their potential. Further, they would be able to determine the potential economic and environmental costs and benefits of various management strategies. By providing an upper bound on C storage in the region (based on sites where those processes have been absent), we place an upper limit on the results of such analyses.

Regional Implications

To estimate the upper bounds of C storage for the PNW region, we multiplied the proportional area of each province (based on the area of the corresponding vegetation provinces in Franklin and Dyrness (1988)) by the average C storage in each province. These area-weighted estimates for each province were then summed. We used the following approximations of the area of each province to calculate the weighted estimates: *P. sitchensis* zone in Oregon (i.e., ORCOAST) was 8 % of the study area; *P. sitchensis* in Washington (i.e., WACOAST) was 9 %; *T. heterophylla* in Oregon (i.e. ORCASC) and Washington (i.e., WACASC) was 32 % and 17 %, respectively; *Pinus ponderosa* (i.e., OREAST) was 13 %; and

A. amabilis (subalpine zone) was 21 % (adapted from Fig. 27 in Franklin and Dyrness (1988)). Since subalpine stands were not represented by our study sites, we used a value of 401 Mg C ha⁻¹ in the *A. amabilis* zone, taken as the average from studies by Boone et al. (1988, Fig.1), Kimmins and Krumlik (1973, Tables 6 and 7 (assuming soil and roots are each 20 % of live biomass)) and Grier et al. (1981, Table 2). Without a more formal geospatial analysis, this weighting procedure is a good first attempt at a regional estimate, allowing us to further constrain our estimate of the upper bounds of C storage. Before weighting, the average, upper bound of C storage was 745 Mg C ha⁻¹ (n = 43 stands) to a depth of 100 cm. After weighting, the average upper bound of C storage was 671 Mg C ha⁻¹. Recalculating to SOC to 50 cm, a depth more amenable to forest sequestration practices in the short-term, the average, upper bound of C storage was 640 Mg C ha⁻¹. For the latter calculation, SOC in the subalpine zone was assumed to be half of that in the former calculation to 100 cm.

At the regional level, exogenous disturbances such as increasing CO₂, natural disturbances, and climate change will further change the regional capacity to store additional C. The eventual regional capacity to sequester C in the PNW may be, therefore, much different than the potential capacity we outline here. Regional predictions of actual carbon sequestration will require a more detailed accounting of all significant endogenous and exogenous factors that control it. However, by constraining these estimates with the potential values we describe, it may be possible to place limits on the system.

Comparison with Global Studies

The C densities we measured in old-growth forests of the PNW are higher than C density values reported for any other type of vegetation, anywhere in the world (**Figure 2.4; Appendix A**). Unfortunately, comparisons of our study to other carbon-density estimates is hampered since estimates often reflect sites whose disturbance histories are poorly documented. The biomass (or C) estimates of other studies often include effects of non-catastrophic, disturbance legacies (e.g. selective logging, light fires) or may represent stands which are in early to middle stages of succession after a stand-clearing disturbance such as a harvest, blow down, or heavy fire. Moreover, definitions of major ecosystem pools (live, detrital, soil) differ among studies. For example, Schlesinger (1977) defined detrital C as “the total carbon in dead organic matter in the forest floor and in the underlying mineral soil layers,” while Grier and Logan (1977) excluded soil C in their definition of detritus. In general, the distinction between litter, detritus, and soil C is not consistent between studies, making comparisons difficult (Matthews 1997).

Other limited studies in the region have demonstrated the potential of PNW old-growth forests to support large amounts of biomass. Fujimori et al. (1976), measuring only stem, branch, and leaf dry weights, reported biomass values of 669 to 882 Mg ha⁻¹ (335 to 441 Mg C ha⁻¹) in *P. sitchensis*, *Tsuga heterophylla*, and *A. amabilis* zones in Oregon and Washington. Means et al. (1999) estimated aboveground biomass (trees, foliage, shrubs, herbs) at the H.J. Andrews forest as 965 ± 174 Mg ha⁻¹ (or 483 ± 87 Mg C ha⁻¹). Grier and Logan (1977), who studied

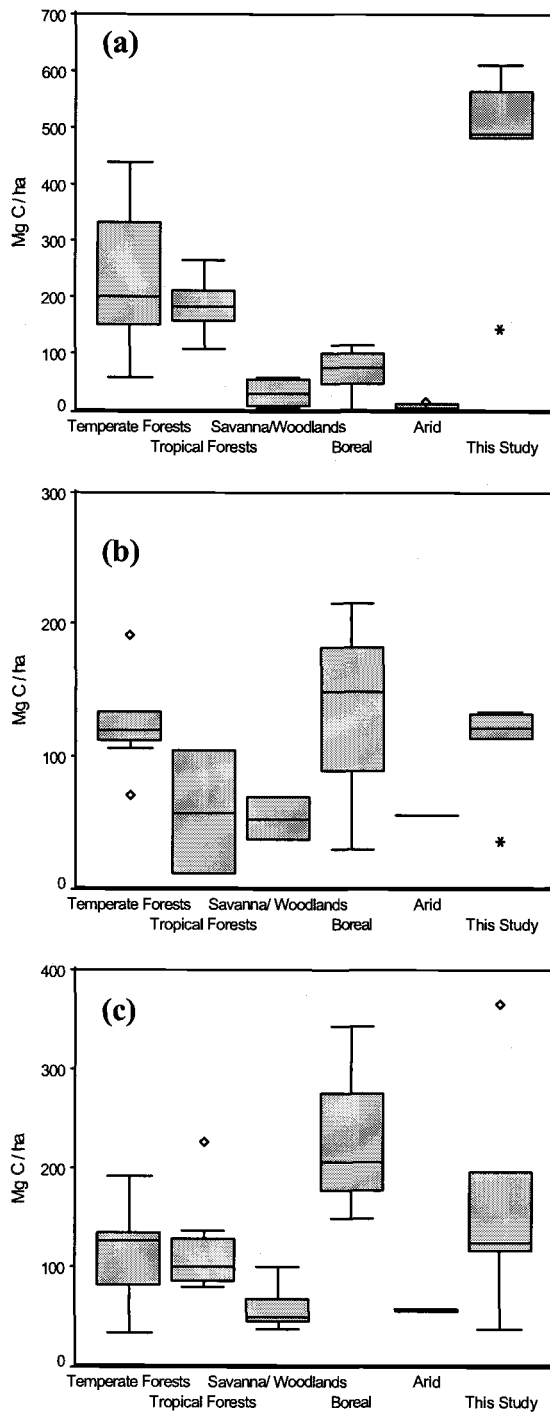


Figure 2.4. Boxplots describing C storage estimates from the literature for (a) live (b) detrital and (c) SOC pools, compared to the average C storage among provinces in the PNW (this study).

a 450-year old-growth stand in Watershed 10 of the H.J. Andrews, found total organic matter accumulations, including SOC to 1 m, ranging from 1008 to 1514 Mg ha⁻¹ (or 504 to 757 Mg C ha⁻¹). These studies at the H.J. Andrews were within the range of TEC that we measured at the H.J. Andrews (445 to 1097 Mg C ha⁻¹).

Why Does Old-growth in the PNW Store So Much C?

Trees in the PNW can reach massive sizes. Mild fall and winter conditions in much of the PNW facilitate continued productivity by coniferous evergreens at a time when deciduous trees are not able to photosynthesize. In addition, long, dry summers further hinder deciduous tree growth (Waring and Franklin 1979). Large conifer trees are able to maintain their growth by continued water conductivity through long, dry summers, which is facilitated with a tracheid xylem structure (Mencuccini and Grace 1996). The absence of frequent fires or storms in the productive regions of the PNW further supports massive trees with long lifetimes (Waring and Franklin 1979). In high-elevation sites, winter dormancy by coniferous tree species facilitates survival in cold conditions (Havrenek and Tranquillini 1995).

The large size of PNW trees means that they occupy a large proportion of ecosystem C storage relative to the national average. For example, Turner et al. (1995) estimated that half of actual total forest C in the conterminous U.S. was in the soil and that only 33 % was in trees. Woody debris represented 10 % of total C; the forest floor was 6 % and the understory was 1 % of total forest C. Birdsey et al. (1993) similarly estimated that only 31 % of total C in the U.S. is currently in tree C (51 % merchantable: 17 % roots, 3 % foliage, 6 % snags, 24 % other) and 59 % was

soil C. Litter, humus and downed, coarse woody debris comprised 9 % while understory was 1 % of total C. These national averages are different than the 15-32 % SOC and 53-67 % tree C in the old-growth stands reported in this study. It should be noted that the absolute amount of SOC in the PNW is higher than the global average, although the relative proportion of ecosystem C that they represent is less due to the large amount of tree C in old-growth PNW forests. The detailed methods used to measure SOC probably allowed us to find higher absolute C stores for this pool. However, the large proportion of tree C in this system, relative to the other studies mentioned above, indicates that the PNW may be more amenable to storing C through management and conservation efforts than other systems which store more C in soil.

C Sequestration and Economic Implications

Future C management (e.g., Parson and Keith 1998) will require information on the upper bounds of C storage and the extent to which current forest C storage differs from it. In the U.S., Birdsey (1992) used national forest inventory data and other selected studies to estimate current (1987) organic C storage for trees, soil, forest floor, and understory vegetation. In this assessment, PNW forests accounted for 39 % of TEC in the United States. Total C averaged 193.6 Mg C ha⁻¹ for Oregon forests and 227.1 Mg C ha⁻¹ for Washington forests (mean = 208.3 Mg C ha⁻¹, weighted by forest area in Birdsey (1992)). Turner et al. (1995) report an average C storage in PNW forests of 330 Mg C ha⁻¹. These studies present estimates that are significantly lower than our regional approximation of the upper bounds of C storage (671 Mg C ha⁻¹ for

TEC₁₀₀ and 640 Mg C ha⁻¹ for TEC₅₀). In fact, our estimate is twice that of Turner et al. (1995) and more than 3 times that of Birdsey (1992).

Subtracting the estimate of Turner et al. (1995) of average current C storage in western Oregon and Washington from the upper bound of C storage in the region, forests could, theoretically, store an additional 310 to 341 Mg C ha⁻¹. To increase the C store to this level would require forest management aimed toward C sequestration, which may include protection from catastrophic, natural disturbances, lengthening of harvest rotations, and improvement in soil C storage.

Given recent estimates of the value of C in economic analyses (e.g., Romm et al. 1998) the average worth of each hectare of forest could be thousands of dollars for additional C sequestration. Multiplied by the area of forest in Oregon and Washington, this additional C storage would be worth billions of dollars (given the current value of the dollar). While we realize it is unlikely that large areas may be converted to old-growth forests given the other demands on timber resources, this rough calculation indicates a significant economic value that C storage could represent in this region.

Conclusions

Old-growth forest ecosystems can be used as an upper bound (or upper limit) on additional C sequestration potential. Currently, forest C storage in the PNW is less than this upper bound due to management practices and natural disturbances that lower the average age of the forests, reducing the time for large tree boles, detrital

biomass, and soil C to accrue. The relative effect of natural disturbances, and human management on future C sequestration can be best gauged by comparisons to the upper bounds of C storage as presented in this study. The upper bound (or limit) of the global, terrestrial biosphere to sequester additional carbon could be improved with similar studies in other regions. If management strategies were such to allow forests to return closer to the C stores found in old-growth forests, the PNW would have considerable ability to sequester additional C. This could have significant economic implications.

Acknowledgments

This research was made possible by funding from the Pacific Northwest Research Station Long-Term Ecosystem Productivity Program, and Interagency Agreement DW 12936179 between USEPA and the Pacific Northwest Research Station. All stands are associated with the H.J. Andrews Long Term Ecological Research (LTER) program, grant number DEB-9632921.

References

- Acker, S. A., P.A. Harcombe, M.E. Harmon, and S.E. Greene. In press. Biomass accumulation over the first 150 years in a coastal Oregon spruce-hemlock forest. *Vegetation Science*.
- Acker, S.A., W.A. McKee, M.E. Harmon, and J.F. Franklin. 1998. Long-term research on forest dynamics in the Pacific Northwest: a network of permanent forest plots. *In Forest Biodiversity in North, Central, and South America and the Caribbean: Research and Monitoring*, F. Dallmeier and J.A. Comiskey (Eds.). The Parthenon Publishing Group, Inc., New York, New York, pp. 93-106.
- Bender, M., C. Field, L.O. Hedin, J. Schimel, E. Sundquist, R. Berner, J. Galloway, F. Mackenzie, M. Torn, K.H. Freeman, J. Hedges, C. Mora, R. Stallard, S.C. Wofsy, and W.H. Schlesinger. 2000. *The Changing C Cycle: A Terrestrial Focus, Report of the Workshop on the Terrestrial C Cycle*. The National Science Foundation, Division of Earth Sciences.
- Birdsey, R.A., A.J. Plantinga, and L.S. Heath. 1993. Past and prospective carbon storage in United States forests. *Forest Ecology and Management* **58**: 33-40.
- Birdsey, R.A. 1992. Carbon storage and accumulation in United States forest ecosystems. USDA Forest Service, Gen. Tech. Rep. WO-59, 51pp.
- Boone, R.D., P. Sollins, and K. Cromack, Jr. 1988. Stand and soil changes along a mountain hemlock death and regrowth sequence. *Ecology* **69**: 714-722.
- Bormann, F.H. and G.E. Likens. 1979. Catastrophic disturbance and the steady state in northern hardwood forest. *American Scientist* **67**: 660-669.
- Brown, R.B. and R.B. Parsons. 1972. Soils of the reference stands - Oregon IBP. Internal Report **128**. College of Forest Resources, University of Washington, Seattle, Washington, 84 pp.
- Brown, S. 1996. Mitigation potential of carbon dioxide emissions by management of forests in Asia. *Ambio* **25**: 273-278.
- Brown, S., A.J.R. Gillespie, and A.E. Lugo. 1991. Biomass of tropical forests of south and southeast Asia. *Canadian Journal of Forest Research* **21**: 111-117.
- Cairns, M.A., S. Brown, E.H. Helmer, and G.A. Baumgardner. 1997. Root biomass allocation in the world's upland forests. *Oecologia* **111**: 1-11.
- Chen, H., M.E. Harmon, and R.P. Griffiths. 2001. Decomposition and nitrogen release from decomposing woody roots in coniferous forests of the Pacific

- Northwest: a chronosequence approach. *Canadian Journal of Forest Research* **31**: 246-260.
- Cohen, W.B., M.E. Harmon, D.O. Wallin, and M. Fiorella. 1996. Two decades of carbon flux from forests of the Pacific Northwest. *BioScience* **46**: 836-844.
- Cooper, C.F. 1983. Carbon storage in managed forests. *Canadian Journal of Forest Research* **13**: 155-166.
- Corti, G., F.C. Ugolini, and A. Agnelli. 1998. Classing the soil skeleton (greater than two millimeters): proposed approach and procedure. *Soil Science Society of America Journal* **62**: 1620-1629.
- Cromack, K., Jr., R.E. Miller, O.T. Helgerson, R.G. Smith, and H.W. Anderson. 1999. Soil carbon and nutrients in a coastal Oregon Douglas-fir plantation with red alder. *Soil Science Society of America Journal* **63**: 232-239.
- Daly, C., R.P. Neilson, D.L. Phillips. 1994. A statistical-topographic model for mapping climatological precipitation over mountainous terrain. *Journal of Applied Meteorology* **33**: 140-158.
- DeBell, D.S. and J.F. Franklin. 1987. Old-growth Douglas-fir and western hemlock: a 36-year record of growth and mortality. *Western Journal of Applied Forestry* **2**: 111-114.
- Dodson, R. and D. Marks. 1997. Daily air temperature interpolation at high spatial resolution over a large mountainous region. *Climate Research* **8**: 2-20.
- Franklin, J. F., T. A. Spies, R. Van Pelt, A. Carey, D. Thornburgh, D.R. Berg, D. Lindenmayer, M. E. Harmon, W. Keeton, and D. C. Shaw. In press. Disturbances and the structural development of natural forest ecosystems with some implications for silviculture. *Forest Ecology and Management*.
- Franklin, J.F. and D.T. Dyrness. 1988. *Natural Vegetation of Oregon and Washington*, Oregon State University Press, Corvallis, Oregon, U.S.A.
- Franklin, J.F., W.H. Moir, M.A. Hemstrom, S.E. Greene, and B.G. Smith. 1988. The forest communities of Mount Rainier National Park. *Scientific Monograph Series Number 19*. U.S. Department of the Interior, National Park Service, Washington, D.C., 194 pp.
- Fujimori, T., S. Kawanabe, H. Saito, C.C. Grier, and T. Shidei. 1976. Biomass and net primary production in forests of three major vegetation zones of the northwestern United States. *Journal of the Japanese Forestry Society* **58**: 360-373.

- Gardner, R.H. B.T. Milne, M.G. Turner, and R.V. O'Neill. 1987. Neutral models for the analysis of broad-scale landscape pattern. *Landscape Ecology* **1**: 19-28.
- Garrison, G.A., J.M. Skovlin, C.E. Poulton, and A.H. Winward. 1976. Northwest plant names and symbols for ecosystem inventory and analysis. Gen. Tech.Rep. **PNW-GTR-46**. Portland, Oregon: USDA, Forest Service, Pacific Northwest Forest and Range Experiment Station, 263 pp.
- Grier, C.C. and R.S. Logan. 1977. Old-growth *Pseudotsuga Menziesii* communities of a western Oregon watershed: biomass distribution and production budgets. *Ecological Monographs* **47**: 373-400.
- Grier, C.C., K.A. Vogt, M.R. Keyes, and R.L. Edmonds. 1981. Biomass distribution and above- and below-ground production in young and mature *Abies amabilis* zone ecosystems of the Washington Cascades. *Canadian Journal of Forest Research* **11**: 155-167.
- Harcombe, P.A. 1986. Stand development in a 130-year-old spruce-hemlock forest based on age structure and 50 years of mortality data. *Forest Ecology and Management* **14**: 41-58.
- Harmon, M.E., K. Bible, M.J. Ryan, H. Chen, and J. Klopatek. In review. Production, respiration, and overall carbon balance in an old-growth *Pseudotsuga/Tsuga* forest ecosystem.
- Harmon, M.E. and J. Sexton. 1996. Guidelines for measurements of woody detritus in forest ecosystems. U.S. LTER Network Office: University of Washington, Seattle, Washington.
- Harmon, M.E., W.K. Ferrell, and J.F. Franklin. 1990. Effects on carbon storage of conversion of old-growth forests to young forests. *Science* **247**: 699-702.
- Havrenek, W.M. and W. Tranquillini. 1995. Physiological processes during winter dormancy and their ecological significance. *In Ecophysiology of Coniferous Forests*, W.K. Smith and T.M. Hinckley (Eds.), Academic Press, San Diego, California, pp. 95-124.
- Houghton, R.A., E.A. Davidson, and G.M. Woodwell. 1998. Missing sinks, feedbacks, and understanding the role of terrestrial ecosystems in the global carbon balance. *Global Biogeochemical Cycles* **12**: 25-34.
- Janisch, J.E. and M.E. Harmon. 2002. Successional changes in live and dead wood stores: Implications for net ecosystem productivity. *Tree Physiology* **22**: 77-89.
- Johnson, E.A. and C.E. Van Wagner. 1985. The theory and use of two fire history models. *Canadian Journal of Forest Research* **15**: 214-220.

- Kauppi, P.E., K. Mielikainen, and K. Kuusela. 1992. Biomass and carbon budget of European forests from 1971-1990. *Science* **256**: 70-74.
- Kimmins, J.P. and G.J. Krumlik. 1973. Comparison of the biomass distribution and tree form of old virgin forests at medium and high elevations in the mountains of South Coastal British Columbia, Canada. IUFRO Working Party on the Mensuration of Forest Biomass, presented in Vancouver, B.C., August 20-24.
- Krankina, O.N. and R.K. Dixon. 1994. Forest management options to conserve and sequester terrestrial carbon in the Russian Federation. *World Resources Review* **6**: 88-101.
- Lassen, L.E. and E.A. Okkonen. 1969. Sapwood thickness of Douglas-fir and five other western softwoods. **FPL-124**, Oregon State University, Corvallis, Oregon, USA.
- Long, J.N. and J. Turner. 1975. Aboveground biomass of understorey and overstorey in an age sequence of four Douglas-fir stands. *Journal of Applied Ecology* **12**: 179-188.
- Marshall, J.D. and R.H. Waring. 1986. Comparison of methods of estimated leaf-area index in old-growth Douglas-fir. *Ecology* **67**: 975-979.
- Matthews, E. 1997. Global litter production, pools, and turnover times: Estimates from measurement data and regression models. *Journal of Geophysical Research*. **102**: 18,771 - 18,800.
- Means, J.E., S.A. Acker, D.J. Harding, J.B. Blair, M.A. Lefsky, W.B. Cohen, M.E. Harmon, and W.A. McKee. 1999. Use of large-footprinting scanning airborne lidar to estimate forest stand characteristics in the western Cascades of Oregon. *Remote Sensing of Environment* **67**: 298-308.
- Means, J.E., H.A. Hansen, G.J. Koerper, P.B. Alaback, and M.W. Klopsch. 1994. Software for Computing Plant biomass - BIOPAK Users Guide. **PNW-GTR-340**, U.S.D.A., Forest Service, Pacific Northwest Research Station.
- Mencuccini, M. and J. Grace. 1996. Hydraulic conductance, light interception and needle nutrient concentration in Scots pine stands and their relations with net primary productivity. *Tree Physiology* **16**:459-468.
- Odum, E.P. 1969. The strategy of ecosystem development. *Science* **164**: 262-269.
- Parson, E.A. and D.W. Keith. 1998. Fossil fuels without CO₂ emissions. *Science* **282**: 1053-1054.

- Pike, L.H., R.A. Rydell, and W.C. Denison. 1977. A 400-year-old Douglas-fir tree and its epiphytes: biomass, surface area, and their distributions. *Canadian Journal of Forest Research* **7**: 680-699.
- Remillard, S.M. 1999. Soil Carbon and Nitrogen in Old-Growth Forests in Western Oregon and Washington, M.S. Thesis, Oregon State University, Corvallis, Oregon, U.S.A.
- Romm, J., M. Levine, M. Brown, and E. Petersen. 1998. A Road map for U.S. carbon reductions. *Science* **279**: 669-670.
- Santantonio, D. and R.K. Hermann. 1985. Standing crop, production, and turnover of fine roots on dry, moderate, and wet sites of mature Douglas-fir in western Oregon. *Annals of Science Forestry* **42**: 113-142.
- Santantonio, D., R.K. Hermann, and W.S. Overton. 1977. Root biomass studies in forest ecosystems. *Pedobiologia* **17**: 1-31.
- Schlesinger, W.H. 1977. Carbon balance in terrestrial detritus. *Annual Review of Ecology and Systematics* **8**: 51-81.
- Turner, D.P., W.B. Cohen, and R.E. Kennedy. 2000a. Alternative spatial resolution and estimation of carbon flux over a managed forest landscape in Western Oregon. *Landscape Ecology* **45**: 441-452.
- Turner, D.P., S.A. Acker, J.E. Means, and S.L. Garman. 2000b. Assessing alternative allometric algorithms for estimating leaf area of Douglas-fir trees and stands. *Forest Ecology and Management* **126**: 61-76.
- Turner, D.P., G.J. Koerper, M.E. Harmon, and J.J. Lee. 1995. A carbon budget for forests of the conterminous United States. *Ecological Applications* **5**: 421-436.
- Turner, J. and J.N. Long. 1975. Accumulation of organic matter in a series of Douglas-fir stands. *Canadian Journal of Forest Research* **5**: 681-690.
- Turner, M.G. 1989. Landscape ecology: the effect of pattern on process. *Annual Review of Ecology and Systematics* **20**: 171-97.
- Ugolini, F.C., G. Corti, A. Agnelli, and F. Piccardi. 1996. Mineralogical, physical, and chemical properties of rock fragments in soil. *Soil Science* **161**: 521-542.
- U.S. Forest Products Laboratory. 1974. Wood Handbook: wood as an engineering material. USDA Agricultural Handbook **72**, Revised.
- Vitousek, P.M. 1991. Can planted forests counteract increasing atmospheric carbon dioxide? *Journal of Environmental Quality* **20**: 348-354.

Waring, R.H. and S.W. Running. 1998. *Forest Ecosystems: Analysis at Multiple Scales*, Academic Press, San Diego, California, 370 pp.

Waring, R.H. and J.F. Franklin. 1979. Evergreen coniferous forests of the Pacific Northwest. *Science* **204**: 1380-1386.

CHAPTER 3**A MODEL TO PREDICT POTENTIAL C STORAGE AS A FUNCTION OF
DISTURBANCE REGIMES AND CLIMATE**

Erica A. H. Smithwick, Mark E. Harmon, and James B. Domingo

Abstract

Disturbances remain a key uncertainty in constraining the global carbon cycle in part because of the difficulty in scaling these fine-scale processes to the global level. Here we present a new model (MAXCARB) that predicts the potential response of carbon (C) storage in live, dead, stable, and forest product pools over a large area (approximately 10^5 ha) to climate and disturbance. To scale the effects of disturbances to broader scales, we simulate disturbance regimes, building on established principles in landscape ecology. For a given disturbance regime, the effects of disturbance events and successional dynamics at the fine scale are simulated by MAXCARB with age-dependent equations that predict how fluxes and mass of C stores change through time. Simulation results from the model compared favorably to simulation results from a finer-scaled model (STANDCARB) indicating that processes and carbon pools were treated consistently between the models. Comparison of model predictions matched data from old-growth forests in the Pacific Northwest, U.S.A, along a wide biogeoclimatic gradient (slope of regression line = 0.92, $r^2 = 0.94$). Analyses of the results indicate that fine-scale heterogeneity in disturbance processes can be captured at broad scales by simulating disturbance regimes rather than discrete disturbance events. Increased understanding of the variation in ecosystem processes with age will facilitate using this scaling approach.

Introduction

Current scientific research on the terrestrial C cycle is focused on constraining global estimates of the “missing” C sink (Dai and Fung, 1993; Ciais, 1995; Goulden et al., 1996; Houghton et al., 1998; Holland and Brown, 1999; Potter et al., 1999; Fung, 2000; Pacala et al., 2001) and locating C sources and sinks regionally (Houghton, 1993; Cohen et al., 1996; Fan et al., 1998; Melillo et al., 1988; Houghton, 1999; Fang et al., 2001; Potter et al., 2001). One goal of C cycle research is to predict the role of the terrestrial biosphere in future mitigation of atmospheric CO₂ increases under changing climate and disturbance conditions. However, the global potential to store C under future disturbance regimes resulting from climate change is not known (Dale, 1997; Schimel et al., 1997).

At intermediate (regional to continental) scales, disturbances are often accounted for indirectly by using historical input data (such as land-cover maps derived from remote sensing) to drive ecosystem models. For example, Schimel et al. (2000) used historical inventory data and satellite maps to drive three different ecosystem models (Biome-BGC, Century, and TEM), which account for increasing CO₂ and climate change, to evaluate C storage by ecosystems of the United States. Potter et al. (2001) combined satellite-derived greenness estimates and fire counts with an ecosystem production model (CASA) to evaluate regional C flux in response to deforestation and biomass burning in tropical forests during the early 1990s. Cohen et al. (1996) used biogeoclimatic maps and satellite land cover maps to drive a regional ecosystem model (LANDCARB) in the Pacific Northwest between 1972 and 1991 to assess how changes in disturbance regimes, from one

consisting of natural fires to one consisting of clear-cut harvesting, affected C storage. The abandonment of former agricultural lands, resulting in afforestation (Houghton et al., 1999), or the encroachment of woody biomass into areas that were previously grazed (Sedjo, 1992; Dixon et al., 1994; Hibbard, 1995), may also result in changes in C storage over time. As all these studies indicate, historical land-use changes may be the dominant factor controlling C storage at regional scales (Casperson et al., 2000).

However, including disturbance processes in global models is difficult because global models tend to be driven, in large part, by ecophysiological factors and therefore have limited capacity to predict the effect of disturbance processes directly (Peng, 2000). At global scales, current dynamic vegetation models assume that climate is the predominant factor controlling the composition and structure of vegetation and largely ignore the effects of disturbances processes (Peng, 2000). Initial attempts to include natural disturbances as part of a larger model (e.g., Lenihan et al., 1998, White et al., 2000) require data that are generally unavailable at broad scales. Moreover, most global models do not simulate anthropogenic disturbances, such as land-use change, into the future (Peng, 2000). To date, an efficient methodology to assess the effect of disturbances on potential C storage at broad scales is lacking.

Predicting the effects of future disturbances on global C cycling would be enhanced by an efficient methodology to scale information on disturbance processes from the regional scale to broader scales. At regional scales, individual disturbance events can be discerned, but at global scales individual disturbance

events are not directly observable, except in rare cases. Therefore, scaling approaches must summarize disturbance processes without explicitly depending on the exact prediction (in space and time) of individual disturbance events, which is impractical at global scales. A way to scale disturbances to broader scales is to use the concept of disturbance regimes. Derived from empirical observations, and building on principles of landscape ecology, a disturbance regime summarizes both the type and frequency of disturbance events for a broad area. It has been used to reconstruct historical forest age-class structures and to explain current age-class distributions of ecosystems within a landscape.

Here, we use the concept of disturbance regimes to predict the impact of simulated disturbances on steady-state C storage. This provides a mechanism to scale the effects of disturbance processes to an area of any size with the same disturbance regime. These concepts are incorporated into a new model (MAXCARB) that predicts the response of potential C storage over a large area (approximately 10^5 ha) to disturbance regimes and climate. By calculating potential C storage in the absence of exogenous disturbances, MAXCARB can be used to investigate the effect of climate on potential C storage at steady state. In addition, by simulating the effects of natural or regulated disturbance regimes on landscape-scale C stores, MAXCARB can be used to investigate the relative effects of different disturbance regimes on potential C storage. In this way, MAXCARB can efficiently and systematically test the effect of changing disturbance regimes and climate on potential C storage. This efficiency is useful for constraining estimates of future C storage at broad scales.

Model Description

Overview

MAXCARB, a computer simulation model written in C⁺⁺, is part of a larger modeling strategy (Cohen et al., 1996), used to measure the temporal and spatial patterns of C storage over the Pacific Northwest region of the United States. In this approach, multiple models are used to simulate processes at different scales. As part of this modeling strategy, MAXCARB is used to constrain regional estimates from the top down by placing an upper limit on production, decomposition, and C stores. Another model, STANDCARB (Harmon and Domingo, 2001; Harmon and Marks, in press), is used to constrain regional estimates from the bottom up by placing limits on the rate that C pools change over time. Actual stores at the regional scale are calculated using LANDCARB (Cohen et al., 1996; Wallin et al., 1996), which responds to observed changes in land-cover, as indicated by remote sensing.

MAXCARB predicts potential C stores in live, dead, stable (decay-resistant), and forest products pools for a steady-state landscape using assumptions of climate and soil constraints on growth and decomposition that are similar to many ecosystem process models (e.g., Running and Coughlan, 1988; Harmon and Marks, in press). Currently, the model is parameterized for the Pacific Northwest region of the United States but it can be parameterized for other regions as well.

The model has two spatial modes: point-mode, where the model computes steady-state C stores for a single site (i.e., location); and grid-mode, where the

model computes stores for a region represented by a rectangular grid of sites. When used to examine regional patterns of steady-state C stores, the region can be divided up into ecoregions, each representing a specific species composition and disturbance regime. Five types of input data are used to predict stores spatially: temperature, precipitation, elevation, solar radiation, and soil characteristics (texture, depth, and rockiness).

MAXCARB consists of three modules: STEADY-STATE, CLIMATE, and DISTURBANCE (**Figure 3.1**). At the center of the model design is the STEADY-STATE Module, which calculates steady-state C stores for all live, dead, stable, and forest product pools. To calculate these stores, the STEADY-STATE Module uses "landscape-average" rate-constants for ecoregions that are computed by the DISTURBANCE Module (**Figure 3.2**). The DISTURBANCE Module computes the rate-constants for each ecoregion by simulating fluxes and stores through time. This simulation includes disturbance events defined by the disturbance regime prescribed for each ecoregion. The user can choose not to run the DISTURBANCE Module, in which case the landscape-average rates can be read from a file manually created by the user, or generated during a previous simulation. The CLIMATE Module adjusts the growth, respiration, and decomposition rates in the STEADY-STATE Module for the combined effects of water, light, and temperature limitations, as specified by the site's climate data.

Temporally, the DISTURBANCE Module operates on an annual time-step, while the CLIMATE Module operates on a monthly time-step. The calculations in the STEADY-STATE Module represent equilibrium solutions (see below) and

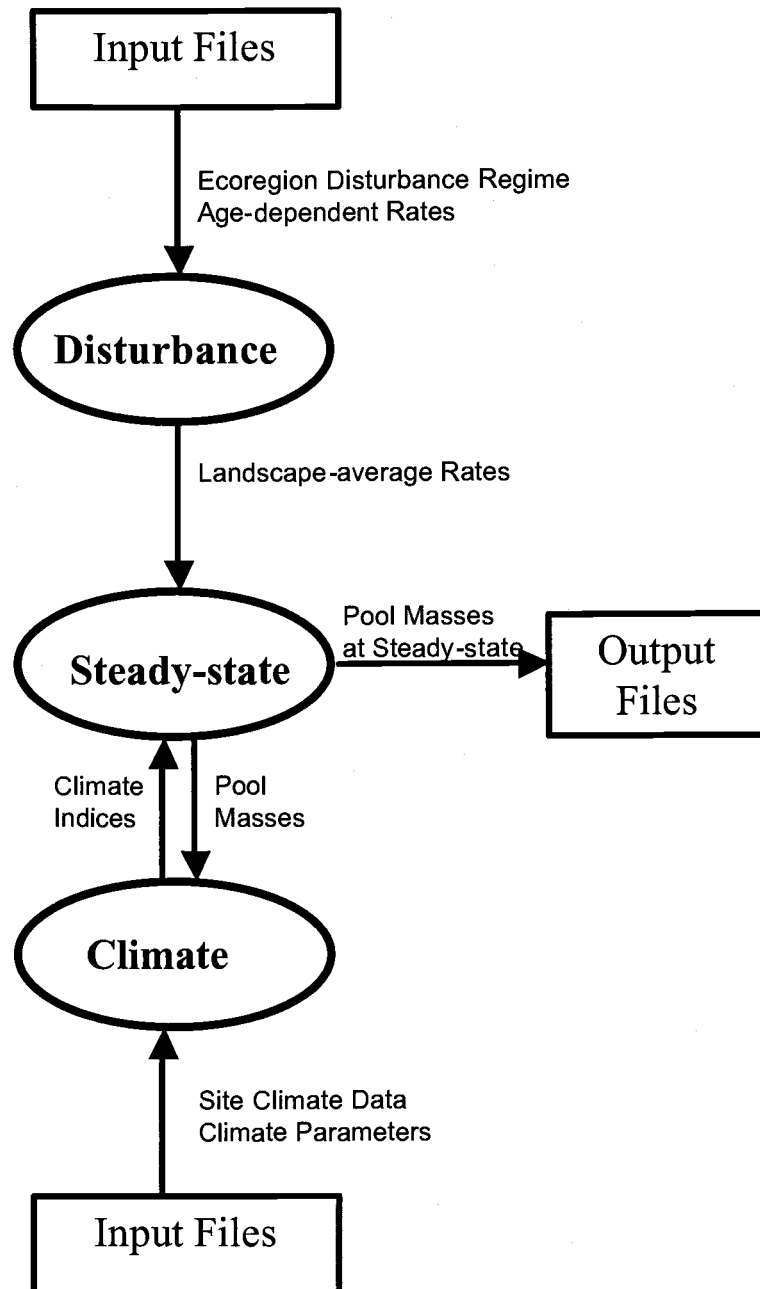


Figure 3.1. Overall conceptual structure of MAXCARB, showing the DISTURBANCE, STEADY STATE, and CLIMATE Modules and their interactions.

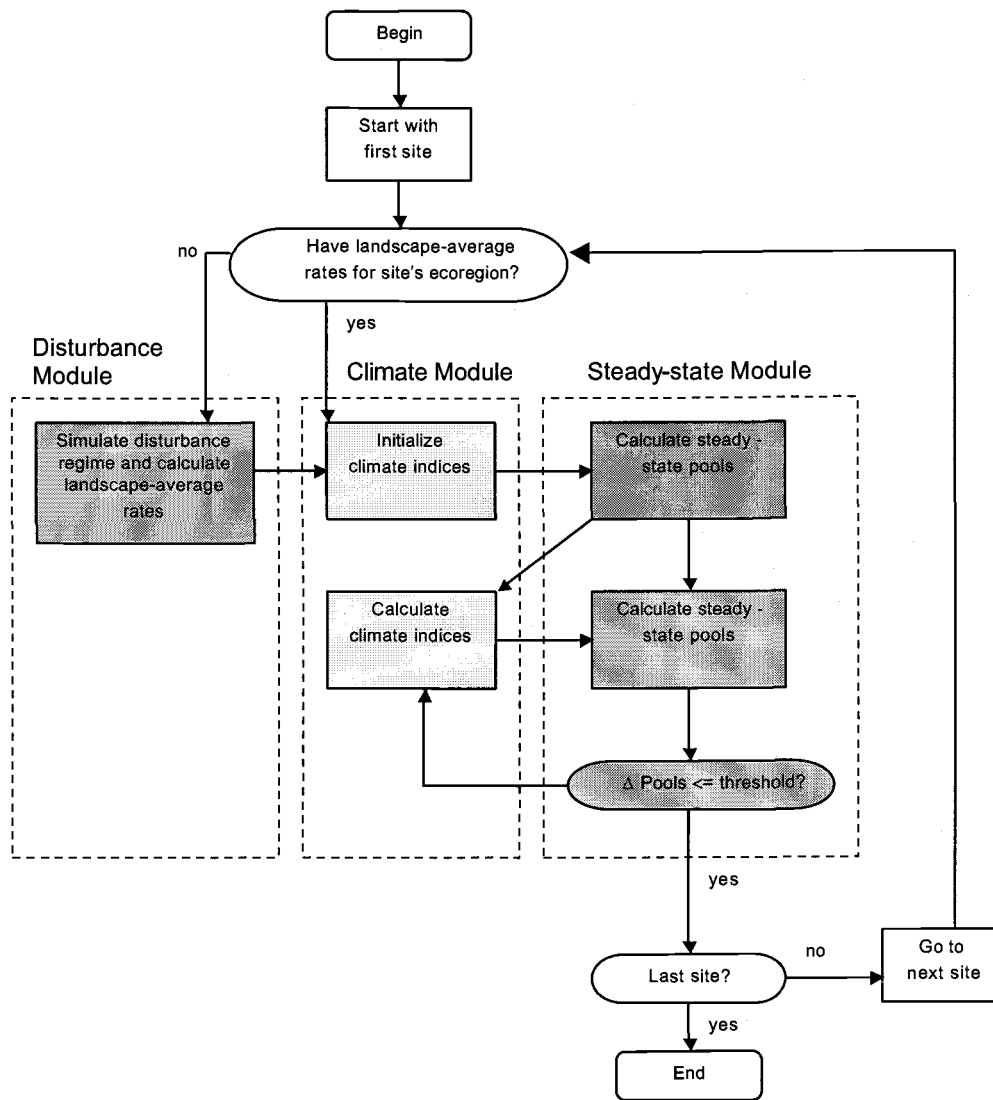


Figure 3.2. Flowchart of the calculations used in the MAXCARB model, showing the relationship between the DISTURBANCE, STEADY-STATE, and CLIMATE Modules.

therefore have no specific time-step. Because they represent steady-state solutions, analysis of transient responses to changes in climate or disturbance regimes with MAXCARB is not recommended.

MAXCARB calculates the effects of disturbance regimes at the ecoregion-scale (typically $> 10^5$ ha). However, MAXCARB calculates the effects of climate at scales for which these data are typically available (approximately 1 ha and greater). By using this approach we are able to portray effects of climate gradients across sites within each ecoregion.

MAXCARB was designed to work with a finer-scale model. The rationale was that an existing, stand-scale model, STANDCARB 2.0 (Harmon and Domingo, 2001), predicts stand-level responses to disturbances (Harmon and Marks, in press) but is inefficient at predicting C storage over broad areas. MAXCARB incorporates the general dynamics of STANDCARB, but is simple enough to facilitate calculations over broad areas. Specifically, STANDCARB 2.0 simulates species succession and replacement due to disturbance, a feature common to gap simulation models (Shugart et al., 1988). STANDCARB also simulates the effect of climate on growth, respiration, and decomposition rates, as in other ecosystem process models. STANDCARB simulates mixed species, mixed age-class forests by simulating a number of cells within a stand. Each cell represents the approximate area occupied by a single, mature tree (between 0.01 and 0.062 ha). Each cell is represented by four layers of vegetation (upper trees, lower trees, shrubs, and herbs), with each vegetation layer having up to seven live parts. Each cell also has nine detrital pools and three stable C pools. MAXCARB simplifies

the dynamics of STANDCARB 2.0 by solving potential C stores with an equilibrium solution, without explicitly tracking the growth of each stand, or every layer and species within each stand. By simplifying the time dynamics, it is possible to extrapolate information across space more efficiently with MAXCARB than STANDCARB by minimizing the number of calculations necessary. However, MAXCARB remains similar to STANDCARB in that it uses the same C pools, climate calculations, and parameterization, thus making it easier to compare the behavior between the two models.

General Approach

MAXCARB predicts potential C stores at steady state by simulating a system in which a constant flux, divided by a modifying rate-constant, yields a constant store at steady-state (Olson, 1963). By definition, an ecosystem at steady-state has equal fluxes into and out of the ecosystem to maintain constant mass:

$$(1) \quad \text{input_flux}_{ss} = \text{output_flux}_{ss}.$$

Rates at steady-state equal the rate at which mass is leaving a pool:

$$(2) \quad \text{rate}_{ss} = \text{flux}_{ss} / \text{mass}_{ss},$$

where mass_{ss} represents the steady-state store for each pool (mass area^{-1}), flux_{ss} equals the steady-state fluxes (inputs) to each pool ($\text{mass area}^{-1} \text{ time}^{-1}$), and rate_{ss} equals the steady-state rate (time^{-1}), which is the rate that mass leaves the pool.

Rearranging, the steady-state mass can be predicted from the steady-state flux and rate:

$$(3) \quad \text{mass}_{ss} = \text{flux}_{ss} / \text{rate}_{ss}.$$

Conceptually, a landscape is composed of multiple ecosystems, the age-structure of which are determined by the landscape's disturbance regime. Thus, the above equations will apply at the landscape scale, as well as the ecosystem scale, as long as the rates, inputs, and masses are averages for all the ecosystems within the landscape, and the disturbance regime is constant. These concepts are useful for MAXCARB as it allows us to scale processes typically employed at an ecosystem scale to a broader scale, given the corresponding rates, fluxes, and masses are known for the larger area. For example, Equation 2 can be described as:

$$(4) \quad \text{rate}_{LA} = \text{flux}_{LA} / \text{mass}_{LA}$$

where rate_{LA} , flux_{LA} , and mass_{LA} , calculated in the DISTURBANCE Module, equal landscape-average values rather than those of a specific ecosystem.

Although one could assume that rate-constants controlling the input and output of mass are the same for each ecosystem age-class, there is increasing empirical evidence, recently reviewed by Bond and Franklin (2002), of significant age-related change at the level of individual trees (Yoder et al., 1994) and forest stands (Janisch and Harmon, 2002; Bond and Franklin, 2002). If ecosystem rate-constants are not actually constant through succession, models that do not account for this age-dependency may incorporate error. To capture these age-related dynamics at broad scales, we used STANDCARB to develop equations that define how rates change as a function of stand age. The age-dependent equations implicitly capture the effects of different species and vegetation layers. Thus, we were able to simplify MAXCARB by not including these successional dynamics explicitly.

In the STEADY-STATE Module, steady-state mass is calculated with the following general equation:

$$(5) \quad \text{mass}_{\text{SS}} = \text{flux}_{\text{SS}} / (\text{rate}_{\text{LA}} * \text{index}_{\text{C}}).$$

Landscape-average rates (rate_{LA}) are passed from the DISTURBANCE Module and then modified by indices calculated in the CLIMATE Module (index_{C}). The climate indices estimate the constraints of temperature, precipitation, and solar radiation on production, respiration, and decomposition.

STEADY-STATE Module

Description

The STEADY STATE Module (**Figure 3.3**) calculates the steady-state stores of seven live C pools, eight dead C pools, three stable pools, and one forest product pool. The live pools are: foliage, sapwood, heartwood, heart rot, branches, coarse roots, and fine roots. Live C pools transfer material to their respective detrital counterpart, with the exception that dead heartwood is a combination of inputs from both heartwood and heart rot. Dead sapwood and dead heartwood are additionally separated into snags and logs so that the effects of position on microclimate can be modeled. All detrital pools can potentially add material to one of the three relatively decay-resistant stable pools: stable foliage, stable wood, and stable soil.

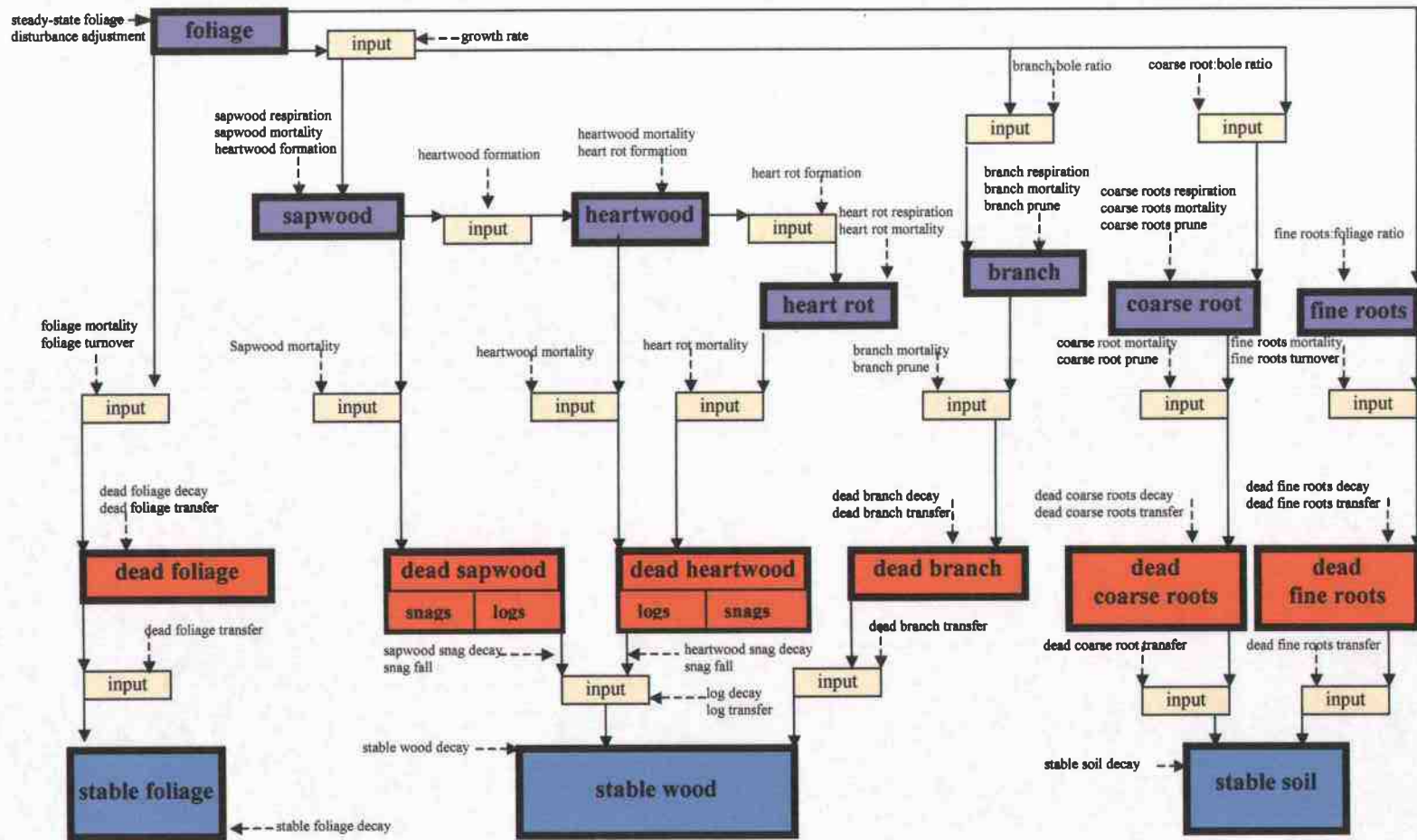


Figure 3.3. Cascade of calculations used in the STEADY-STATE Module to calculate landscape-average, steady-state mass.

Calculations

Foliage and fine-root stores are solved directly from ecoregion-specific parameters, rather than Equation 5. The foliage stores for a given disturbance regime and climate are determined by the steady-state foliage and the degree to which disturbances reduce foliage from steady-state stores (calculated in the DISTURBANCE Module). The steady-state, fine-root stores are determined by the fine-root to foliage ratio, calculated in the DISTURBANCE Module.

The steady-state C store for all other C pools is calculated in a cascade of equations (**Figure 3.3**). The steady-state C store is equal to the input flux (from the pools “above” the pool of interest, i.e., the “donor” pool) divided by the rates modifying the output of mass (to the pool “below” it in the cascade) (Equation 5; specific equations described in **Appendix D**). Input fluxes are calculated from the mass of the *contributing* pools multiplied by landscape-average rates derived from the DISTURBANCE Module. Output fluxes are calculated from the mass of the *current* pool multiplied by landscape-average rates from the DISTURBANCE Module. The CLIMATE Module further modifies respiration, decay, and transfer rates for the given site by calculating climate indices.

CLIMATE Module

Description

The CLIMATE Module is derived from STANDCARB 2.0 and explained in detail elsewhere (Harmon and Domingo, 2001). We will only review its general methodology here (equations in **Appendix E**). The CLIMATE Module estimates the effect of temperature, precipitation, and solar radiation on production, respiration, and decomposition. These effects are calculated each month and then averaged yearly to yield the annual indices used by the STEADY-STATE Module.

Calculations

Production, respiration, and decomposition rates are potentially constrained by available light, mean monthly temperature, and/or monthly moisture conditions. Light limitations constrain production by modifying foliage mass. Temperature limitations on growth are calculated by assuming there is an optimal mean daytime temperature and growth decreases when temperatures are above or below this optimum (Running and Coughlan, 1988). Water limitations are calculated by assuming that there is an exponential reduction in production due to soil moisture limitations (Emmingham and Waring, 1977).

Available water is calculated by first calculating precipitation interception. Interception by the canopy, woody detritus, and forest floor is calculated sequentially. First, canopy interception is calculated assuming that interception of precipitation increases linearly with increasing foliage mass. Woody detritus (dead

sapwood, dead heartwood, and dead branches) intercepts precipitation that was not intercepted by the canopy. The interception by each dead wood pool is calculated as a function of its mass, current water store, and the maximum moisture content defined for that pool. Precipitation not intercepted by the canopy or dead wood pools enters the forest floor (dead foliage and stable foliage). Interception by the dead foliage and stable foliage pools is a function of the mass of each pool, its current water store, and the maximum moisture content specified for each pool.

Monthly total potential evapotranspiration is calculated using a modification of the Priestly-Taylor method (Bonan, 1989; Jones, 1992), which estimates total evaporative flux over a wet surface. Total potential evapotranspiration for a month is assumed to be proportional to the estimated monthly solar irradiance and the monthly mean air temperature. The constants used to solve the Priestly-Taylor method are empirically derived after Jensen and Haise (1963) from elevation and mean minimum and maximum daily temperatures for the warmest month of the year. To estimate the potential amount of transpiration by plants, total potential evapotranspiration is reduced by the amount of evaporation from canopy interception and detritus pools. This yields a monthly potential transpiration loss assuming that leaf mass and soil water stores are at a maximum. The actual transpiration losses each month are controlled by the soil water stores and the foliage mass. The effect of foliage mass is linear and determined by the ratio of current-year foliage mass to steady-state foliage mass. The effect of soil moisture on transpiration is calculated by assuming that when the soil water potential is below -0.3 MPa, transpiration decreases exponentially (Emmingham and Waring, 1977). Volumetric moisture

content is converted to water potential using a reciprocal function similar to Running and Coughlan (1988).

Detrital pool and mineral soil moisture content are calculated monthly and represent the balance of inputs through precipitation and outputs via evapotranspiration. For mineral soil, the monthly input is the water that has not been intercepted by the canopy, dead wood, or the forest floor pools. The loss of water from mineral soil is controlled solely by plant transpiration, assuming evaporative losses from mineral soil are minimal. The rate of water loss from detrital pools is calculated from the monthly evaporative demand (a function of radiation and temperature) and a pool-specific drying constant.

We assume that moisture controls decomposition in two ways. The first is by matric potential, which limits decomposition when the fiber saturation point is reached. The second is by low oxygen diffusion when the moisture content is high, which significantly limits coarse wood decomposition (Harmon et al., 1986). We model the matric potential and diffusion limitation portions separately from the minimum and maximum moisture contents. The overall effect of moisture is calculated by multiplying these two indices.

Temperature controls decomposition in two ways. First, there is an increase in respiration rate with temperature following a Q_{10} curve. Second, there is a lethal temperature limit that arrests decomposer activity. These functions are calculated from the Q_{10} rate, monthly mean air temperature, and monthly optimum temperature for decomposition. The combined effects of moisture and temperature on

decomposition are calculated by multiplying the moisture and temperature-limitation indices.

DISTURBANCE Module

Description

The DISTURBANCE Module (**Figure 3.4**) calculates landscape-average rate-constants for each ecoregion that are used by the STEADY-STATE Module. The rationale for this module is that rates controlling allocation, growth, and decomposition change as a forest ages. Following a disturbance, live, dead, and stable C are recalculated given rate-constants for the new stand age. Currently, MAXCARB only supports catastrophic disturbances, which kill all live plants and reset the age of the stand to zero. The return interval (the number of years between disturbance events) is determined by a user-prescribed disturbance regime for that ecoregion. There are two general types of disturbance regimes simulated in MAXCARB: regulated and natural. Disturbances that leave the living stand relatively intact (e.g., gap formation) are included implicitly.

By definition, forests managed in a regulated disturbance regime are represented by an equal distribution of age-classes on the landscape; thus, the same stand area is available for harvest each year. It follows that disturbances in a regulated regime reoccur at a given location at an interval equal to the regime's disturbance interval, e.g., a site with a 100-year, clear-cut, harvest regime will be harvested every 100 years. Sites are never older than the user-defined disturbance

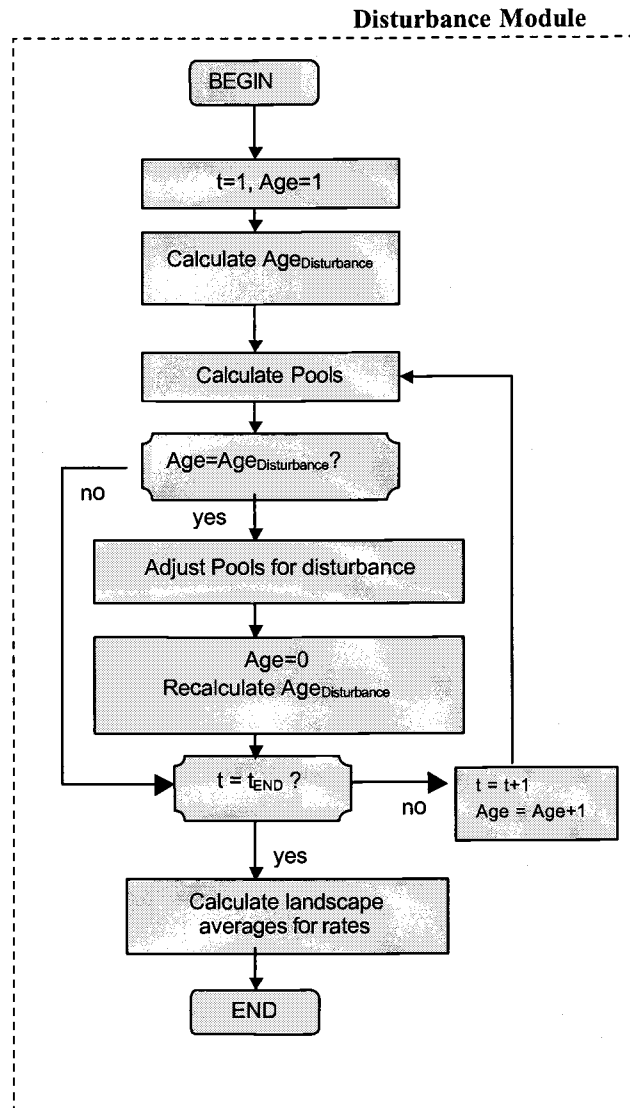


Figure 3.4. Flowchart of the calculations used in the DISTURBANCE Module.

interval. Building on these landscape-scale concepts, regulated disturbance regimes in MAXCARB are simulated through time for a given ecoregion. The user sets the disturbance interval, which exactly defines the number of years between disturbance events.

In a natural disturbance regime, a Poisson random process determines the occurrence of disturbance events through time (**Figure 3.5**). For simplicity, MAXCARB simulates a natural disturbance regime with a negative exponential distribution (Van Wagner, 1978). The negative exponential distribution, and the related Weibull distribution, form the basis of the most common conceptual models used in the literature to explore the recurrence of disturbance events on a landscape (Johnson and Van Wagner, 1985; Van Wagner, 1978; Johnson and Gutsell, 1994). Simulating natural disturbance regimes with a negative exponential, rather than the Weibull distribution, assumes that stand age does not affect the susceptibility of the stand to the natural disturbance event. Thus, stands may survive past the mean disturbance interval due to random chance (see the tail of the distribution in **Figure 3.5**), not because old-stands are less susceptible to burning, as in the Weibull distribution. Eventually, our goal is to allow the user to choose the appropriate probability distribution function for their area of interest.

Calculations

The DISTURBANCE Module calculates C stores through time for an ecoregion. Carbon stores and fluxes are calculated for all pools described in the STEADY-STATE Module. Rather than spatially track the stores and fluxes at

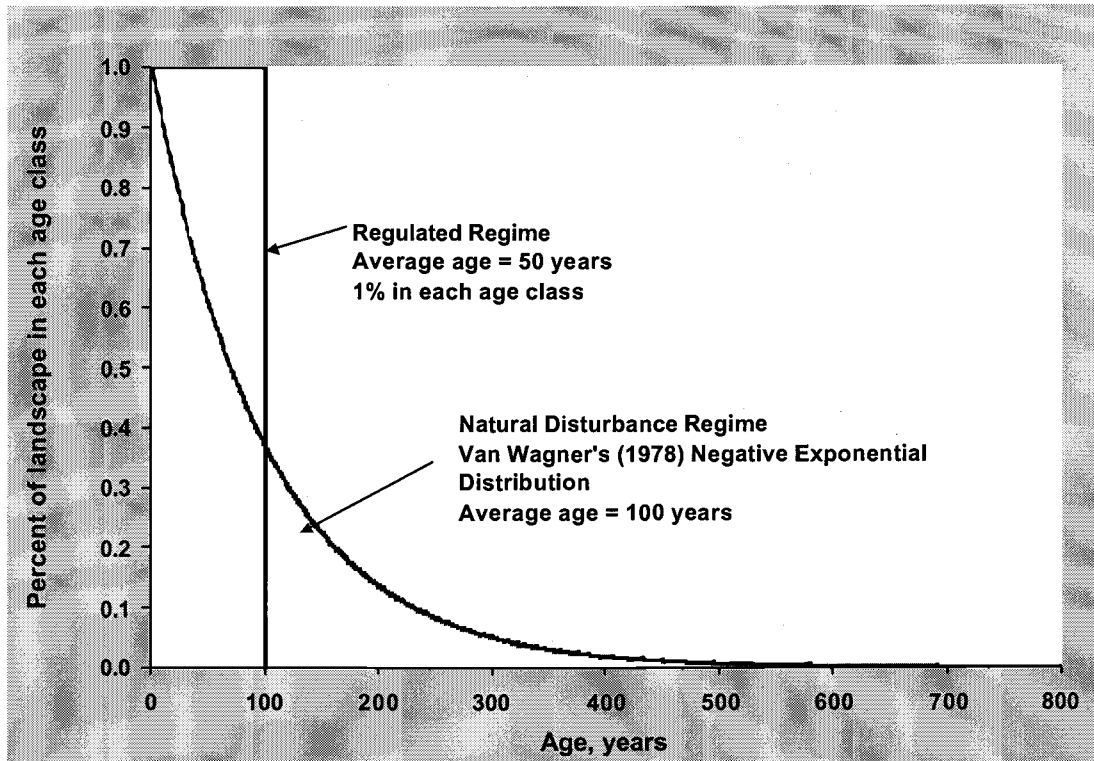


Figure 3.5. Conceptual representation of the age-class structure for regulated and natural disturbance regimes.

multiple locations within a landscape in a short period of time, we calculate the stores of C within a single ecoregion over a long period of time to calculate landscape-average rate-constants. These calculations are based on the same landscape-scale principles as a spatial simulation, although here we substitute space for time. This assumes that there is no significant spatial interaction between the age-classes in the landscape affecting C storage.

The C stores for each pool are a function of the stores in the previous year, plus inputs and outputs from the pool over that year. The general equation for these calculations is:

$$(6) \quad \textit{pool:mass (age)} = \textit{pool:mass (age-1)} + \textit{input:flux} - \textit{output:flux}$$

The calculations are based on the same pools in the STEADY-STATE Module, so there is also a similar set of cascading calculations between pools. Input fluxes are calculated from the mass of contributing pools and rate constants modifying the input to the current pool. Output fluxes are calculated from the mass of the current pool and rate constants modifying the transfer of mass to subsequent pools (transfer rates, mortality rates, formation rates, or pruning rates), the loss of mass to the atmosphere (respiration rates for live pools, and decay rates for detrital pools), and the loss or transfer of mass due to disturbance-events. Output fluxes will be a function of some combination of these transfers and losses, depending on the pool being calculated. For example, live pools do not have a decay loss so they are a function of transfers and respiration losses only. Equations are described in detail in **Appendix C**.

After the fluxes and pool masses are calculated for the current simulation year, running totals for each of these values are updated. When a disturbance event occurs, the stand age is reset to zero, the stand develops again, and masses and fluxes are recalculated at the new stand age. The longer the disturbance interval for a natural disturbance regime, the longer the simulation must be run to capture the average dynamics of the site through time.

To calculate the landscape-average rate constants, the DISTURBANCE Module uses the same equation as the STEADY-STATE Module, but solves for the landscape-average rates using the sum of the masses and fluxes (described generally in Equation 4):

$$(7) \quad \text{Rate}_{\text{LA}} = \frac{\sum_{t=0}^{\text{Time_End}} \text{Flux}_t}{\sum_{t=0}^{\text{Time_End}} \text{Mass}_t}$$

The landscape-average rate constants are thus a function of the disturbance regime, since the average age of the landscape is determined by the frequency of the disturbance event since the fluxes and masses of the pools are determined by age-dependent rates.

Disturbance Event Transfers

When a disturbance event occurs, the DISTURBANCE Module determines the amount of C that is transferred to other pools (i.e., from live pools to dead pools), or lost (i.e., to the atmosphere, in the case of a fire). If the disturbance is a harvest, the DISTURBANCE Module determines the amount of bole mass removed to the

forest products pool and the amount of live pool mass transferred to the dead pool. If the disturbance is a fire, the DISTURBANCE Module determines the amount of mass that is lost to the atmosphere through combustion and the amount of live pool mass transferred to the dead pool. Each live and dead pool may be consumed by fire to a different degree, as specified by the user.

Age-dependent Rate Functions

Carbon fluxes and stores in the DISTURBANCE Module are modified by rate functions that can be either constant or dynamic. As an example of dynamic rate functions, mortality may be higher during middle stages of succession due to stem competition. However, since equations describing dynamic changes in rates with ecosystem age are currently uncommon, we tested both approaches to parameterize the DISTURBANCE Module. We first developed equations describing how ecosystem rates change with time based on the output from multiple runs of the more-detailed model, STANDCARB 2.0. STANDCARB was run for a 10 x 10 grid of cells for 1000 years and outputs were analyzed to estimate the change in the following rates through time: allocation ratios of live parts, formation of heartwood and heart-rot, respiration of live parts, tree mortality, branch and coarse-root pruning, decay and turnover of dead pools, and transfer rates to stable pools. Independent simulations were run for scenarios with a clear-cut harvest interval of 50, 100, and 150 years, to determine the effects of disturbance on modifying rate-constants through time. Each simulation was repeated 5 times to minimize the variability common to gap-phase models; yearly output from the model was averaged for the 5

simulations. Functions were fit to the output that described the general trend in rates or pools through time (**Figure 3.6** and **Figure 3.7**; **Appendix C**). Functions fit one of several forms, including a step function, the Chapman-Richards equation (Causton et al., 1978, Cooper, 1983, Richards, 1959), or a modification of the Chapman-Richards equation.

In the second method, we used rate constants derived by calibrating MAXCARB to STANDCARB. These rate constants do not reflect a single species or lifeform, but rather, they capture the general dynamics through time of the STANDCARB model. Therefore, they provide a straightforward test of the conceptual design of the model and form the basis of results presented in this paper.

Simulation Experiments

To demonstrate the potential of MAXCARB to predict C storage over a broad area, we ran simulations with the model in several ways. Our goal was to demonstrate that MAXCARB is consistent with its conceptualization, facilitating its use at regional scales. First, we ran MAXCARB separately for 50-year and 200-year natural disturbance (fire) regimes to demonstrate the effect of disturbance interval on flux, mass, and landscape-average rate calculations in the DISTURBANCE Module.

Second, we tested the sensitivity of MAXCARB to disturbance interval, running separate simulations for 40-, 60-, 80-, 100-, or 120-year regulated disturbance regimes (harvest + site preparation fire) for the H.J. Andrews in the

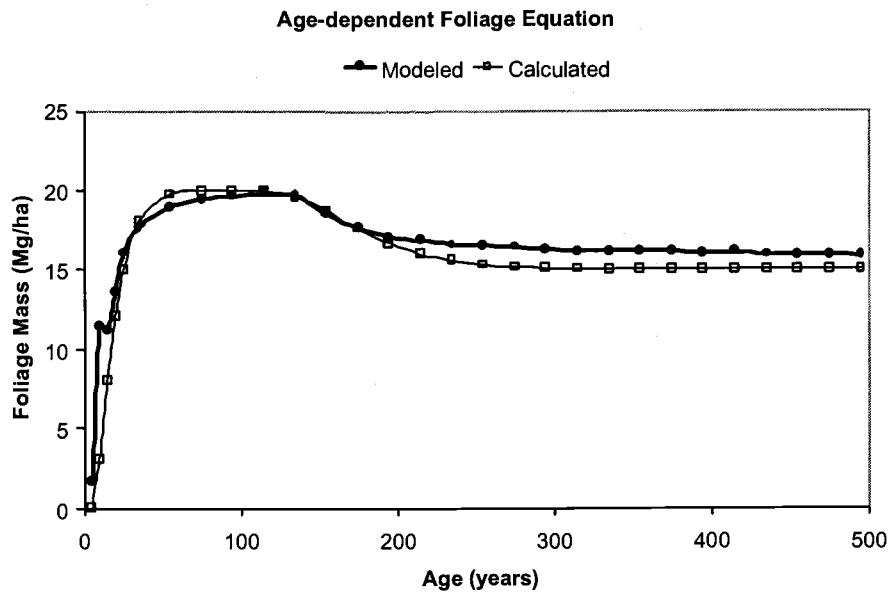


Figure 3.7. Example of dynamic rate function for foliage mass used in the DISTURBANCE Module. Modeled lines represent output from the STANDCARB model, while Calculated lines represent the fit of the rate-function.

Oregon Cascades. We compared results to C stores predicted by the STANDCARB model (Harmon and Marks, in press).

Third, we calibrated the age-dependent rate file in the DISTURBANCE Module of MAXCARB with parameters derived from diagnostic output from STANDCARB. Both models were parameterized for Douglas-fir in the Oregon Cascades at the H.J. Andrews. We compared steady-state live, dead, and stable pools from MAXCARB to similar pools calculated by 1000-year simulations with STANDCARB. Comparisons of C pools in these tests verified whether steady-state stores could be predicted more efficiently using MAXCARB.

Fourth, we performed a sensitivity test on the age-dependent rates in the DISTURBANCE Module, which, we expected, were the largest source of potential error. Our goal was to determine how potential changes in disturbance regimes might affect total C stores at steady-state. We did this by changing each parameter in the rate file independently two times, +10 % and -10 % of its initial value, and reran the simulation, comparing the effect of this change on total C stores at steady-state.

Finally, we used MAXCARB to predict the steady-state C stores for multiple sites along a broad biogeoclimatic gradient and compared the results to observed old-growth C stores (Smithwick et al., in press). Each site was run using climate and radiation characteristics by using its closest climate and radiation station, determined from the Western Regional Climate Center and the Solar Radiation Monitoring Laboratory at the University of Oregon, respectively. Soil characteristics were

defined from the H.J. Andrews Long Term Ecological Research databank (<http://www.fsl.orst.edu/lter/datafr.htm>).

Results

Simulating Natural Disturbance Regimes

Simulations of natural fire regimes with the DISTURBANCE Module indicated that as the mean return time of fires lengthened, fires occurred less frequently but resulted in greater losses of mass for each fire (**Figure 3.8**). Occasionally, natural fires occurred at shorter intervals in the longer regime, each of which resulted in less loss of mass. However, averaging over time, more mass was lost to the atmosphere for longer disturbance intervals since mass had a longer time to accrue (Harmon et al., 1990; **Figure 3.9**). The disturbance regime also affected fluxes through time. For instance, total respiration losses were larger for the 200-year regime than the 50-year regime (**Figure 3.10**) since respiration is a function of pool-specific respiration rates and pool mass, which is affected by disturbance. As a result of these changes in fluxes and mass (Equation 4), the landscape-average rate of burn loss was lower for the 200-year regime than the 50-year regime (**Figure 3.11**). As a consequence of these changes in landscape-average rates in the DISTURBANCE Module, the 200-year regime stored 31.2 % more total C at steady-state than the 50-year regime (891.9 Mg C ha⁻¹ vs. 613.4 Mg C ha⁻¹).

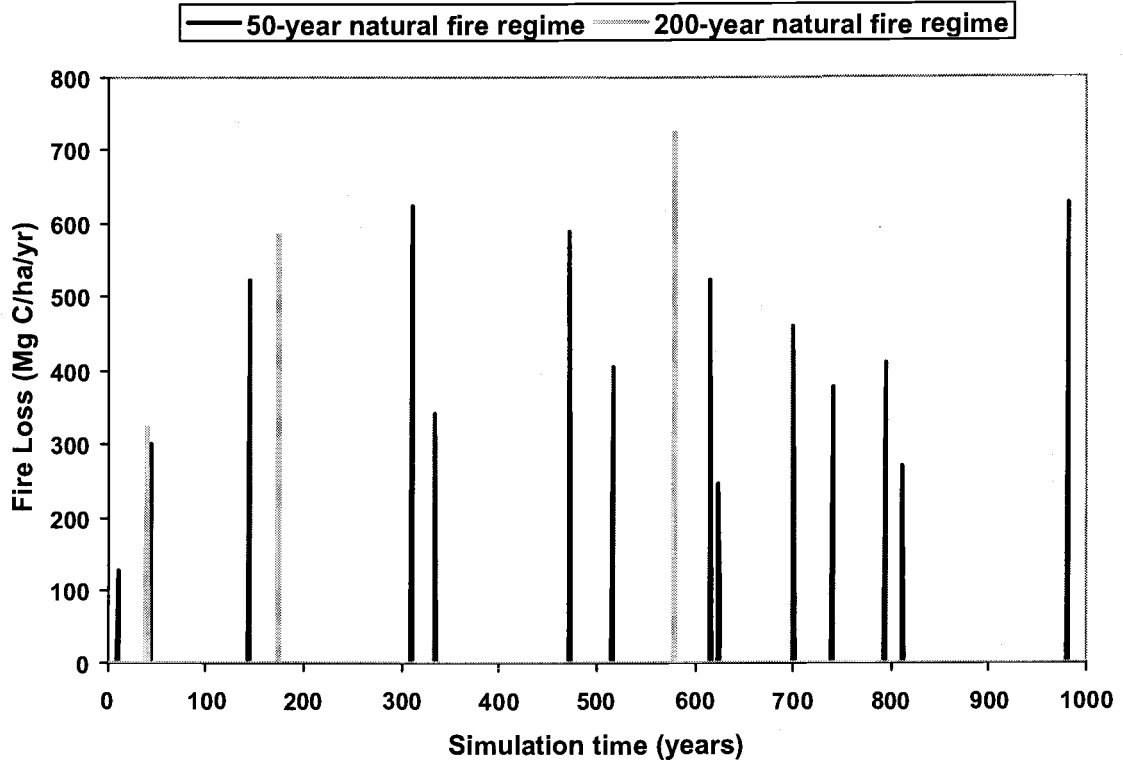


Figure 3.8. Comparison of fire flux (loss) between a 200-year and 50-year natural disturbance (fire) regime.

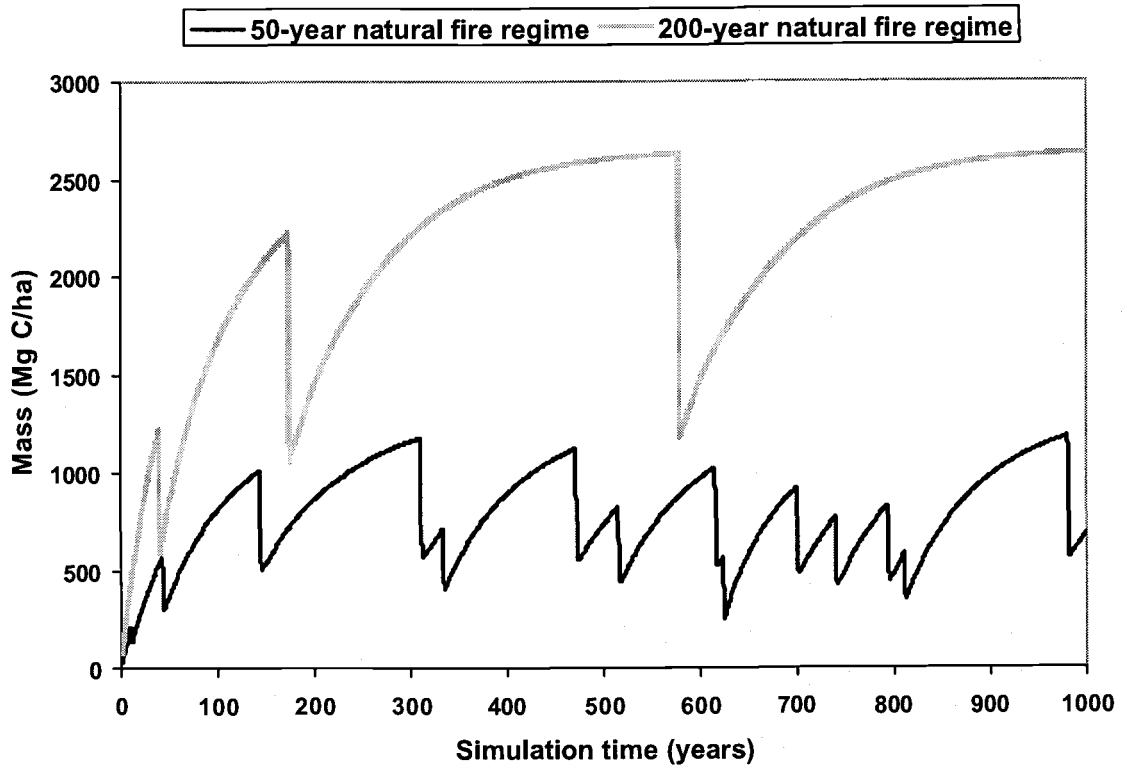


Figure 3.9. Comparison of total mass through time for a 200-year and a 50-year natural disturbance (fire) regime.

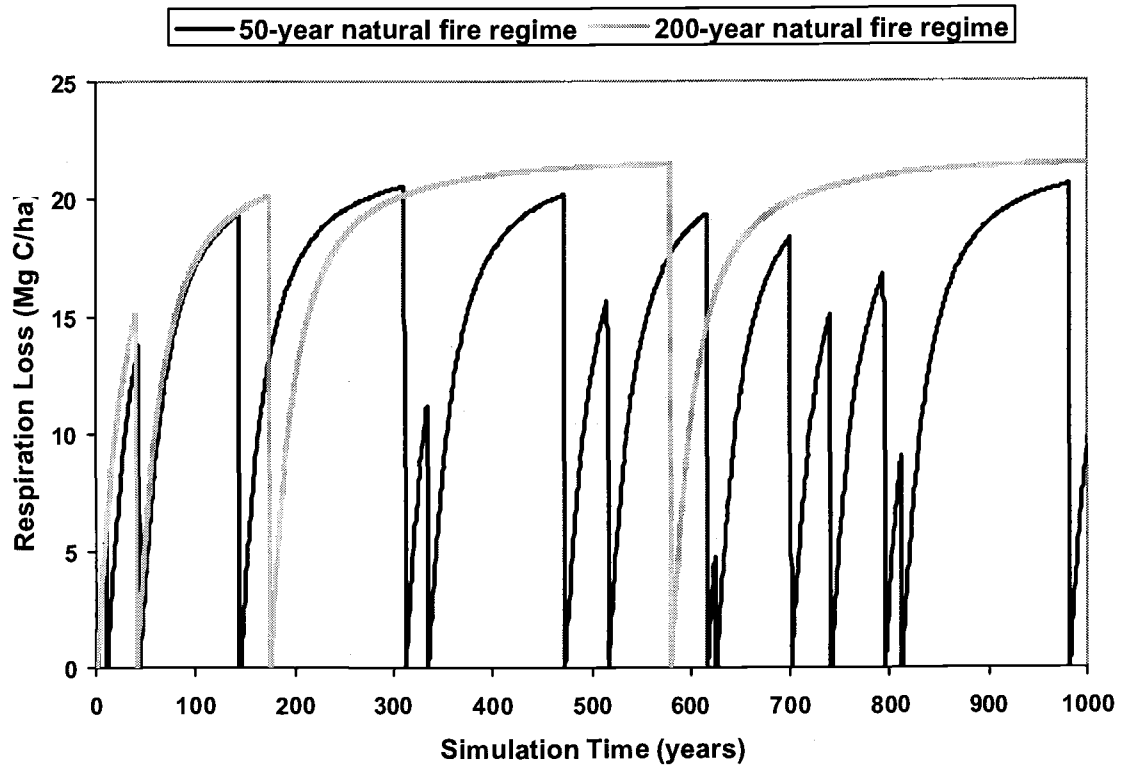


Figure 3.10. Comparison of the respiration flux (loss) of total carbon between a 200-year and a 50-year natural disturbance (fire) regime.

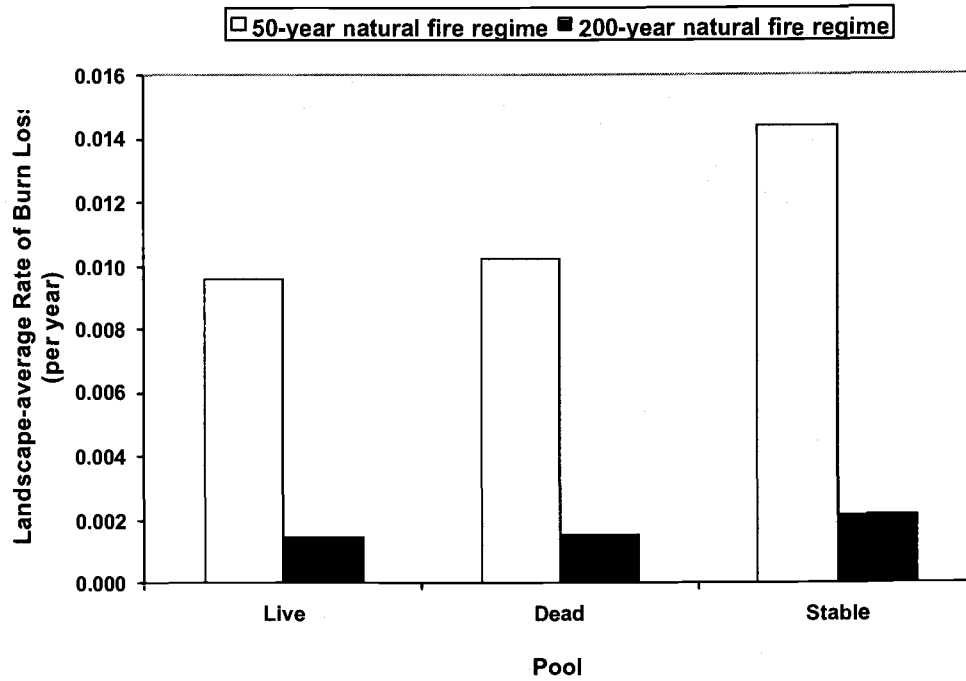


Figure 3.11. Landscape-average rates of burn loss calculated in the DISTURBANCE Module for live, dead, and stable pools.

Simulating Regulated Disturbance Regimes

Simulations of regulated disturbance regimes with the DISTURBANCE Module demonstrated that as the rotation interval increased, the steady-state store of C increased (**Figure 3.12**). Thus, at a rotation interval of 40 years, the live and dead stores of C predicted by MAXCARB were only 36 % of the C stores that would be stored in the absence of any disturbances. As the time between harvests increased, the landscape stored proportionately more so that in a 120-year rotation interval, 64 % of the maximum was stored. Both STANDCARB and MAXCARB predicted a similar rate of increase in landscape C stores with a lengthening of the disturbance regime (**Figure 3.12**). MAXCARB predicted higher C stores compared to STANDCARB because MAXCARB was parameterized for Douglas-fir and STANDCARB was parameterized for mixed stands of Douglas-fir and western hemlock. Importantly, MAXCARB predicted these results in a fraction of the time (several minutes) than the more detailed model, STANDCARB (several hours). Thus, these tests showed that one could more efficiently predict steady-state C stores using MAXCARB than STANDCARB.

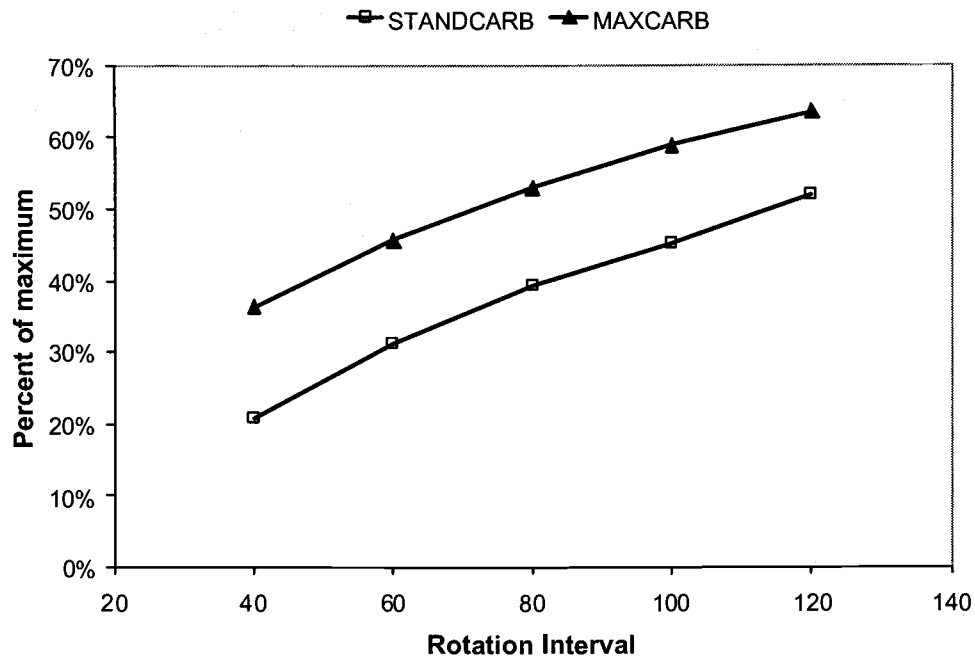


Figure 3.12. Effect of rotation interval on landscape-average, steady-state carbon stores, expressed as a percent of maximum total stores. STANDCARB data is taken from Harmon and Marks (in press).

Calibration with STANDCARB

Steady-state C stores from MAXCARB and STANDCARB compared favorably between the two models (**Figures 3.13, 3.14, and 3.15**) after calibration of the age-dependent rates in the DISTURBANCE Module of MAXCARB (**Table 3.1**). Standard errors for STANDCARB represent deviations from multiple runs of a stochastic model, but it was not possible to calculate standard errors for MAXCARB since results are equilibrium solutions. Thus, if MAXCARB C stores were ± 2 standard errors of both STANDCARB, we assumed the MAXCARB results were not significantly different. All live, dead, and stable C pools predicted by MAXCARB were within 2 standard errors of the STANDCARB results except for the dead branch pool ($11.8 \pm 1.2 \text{ Mg C ha}^{-1}$ for STANDCARB and 9.6 Mg C ha^{-1} for MAXCARB) and the stable soil pool ($137 \pm 5.7 \text{ Mg C ha}^{-1}$ for STANDCARB and $130.7 \text{ Mg C ha}^{-1}$ for MAXCARB). Total C stores (live + dead + stable pools) were $1060.8 \pm 105.2 \text{ Mg C ha}^{-1}$ for STANDCARB and $1034.9 \text{ Mg C ha}^{-1}$ for MAXCARB.

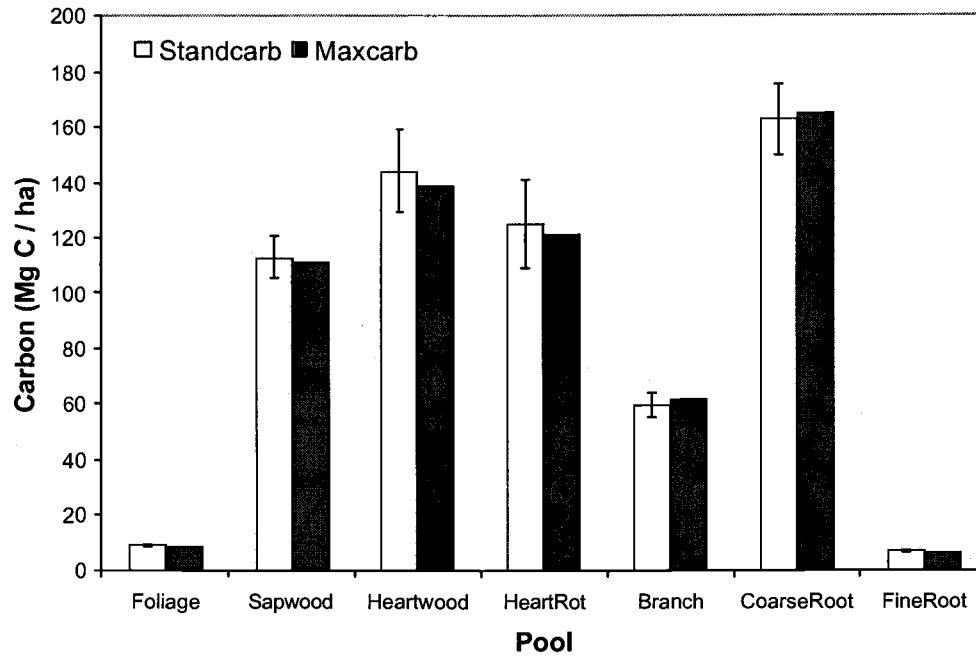


Figure 3.13. Comparison of MAXCARB and STANDCARB steady-state carbon stores for all live pools.

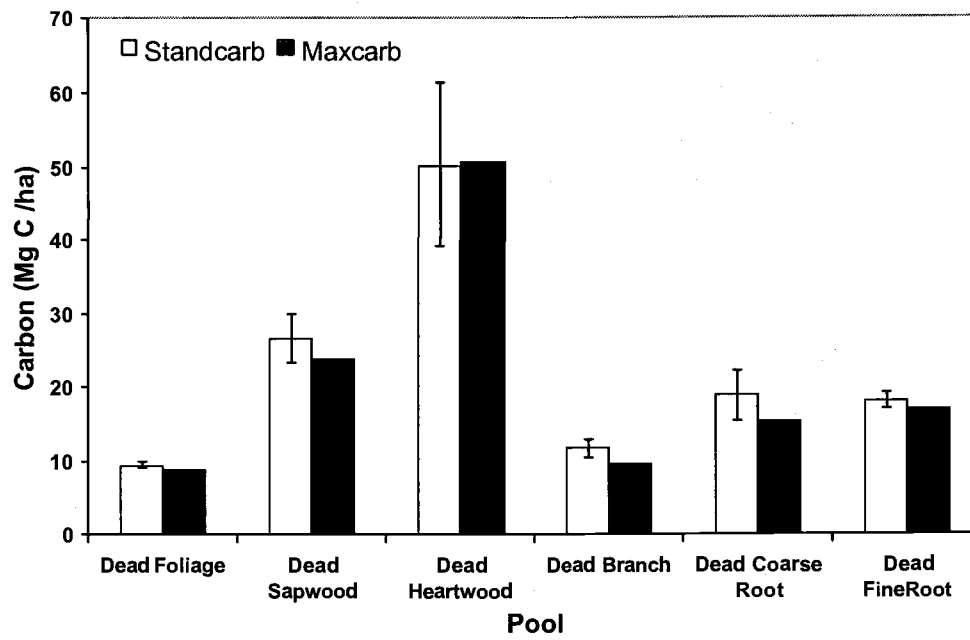


Figure 3.14. Comparison of MAXCARB and STANDCARB steady-state carbon stores for all dead pools.

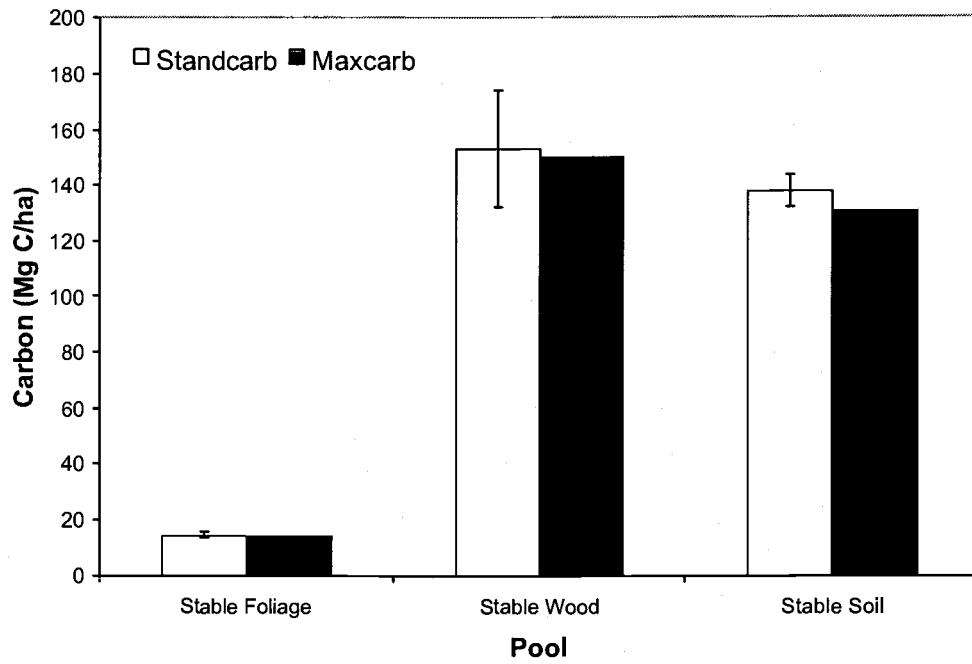


Figure 3.15. Comparison of MAXCARB and STANDCARB steady-state carbon stores for all stable pools.

Table 3.1. Constants in the DISTURBANCE Module after calibration with STANDCARB.

Name	Value	Units
Foliage Mass	17.8	Mg /ha
Bole growth efficiency	1.0	unitless
Live Pool Ratios		
Branch to bole ratio	0.45	unitless
Coarse root to bole ratio	0.75	unitless
Fine root to foliage ratio	0.75	unitless
Bole Formation Rates		
Heartwood formation	0.02	yr ⁻¹
Heartrot formation	0.01	yr ⁻¹
Respiration Rates		
Sapwood respiration	0.025	yr ⁻¹
Heart rot respiration	0.006	yr ⁻¹
Branch respiration	0.015	yr ⁻¹
Coarse root respiration	0.015	yr ⁻¹
Turnover Rates		
Foliage turnover	0.2	yr ⁻¹
Fine root turnover	0.5	yr ⁻¹
Pruning Rates		
Branch pruning	0.02	yr ⁻¹
Coarse root pruning	0.005	yr ⁻¹
Tree Mortality	0.006	yr ⁻¹
Input Decay Rates		
Dead foliage decay	0.15	yr ⁻¹
Dead sapwood decay	0.03	yr ⁻¹
Dead heartwood decay	0.01	yr ⁻¹
Dead branch decay	0.10	yr ⁻¹
Dead coarse root decay	0.07	yr ⁻¹
Dead fine root decay	0.15	yr ⁻¹
Stable Decay Rates		
Stable foliage decay	0.12	yr ⁻¹
Stable wood decay	0.04	yr ⁻¹
Stable soil decay	0.02	yr ⁻¹
Transfer Rates		
Dead foliage transfer	0.15	yr ⁻¹
Dead sapwood snags transfer	0.07	yr ⁻¹
Dead sapwood logs transfer	0.03	yr ⁻¹
Dead heartwood snags transfer	0.15	yr ⁻¹
Dead heartwood logs transfer	0.037	yr ⁻¹
Dead branch transfer	0.15	yr ⁻¹
Dead coarse roots transfer	0.08	yr ⁻¹
Dead fine roots transfer	0.10	yr ⁻¹

Comparison with Observed Old-growth Forest Data at H.J. Andrews

There is good agreement between all three sources of steady-state C-store predictions at the H.J. Andrews: STANDCARB, MAXCARB, and old-growth forest data, which were described in **Table 2.2** and Smithwick et al. (in press) (**Figure 3.16**). Standard errors for the old-growth data reflect the variation among 14 stands sampled at the H.J. Andrews. The largest pools (live boles (stem wood and stem bark), dead wood, and stable soil) were not significantly different between the models and the old-growth data. Modeled predictions of live foliage C, live branch C, live coarse root C, and dead coarse root C were significantly greater than observed old growth data, while live fine roots and fine wood debris (dead branches) were significantly less. Live pools equaled $620.3 (\pm 57.0) \text{ Mg C ha}^{-1}$ for STANDCARB, $614.3 \text{ Mg C ha}^{-1}$ for MAXCARB, and $557.2 (\pm 45.6) \text{ Mg C ha}^{-1}$ for the old-growth forest. Dead pools equaled $149.4 (\pm 21.4) \text{ Mg C ha}^{-1}$ for STANDCARB, $139.8 \text{ Mg C ha}^{-1}$ for MAXCARB, and $132.0 (\pm 23.3) \text{ Mg C ha}^{-1}$ for the old-growth forest. Total C for the old-growth forest at the H.J. Andrews was $811.7 (\pm 76.6) \text{ Mg C ha}^{-1}$. Total C for STANDCARB and MAXCARB was considerably greater when the stable wood pool was included ($1060 (\pm 105.2) \text{ Mg C ha}^{-1}$ and $1035.0 \text{ Mg C ha}^{-1}$, respectively) and comparable when the stable wood pool was excluded ($907.5 (\pm 84.1) \text{ Mg C ha}^{-1}$ and $884.8 \text{ Mg C ha}^{-1}$, respectively). This test indicates good agreement between modeled and observed steady-state C stores at the site-level. However, agreement could be improved through better parameterization of rates controlling stable pools.

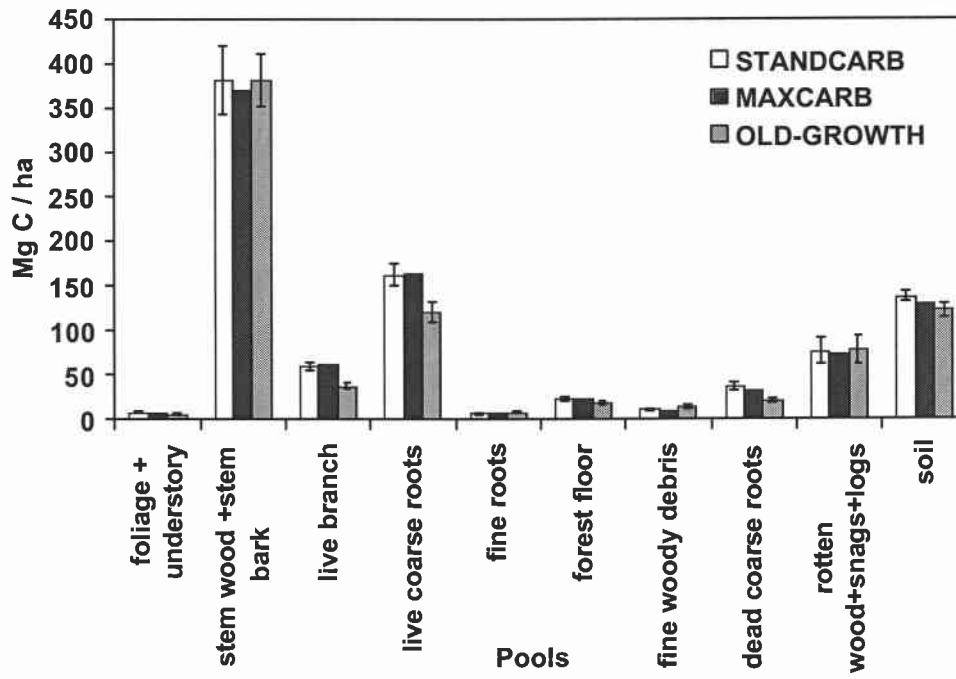


Figure 3.16. Comparison of steady-state carbon stores in live, dead, and stable pools between STANDCARB, MAXCARB, and old-growth forest data (H.J. Andrews, Oregon Cascades). Error bars represent two standard errors around the mean.

Sensitivity Analysis

Generally, total C stores predicted by MAXCARB were not sensitive to 10 % changes of the rates in the DISTURBANCE Module. Tree mortality was the most sensitive parameter (initially set at 0.6 % yr⁻¹, **Table 3.1**). Total C stores increased 4 % when mortality was reduced 10 % (**Figure 3.17**). The next most sensitive parameters were respiration rates and allocation ratios. However, changing allocation ratios or respiration rates by ± 10 % did not change total C stores by more than 2 % (**Figures 3.18 and 3.19**).

Comparison with Observed Old-growth Forest Data in the PNW

MAXCARB showed good agreement between predicted (modeled) and observed results among multiple sites in the Pacific Northwest (**Figure 3.20**). A comparison of predicted and observed results was made by evaluating the slope of the regression line, fitting the predicted data, to the 1:1 line, which reflects perfect agreement between predicted and observed data. The slope of the regression line was 0.92, indicating a close agreement between steady-state C stores predicted by MAXCARB and the old-growth data ($y = 0.9201x + 132.27$, $r^2 = 0.944$). In general, MAXCARB seemed to overpredict steady-state C stores, as indicated by the positive intercept. However, the relationship between predicted and observed varied between sites. Among the sites examined, eastern Oregon stored the least amount of C at steady state for both MAXCARB predictions and observed data. MAXCARB predicted a store of 310 Mg C ha⁻¹, which is more than the 195 Mg C ha⁻¹

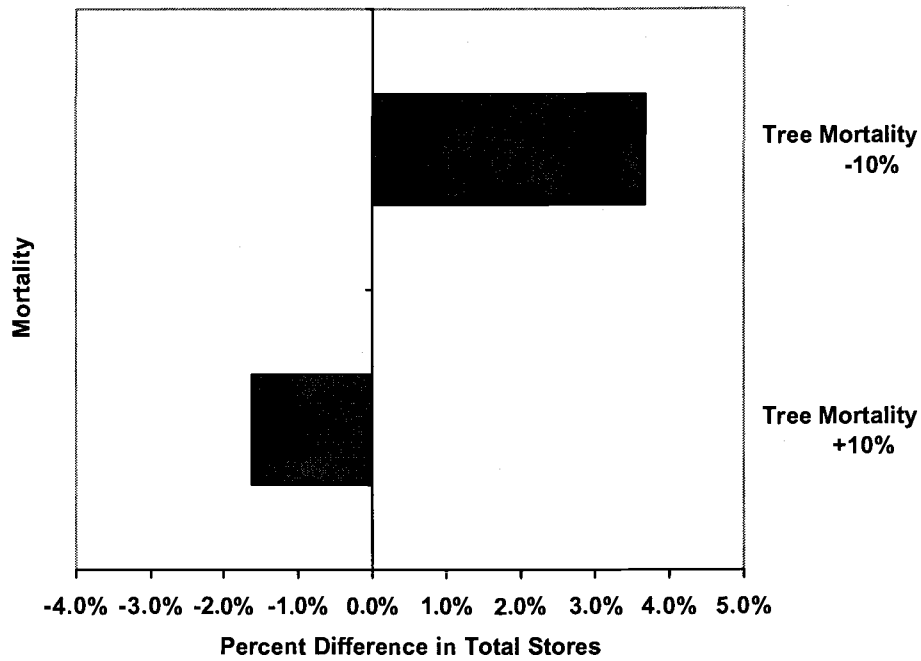


Figure 3.17. Results of a sensitivity test on the rates in the DISTURBANCE Module, showing the effect of changing tree mortality rates $\pm 10\%$ on total carbon stores.

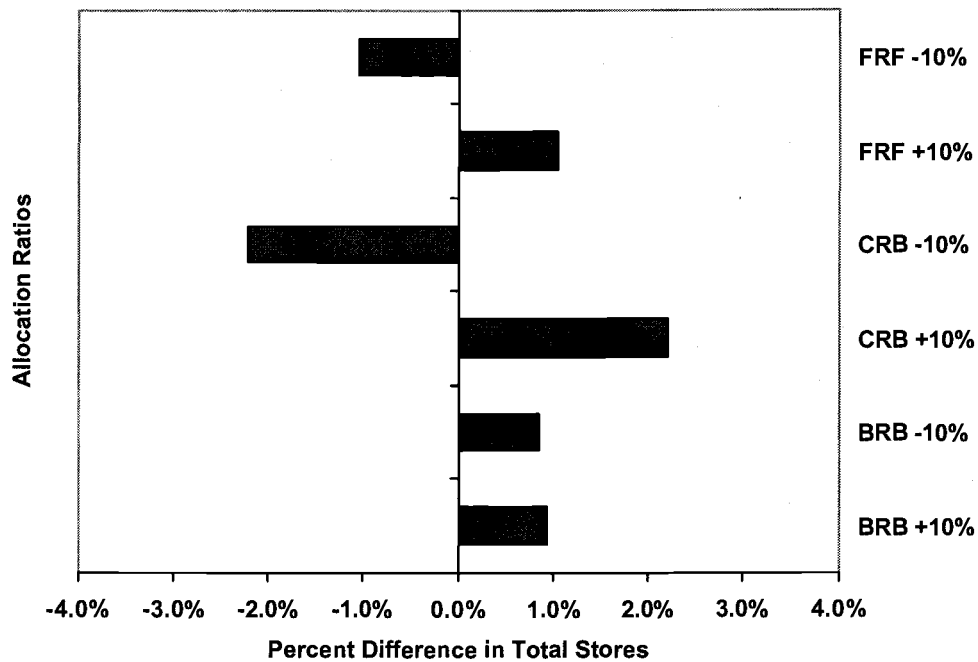


Figure 3.18. Results of a sensitivity test on the rates in the DISTURBANCE Module, showing the effect of changing allocation ratios $\pm 10\%$ on total carbon stores (FRF = fine root to foliage ratio, CRB = coarse root to bole ratio, and BRB = branch to bole ratio).

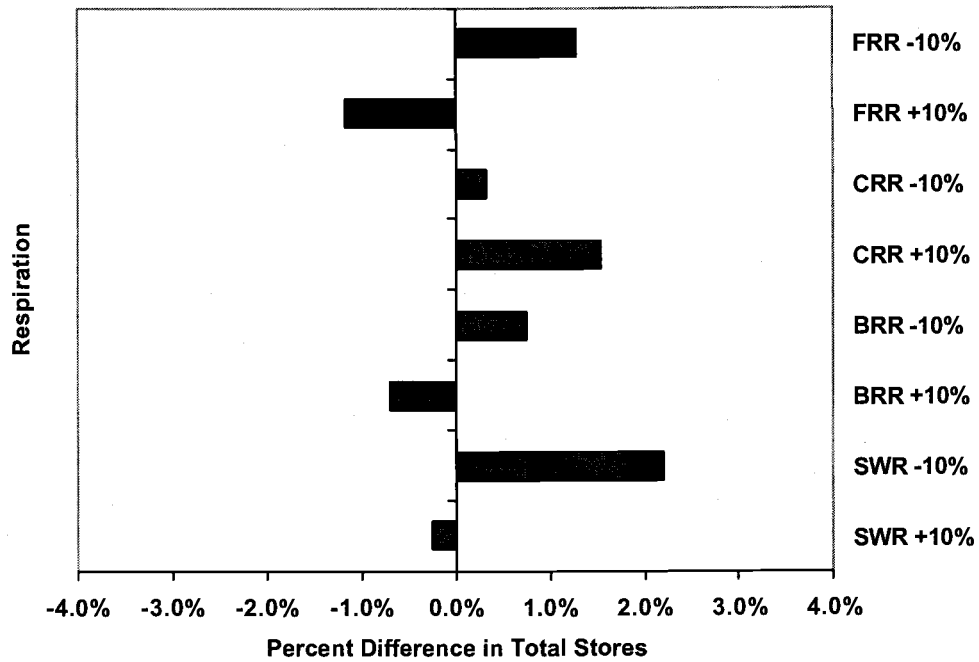


Figure 3.19. Results of a sensitivity test on the rates in the DISTURBANCE Module, showing the effect of changing respiration rates $\pm 10\%$ on total carbon stores (FRR = fine root respiration, CRR = coarse root respiration, BRR = branch respiration, SWR = sapwood respiration).

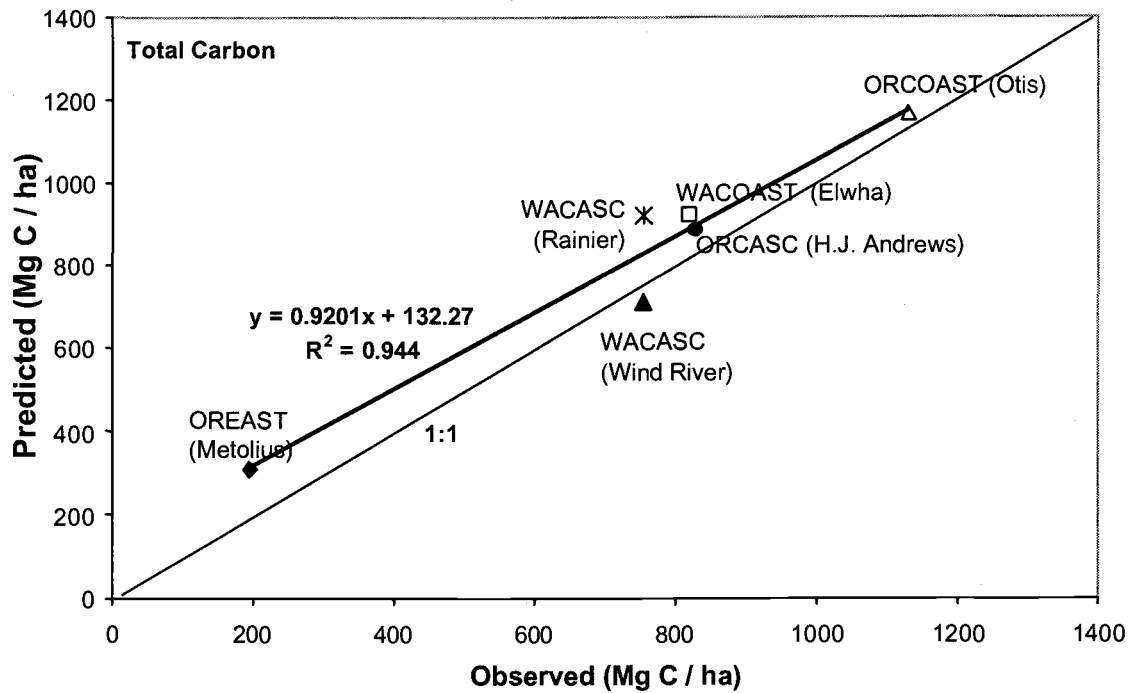


Figure 3.20. Predicted (MAXCARB) vs. observed (old-growth forest data) steady-state carbon stores. OREAST = Eastern Oregon, WACASC = Washington Cascades, WACOAST = Washington Coast, ORCASC = Oregon Cascades, ORCOAST = Oregon Coast. Names in parentheses represent the climate site for which MAXCARB was parameterized.

(range 158 to 232 Mg C ha⁻¹) measured in the field (**Table 2.2**, Smithwick et al., in press). The Washington Cascades sites were predicted by MAXCARB to store 921 Mg C ha⁻¹ at Rainier and 712 Mg C ha⁻¹ at Wind River, whereas the mean store for old-growth stands was 754 Mg C ha⁻¹. The range of values from the old-growth stands sampled in the Washington Cascades was actually between 463 Mg C ha⁻¹ and 1050 Mg C ha⁻¹, encompassing the values predicted by MAXCARB. Coastal Washington was predicted by MAXCARB to store 921 Mg C ha⁻¹, which was within the range of the observed data (623 to 993 Mg C ha⁻¹) but lower than the mean C store in coastal Washington (820 Mg C ha⁻¹). MAXCARB may predict greater steady-state C stores in coastal Washington than was observed because MAXCARB was parameterized for the Elwha climate station, which is at a lower elevation than the observed stands (located at a higher elevation within the Olympic National Park (Chapter 2)). The closest agreement between observed and predicted C stores was at the Oregon coast site, which was predicted by MAXCARB to store 1167 Mg C ha⁻¹, while the average for the old-growth forest was 1130 Mg C ha (range = 1006 to 1245 Mg C ha⁻¹).

Steady-state C storage in coastal Washington more closely resembled storage in the Washington and Oregon Cascades sites than in coastal Oregon. Sites in the Cascades exhibit a wider range in temperature minimums and maximums through the year compared to coastal sites (**Table 3.2, Figure 3.21**). The Washington coast site receives less precipitation than the Oregon coast site through the year (**Table 3.2, Figure 3.22**). Thus, the low precipitation in coastal Washington may explain the lower C storage compared to coastal Oregon.

Table 3.2. Site parameter values used in the CLIMATE Module of MAXCARB to predict total carbon stores at steady-state for multiple sites in the Pacific Northwest, U.S.A.

Site	Ecoregion	Monthly Min. Temp ^a (°C)	Mean Monthly Max. Temp ^a (°C)	Mean Total Annual Precip. ^a (cm)	Mean Monthly Radiation ^b (cal cm ²)	Soil Texture ^c
H.J. Andrews	ORCASC	3.1	17.8	173.8	344.0	silty-clay-loam
Wind River	WACASC	2.6	15.4	260.7	329.8	loam
Rainier	WACASC	2.9	11.7	175.2	344.0	loamy-sand
Metolius	OREAST	0.7	16.4	26.5	362.6	silt-loam
Cascade Head	ORCOAST	5.8	15.0	250.6	313.8	silty-clay-loam
Olympic NP	WACOAST	4.3	14.1	142.1	311.1	silt-loam

^a Monthly temperature and precipitation data was taken from sites listed in the Western Regional Climate Center; sites were chosen based on geographic proximity to forest sites (ORCASC = H.J. Andrews, Oregon; WACASC (Wind River) = Wind River, Washington; WACASC (Rainier) = Rainier (Carbon River), Washington; OREAST = Metolius, Oregon; ORCOAST = Otis, Oregon; WACOAST = Elwha Ranger Station, Washington)

^b Monthly radiation taken from the Solar Radiation Monitoring Laboratory, University of Oregon; sites were chosen based on geographic proximity to forest sites (WACASC (Wind River) = Hood River, Oregon; OREAST = Bend, Oregon; ORCOAST = Coos Bay, Oregon; WACOAST = Forest Grove, Oregon). ORCASC radiation taken from the H.J. Andrews LTER databank and was assumed to be the same for WACOAST (Rainier).

^c Soil texture was based on data in the H.J. Andrews LTER databank and personal communication with S.M. Remillard.

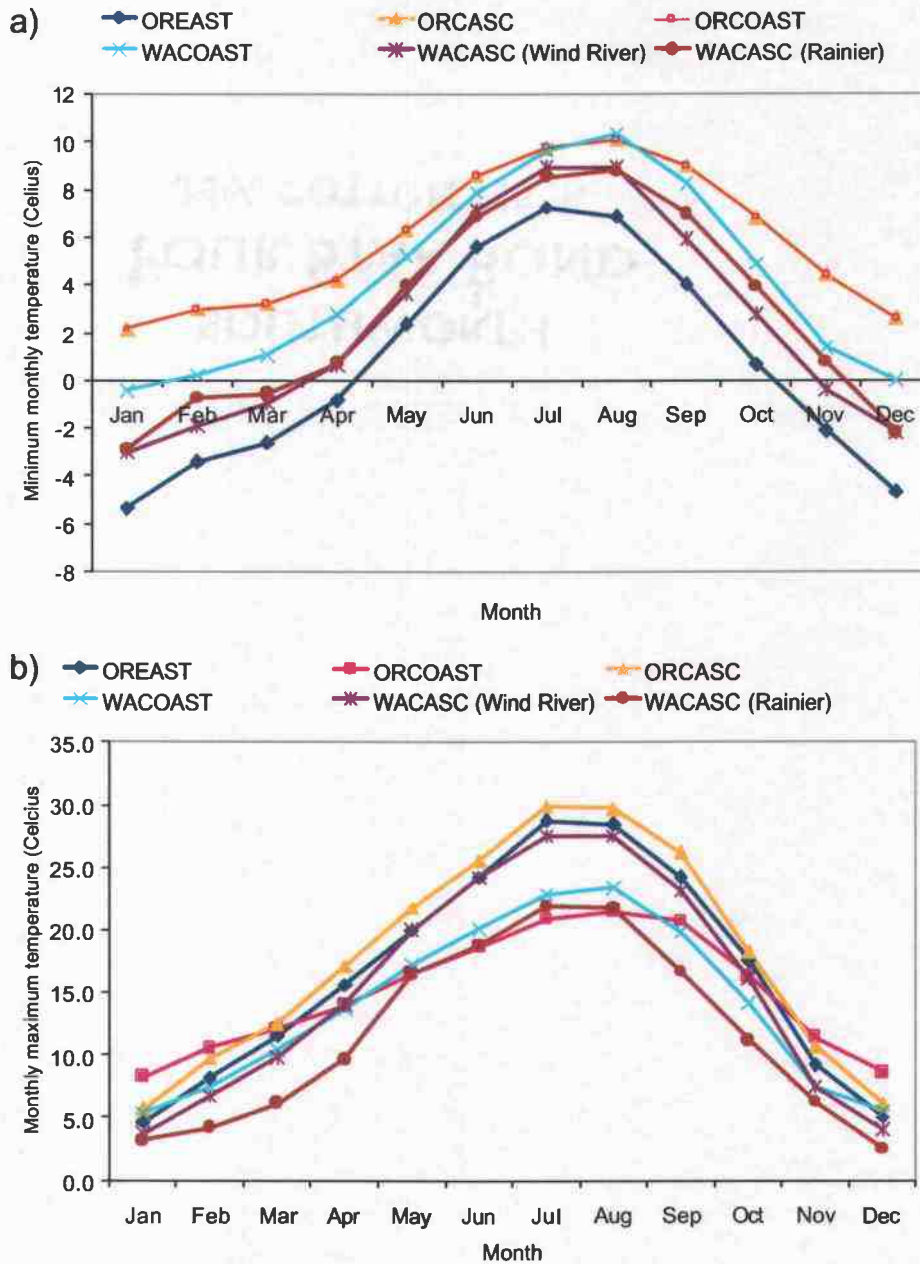


Figure 3.21. Temporal variation in (a) monthly minimum and (b) monthly maximum temperature for the five ecoregions represented by old-growth forest data.

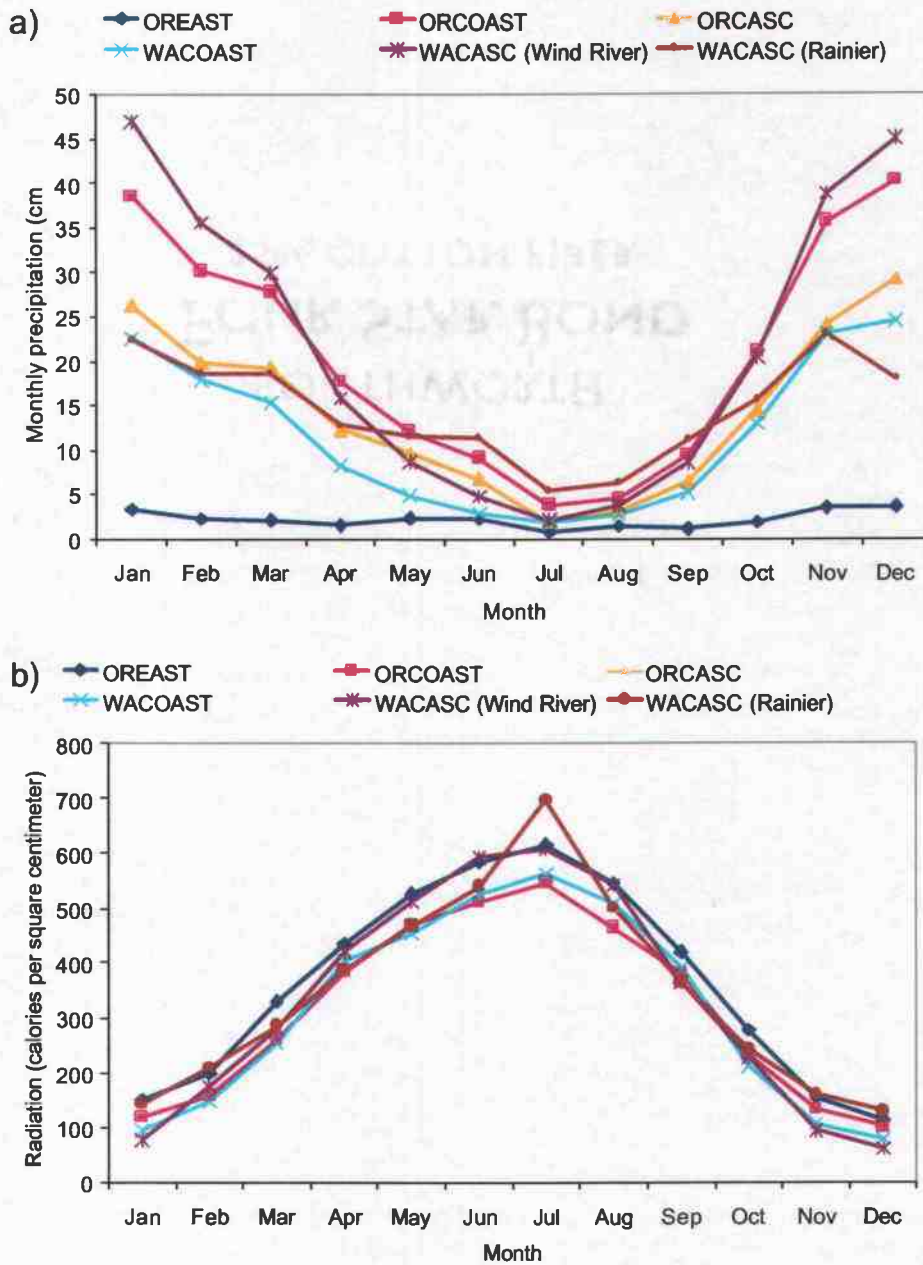


Figure 3.22. Temporal variation in (a) monthly precipitation and (b) monthly radiation for the five ecoregions represented by old-growth forest data.

Differences between observed and predicted steady-state C stores are better explained by differences in mean annual precipitation (**Figure 3.23**) than by other climate variables (data not shown); however, the relationship was weak. As precipitation decreased, the differences between the predicted and observed values increased ($R^2 = 0.41$). This indicates that the model did a better job predicting steady-state C stores in regions that receive greater precipitation compared to sites that receive less.

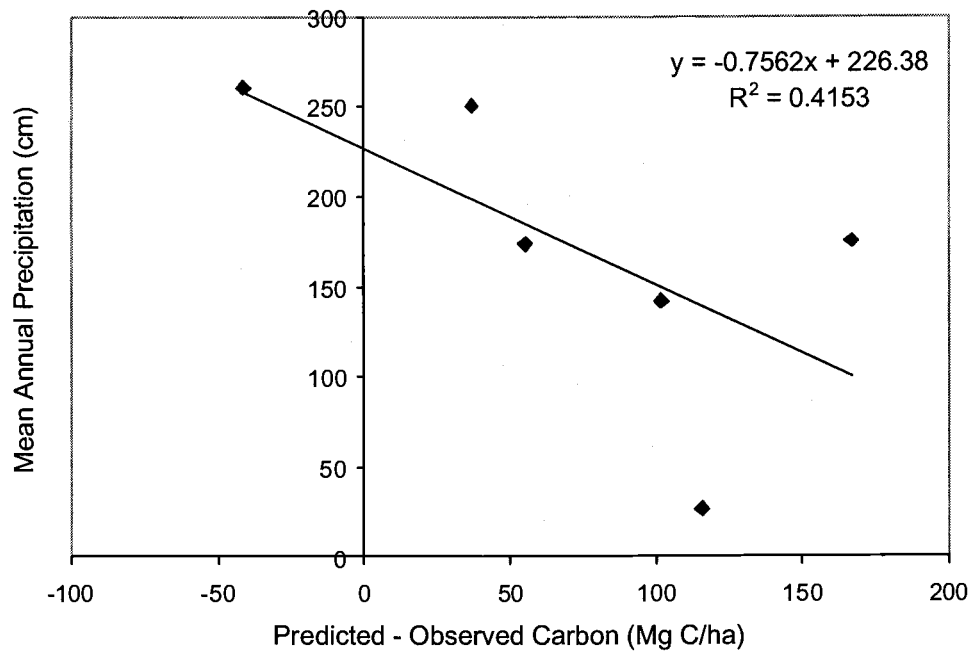


Figure 3.23. Linear regression between mean annual precipitation of observed (old-growth forest sites) and the difference between predicted (MAXCARB) and observed carbon stores at steady-state.

Discussion

To constrain uncertainty of the terrestrial biosphere's role in the global C cycle, it is helpful to bound predictions, particularly when human impacts, which may change the pace and direction of system trajectories, are unknown. Baseline studies provide a lower bound to system dynamics (what is the system's origin?) (Bender et al., 2000). It is equally helpful to place an upper bound (what is the upper limit of the system's response?), although these studies are rare. In MAXCARB, we present a model that can predict an upper bound of forest C storage at steady-state. The prediction can be useful for heuristic purposes to explore how uncertainty is affected by forcings outside the equilibrium state, such as from climate change.

In addition, MAXCARB operates at the regional scale, providing a means of characterizing uncertainties at broader and finer scales. This is because highlighting the significant processes at regional scales allows a better characterization of the important processes at broader and finer scales. Specifically, regional processes are constrained by processes at the global scale while finer-scale processes provide the mechanistic understanding necessary to predict regional-scale dynamics (O'Neill, 1988).

As part of this process, understanding the role of disturbances at regional scales is critical for constraining estimates of the role of the terrestrial biosphere in mitigation of atmospheric CO₂ increases (Potter et al., 1999; Schimel et al., 2001). For instance, Kurz and Apps (1999) recently assessed net ecosystem productivity in Canada's forests over a 404 Mha area and showed that increases in fires and insect damage have reduced C storage over the region.

Using MAXCARB, we studied the potential response of C storage to changes in disturbance regimes at the regional scale. Results indicated that lengthening the landscape rotation interval in a regulated (clear-cut) disturbance regime increased steady-state C storage, implying that C sequestration potential is partially determined by the disturbance regime. Specifically, landscape-average rates, which constrain steady-state C storage, were dependent on the simulated disturbance regime. These rates provide a mechanism whereby information on disturbance processes from regional scales can be translated to broader scales. Specifically, landscape-average rates could be used to modify parameters in a broad-scale model for disturbance regimes at regional scales. Because MAXCARB is an efficient model in terms of the time required for simulations, this is a tractable approach at broad scales.

We evaluated results of MAXCARB by comparing results with STANDCARB and with data from old-growth forests. While this is not an independent validation (since landscape-average rates from the DISTURBANCE Module are used to calculate steady-state C stores), it demonstrates that the same solution can be achieved with the more efficient model.

Comparisons between modeled predictions and observed data for the H.J. Andrews generally showed good agreement for most pools from both models. Differences for some pools, e.g., live coarse roots and live branches, may be because old-growth estimates were derived with allometric equations, or they may be due to parameterization of the model. The good agreement between the observed and modeled stable soil C pool is significant since this pool is the last pool in the cascade of equations in MAXCARB and is most likely to be in error as errors from preceding

calculations accumulate. Again, while not a validation of the model, this suggests that errors did not substantially accumulate during the cascade of equations.

There was also good agreement between predicted and observed old-growth data at multiple sites in the PNW. However, we did not include the stable wood pool in this comparison, which would have increased the difference between predicted and observed steady-state C stores. Comparing predicted and observed stable wood pools is difficult since dead and stable pools are not distinguished in the observed data, but are separately modeled in MAXCARB. Also, parameterization of stable wood is difficult because the steady-state C store is determined by transfer (e.g., snag fall) and decay rates. Either of these rates may be in error. More information is needed to assess decay and transfer rates of dead wood at the landscape-level to better evaluate model predictions.

Despite these caveats, we were able to predict steady-state C stores reasonably well compared to data from old-growth forests, in response to a wide variation in biogeoclimatic conditions in the PNW. As outlined by Smithwick et al. (in press, Chapter 2), eastern Oregon stored the least C at steady-state, while coastal Oregon stored the most. Eastern Oregon appears to be limited by precipitation and extreme minimum and maximum temperatures, while coastal Oregon enjoys mild winters and a less-severe summer drought. Precipitation and temperature are variable in the Washington and Oregon Cascades resulting in intermediate steady-state C stores for sites in these ecoregions. While the site we modeled at the Washington coast has moderate temperature ranges, it receives less precipitation than the Oregon coast, resulting in a lower steady-state C store. Differences between

predicted and observed values appear to be inversely related to mean annual precipitation, indicating MAXCARB yields increasing error at drier sites.

MAXCARB is one of many models being developed to capture fine-scale dynamics at broader scales. For example, Amiro et al. (2000) suggested that NPP trajectories could be used as spatial averages to support broader-scale carbon models in fire-prone regions of Canada. Leibowitz et al. (2000) developed a general framework for assessing landscape-level functions based on the operation of ecosystem units comprising the landscape. Moorcroft et al. (2001) present a new model (ED) to scale gap-models to large scales, accounting for stochastic disturbance events operating at the level of the individual. Similar to MAXCARB, ED attempts to capture processes, including disturbances, at large scales without modeling individual organisms, thereby increasing computer efficiency at broad scales. The methodology with ED is statistically-based, capturing the size- and age-structured variability that is inherent in sub-grid cell heterogeneity.

In both MAXCARB and ED, rules governing the sub-grid cell heterogeneity and processes are not well understood and require more research. In MAXCARB, we assume that disturbance events over a landscape can be simplified with a disturbance regime. The assumption that a landscape is in steady-state with regard to its disturbance regime is robust over very long time scales and across broad spatial resolutions. However, in actual landscapes, and for shorter time-scales and narrower spatial domains, these assumptions may be invalid. Few empirical studies exist over the long time periods and broad spatial scales as is needed to evaluate error in these conceptual models. Error may be incorporated in MAXCARB by assuming steady-

state landscapes if species dispersal and migration are not fully accounted for. For example, the age-dependent functions in MAXCARB's DISTURBANCE Module presume the user is able to define a priori the species composition after disturbance events (integrating any dynamic changes in species composition during succession). In reality, for very short, repeated disturbance intervals, late-successional species may not be able to successfully regenerate and may not be able to migrate into the stand. At very long disturbance intervals, early successional species may disappear from the system if their dispersal is limited. However, these errors should not substantially affect the estimates of steady-state C stores presented here, given the long lifespan of tree species in the PNW and the rotation intervals we used. However, caution should be used when applying the model to other areas where species may have shorter lifespans and disturbances are infrequent or rare.

The landscape-level concept of simulating disturbance events based on a probability distribution builds on established concepts in forestry, ecosystem science, and landscape ecology. For example, at the stand-scale, the classic "J-shaped" curve is used to describe the sustainable distribution of height and diameter classes of uneven-aged forests. At the landscape scale, there are many probability distributions that have been put forth to capture the dynamics of natural disturbance events through time. For example, Zhang et al. (2001) recently suggested that mixed Weibull distributions might ultimately be used to capture dynamics in uneven-aged stands. These disturbance distributions require continued empirical testing to be used with confidence at broad scales. A future improvement to MAXCARB may be

the user-defined option of choosing one of a family of distributions to determine how the choice affects potential carbon storage.

One limitation of assessing ecological processes at broad spatial and temporal scales is understanding and summarizing successional trends (Amiro et al., 2000). This is particularly evident with MAXCARB as age-dependent functions are critical for correctly parameterizing the DISTURBANCE Module. In this paper, we present data using age-dependent rates derived with simulations from the STANDCARB model. A sensitivity test on these rates showed that total stores were not greatly affected by moderate changes ($\pm 10\%$). Yet, there remains considerable uncertainty for some parameters, such as allocation ratios, suggesting that even a change in 10% of the original value may not reflect the uncertainty in that parameter. More empirical work is needed to narrow the uncertainty of these parameters. In the meantime, continued work with other models, such as STANDCARB, may allow better parameterization. The relatively good fit between total stores of both models and field data indicates that further improvement of parameters may be minimal to significantly improve agreement. Summarizing changes in ecosystem function with age is an emerging, evolving arena of research (Bond and Franklin, 2002) and as new empirical knowledge is gained at finer scales, it can be incorporated into the MAXCARB structure.

Another source of potential error in MAXCARB is the assumption that spatial interaction of heterogeneous patches does not significantly affect steady-state C stores. Future grid-mode simulations of MAXCARB may incorporate error by not accounting for the effect of spatial interactions (see Chapter 4). More research

would clarify the importance of sub-grid cell heterogeneity. Pierce and Running (1995) assessed the significance of averaging sub-grid cell variations on estimates of net primary production and concluded that aggregating climate indices to a 1-degree land surface area was more important in causing error than aggregating topographical, soils, and vegetation variation. To avoid this problem, MAXCARB's design allows for climate variation at the scale at which data is available, within broader regions of disturbance regimes.

MAXCARB also does not include the constraints of nutrient cycling on potential C stores. This simplification was made although nitrogen and other nutrients can constrain growth in this region. Therefore, application of the current MAXCARB model to situations with these limitations may incorporate error.

Assessing error when information is translated from fine to broad scales is difficult. Translating processes at finer scales as a functional response at a larger scale can lead to error (King et al. 1991). Precisely defining functionality at larger scales is a challenge since most empirical data is derived at the plot level. We suggest that the landscape scale is an appropriate level on which to examine disturbance processes. Predicting steady-state C stores across a wide gradient of climate, soils, and disturbance regimes at the regional scale facilitates assessment of the relative importance of these interacting factors on C storage in the long term.

Conclusions

Scaling mechanisms are needed to incorporate disturbance processes at broad scales efficiently and accurately. We present a new model that is able to predict potential carbon stores across a given region in response to biogeographical variation in climate, soils, dominant species composition and, importantly, the effect of disturbance regimes. By assessing disturbance regimes at the landscape-scale, we were able to implicitly include disturbance processes at a broad scale without having to individually model each stand within the landscape. We used information about a landscape's steady-state disturbance regime to calculate landscape-average rate constants that determine its steady-state mass. We used a detailed succession model to predict changes in key rates at broad scales, negating the need to model successional pathways explicitly.

By comparing this model to data from old-growth forests and to steady-state results from a finer-scale model, we have confidence that MAXCARB can constrain estimates of the upper bounds of C storage in the PNW. Additionally, we also found that, as the disturbance interval was lengthened, the potential amount of total C stores on the landscape increased.

Currently, disturbance is a key uncertainty in global carbon studies, and MAXCARB could be used to parameterize global models for the effect of disturbance at regional scales and to assess the relative effect of disturbances on potential C storage.

Acknowledgments

This research was made possible by funding from the Pacific Northwest Research Station Long-Term Ecosystem Productivity Program, an NSF Graduate Research Traineeship award to Oregon State University, and Interagency Agreement DW 12936179 between USEPA and the Pacific Northwest Research Station. All stands are associated with the H.J. Andrews Long Term Ecological Research (LTER) program, grant number DEB-9632921.

References

- Amiro, B.D., Chen, J.M. and Liu J. 2000. Net primary productivity following forest fire for Canadian ecoregions. *Can. J. For. Res.* 30, 939-947.
- Bender, M., Field, C., Hedin, L.O., Schimel, J., Sundquist, E., Berner, R., Galloway, J., Mackenzie, F., Torn, M., Freeman, K.H., Hedges, J., Mora, C., Stallard, R., Wofsy, S.C., and Schlesinger, W.H. 2000. The Changing C Cycle: A Terrestrial Focus, Report of the Workshop on the Terrestrial C Cycle. The National Science Foundation, Division of Earth Sciences.
- Bonan, G.B. 1989. A computer model of the solar radiation, soil moisture, and soil thermal regimes in boreal. *Ecol. Model.* 45, 275-306.
- Bond, B.J. and J.F., Franklin. 2002. Aging in Pacific Northwest forests: a selection of recent research. *Tree Physiology* 22: 73-76.
- Caspersen, J.P., Pacala, S.W., Jenkins, J.C., Hurtt, G.C., Moorcroft, P.R., and Birdsey, R.A. 2000. Contributions of land-use history to C accumulation in U.S. forests. *Science* 290, 1148-1151.
- Causton, D.R., Elias, C.O., and Hadley, P. 1978. Biometrical studies of plant growth. *Plant, Cell, and Environ.* 1, 163-184.
- Ciais, P. 1995. A large northern hemisphere terrestrial CO₂ sink indicated by the ¹³C/¹²C ratio of atmospheric CO₂. *Science* 269, 1098-1102.
- Cohen, W.B., Harmon, M.E., Wallin, D.O., and Fiorella, M. 1996. Two decades of C flux from forests of the Pacific Northwest. *Bioscience* 46, 836-844.
- Cooper, C.F. 1983. C storage in managed forests. *Can. J. For. Res.* 13, 155-166.
- Dai, A. and Fung, I.Y. 1993. Can climate variability contribute to the "missing" CO₂ sink? *Global Biogeochem. Cycles* 7, 599-609.
- Dale, V.H. 1997. The relationship between land-use change and climate change. *Ecol. Appl.* 7, 753-769.
- Dixon, R.K., Brown, S., Houghton, R.A., Solomon, A.M., Trexler, M.C., and Wisniewski, J. 1994. C pools and flux of global forest ecosystems. *Science* 263, 185-190.
- Emmingham, W.H. and Waring, R.H. 1977. An index of photosynthesis for comparing forest sites in western Oregon. *Can. J. For. Res.* 7, 165-174.

- Fan, S., Gloor, M., Mahlman, J., Pacala, S., Sarmiento, J., Takahashi, T., and Tans, P., 1998. A large terrestrial C sink in North America implied by atmospheric and oceanic C dioxide data and models. *Science* 282, 442-446.
- Fang, J., Anping, C., Peng, C., Zhao, S., and Ci, L. 2001. Changes in forest biomass C storage in China between 1949 and 1998. *Science* 292, 2320-2322.
- Fung, I. 2000. Variable C Sinks. *Science* 290, 1313.
- Goulden, M.L., Munger, J.W., Fan, S-M, Daube, B.C., and Wofsy, S.C. 1996. Measurements of C sequestration by long-term eddy covariance: methods and a critical evaluation of accuracy. *Global Change Biol.* 2, 169-182.
- Harmon, M.E., Franklin, J.F., Swanson, F.J., Sollins, P., Gregory, S.V., Lattin, J.D., Anderson, N.H., Cline, S.P., Aumen, N.G., Sedell, J.R., Leinkaemper, G.W., Cromack Jr., K., and Cummins, K.W. 1986. Ecology of coarse woody debris in temperate ecosystems. *Adv. Ecol. Res.* 15, 133-302.
- Harmon, M.E., Ferrell, W.K., and Franklin, J.F. 1990. Effects on carbon storage of conversion of old-growth forests to young forests. *Science* 247, 699-702.
- Harmon, M.E. and Domingo, J.B. 2001. A user's guide to STANDCARB version 2.0: A model to simulate the C stores in forest stands. Department of Forest Science, Oregon State University, Corvallis, Oregon.
- Harmon, M.E. and Marks, B. In press. Effects of silvicultural treatments on carbon stores in Douglas-fir/western hemlock Forests in the Pacific Northwest, USA. *Can. J. For. Res.*, In Press. Harmon, M. E. and B. Marks.
- Hibbard, K.A. 1995. Landscape Patterns of C and Nitrogen Dynamics in a Subtropical Savanna: Observations and Models. Ph.D. Dissertation, Texas A&M University.
- Holland, E.A. and Brown, S. 1999. North American C Sink: Technical Comments. *Science* 283, 1815a.
- Houghton, R.A. 1993. Is C accumulating in the northern temperate zone? *Global Biogeochem. Cycles* 7, 611-617.
- Houghton, R.A. 1999. The annual net flux of C to the atmosphere from changes in land use 1850-1990. *Tellus* 51B, 298-313.
- Houghton, R.A., Davidson, E.A., and Woodwell, G.M. 1998. Missing sinks, feedbacks, and understanding the role of terrestrial ecosystems in the global C balance. *Global Biogeochem. Cycles* 12, 25-34.
- Houghton, R.A., Hackler, J.L., and Lawrence, K.T. 1999. The U.S. C budget: contributions from land-use change. *Science* 285, 574-578.

- Janisch, J.E. and Harmon, M.E. 2002. Successional changes in live and dead wood stores: Implications for net ecosystem productivity. *Tree Phys.* 22, 77-89.
- Jensen, M.E. and Haise, H.R. 1963. Estimating evapotranspiration from solar radiation. *J. Irrigation and Drainage Engineering* 89, 15-41.
- Johnson, E.A. and Gutsell, S.L. 1994. Fire frequency models, methods and interpretations. *Adv. in Ecol. Res.* 25, 239-287.
- Johnson, E.A. and Van Wagner, C.E. 1985. The theory and use of two fire history models. *Can. J. For. Res.* 15, 214-220.
- Jones, H.G. 1992. *Plants and microclimate: a quantitative approach to environmental plant physiology.* Cambridge University Press.
- King, A.W., Johnson, A.R. and O'Neill, R.V. 1991. Transmutation and functional representation of heterogeneous landscapes. *Lands. Ecol* 5: 239-253.
- Kurz, W.A. and Apps, M.J.. A 70-year retrospective analysis of carbon fluxes in the Canadian forest sector. *Ecol. Appl.* 9, 526-547.
- Lenihan, J.M., Daly, C., Bachelet, D., and Neilson, R.P. 1998. Simulating broad-scale fire severity in a dynamic global vegetation model. *Northwest Science* 72, 91-103.
- Leibowitz, S.G., Loehle C., Lin, B.-L. and Preston E.M. 2000. Modeling landscape functions and effects: a network approach. *Ecol. Model.* 132: 77-94.
- Melillo, J.M., Fruci, J.R., Houghton, R.A., Moore, B., and Skole, D.L. 1988. Land-use change in the Soviet Union between 1850 and 1980: Causes of a net release of CO₂ to the atmosphere. *Tellus* 40B. 116-128.
- Moorcroft, P.R., G.C. Hurtt, and S.W. Pacala. 2001. A method for scaling vegetation dynamics: the Ecosystem Demography model (ED). *Ecol. Monographs* 71, 557-586.
- Olson, J.S. 1963. Energy storage and the balance of producers and decomposers in ecological systems. *Ecol.* 44, 322-331.
- O'Neill, R.V. 1988. Hierarchy theory and global change. In: Rosswall, T., Woodmansee, R.G., and Risser, P.G. (Eds.) *Scales and Global Change.* John Wiley & Sons, Ltd., pp 29-45.
- Pacala, S.W., Hurtt, G.C., Baker, D., Peylin, P., Houghton, R.A., Birdsey, R.A., Heath, L.S., Sundquist, E., Stallard, R., Ciais, P., Moorcroft, P.R., Casperson, J.P., Shevliakova, E., Moore, B., Kohlmaier, G., Holland, E.A., Gloor, M., Harmon, M.E., Fan, S.-M., Sarmiento, J., Goodale, C.L., Schimel, D., and

- Field, C.B. 2001. Consistent land- and atmosphere-based U.S. C sink estimates. *Science* 292, 2316-2319.
- Peng, C. 2000. From static biogeographical model to dynamic global vegetation model: a global perspective on modeling vegetation dynamics. *Ecol. Model.* 135, 33-54.
- Pierce, L.L. and Running, S.W. 1995. The effects of aggregating sub-grid land surface variation on large-scale estimates of net primary production. *Landscape Ecol.* 10, 239-253.
- Potter, C.S., Klooster, S., and Brooks, V. 1999. Interannual variability in terrestrial net primary production: exploration of trends and controls on regional to global scales. *Ecosystems* 2: 36-48.
- Potter, C., Genovese, V.B., Klooster, S.A., Bobo, M., and Torregrosa, A. 2001. Biomass burning losses of C estimated from ecosystem modeling and satellite data analysis for the Brazilian Amazon region. *Atmos. Environ.* 35, 1773-1781.
- Richards, F.J. 1959. A flexible growth function for empirical use. *J. Exper. Bot.* 10, 290-300.
- Running, S.W. and Coughlan, J.C. 1988. A general model of forest ecosystem processes for regional applications I. Hydrologic balance, canopy gas exchange and primary production processes. *Ecol. Model.* 42, 125-154.
- Schimel, D.S., House, J.I., Hibbard, K.A., Bousquet, P., Ciais, P., Peylin, P., Braswell, B.H., Apps, M.J., Baker, D., Bondeau, A., Canadell, J., Churkina, G., Cramer, W., Denning, A.S., Field, C.B., Friedlingstein, P., Goodale, C., Heimann, M., Houghton, R.A., Melillo, J.M., Moore III, B., Murdiyarso D., Noble, I., Pacala, S.W., Prentice, I.C., Raupach, M.R., Rayner, P.J., Scholes, R.J., Steffen, W.L., Wirth, C. 2001. Recent patterns and mechanisms of carbon exchange by terrestrial ecosystems. *Nature* 414, 169-172.
- Schimel, D., Melillo, J., Tian, H., McGuire, A.D., Kicklighter, D., Kittel, T., Rosenbloom, N., Runnings, S., Thornton, P., Ojima, D., Parton, W., Kelly, R., Sykes, M., Neilson, R., Rizzo, B. 2000. Contribution of increasing CO₂ and climate to carbon storage by ecosystems in the United States. *Science* 287, 2004-2006.
- Schimel, D.S., VEMAP Participants, and Braswell, B.H. 1997. Continental scale variability in ecosystem processes: models, data, and the role of disturbance. *Ecol. Monog.* 67, 251-271.
- Sedjo, R.A. 1992. Temperate forest ecosystems in the global C cycle. *Ambio* 21, 274-277.

- Shugart, H.H., Michaels, P.J., Smith, T.M., Weinstein, D.A., and Rastetter, E.B. 1988. Simulation models of forest succession. In: Rosswall, T., Woodmansee, R.G., Risser, P.G. (Eds.) Scales and Global Change. John Wiley & Sons, Ltd., New York.
- Smithwick, E.A.H., Harmon, M.E., Domingo, J.B. In press. Potential upper bounds of carbon stores in forests of the Pacific Northwest. *Ecological Applications*.
- Van Wagner, C.E. 1978. Age-class distribution and the forest fire cycle. *Can. J. For. Res.* 8, 220-227.
- Wallin, D.O., Swanson, F.J., Marks, B., Cissel, J.H., Kertis, J., 1996. Comparison of managed and pre-settlement landscape dynamics in forest of the Pacific Northwest, USA. *For. Ecol. Manag.* 85, 291-309.
- White, A., Cannell, M.G.R., and Friend, A.D. 2000. The high latitude terrestrial carbon sink: a model analysis. *Global Change Biol.* 6, 227-245.
- Yoder, B.J., Ryan, M.G., Waring, R.H., Schoett, A.W., Kaufman, M.R., 1994. Evidence of reduced photosynthetic rates in old trees. *For. Sci.* 40, 513-527.
- Zhang, L., Gove, J.H., Liu, C., Leak, W.B. 2001. A finite mixture of two Weibull distributions for modeling the diameter distributions of rotated-sigmoid, uneven-aged stands. *Can. J. For. Res.* 31, 1654 – 1659.

CHAPTER 4

**EXAMINING MULTISCALE EFFECTS OF LIGHT LIMITATIONS AND
EDGE-INDUCED MORTALITY ON CARBON STORES IN
FOREST LANDSCAPES**

Erica A. H. Smithwick, Mark E. Harmon, and James B. Domingo

Abstract

Analyses of carbon (C) dynamics at broad scales usually do not consider spatial interactions. The assumption is that C dynamics can be modeled within homogenous patches (i.e., even-aged) and then summed to predict broad-scale dynamics (an additive approach). We reexamine this additive approach by using a forest process model to estimate the relative effects of edge-induced, tree mortality (mainly due to wind) and light limitations on C dynamics in artificial forest landscapes with various spatial structures. We analyzed simulation results to examine possible emergent behaviors due to spatial interactions at multiple levels of pattern-process interactions. Emergent (i.e., non-additive) behaviors were observed at all levels of scale examined, indicating that emergent behaviors did not necessarily cease as one proceeded from the patch to the landscape level, as we had expected. However, the magnitude of the emergent behaviors depended on the level of spatial interaction considered as well as the type and intensity of the processes that were included. In all cases, patch-to-patch interactions resulted in significant emergent behaviors when process interactions were strong but were not significant when interactions were weaker. In one case, the magnitude of emergent behaviors differed among the landscapes, indicating that patch-to-patch interactions may not be accounted for by a simple correction for edge effects unless spatial interactions are addressed. The implication is that some dynamics of C flux processes in fragmented landscapes may not be captured at broad-scales using an additive approach, whereas in other cases spatial interactions are small enough to be ignored.

Introduction

Quantifying the exchange of C between the terrestrial biosphere and the atmosphere is necessary to constrain the global C budget and potentially manage for C sequestration (e.g., Brown 1996; Schultze et al. 2000; Watson et al. 2000). As a result, estimates of C exchange over broad scales are needed to validate regional and global C models. Since it is impractical to directly measure C flux for every ecosystem over a broad area, it is necessary to make assumptions about how to scale local information derived from select sites to a larger area.

A simple way to scale information to broader extents is through a 'distributional' or 'additive' approach (Baker 1989) and, traditionally, many C flux research projects have been attempted in this way (e.g., Cohen et al. 1996; Houghton et al. 2000). Carbon flux has a strong vertical component in that C is transferred from the biosphere to the atmosphere through decomposition and respiration, and from the atmosphere to the biosphere through photosynthesis. Thus, when accounting for the net flux of an ecosystem, the balance of vertical inputs and outputs should indicate the directionality of C transfer either into the ecosystem or the atmosphere. It follows that by knowing the net C flux of several landscape elements, and summing the fluxes for the area of each landscape element, it should be possible to calculate the net landscape flux.

However, processes affecting C flux such as mortality, respiration, and decomposition may change horizontally across forest edges, influencing C storage in neighboring patches. These horizontal processes have been inadequately described in most carbon flux research. The change in horizontal processes can be

linear or non-linear across this zone. If the change is linear, the response at the edge is a result of the degree of mixing of the two neighboring patches (the “matrix effect” of Lidicker (1999)). An additive model can handle this linear change. By contrast, if the change is non-linear (enhanced, diminished, or asymptotic), the response of the system at the edge cannot be explained completely by the mixing of the two neighboring patches. As a result, averaging the properties of the neighboring patches is not sufficient to predict behavior at broad-scales using traditional additive approaches (Lidicker 1999). Therefore, landscape-level estimates of C flux may diverge from patch-level estimates if these horizontal processes are included. The differences between the two approaches can be attributed to landscape-level “emergent behaviors” (i.e., behaviors at the landscape scale that cannot be predicted solely from the additive properties of the patches).

A landscape, which, by the definition we employ here, is composed of patches of interacting stands or ecosystems (Forman and Godron 1981), is a useful spatial unit in which to evaluate the impact of forest edges at broad scales. If emergent behavior is important, landscape C flux may be dependent on patch topology, the spatial relationships among patches in a landscape. Indeed, a central tenet of landscape ecology is that spatial heterogeneity and scale matter when interpreting ecological patterns and processes (Risser 1987, Wiens 1998). Since forest edges are common components of many landscape mosaics (Forman and Godron 1981; Franklin and Forman 1987), horizontal processes across forest edges may be important in landscape-scale C budgets. Theoretically, it has been shown

that the spatial patterns of edges on the landscape, created by different disturbance regimes, result in different ecological responses (Franklin and Forman 1987).

Recent evidence suggests that at short time-scales the horizontal flux of C can be significant, even in areas presumed homogenous. Interpretation of the resultant flux over a broad area must account for this horizontal heterogeneity. For example, eddy correlation techniques were designed to measure the vertical flux of CO₂ and water vapor between the vegetation, soil, and atmosphere over an ecosystem, allowing the calculation of the net amount of material entering and leaving the ecosystem at a very fine temporal resolution over a fairly broad area. However, due to horizontal movement of air masses, the source area of the measured fluxes does not necessarily equal the "footprint" of the eddy flux tower (Turner and Gregory, in review ; Kaharabata et al. 1997; Wofsy et al. 1993; Goulden et al. 1996). The direction and magnitude of this source discrepancy may change at time scales of hours (differing wind directions) to decades (changing land types and/or age-class structure), making it difficult to avoid. Airborne and eddy-flux measures of C exchange may not agree due to fine-scale spatial heterogeneity (Desjardins et al. 1997), indicating that simple additive approaches may not be sufficient to capture broad-scale fluxes.

Research on long-term edge effects, primarily from observational field studies, also indicates important horizontal effects across forest edges. Particularly, increased light penetration and susceptibility to wind turbulence cause differences between the edge and the interior. Increased light at forest edges causes a difference in the competitive advantage of different species and life forms, although

the effect is dependent on stand age, aspect, and moisture conditions (Ranney et al. 1981; Lovejoy et al. 1984; Williams-Linera 1990). In addition to changes in light conditions, the openings at forest edges often result in increased exposure to wind and thus increased rates of tree-mortality. In the tropics, Laurance et al. (1997) found that, with time, carbon stores of live vegetation within 100 m of an edge boundary were reduced 36 % compared to that before fragmentation. In the same area, Laurance et al. (1998) showed that the mean mortality rate was 3 to 4 times higher in forests within 60 m of edges (4.01 % vs. 1.27 %), while Ferreira and Laurance (1997) reported mortality rates that were elevated 7 or 8 times in edge plots compared to interior forest plots. In Panama, Williams-Linera (1990) showed that the edge to interior ratio of trees that died after the edges were created was 14:1. In North American temperate forests, increased mortality at edges in old-growth Douglas-fir (*Pseudotsuga menzeizii*) has also been recorded. Eighty-percent of the blow-down associated with a forest windthrow event in the Bull Run Basin in northwestern Oregon was due to the proximity of the stands to recent clear-cut edges (Sinton et al. 2000). Chen et al. (1992) showed a greater number of snags and logs at forest edges, indicating elevated rates of tree-mortality at forest edges compared to the interior forest.

Light and wind interact in the edge zone, causing concomitant changes. For example, windthrow in the Bull Run Basin has favored the development of shade-tolerant species along edges and reduced the presence of old-growth Douglas-fir, which is susceptible to wind mortality after being newly exposed (Sinton et al. 2000). A similarly complex response to light and wind was observed at Wind

River, in southern Washington, where Douglas-fir and western hemlock (*Tsuga heterophylla*) seedlings increased, but Pacific Silver fir (*Abies amabilis*) seedlings and saplings decreased in abundance (Chen et al. 1992). In the tropics, secondary plant species that depend on high light conditions are able to invade reserve margins as prevailing winds cause an increase in standing dead, broken, and fallen trees (Lovejoy et al. 1984). Thus, multiple ecological processes may operate simultaneously at patch edges (particularly light and wind), potentially resulting in complex emergent behavior that cannot be assessed by examining processes independently.

In this paper, we use a forest process model (STANDCARB) to simulate the effects of wind mortality and light limitations on carbon storage within different artificial landscape structures. Our general research question is: can landscape carbon storage be predicted using the additive approach, whereby the value of the landscape is equal to the area-weighted sum of the properties of the patches? Specifically, does the interaction of these two processes (light and wind) result in non-linear interactions among patches that are not predictable using additive approaches? Finally, if emergent behaviors (defined here as the differences beyond expected variation of an additive model) are present at one spatial scale due to interactions at the lower levels, do they cease to be important at broader scales?

There were two specific objectives with this modeling exercise. The first objective was to analyze the effect of cell-to-cell interactions at the stand scale. Here, a cell is approximately 0.03 ha, which represents the area that would be occupied by a typical mature tree in the Pacific Northwest. Cell-to-cell interactions

are determined by examining results within a homogenous landscape, i.e., where there is only one type of patch and thus no patch-to-patch interactions. The second objective was to analyze the effects of patch-to-patch interactions at the landscape scale. A patch represents a collection of cells within a simulated landscape. Patch size ranged from 0.03 ha to approximately 5 ha, depending on the type of artificial landscape being simulated. Interactions between patches are determined by examining results within heterogeneous landscapes, where there is a mix of old and young age-classes on the landscape. We also examined the effect of patch structure in a landscape, i.e., the arrangement of patches, as it might affect possible emergent behavior at the landscape scale. By comparing results at two scales of interaction, our goal was to determine if carbon storage was predictable using an additive approach, or, conversely, whether emergent behaviors due to the interaction of light and wind processes were evident. Despite a generally accepted notion that spatial heterogeneity is important (King et al. 1991; Risser 1999), it is difficult to determine at what scale, and under what circumstances, this is so. The goal of this research is to elucidate the scales over which assumptions of spatial homogeneity will hold. This research has significant implications for carbon cycle modeling since carbon models that operate at broad scales make assumptions of spatial homogeneity, although the implications may extend to other ecological fields in which spatial scale is important.

Methods

Model Description

STANDCARB v.2.0 (Harmon and Domingo 2001; Harmon and Marks, in press) was used in these simulations. This model simulates the dynamics of live and dead pools of carbon in mixed-species, mixed-age-class, forest stands and is also able to simulate the effects of harvests or fire on carbon storage.

STANDCARB is similar to gap models since each stand is simulated with many replicate cells, which are then averaged to obtain stand values. In addition, STANDCARB can be parameterized for specific species based on characteristics defining their growth, mortality, and decomposition. As a result, the species composition changes through time during succession in response to the species' competitiveness. STANDCARB is also similar to many ecosystem-process models in that growth, mortality, decomposition, and other significant ecosystem processes are calculated in response to abiotic factors such as climate and site characteristics. Temporally, STANDCARB is run on an annual time step for all live and dead carbon pools through succession, although climate variables, affecting tree establishment, growth, and decomposition are computed monthly.

Within each cell in STANDCARB, there are 4 vegetation layers (upper tree, lower tree, shrub layer, and herb layer), each of which has up to seven live pools, eight detrital pools, and three stable carbon pools (**Figure 4.1**). For example, the upper and lower tree layers are comprised of seven live pools: (1) foliage, (2) fine-roots, (3) branches, (4) sapwood, (5) heartwood, (6) coarse-roots, and (7) heart-rot.

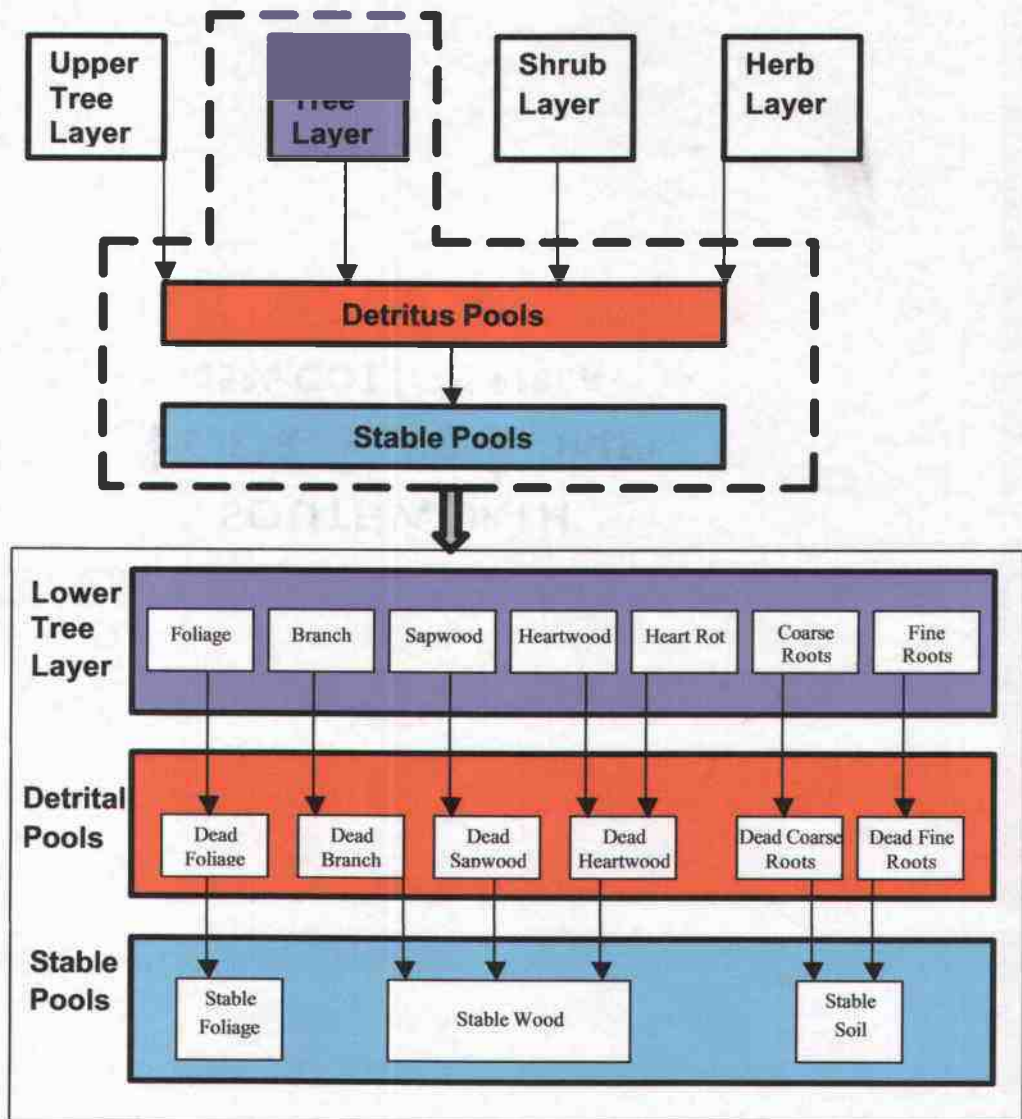


Figure 4.1. Conceptual structure of carbon pools and vegetation layers for STANDCARB 2.0.

Shrubs do not have heartwood or heart-rot since they do not form a bole, and herbs do not have any woody components. Each tree layer can be a different species, whereas the shrub and herb layers are each represented by a single “species.” Live carbon pools transfer material to their detrital counterpart to account for the pools available for decomposition processes. Dead sapwood and dead heartwood are additionally separated into snags and logs so that the effects of position on microclimate can be modeled. All detrital pools in a cell can potentially add material to the three, relatively decay-resistant, stable C pools: (1) stable foliage, (2) stable wood, and (3) stable soil.

Here, we describe a modification to STANDCARB that allows the model to calculate tree exposure to wind at each cell and to increase natural tree-mortality rates in proportion to increased tree exposure. With this change, cells in STANDCARB can interact spatially with both light and wind, which affects growth, decomposition, and mortality processes within cells.

Modeling Light Processes

Light influences several processes in STANDCARB: (1) the establishment of tree species based on their light requirements, (2) growth rates through modification of foliage mass, and (3) decomposition, through influences in detritus moisture contents. To determine the direct and diffuse light reaching a particular cell, STANDCARB uses a function called NeighborLight. NeighborLight calculates the angle to the tallest tree along each of 8 cardinal transects surrounding the cell of interest (**Figure 4.2**). By knowing the angle of the sun from the cell of

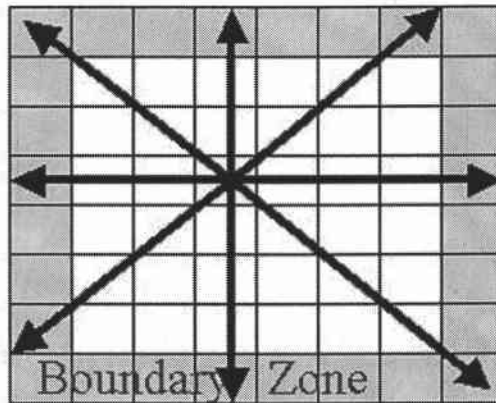


Figure 4.2. Arrangement of cells in STANDCARB, representing the spatial structure used to calculate light limitations and wind mortality. A boundary zone surrounds the simulation cells, representing vegetation outside of the simulation area. The arrows indicate the directions of transects used to determine shading effects and exposure to wind.

interest, given information about the latitude, aspect, and slope of the site being simulated, it is possible to calculate the direct and diffuse light reaching the cell. For diffuse light, the average angle from these 8 transects is used to calculate incoming radiation. For direct light, a weighted average of the E, SE, S, SW, and W transects is used (Harmon and Domingo 2001). In addition, cell width (which can be set by the user) determines the amount of light entering a cell since, for a given height, wider cells allow more direct and diffuse light to enter. This is important because the minimum light requirements are different for different tree species, and the species composition will affect the amount of carbon that is predicted. We ran a series of simulations to test the effect of cell width of 15 m, 20 m, and 25 m on carbon and found a significant response of cell width on carbon storage, with larger cells retaining more carbon than smaller cells. We chose an intermediate cell width of 17 m, which is approximately equal to the canopy width of old-growth trees in the Pacific Northwest. All simulations that are described in this paper were run with a 20 x 20 cell matrix, for a total of 400 cells, representing an area of 115,600 m² (or 11.56 ha).

Modeling Wind Mortality

We recognize that wind is an especially complex process in forest ecosystems and we do not attempt to mimic its behavior exactly. Rather, we estimated its effect by making the assumption that tree mortality is augmented by increased exposure to wind. We refer to “wind mortality” for simplification, although we imply that there is, more explicitly, an elevated tree-mortality rate

where cells are more-exposed, as at patch edges. We modeled exposure as a function of slope, aspect, and tree heights, which are important factors resulting in higher mortality rates at forest edges after catastrophic wind events (Lovejoy et al. 1984; Foster 1988; Foster and Boose 1992; Chen et al. 1992).

In previous versions of STANDCARB, tree mortality is initially high due to tree competition and then decreases to a density-independent value that is a function of the maximum age of the tree species, which sets the probability that the tree will die in any given year. Here, we assumed that mortality in a cell would increase due to wind turbulence in cells that were more exposed relative to those that were more sheltered. We took advantage of the existing model structure in NeighborLight to calculate a new function, called NeighborWind, to calculate the relative exposure of trees in a cell. NeighborWind determines exposure to wind by calculating the angle from the tree height in the cell of interest to the average tree height along each of the 8 surrounding transects (**Figure 4.2**). The length of the transect (the number of cells from which average transect height is calculated) is set by the user. In these simulations, we used a transect length of 10 cells (170 m for a cell width of 17 m). NeighborWind then takes the average angle for the 8 transects. The angle is normalized so that negative numbers indicate increased exposure (the tree in the cell of interest is taller than neighboring cells, meaning it has a higher mortality rate). The transects can also be weighted by aspect so that if there is a directionality to the wind-induced mortality, it can be specified by the user. However, in this paper, all the transects received equal weighting. We then defined a new parameter, k , to equal the ratio of the maximum mortality rate at a

completely exposed cell to the base mortality rate (**Figure 4.3**). We used k values equal to 2, 3, 5, or 8 times the baseline mortality rate, which are realistic estimates for increased wind mortality at edges given the current literature (Laurance et al. 1998; Ferreira and Laurance 1997; Chen et al. 1992). Both NeighborLight and NeighborWind can be set by the user as either on or off, which allows the user to manipulate the interactions of light and wind during the simulations.

Model Parameterization and Calibration

To calibrate the model, we used data from old-growth stands in the H.J. Andrews LTER permanent plot network (Acker et al. 1998) reported in Smithwick et al. (in press). The goal of this calibration was to fit the relative proportion of pools in the old-growth forest data (presumed to be at steady-state by Smithwick et al. (in press)) to the steady-state model results (average of years 500 to 1000). The categories reported in Smithwick et al. (in press) did not exactly match those output from the model so it was necessary to assign pools to their appropriate category (**Table 4.1**). Then, we adjusted the model parameters in the mortality, growth, site, and decomposition driver files in STANDCARB to match the relative proportion of pools in the old-growth field data. For simplicity, we presumed an equal ratio of Douglas-fir and western hemlock tree seedlings to initiate the simulations.

Parameters affecting mortality, pruning, and turnover varied between species. The maximum mortality rate was lower for Douglas-fir (0.009 yr^{-1}) than for western hemlock (0.011 yr^{-1}) and the maximum age for Douglas-fir was set at 1200 years versus 800 years for western hemlock. Pruning rates for branches and

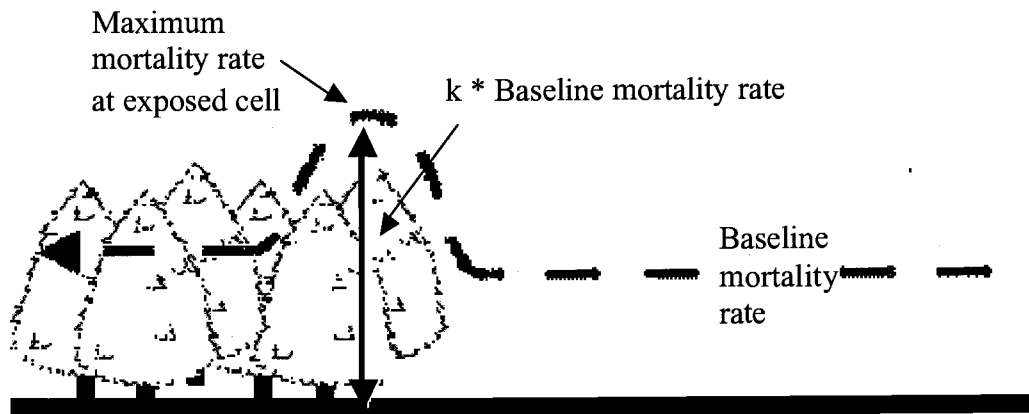


Figure 4.3. Graphical representation of elevated mortality rates across an edge. In STANDCARB, k is equal to the wind mortality rate divided by the baseline (“gap-phase”) mortality rate.

Table 4.1. Calibration of modeled carbon pools in STANDCARB v.2.0 to old-growth forest pools (Smithwick et al., in press).

Old-growth Pools	% of Total	Standcarb Pools	% of Total
Live Branch	4.1	Live Branch	4.7
Dead Branch	0.8		
Foliage	0.6	Foliage	0.9
Stem Wood	46.4	Sapwood+Heartwood+Heartrot	43.2
Fine Roots	1.0	Fine Roots	0.7
Coarse Roots	14.8	Coarse Roots	13.6
Fine Woody Debris	1.7	Dead Branch	1.3
Dead Roots	2.6	Dead (Fine + Coarse) Roots	3.5
Forest Floor	2.3	Dead Foliage + Stable Foliage	2.5
Rotten Wood	1.4	Stable Wood	2.2
Soil	14.9	Soil	15.6
Logs	5.1	Non-salvagable Logs	7.3
Snags	4.4	Non-salvagable Snags	4.4

coarse-roots were the same for both species (0.02 yr^{-1} and 0.005 yr^{-1} , respectively). Time close, the time required for the tree to have its maximum branch extension, was set at 120 years for Douglas-fir and 100 years for western hemlock. Foliage turnover rates were slightly faster for western hemlock (0.25 yr^{-1} vs. 0.20 yr^{-1}) than Douglas-fir as the latter retains leaves longer, but fine root turnover rates were the same (0.5 yr^{-1}).

Growth parameters were also slightly different between species. Western hemlock was set to establish when only 5 % of the total available light reached the cell, but Douglas-fir, which generally requires more light for establishment, was set to require 10 % of total light for successful establishment. Both species had similar allocation ratios of fine roots to foliage (0.33) but Douglas-fir had higher rates of heartwood formation than western hemlock (0.059 yr^{-1} vs. 0.022 yr^{-1}), reflecting its thinner sapwood, a higher coarse root to bole ratio (0.62 vs. 0.52), and a lower branch to bole ratio (0.11 vs. 0.34).

Finally, decomposition parameters, which affect the rates of decay and turnover, were different for different tree species and different carbon pools. Foliage, fine-roots, coarse-roots, and branch decay rates (0.15 yr^{-1}), as well as sapwood decay rates (0.07 yr^{-1}), were the same for both species. Heartwood decay was slower for Douglas-fir (0.02 yr^{-1}) than for western hemlock (0.07 yr^{-1}). Stable soil decay rates were set at 0.007 yr^{-1} to mimic the relatively high decomposition resistance of this pool. All dead pools transferred material to the stable pools at differing rates. The rate of transfer from the dead foliage pool to the stable foliage pool was 0.057 yr^{-1} , which indicates a relatively fast decomposition rate of the dead

foliage pool. By contrast, the rate of transfer from the dead branch pool to the stable wood pool was 0.003 yr^{-1} , which indicates a slower rate of decomposition for wood pools.

Model Simulation Experiments

We used STANDCARB in 1000-year simulation experiments of artificial landscapes with varying age-class structures, representing a range of possible management regimes: Landscape Y (100% Young), Landscape OG (100% Old-Growth), Landscape AIC (50% young and 50% old, Aggregated Interior Cut), Landscape AIF (50% young and 50% old, Aggregated Interior Forest), Landscape CH (50% young and 50% old, Checkerboard cut), and Landscape AD (50% young and 50% old, Aggregated Directional cut, where the upper half is cut and the lower half remains uncut) (**Figure 4.4**). For landscapes with a simulated harvest regime (all except Landscape OG), STANDCARB was run 2 times, one with a harvest regime of 50 years and one with a harvest regime of 100 years. All harvests occurred after year 500, once the species composition had stabilized. For example, the 100-year harvest patterns were prescribed at years 500, 600, 700, 800, 900, and 1000. Only years 500 to 1000 were used to calculate results. For brevity, only the 100-year simulations will be described here but results for both regimes were similar.

Simulations were run with one of four interactions of light limitations and wind mortality: (1) light limitations OFF and wind mortality OFF, which served as a control, (2) light limitations ON, wind mortality OFF, (3) light limitations OFF

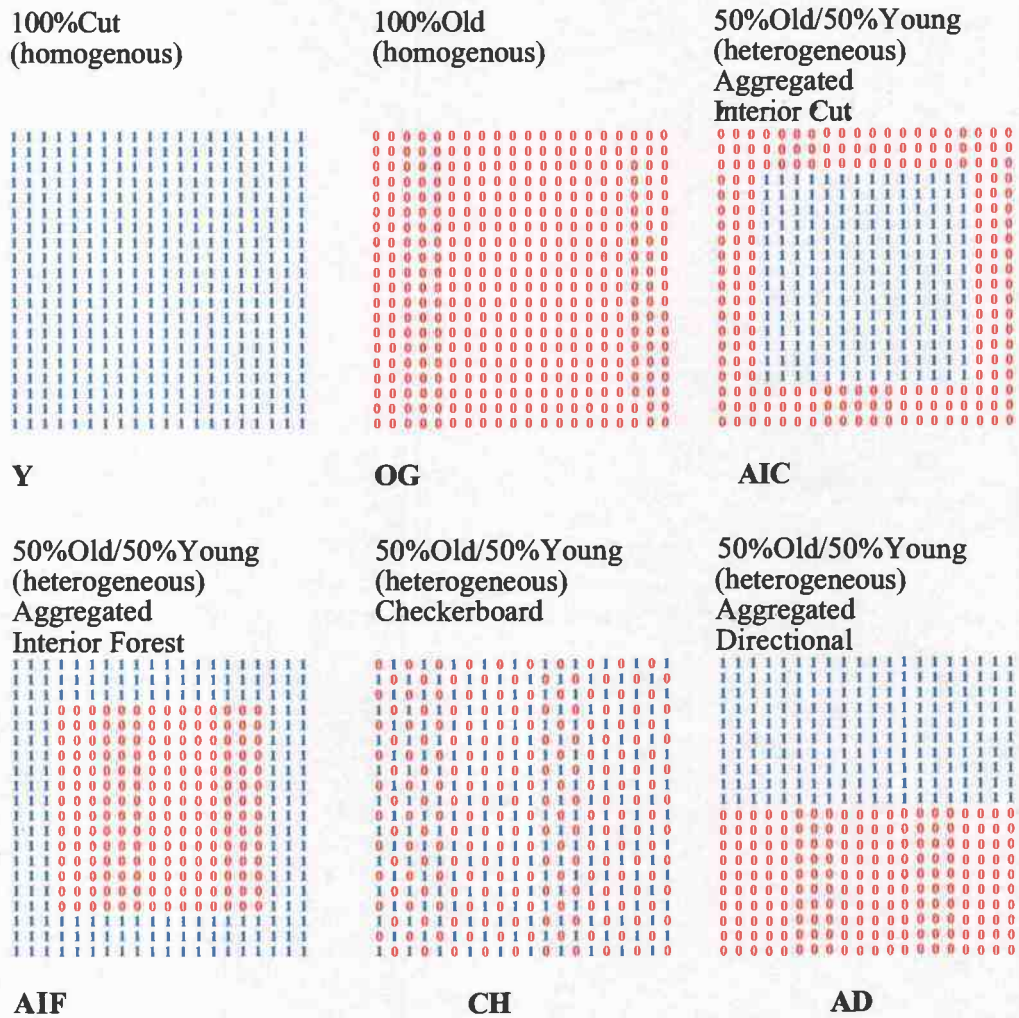


Figure 4.4. Artificial landscape cutting patterns used to drive the model (0=uncut, 1=cut). Each cutting pattern was used for simulations of 100-year and 50-year harvesting regimes. Each pattern describes a landscape with either a homogenous (Y, OG) or heterogeneous (AIC, AIF, CH, AD) patch structure.

and wind mortality ON, and, finally, (4) light limitations ON and wind mortality ON, which simulated the interaction between the processes. For all simulations in which wind mortality was included, simulations were run at k set to 2, 3, 5, or 8.

We tested for statistical significance of emergent behaviors by first identifying the control (or additive) calculation for each case (detailed below and in **Table 4.2**). We then compared the control to the appropriate simulation results, in which the interactions of interest were present. We tested for statistical significance by first calculating the standard deviation from the mean of the five replicate runs of the model for the simulation of interest. It is necessary to account for this expected variability in model results since STANDCARB has stochastic elements. We then compared the mean of the control to that of the simulation. If that difference was greater than two standard deviations, then we considered it to be significant. This is a conservative test since it implies that 95% of the observations do not overlap the mean. If, after accounting for the variability in the model, the mean of the simulation was significantly different from the control, then we considered emergent behaviors to be present.

Stand Scale

To observe the effects of light and wind processes on carbon stores at the stand scale, we were interested in the cell-to-cell interactions within a patch and not the spatial variability between patches. Thus, these comparisons were made in Landscape OG and Landscape Y, which are homogeneous patch-types.

We examined emergent behaviors among 3 types of cell-to-cell interactions at the stand scale: (1) cell-to-cell, (2) cell-to-cell * process, and (3) cell-to-cell * age (Table 4.2). The first interaction (cell-to-cell) reflected the interaction between cells with regard to a certain process, i.e., light or wind. The goal was to determine the relative effect of light and wind on carbon stores, relative to when neither is included.

The second interaction (cell-to-cell * process) reflected the interactions of light and wind processes acting together and not their individual effects. Our assumption was that an additive combination of the effects of light limitations on carbon stores, simulated independently (C_L), and the effects of wind mortality on carbon stores, simulated independently (C_W), should equal the carbon stores when both light and wind processes were included together in the same simulation (C_{LW}). It follows that any difference in carbon stores would be due to an emergent behavior, that is, behavior not predictable by a combination of the processes simulated independently.

The third type of interaction (cell-to-cell * age) reflects the interactions due to the age of the landscape. Simply, we asked whether cell-to-cell interactions are different between Landscape OG and Landscape Y. Our hypothesis was that older landscapes, which exhibit more tree height variability, might result in larger emergent behaviors than young landscapes, which have a more uniform canopy height distribution. Emergent behaviors are indicated as significant differences between results of Landscape OG and those of Landscape Y.

The establishment and persistence of a species in the stand is a function of

Table 4.2. Description of methodology used to test for emergent behaviors at various levels of spatial interaction. C_L = carbon (C) stores for simulation with only light limitations included, C_W = carbon stores for simulation with only wind mortality included, C_{LW} = carbon stores when both were included, and C_\emptyset = carbon stores when neither process was included in the simulation experiments. OG is the old-growth age-class structure; Y is the young age-class structure; OG*Y is any heterogeneous age-class structure, representing AIC, AIF, CH, and AD (Figure 4.3).

Level of Interaction	Control	Treatment	Emergent Behaviors Question
Cell-to-cell	$C_{\emptyset-OG}$ (or $C_{\emptyset-Y}$) $C_{\emptyset-OG}$ (or $C_{\emptyset-Y}$)	C_{W-OG} (or C_{W-Y}) C_{L-OG} (or C_{L-Y})	Do cells interact within homogenous landscapes?
Cell-to-cell * process	$(C_{W-OG} / C_{\emptyset-OG}) * (C_{L-OG} / C_{\emptyset-OG})$ $(C_{W-Y} / C_{\emptyset-Y}) * (C_{L-Y} / C_{\emptyset-Y})$	$C_{LW-OG} / C_{\emptyset-OG}$ $C_{LW-Y} / C_{\emptyset-Y}$	Do the processes interact within homogenous landscapes?
Cell-to-cell * age	C_{W-OG} (or C_{W-Y}) C_{L-OG} (or C_{L-Y}) C_{LW-OG} (or C_{LW-Y})	C_{W-Y} (or C_{W-OG}) C_{L-Y} (or C_{L-OG}) C_{LW-Y} (or C_{LW-OG})	Do the process effects vary with landscape age?
Patch-to-patch	$(C_{W-OG} + C_{W-Y})/2$ $(C_{L-OG} + C_{L-Y})/2$ $(C_{LW-OG} + C_{LW-Y})/2$	C_{W-OG*Y} C_{L-OG*Y} $C_{LW-OG*Y}$	Do patches interact within heterogeneous landscapes?
Patch-to-patch * process	$(C_{L-OG*Y} / C_{\emptyset-OG*Y}) * (C_{W-OG*Y} / C_{\emptyset-OG*Y})$	$C_{LW} / C_{\emptyset-OG*Y}$	Do the processes interact within heterogeneous landscapes?
Patch-to-patch * structure	average (C_{W-OG*Y}) average (C_{L-OG*Y}) average $(C_{LW-OG*Y})$	C_{W-OG*Y} C_{L-OG*Y} $C_{LW-OG*Y}$	Do the process effects vary with patch age structure?

the available light and mortality rates and therefore, we expected, would be determined by the particular light and wind processes included in the simulation. In particular, the species composition of a simulation would be determined by whether or not light and wind processes were allowed to interact between cells in a homogenous stand. Growth, respiration, and decomposition rates are parameterized differently for different species in STANDCARB and, as a result, carbon stores are likely to be affected by a change in species composition.

Landscape Scale

To determine whether patch-to-patch interactions caused emergent behavior at the landscape scale, we used artificial landscapes with a heterogeneous patch structure. A patch ranged in size from just one cell (0.03 ha) for Landscape CH to 50 % of the cells in the landscape, or approximately 5 ha for Landscapes AD, AIC, AIF. We examined 3 types of patch-to-patch interactions: (1) patch-to-patch, (2) patch-to-patch * process, and (3) patch-to-patch * structure (**Table 4.2**). The first interaction (patch-to-patch) reflects the interaction of patches within heterogeneous landscapes with regard to a certain process. Our goal was to determine whether carbon storage in heterogeneous landscapes is equal to the average of independent simulations of Landscape OG and Landscape Y, since heterogeneous landscapes are simply an equal mixture of old and young age-classes.

The second type of interaction (patch-to-patch * process) reflects the interaction of processes in heterogeneous landscapes. This type of interaction is

similar to the cell-to-cell * process interaction, except that we are now concerned with heterogeneous rather than homogenous landscapes.

The third type of interaction (patch-to-patch * structure) reflects possible emergent behaviors due to the effect of spatial structure, i.e., the arrangement of patches on the landscape. To test for emergent behaviors, we compare each heterogeneous landscape to the mean of all the heterogeneous landscapes. If there are no emergent behaviors, each landscape should be approximately equal to the mean. Differences from the mean, therefore, reflect emergent behaviors caused by the spatial arrangement of the patches on the landscape.

To further explore patch-to-patch interactions, we modified STANDCARB to predict average carbon across "zones" of the simulated stand. The user can designate a cell or group of cells as a unique zone. Carbon stores in each zone are then the average of the carbon stores from each cell in that zone. Here we present results from Landscape AD, in which a zone represents one row of cells (**Figure 4.5**). In this way, average carbon stores could be output horizontally across the landscape, allowing modeled responses to be evaluated spatially between patches, i.e., from a cut region to an uncut region (across an "edge"). To determine whether carbon was changed at the edge, we calculated the average live and dead carbon for years 500 to 1000 (in foliage, fine-roots, branches, sapwood, heartwood, coarse-roots, and heart-rot pools), as well as their totals in each of the 20 zones. In Landscape AD, half the stand was cut every 100 years and half remained uncut. Therefore, 10 zones represented re-growing vegetation from the disturbance event (zones C0 through C9), while 10 zones represented old-growth forest (zones U0

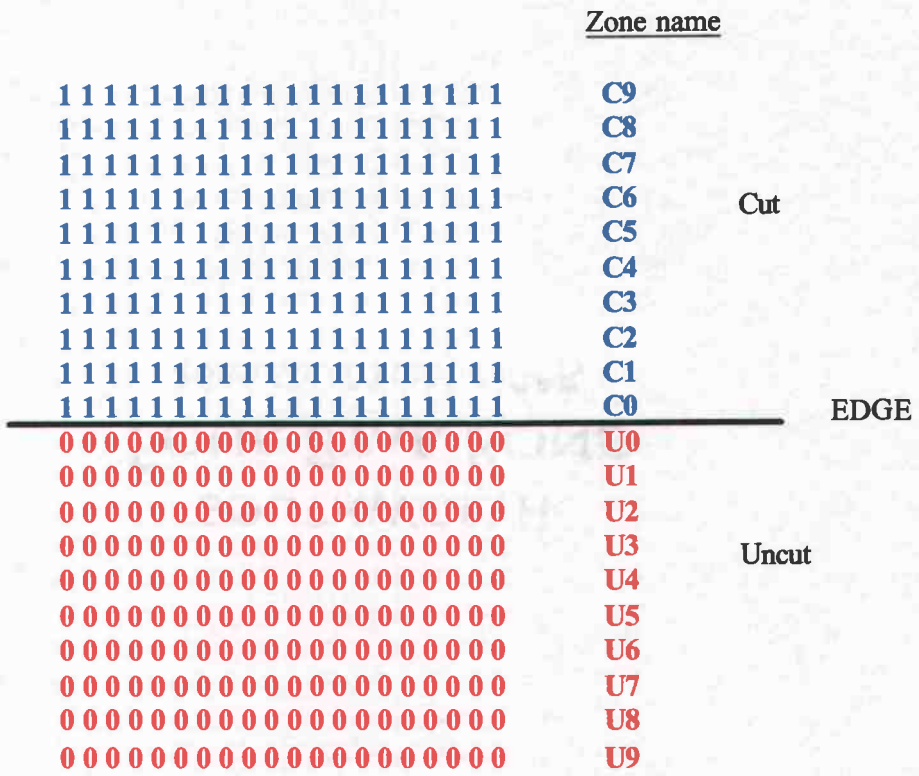


Figure 4.5. Example of the zones used to calculate carbon stores within Landscape AD.

through U9). The border of the patches was thus between zone C0 and zone U0, although the effect to which the carbon stores were affected by the processes was examined in zones “deeper” within each patch type.

Results

Cell-to-Cell Patterns in Carbon Stores

Light and wind processes within homogenous patches affected carbon stores differently. For example, light limitations were more important than wind mortality in changing total forest carbon until wind mortality was set very high ($k=8$) (**Figure 4.6**). In Landscape OG, light limitations caused a reduction of total carbon of 369 Mg C ha^{-1} from the control ($1204 \text{ Mg C ha}^{-1}$ minus 835 Mg C ha^{-1}) (**Table 4.3**). When wind mortality was included, total carbon was reduced by 114 Mg C ha^{-1} ($k=2$), 213 Mg C ha^{-1} ($k=3$), 332 Mg C ha^{-1} ($k=5$), and 434 Mg C ha^{-1} ($k=8$). Thus, at low k values, light limitations reduced carbon stores 2 to 3 times more than wind mortality; as k was increased, the effect of wind mortality on decreasing carbon stores became similar to the effect of light limitations.

When wind was included in the simulations, total carbon stores appeared less responsive than if live or dead stores were analyzed separately, due to the compensatory dynamics of live and dead stores with regard to wind mortality (**Figure 4.7**). Specifically, in all cases, when light-limitations were included, there was a decrease in both live and dead stores; yet, when wind mortality was included, live carbon decreased but dead carbon *increased* relative to the control.

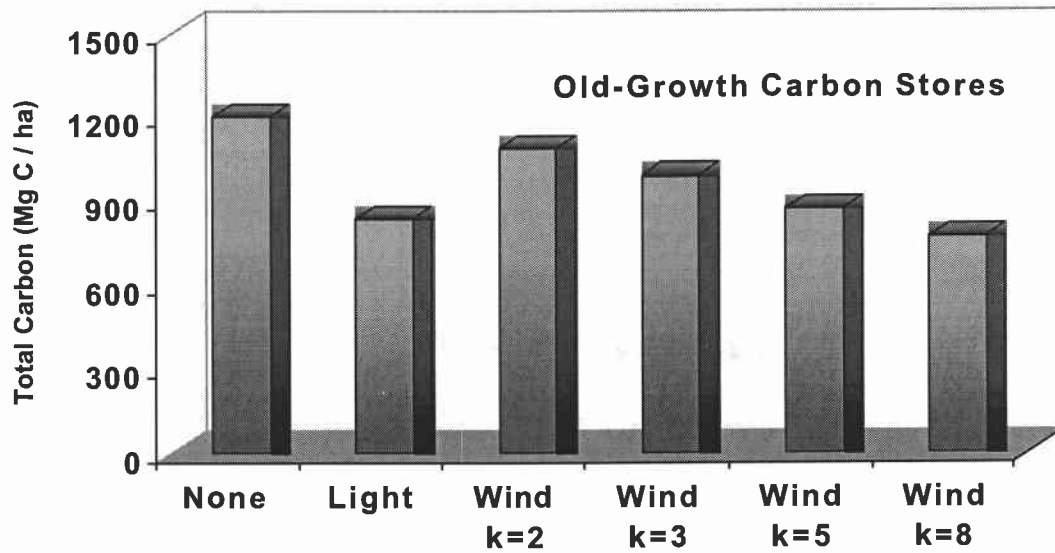


Figure 4.6. Total (live+dead+stable) carbon stores in Landscape OG as a function of processes included in the simulations: None (neither light limitations or wind mortality included), Light (only light limitations included), Wind (only wind mortality included, at various levels of k)

Table 4.3. The effect of Neighbor functions (wind and/or light) on average carbon stores (calculated for years 500 through 1000) for different landscape cutting patterns (OG = old-growth, Y = young, AIC = aggregated interior cut, AIF = aggregated interior forest, CH = checkerboard, AD=aggregated directional; **Figure 4.3**). Standard deviations are in parentheses, rounded to nearest whole number. Only results from the 100-year cutting patterns are shown.

Neighbor	k value	Landscape					
		OG	Y	AIC	AIF	CH	AD
LIVE							
None	na	825(12.5)	248(1.1)	540(4.7)	542(9.4)	541(14.7)	541(3.6)
Light	na	572(2.4)	245(0.4)	409(6.0)	395(6.2)	415(9.9)	402(10.9)
Wind	2	655(3.2)	231(0.4)	433(5.2)	439(2.7)	419(7.9)	426(6.3)
Wind	3	526(8.9)	216(0.6)	361(6.2)	366(7.2)	347(3.6)	361(4.7)
Wind	5	382(3.8)	171(0.3)	253(3.4)	260(3.2)	238(2.4)	281(2.7)
Wind	8	273(2.1)	148(0.1)	191(2.8)	195(1.7)	182(2.1)	216(1.2)
Light+Wind	2	475(6.5)	239(0.5)	354(4.6)	341(5.7)	350(3.9)	350(3.3)
Light+Wind	3	409(6.1)	233(0.5)	317(4.5)	310(5.0)	314(5.5)	312(3.6)
Light+Wind	5	341(5.9)	196(0.4)	212(1.6)	211(2.7)	208(1.8)	273(4.4)
Light+Wind	8	283(2.3)	184(1.2)	183(1.0)	183(1.6)	179(0.9)	237(2.0)
DEAD							
None	na	288(3.6)	164(0.6)	226(1.6)	226(4.3)	225(4.9)	223(3.2)
Light	na	186(2.8)	158(1.3)	161(1.1)	154(1.3)	158(3.2)	162(2.7)
Wind	2	336(1.8)	182(0.2)	261(2.8)	257(2.1)	265(1.5)	262(2.4)
Wind	3	363(3.7)	198(1.1)	281(1.6)	278(3.1)	284(3.4)	281(1.8)
Wind	5	384(1.1)	205(0.6)	298(2.2)	296(1.9)	301(0.9)	303(2.4)
Wind	8	388(1.0)	223(0.2)	307(1.0)	306(1.1)	307(0.2)	316(1.4)
Light+Wind	2	194(5.1)	163(1.4)	173(1.5)	166(3.9)	172(2.4)	170(3.2)
Light+Wind	3	199(5.3)	168(1.2)	180(1.2)	173(2.5)	180(1.6)	179(2.3)
Light+Wind	5	211(2.9)	156(0.5)	159(1.1)	153(1.6)	159(1.2)	189(2.8)
Light+Wind	8	232(1.2)	167(0.8)	175(0.8)	169(1.0)	173(0.9)	205(1.2)

Table 4.3. (Continued)

Neighbor	k value	Landscape					
		OG	Y	AIC	AIF	CH	AD
STABLE							
None	na	90(0.3)	72(0.4)	81(0.3)	81(0.5)	81(0.5)	81(0.3)
Light	na	81(0.4)	70(0.1)	72(0.3)	71(0.4)	72(0.5)	73(0.6)
Wind	2	97(0.5)	73(0.2)	85(0.6)	85(0.4)	86(0.2)	85(0.3)
Wind	3	101(0.5)	74(0.2)	88(0.2)	88(0.3)	89(0.2)	88(0.4)
Wind	5	106(0.2)	59(0.1)	70(0.4)	70(0.3)	71(0.2)	91(0.2)
Wind	8	109(0.1)	61(0.1)	72(0.2)	72(0.1)	72(0.1)	94(0.3)
Light+Wind	2	84(0.7)	70(0.2)	76(0.1)	75(0.8)	76(0.4)	76(0.5)
Light+Wind	3	86(1.4)	71(0.3)	79(0.5)	76(0.8)	79(0.1)	78(0.5)
Light+Wind	5	91(1.2)	52(0.1)	50(0.3)	49(0.2)	49(0.3)	81(0.8)
Light+Wind	8	96(0.5)	53(1.0)	52(0.3)	51(0.1)	51(0.2)	84(0.4)
TOTAL							
None	na	1203(16.5)	484(2.2)	847(6.6)	848(14.1)	847(20.1)	845(7.1)
Light	na	839(5.5)	473(1.9)	643(7.4)	620(7.9)	646(13.5)	636(14.2)
Wind	2	1089(5.4)	487(0.8)	780(8.6)	781(5.2)	770(9.5)	773(8.9)
Wind	3	991(13.1)	488(1.9)	730(8.0)	734(6.5)	720(7.3)	730(6.9)
Wind	5	871(5.1)	435(1.0)	621(6.0)	626(5.4)	610(3.5)	675(5.3)
Wind	8	770(3.2)	432(0.5)	571(4.1)	573(2.9)	562(2.4)	626(2.9)
Light+Wind	2	753(12.3)	473(2.1)	602(6.2)	582(10.4)	598(6.6)	595(7.0)
Light+Wind	3	695(12.8)	471(2.0)	576(6.2)	560(8.2)	572(7.1)	569(6.5)
Light+Wind	5	643(10.0)	403(1.0)	421(3.0)	414(4.5)	415(3.3)	544(8.0)
Light+Wind	8	610(3.9)	404(1.4)	410(2.0)	403(2.7)	403(1.9)	527(3.6)

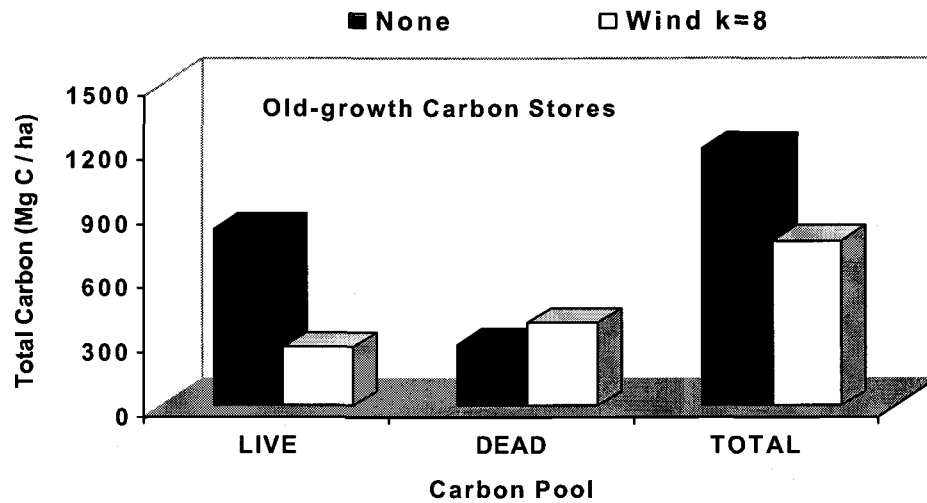


Figure 4.7. Old-growth carbon stores in live, dead, and total carbon pools as a function of simulations with either no light limitations or wind mortality (None), or simulations with wind mortality set to $k=8$ (Wind $k=8$).

For instance, in Landscape OG, when wind mortality was included independently, live carbon decreased 552 Mg C ha^{-1} (825 Mg C ha^{-1} for the control to 273 Mg C ha^{-1} when k was set to 8) (Table 4.3) and dead carbon increased 100 Mg C ha^{-1} (288 Mg C ha^{-1} for the control to 388 Mg C ha^{-1} when k was set to 8). Thus, the change in total carbon stores (after accounting for the small change in stable pools) was 433 Mg C ha^{-1} . We initially tested emergent behaviors for each of the live, dead, stable, and total pools. For simplicity, only tests for total carbon will be presented in the results, although it should be recognized that these integrate the differences in live, dead, and stable stores.

Cell-to-Cell Emergent Behaviors

For all simulations in Landscape OG, carbon stores were significantly different from the control (e.g., after accounting for 95 % of the model variation) (Figure 4.8). When only light limitations were included, total carbon stores were reduced 30.3 % (standard deviation (SD) = 1.3 %) from the control. When only wind mortality was included (at k set to 8), carbon stores were reduced by 36.0 % (SD = 0.8 %). When both light limitations and wind mortality were included, carbon stores were reduced by approximately 49.3 % (SD = 1.3%) ($k = 8$).

In contrast, emergent behaviors in Landscape Y were not consistently observed. For example, when only light limitations were included, emergent behaviors were not significant. When wind mortality was included, results were significant only when k was set to 5 or greater. The largest reduction

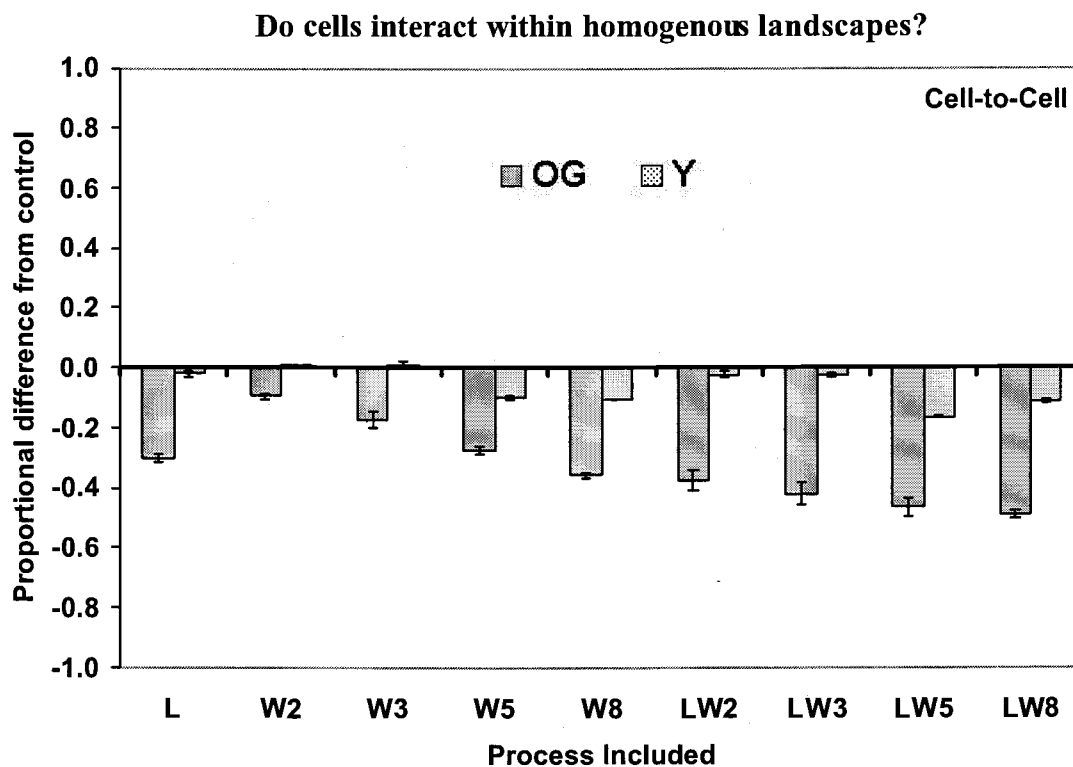


Figure 4.8. Emergent behaviors due to interactions at the cell-to-cell level. Values represent the proportional difference of the treatments from the control. The control is defined in **Table 4.2**. Values different from 0 reflect emergent behaviors. Error bars represent two standard deviations from the mean of five repetitions for each simulation.

(approximately $16.6\% \pm 0.5\%$) was when light and wind were both included and k was set to 5.

*Cell-to-Cell * Process Patterns in Species Dynamics*

Species composition, as evidenced by the number of upper trees in the canopy, was affected by whether light limitations or wind mortality was included. When wind mortality was modeled in the absence of light limitations, there was a sinusoidal pattern in species dominance in the upper canopy through time, the amplitude of which increased as the k value increased (**Figure 4.9**). Western hemlock first appeared in the canopy after canopy closure, due to gap formation of the Douglas-fir. The sinusoidal pattern of species dominance continued through the simulation since both Douglas-fir and western hemlock were able to re-enter the upper canopy due to advanced regeneration in the lower tree layer. With higher k -values, these oscillations resulted in increasing oscillations of carbon stores (**Figure 4.10**). Typically, Douglas-fir would not be able to re-enter the canopy due to its higher light requirements for establishment. Indeed, with light limitations included, Douglas-fir never received enough light to re-enter the upper canopy after the initial canopy closure (**Figure 4.11**) and the canopy continued to be dominated by western hemlock. The timing of the initial transition from Douglas-fir to western hemlock was also determined by which processes were allowed to interact. When k was increased from 3 to 8 the transition to western hemlock from Douglas-fir was about 50 years earlier, indicating that western hemlock was able to dominate earlier by replacing Douglas-fir more quickly, essentially hastening the succession

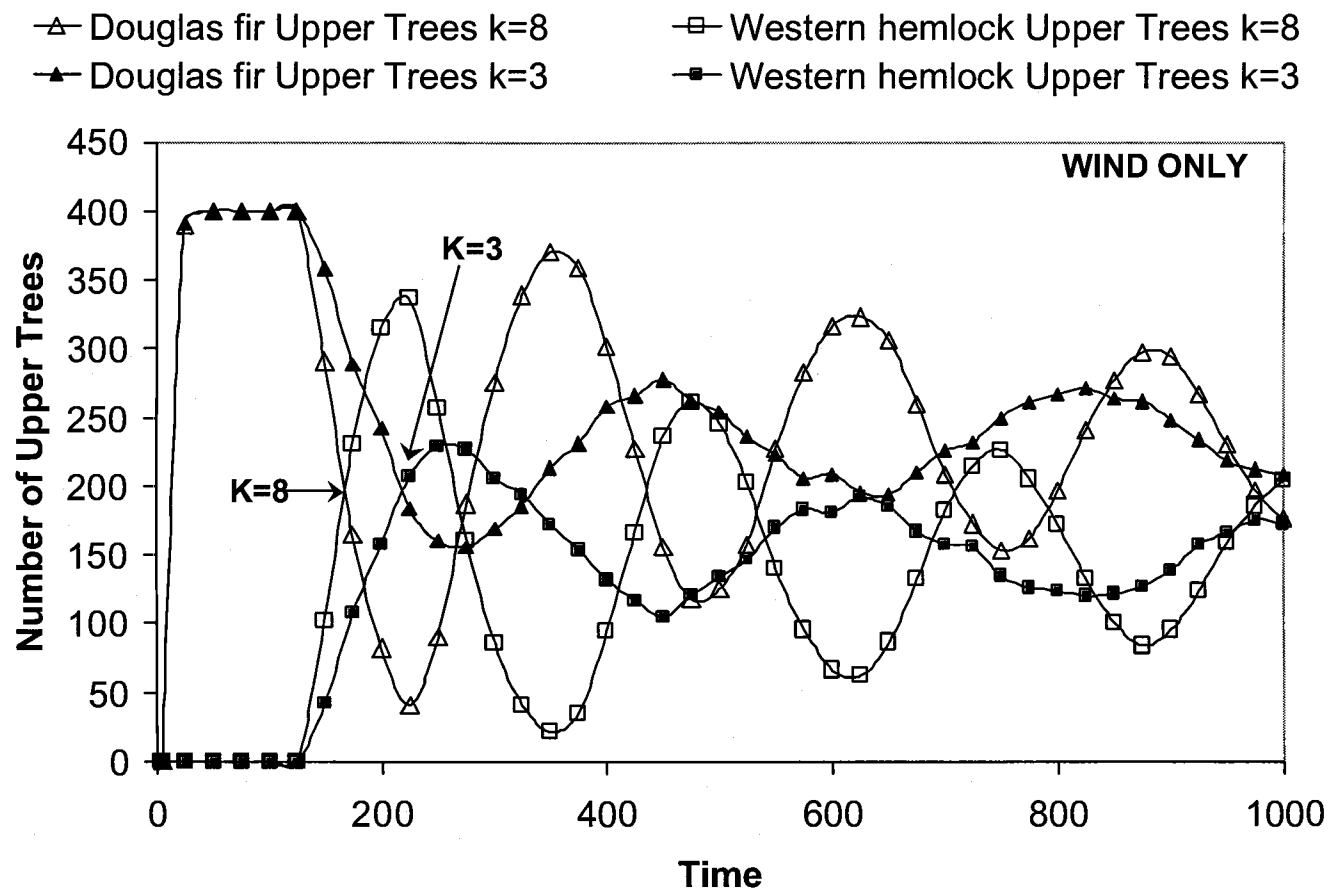


Figure 4.9. Effect of increasing k values on the number of upper trees for PSME (Douglas-fir, *Pseudotsuga menziesii*) and TSHE (western hemlock, *Tsuga heterophylla*) for simulations with only wind mortality included.

Landscape OG

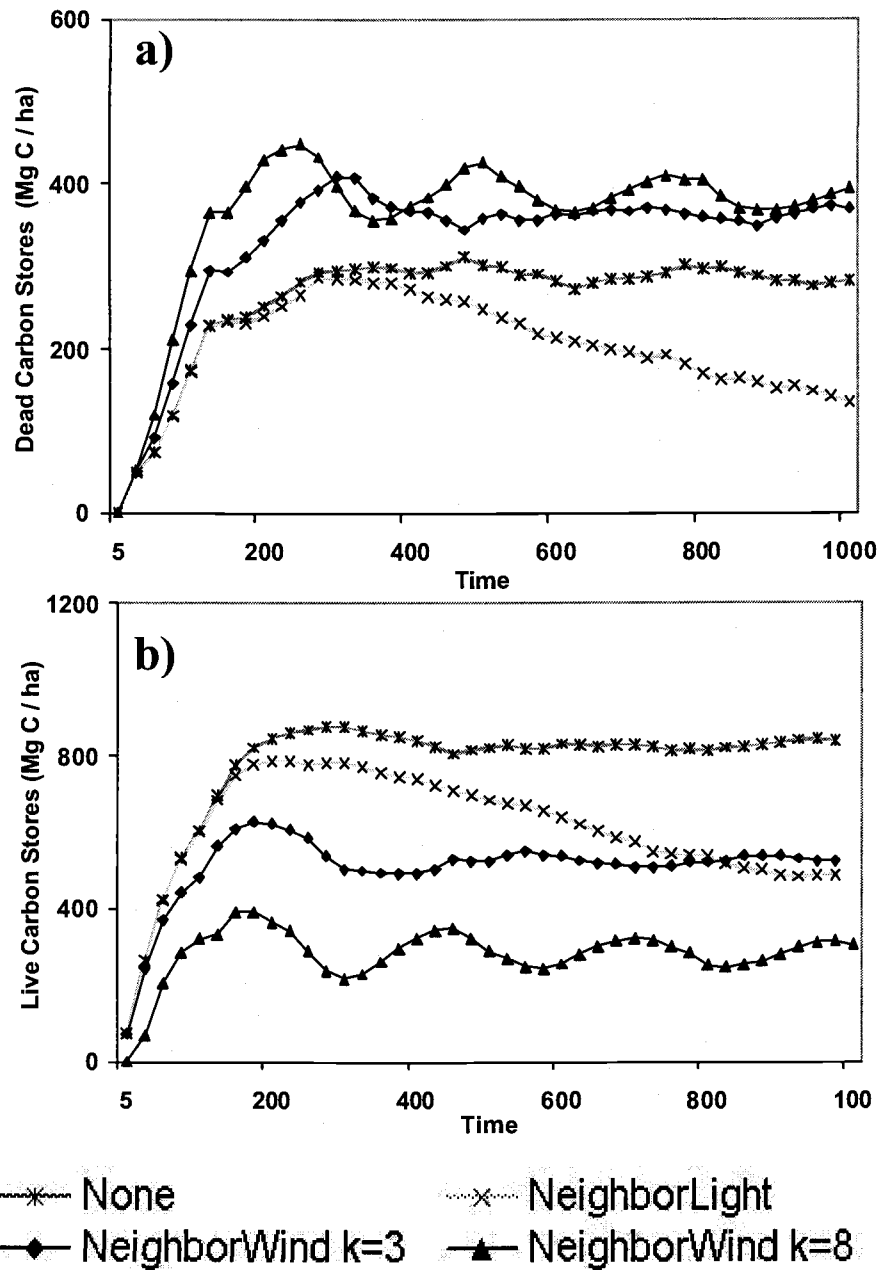


Figure 4.10. The trend in (a) total dead and (b) total live carbon through time for simulations with only wind mortality included (k set to 3 or 8), only light limitations included, or neither included (None) for Landscape OG (old-growth). Note the different y-axis range between live and dead carbon.

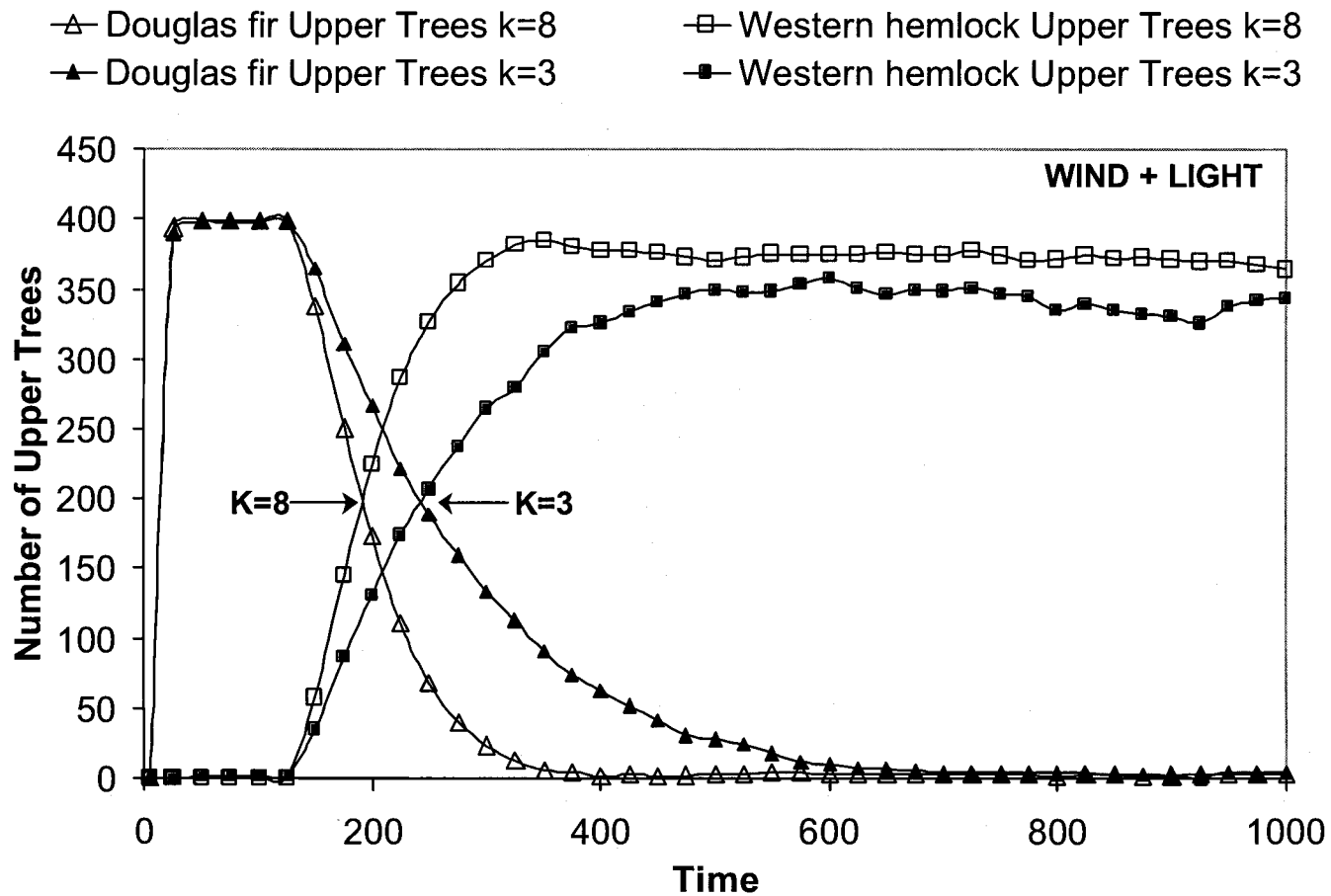


Figure 4.11. Effect of increasing k values on the number of upper trees for PSME (Douglas-fir, *Pseudotsuga menziesii*) and TSHE (western hemlock, *Tsuga heterophylla*) for simulations with both light limitations and wind mortality included.

process (**Figure 4.9** and **Figure 4.11**). The effect of this transition was not due to light limitations since the pattern developed both when light limitations were included as well as when they were not; rather, the earlier transition was most likely due to the faster removal of the upper canopy tree-species at higher levels of wind mortality.

Cell-to-Cell * Process Emergent Behaviors

In this test, significant differences from the control were apparent when k was set to 5 or 8 but were not significant at lower levels of wind mortality (**Figure 4.12**). The direction of these differences (less than or greater than the control) differed between the two landscapes. In Landscape OG, carbon stores were 5.8 % (± 3.1 %) greater when the processes interacted when k was set to 5, and 13.7 % (± 1.3 %) greater when k was set to 8, compared to that calculated using the additive approach. In contrast, in Landscape Y, carbon stores were 5.2 % (± 0.5 %) lower when k was set to 5 and only 1.6 % (± 0.5 %) higher when k was set to 8.

Cell-to-Cell * Age Patterns in Carbon Stores

When there was a regular harvest event across the stand (Landscape Y), the effect of light limitation and wind mortality processes was reduced compared to the older landscape (Landscape OG). For example, in Landscape OG, both light limitations and wind mortality reduced carbon stores from the control, when neither

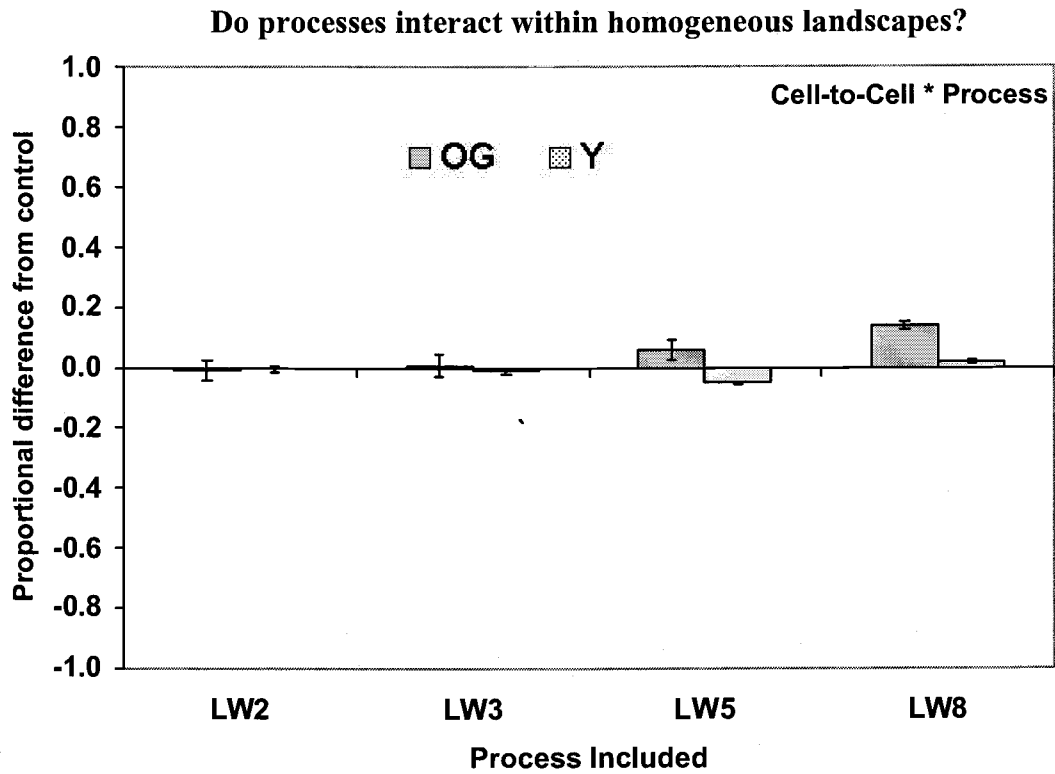


Figure 4.12. Emergent behaviors due to the cell-to-cell * process interactions. Values represent the proportional difference of the treatments from the control. The control is defined in **Table 4.2**. Values different from 0 reflect emergent behaviors. Error bars represent two standard deviations from the mean of five repetitions for each simulation.

was included (**Figure 4.10**). However, in Landscape Y (**Figure 4.13**), the simulations that included light limitations are indistinguishable after year 500 from the control, indicating that light interactions were less pronounced in the younger landscape than the older landscape.

Cell-to-Cell * Age Emergent Behaviors

Emergent behaviors resulting from cell-to-cell interactions in Landscape OG were higher than those in Landscape Y for all simulations (**Figure 4.14**). Emergent behaviors were 28.7 % (± 0.2 %) higher in Landscape OG than Landscape Y when only light was included and between 30.0 % (± 0.02 %) and 40.0 % (± 0.2 %) higher when both light and wind interacted.

Patch-to-Patch Patterns Across Edge Zones

Results across edge zones in Landscape AD showed that carbon stores were affected both by light limitations and wind mortality, indicating that patch-to-patch interactions were important. The relative effect of these processes at the edge was different depending on the type of interaction included and the pools considered (i.e., live, dead, stable, or total).

Landscape Y

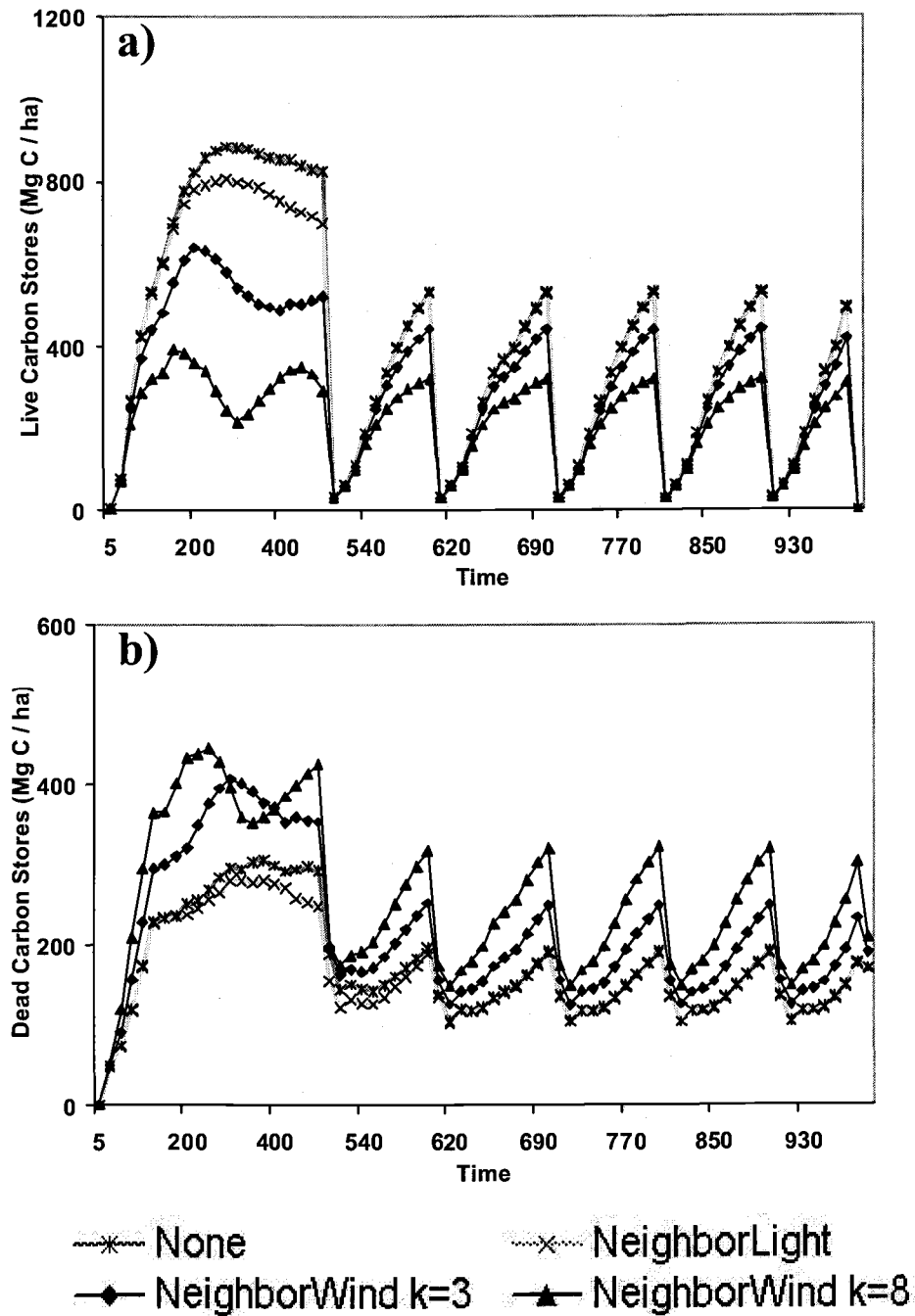


Figure 4.13. The trend in (a) total live and (b) total dead carbon through time for simulations with only wind mortality included (k set to 3 or 8), only light limitations included, or neither included (None) for Landscape Y (young). Note the different y-axis range between live and dead carbon.

Does the process effect vary with landscape age?

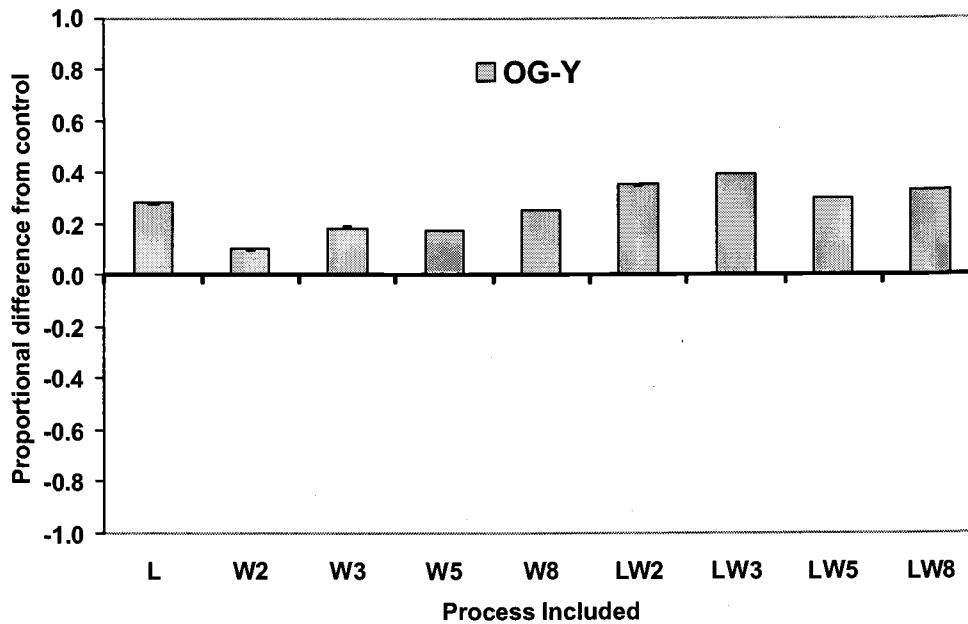


Figure 4.14. Emergent behaviors due to the cell-to-cell * age interactions. Values represent the proportional difference of the treatments from the control. The control is defined in **Table 4.2**. Values different from 0 reflect emergent behaviors. Error bars represent two standard deviations from the mean of five repetitions for each simulation.

Live Stores

In the cut and uncut patch, light limitations and wind mortality processes had different effects on live carbon across all zones (**Figure 4.15, 4.16, and 4.17**). In the cut patch, live carbon stores for all pools were decreased for at least 3 zones from the edge (equivalent to approximately 50 m) when only light limitations were included. In contrast, when only wind mortality was included, live carbon stores across the cut patch were not affected (at any k-value).

In the uncut patch, live carbon in zone 'U0' (one cell width into the uncut patch) was greater than the average carbon stores across all zones in the uncut patch when only light limitations were included. This is presumably due to the increase of light at the edge. Yet, when only wind mortality was included, the live carbon stores decreased for all pools in zone 'U0', due to the increased exposure to wind at the edge. As an example of the effect of wind mortality, the average store of live heartwood in the uncut patch across all zones was $193 \pm 5.4 \text{ Mg C ha}^{-1}$ but was only 181 Mg C ha^{-1} at the edge, a difference of approximately 12 Mg C ha^{-1} . As k was increased, these differences ranged from 16 to 23 Mg C ha^{-1} (**Figure 4.16a**). Sapwood also decreased between 6 and 9 Mg C ha^{-1} at the edge with wind mortality, depending on the k value (**Figure 4.16b**). When light limitations and wind mortality were both included, there was an increase in live carbon near the edge of the uncut patch, indicating the dominating effect of light, despite decreases in live carbon stores due to wind mortality.

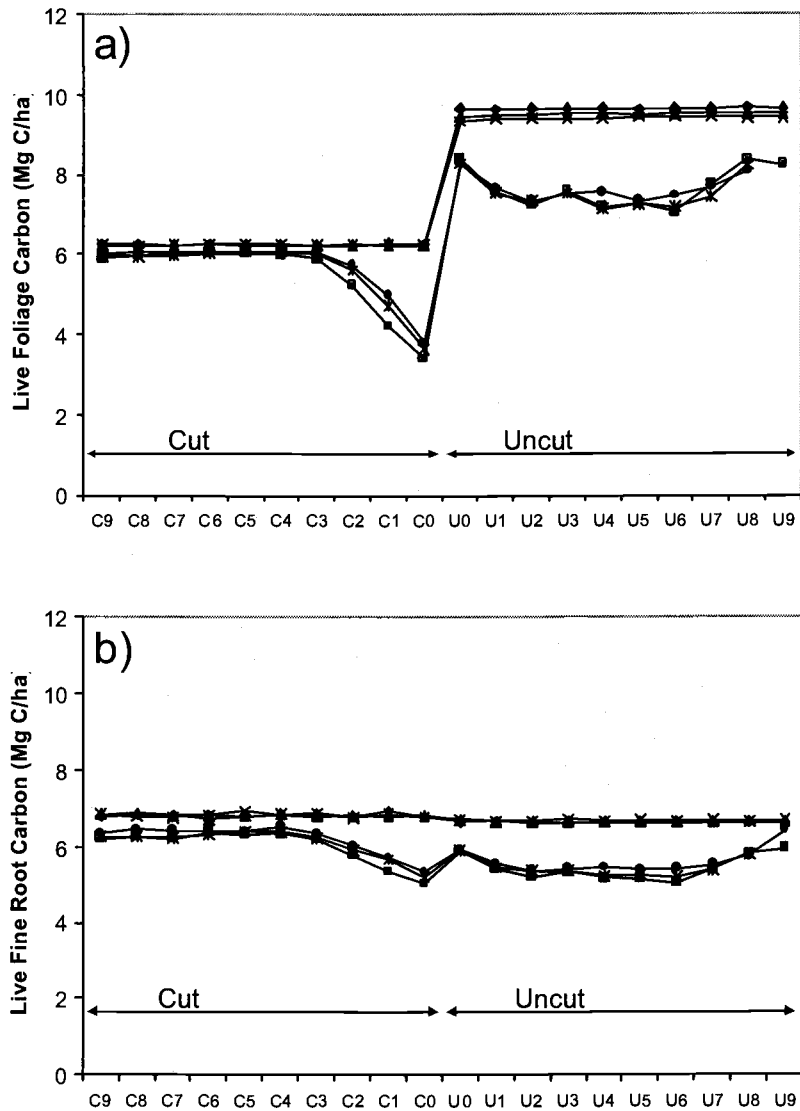
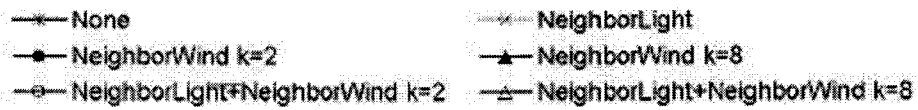


Figure 4.15. Live carbon by zone for different light and wind simulations for (a) foliage and (b) fine-root pools in Landscape AD. Zones C0 to C9 are cut every 50 years after year 500, while zones U0 to U9 remain uncut. Results are the average for years 500 to 1000 for each zone.

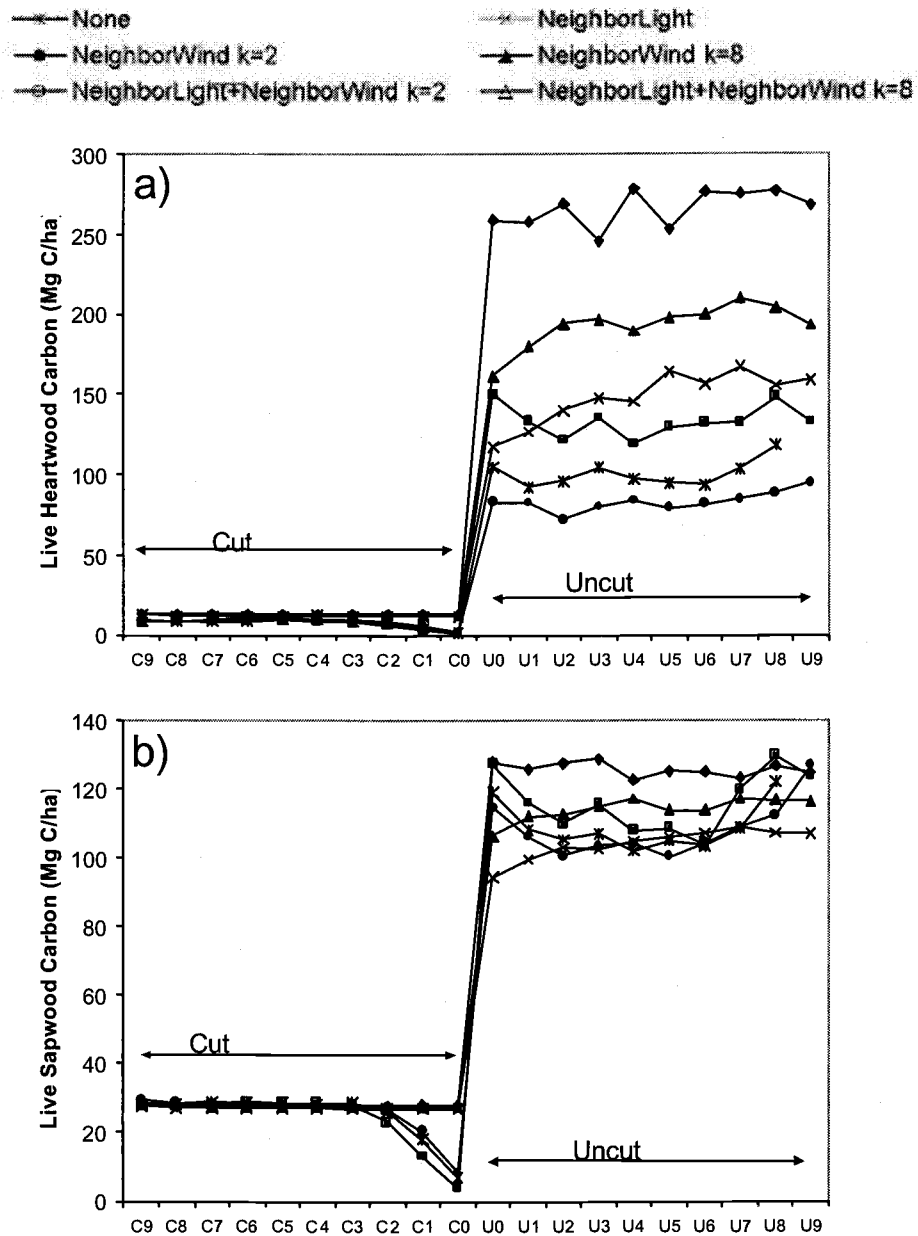


Figure 4.16. Live carbon by zone for different light and wind simulations for (a) heartwood and (b) sapwood pools in Landscape AD. Zones C0 to C9 are cut every 50 years after year 500, while zones U0 to U9 remain uncut. Results are the average for years 500 to 1000 for each zone. Note different y-axis scales.

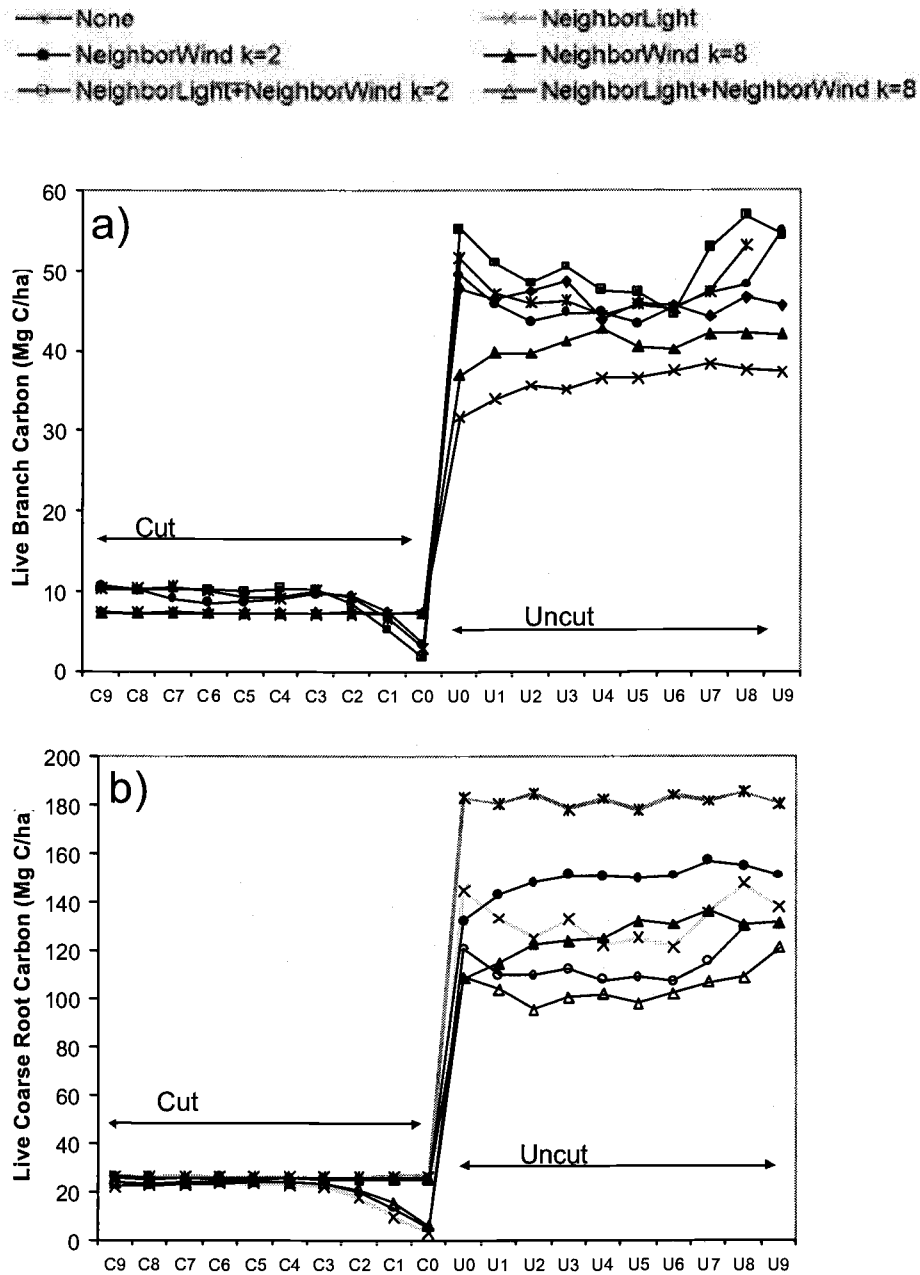


Figure 4.17. Live carbon by zone for different light and wind simulations for (a) branch and (b) coarse root pools in Landscape AD. Zones C0 through C9 are cut every 50 years after year 500, while zones U0 through U9 remain uncut. Results are the average for years 500 to 1000 for each zone. Note different y-axis scales.

Dead Stores

Dead carbon pools in the cut patch showed a decrease within three zones of the edge when only light limitations were included (**Figure 4.18, 4.19, and 4.20**). When only wind mortality was included, there were no observable differences at the edge, although the absolute amount of dead carbon was higher than for the control (no light or wind) for all zones in the cut patch, due to the increased mortality.

Dead carbon pools in the uncut patch increased near the edge when wind mortality was included, although this effect was only apparent for dead sapwood (**Figure 4.19b**) and, similar to the live pools, was observable for only one zone width. Dead sapwood increased from an average of $57 \pm 3.6 \text{ Mg C ha}^{-1}$ across all zones to 65 Mg C ha^{-1} in zone 'U0' when k was set to 2. When k was set to 8, dead sapwood averaged $124 \text{ Mg C ha}^{-1} \pm 7.1 \text{ Mg C ha}^{-1}$ across all zones but was 141 Mg C ha^{-1} in zone 'U0'. This is an increase near the edge of almost 17 Mg C ha^{-1} . Differences between the average carbon across all zones and the carbon in zone 'U0' were not significant for other pools, averaging around 1 Mg C ha^{-1} . When both light limitations and wind mortality were included, carbon stores were generally within the range of carbon stores in simulations when each process was simulated independently. However, when the processes interacted at k set to 8, dead branch carbon storage was consistently higher for the uncut patch, and somewhat higher at the edge of the cut patch, compared to other pools (**Figure 4.20a**).

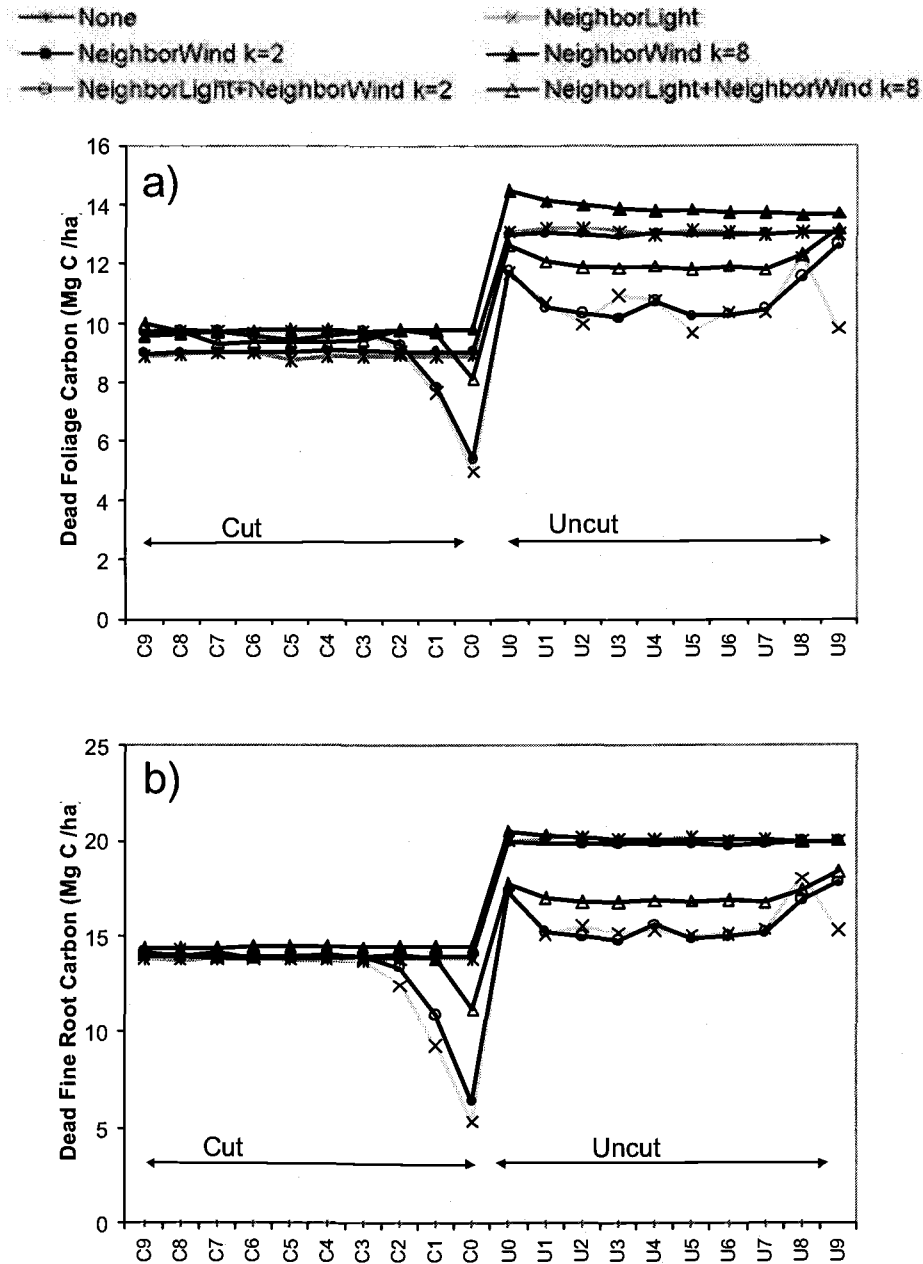


Figure 4.18. Dead carbon by zone for different light and wind simulations for (a) foliage, and (b) fine root carbon pools for Landscape AD. Zones C0 through C9 are cut every 50 years after year 500, while zones U0 through U9 remain uncut. Results are the average for years 500 to 1000 for each zone. Note different y-axis scales.

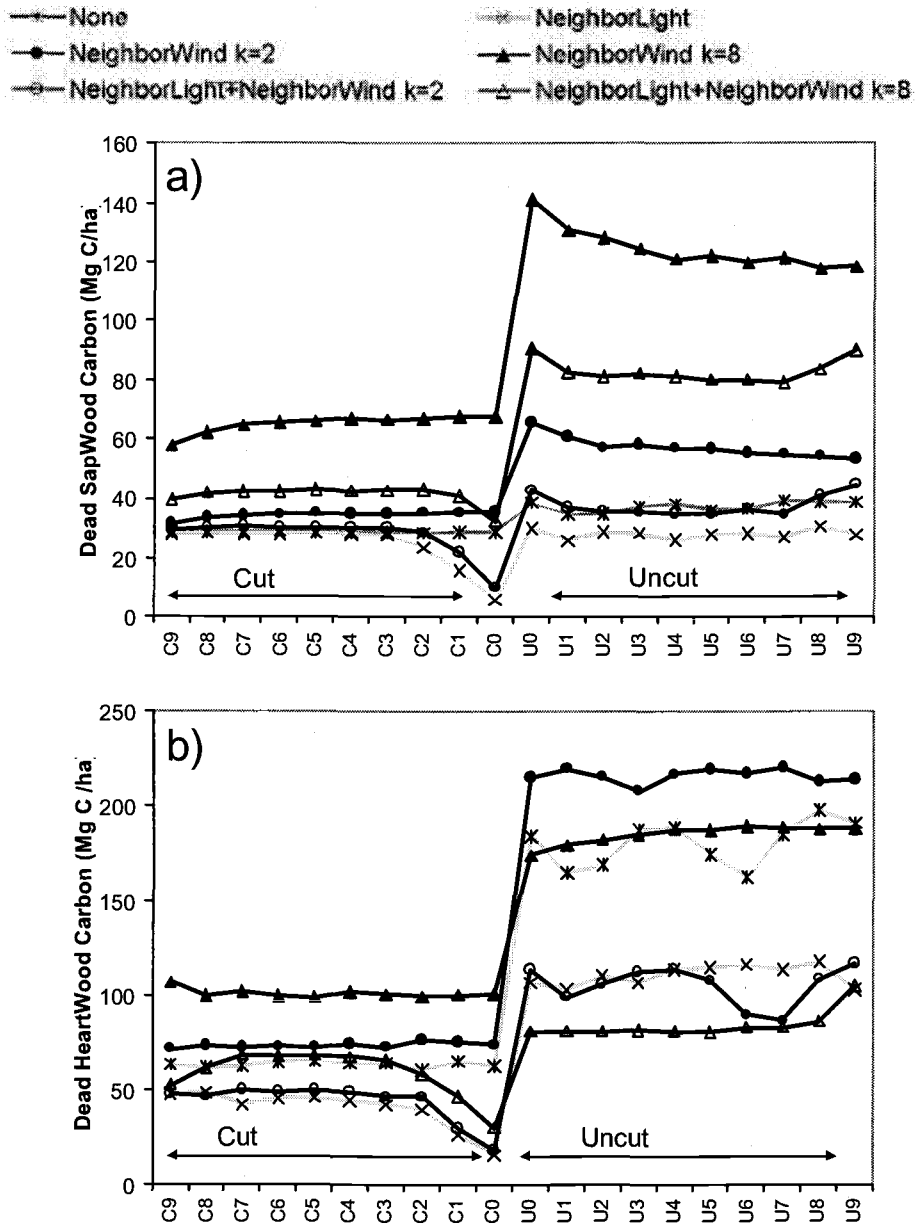


Figure 4.19. Dead carbon by zone for different light and wind simulations for (a) sapwood and (b) heartwood pools in Landscape AD. Zones C0 through C9 are cut every 50 years after year 500, while zones U0 through U9 remain uncut. Results are the average for years 500 to 1000 for each zone. Note different y-axis scales.

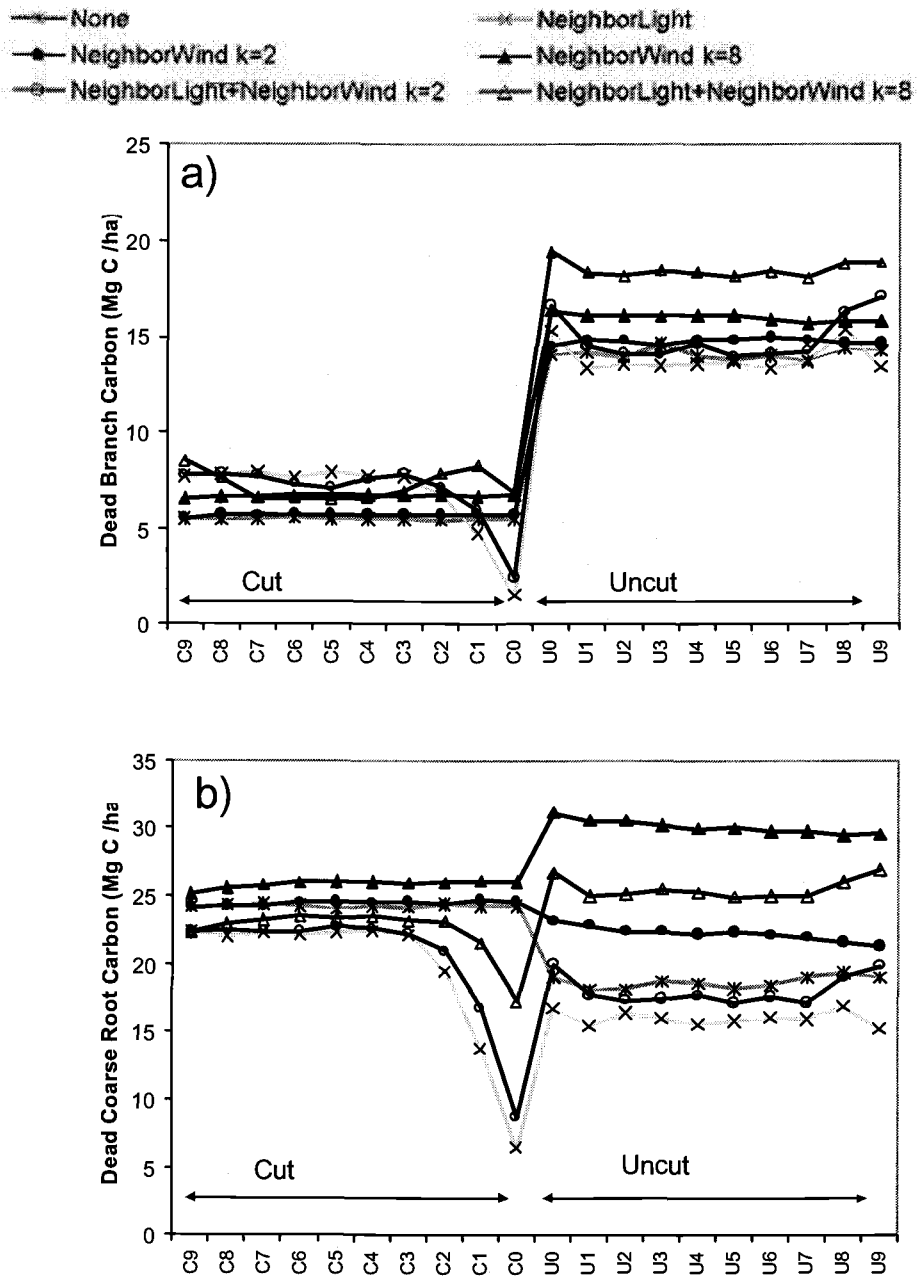


Figure 4.20. Dead carbon by zone for different light and wind simulations for (a) branch and (b) coarse root pools in Landscape AD. Zones C0 through C9 are cut every 50 years after year 500, while zones U0 through U9 remain uncut. Results are the average for years 500 to 1000 for each zone. Note different y-axis scales.

Total Stores

Total live carbon stores (the sum of all the live pools) in the cut patch averaged $200 \pm 62.7 \text{ Mg C ha}^{-1}$ across all zones when only light limitations were included (**Figure 4.21a**). However, near the edge of the cut patch (zone C0), the total live carbon store was 47 Mg C ha^{-1} , a decrease of 154 Mg C ha^{-1} . The difference was negligible (1 Mg C ha^{-1}) for zones C3 to C9, indicating that most of the reduction in carbon stores due to light limitations was at the edge of the cut stand. When only wind mortality was included, the reductions in total live biomass at the edge compared to the average of all zones in the cut patch ranged from 2 (when k was set to 2) to 78 Mg C ha^{-1} (when k was set to 8). When both light limitations and wind mortality were included, total live stores decreased at the edge of the cut patch (up to 137 Mg C ha^{-1} , when k was set to 2), similar to the simulations with only light included. In the uncut patch, for all simulations, total live carbon stores did not appear to change significantly across the zones.

Total dead carbon stores (the sum of all the dead pool results in **Figure 4.21b**) showed no change across all zones in the cut patch. In the uncut patch, total dead pools were increased near the edge, from 3 Mg C ha^{-1} (with light limitations) to 19 Mg C ha^{-1} (with light limitations and wind mortality, $k=2$).

Total carbon pools (total live + total dead + total stable) (**Figure 4.22b**) showed no significant trend near the edge in the uncut patch. In the cut patch, there was a decrease in carbon stores near the edge, ranging from large differences such as 254 Mg C ha^{-1} when only light limitations were included and 230 Mg C ha^{-1} when both light limitations and wind mortality were included ($k=5$) to smaller

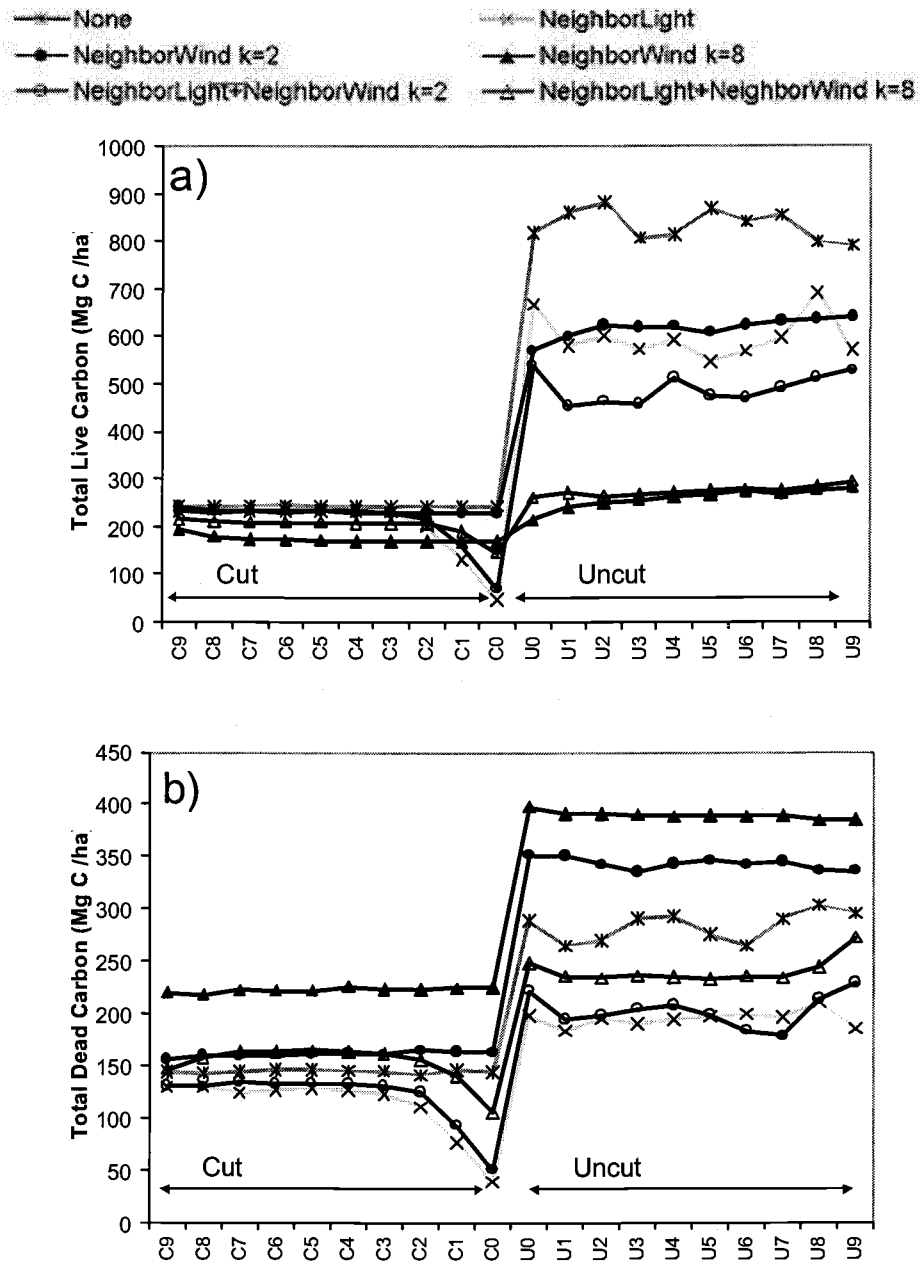


Figure 4.21. Effect of light limitations and wind mortality on: (a) total live and (b) total dead carbon, by zone, in Landscape AD. Zones C0 through C9 are cut every 100 years after year 500, while zones U0 through U9 remain uncut. Results are the average for years 500 to 1000 for each zone.

— None
 — NeighborWind k=2
 — NeighborLight+NeighborWind k=2
 — NeighborLight
 — NeighborWind k=8
 — NeighborLight+NeighborWind k=8

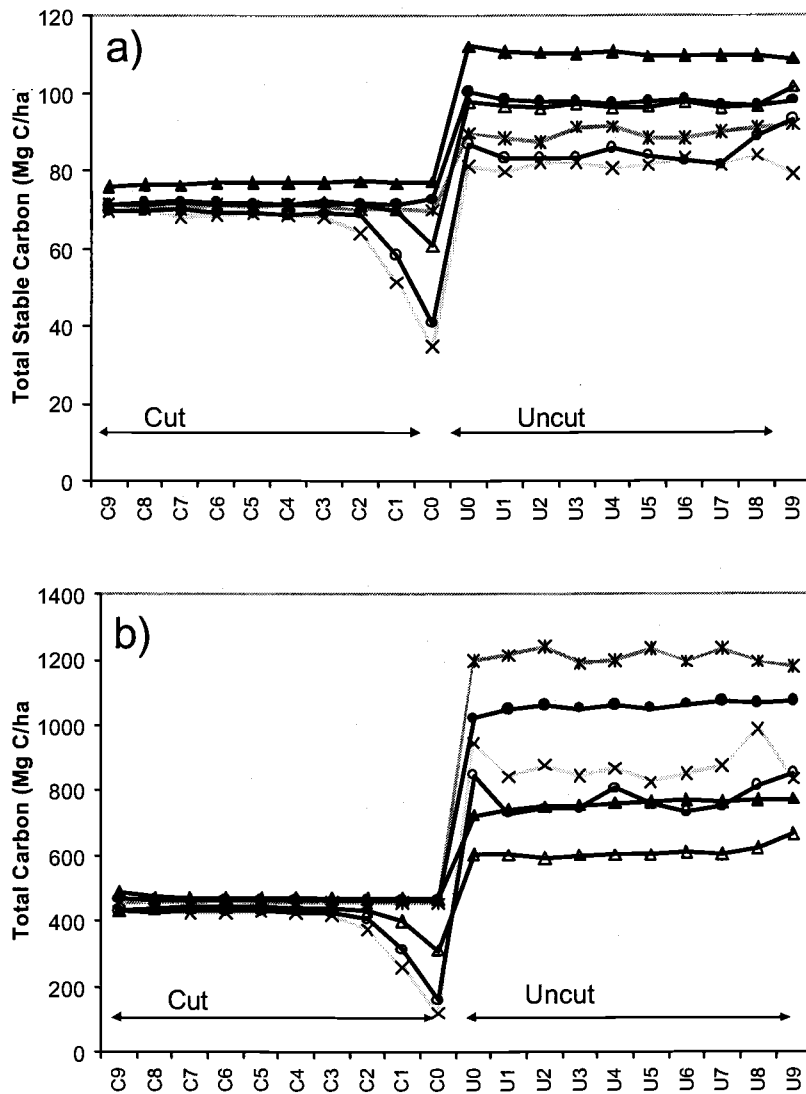


Figure 4.22. Effect of light limitations and wind mortality on: (a) total stable and (b) total (live+dead+stable) carbon, by zone, in Landscape AD. Zones C0 through C9 are cut every 100 years after year 500, while zones U0 through U9 remain uncut. Results are the average for years 500 to 1000 for each zone

differences such as 1 or 2 Mg C ha⁻¹ when only wind mortality was included (k=2, 3, and 8).

Patch-to-Patch Emergent Behaviors

Emergent behaviors due to patch-to-patch interactions were evidenced by differences between the carbon stores in heterogeneous landscapes and the carbon stores of independent simulations of old growth and young landscapes that were additively combined (**Figure 4.23**). However, emergent behaviors were not significant until the k value was set to 5 or 8. At these high k values, landscapes AIC, AIF, and CH had 21 or 22 % (± 2.0 %) less carbon in the heterogeneous landscapes than would be predicted from an additive approach. In contrast, landscape AD had between 4.0 % (± 2.0 %) and 1.0 % (± 3.0 %) greater total carbon stores.

Patch-to-Patch * Process Emergent Behaviors

Emergent behaviors due to patch-to-patch * process interactions were significant when k was set to 3, 5, or 8 for all heterogeneous landscapes (**Figure 4.24**). Differences from the control are small when k is set to 3 (4.0 % SD = 2 %). When k is set to 5, landscape AIC, AIF, and CH are approximately 11.0 % (SD = 2.0 %) lower and landscape AD is 7.0 % (SD = 3.0 %) higher than the control. When k is set to 8, landscapes AIC, AIF, and CH are about 5.0 % (SD = 1.0 %) lower than the control, although landscape AD is 12.0 % (SD = 1.0 %) higher.

Do patches interact within heterogeneous landscapes?

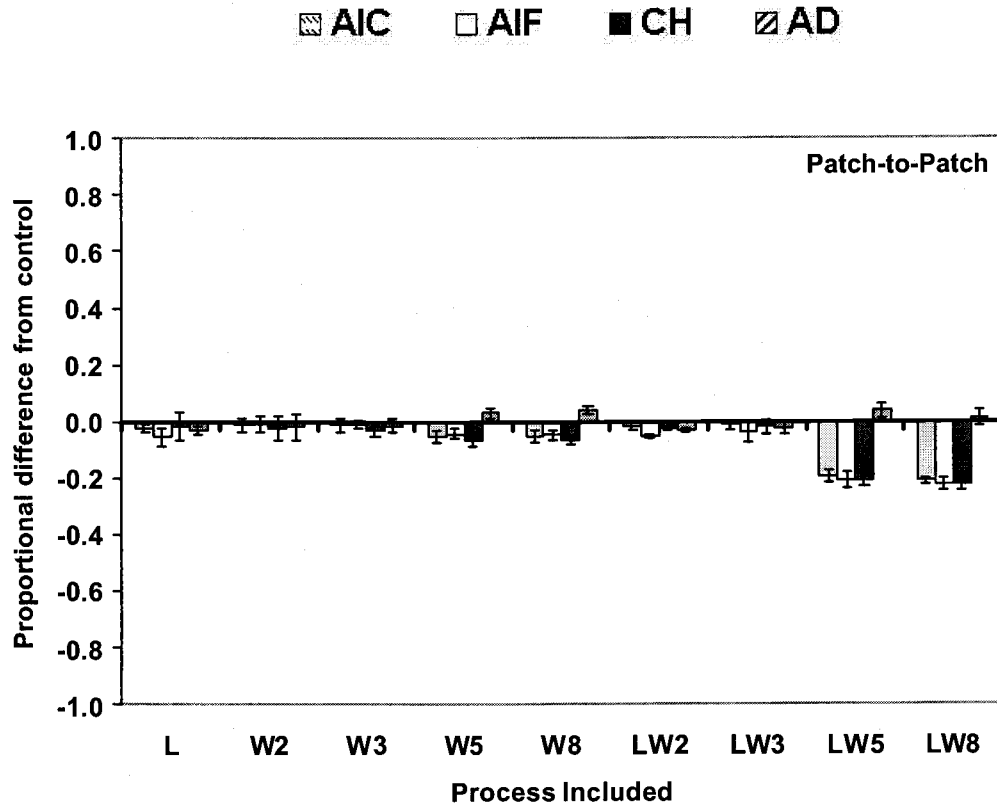


Figure 4.23. Emergent behaviors due to patch-to-patch interactions. Values represent the proportional difference of the treatments from the control. The control is defined in **Table 4.2**. Values different from 0 reflect emergent behaviors. Error bars represent two standard deviations from the mean of five repetitions for each simulation.

Do processes interact within heterogeneous landscapes?

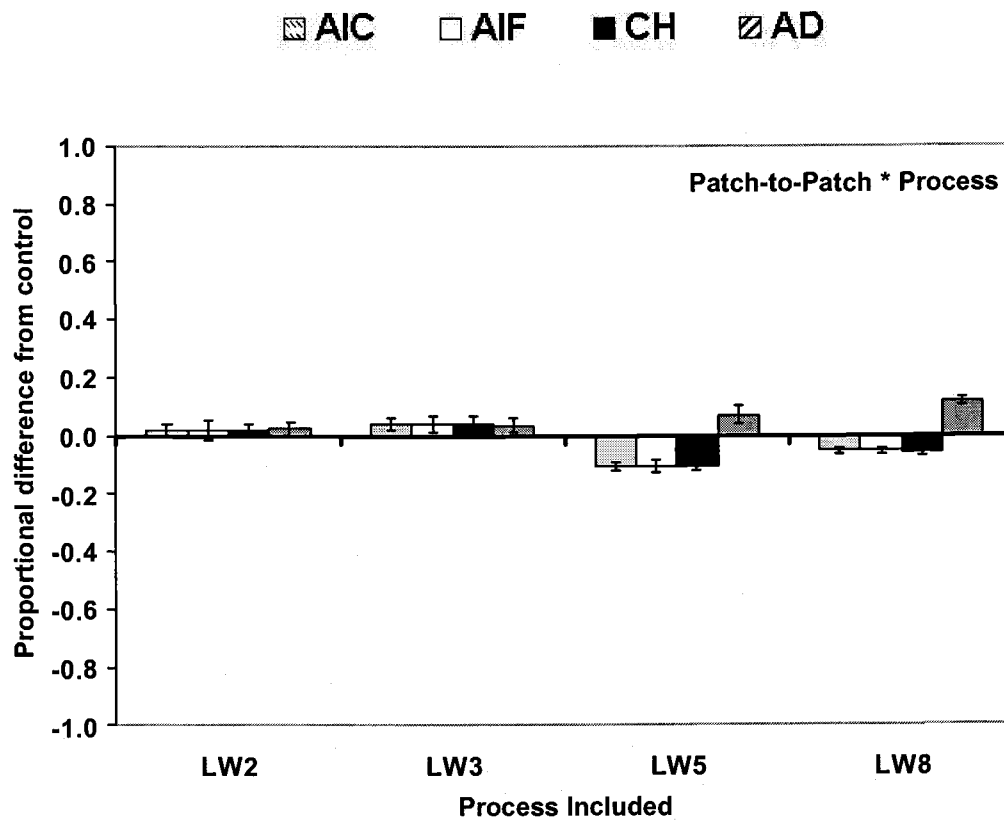


Figure 4.24. Emergent behaviors due to patch-to-patch * process interactions. Values represent the proportional difference of the treatments from the control. The control is defined in **Table 4.2**. Values different from 0 reflect emergent behaviors. Error bars represent two standard deviations from the mean of five repetitions for each simulation.

Patch-to-Patch * Structure Emergent Behaviors

The arrangement of patches on a heterogeneous landscape did not result in emergent behaviors until k was set to 5 or 8 (**Figure 4.25**). The magnitude of the emergent behaviors, as evidenced by the proportional difference from the control (**Figure 4.2**), was dissimilar among different heterogeneous landscapes; the largest differences were found when light and wind interacted. When k was set to 5 or 8, landscapes AIC, AIF, and CH had between 6.0 % and 8.0 % (SD = 1.7 to 3.6 %) lower biomass than the average carbon store of the simulated landscapes. Landscape AD showed an opposite trend, being 21.0 % (SD = 1.7 to 3.6 %) higher than the control.

Discussion

Light and wind processes, which affect forest carbon storage, are complex in spatially heterogeneous landscapes. For example, increased mortality at forest edges may or may not be compensated for by increased growth of trees and shrubs in response to changed light environments. In addition, potential changes in species composition due to new edge openings may modify growth and decomposition processes. Given the uniqueness of the edge zone, understanding these compensatory processes in the edge zone is important at local scales. At broad scales, the influence of the edge zone is less clear. First, the effect of forest edges may be minimal relative to the broad scale patterns that are of interest. Second, if processes are linear across edges, it is possible that edge effects will be

Does the effect of the process vary with different landscape age structure?

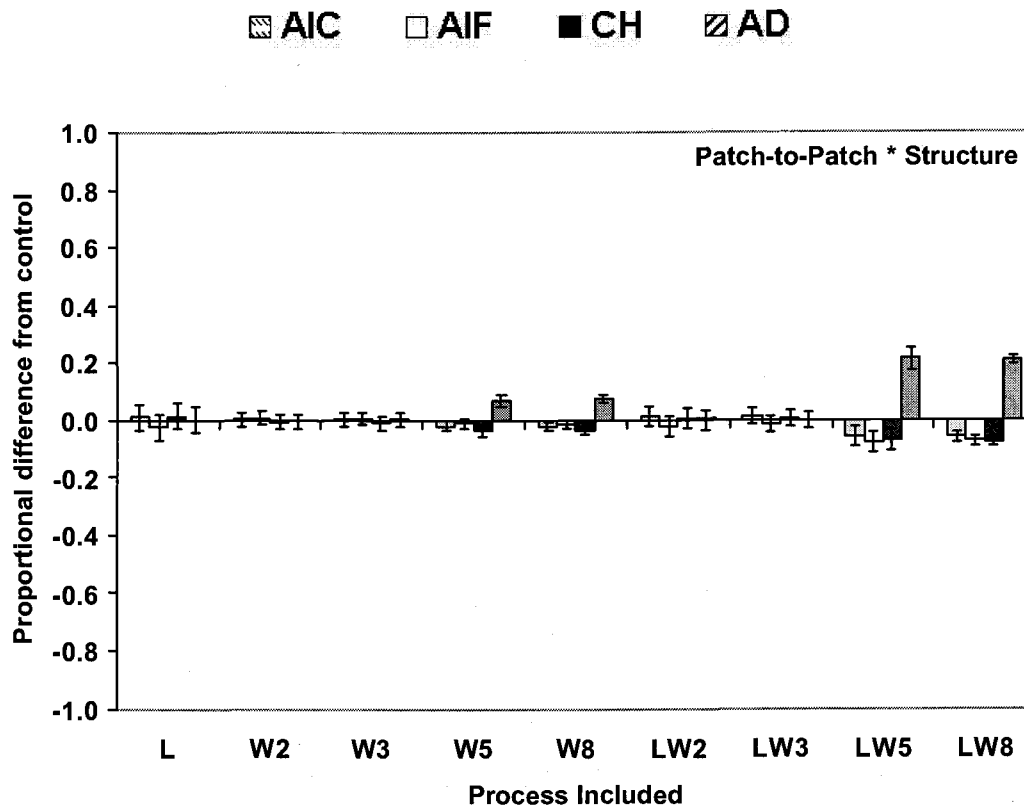


Figure 4.25. Emergent behaviors due to patch-to-patch * structure interactions. Values represent the proportional difference of the treatments from the control. The control is defined in **Table 4.2**. Values different from 0 reflect emergent behaviors. Error bars represent two standard deviations from the mean of five repetitions for each simulation. Comparisons between bars reflect differences between landscapes, due to the different age structures.

minimal at broad scales as edge effects are averaged out across patches. Third, if edge effects are predictable at broad scales, it may be possible to use the edge zone as another unit in an additive approach. However, if multiple processes interact in heterogeneous landscapes, it is likely that edge effects will not be predictable at broad scales due to emergent behaviors. Our modeling exercises were based on a simple analysis of only two processes, light limitations and wind mortality, which are affected by the spatial heterogeneity of tree heights of only two species, Douglas-fir and western hemlock. Simulations were also performed over artificial landscapes for simplicity and do not capture the natural complexity of real landscapes. Nevertheless, results suggest that, in some instances, these processes may lead to emergent behaviors that influence carbon storage at multiple scales, including the landscape level. In such instances, scaling of information from the patch scale to the landscape scale may result in an inaccurate prediction at broader scales.

Our results indicated that increased exposure to wind caused an increase in the dead carbon stores by increasing mortality. These results were not surprising given our assumption that wind increases levels of tree mortality. However, the pattern was less obvious when looking at total carbon stores. In fact, total carbon stores decreased because the reduction in live carbon stores was greater than the increase in dead carbon stores. Thus, the results stress the importance of looking at results for all significant ecosystem pools of carbon because totals hide important changes within specific pools. This was apparent when looking at the average carbon stores for a landscape, the zoned results within a landscape patch, or the time trends.

In addition to increasing dead carbon stores, increased levels of wind mortality caused changes in species composition. In STANDCARB, species respond differently to the same environmental conditions (e.g., the light environment). As a result, earlier openings in the canopy due to wind may accelerate increases in shade-tolerant species undergoing advance regeneration. Changes in species composition may also affect carbon stores indirectly since species influence rates of growth, respiration, and decomposition differently. Our results indicated that species transitions were accelerated with increasing wind mortality, resulting in simultaneous changes in carbon stores. While others have demonstrated that the creation of new edge environments may lead to changes in species composition (Sinton et al. 2000; Chen et al. 1992), there has been little work to relate these changes to carbon stores. A combination of targeted modeling and fieldwork is necessary to determine the persistence of these potential changes in ecosystem succession and to attribute changes in carbon (or nutrient) stores either to the interaction of multiple processes or to a specific process.

By simulating a zone structure within our simulated landscapes, we were able to examine the location of "edge effects" due to wind and/or light. Our results indicate that the effects of light limitations were primarily located at the edge since carbon stores were reduced in the cut patch for at least 50 m, presumably due to shading by the uncut patch. The relative response of light limitations was varied for different pools of carbon, e.g., a larger increase in dead sapwood than other pools at high levels of wind mortality. However, we did not detect the effects of wind mortality in cut patches beyond one cell width. There may be several reasons for

this. First, given the relatively coarse resolution of the cells, we may have missed finer-scale dynamics. Second, and probably more importantly, a limitation of STANDCARB is that each cell can only be affected by wind mortality once per year. Thus, there is a time step limit on wind propagation through a stand and continuous effects of wind mortality within a year cannot be simulated. In future modeling of edge effects it would be helpful to consider shorter time-steps for wind disturbances within a year.

We did not include many other processes known to be potentially important at forest edges and which may influence carbon stores in fragmented landscapes. For example, future modeling would be improved by incorporating the transfer of material between neighboring cells, i.e. the exchange of fallen wood, or the competition of roots below-ground. These relationships were not included here given the complex nature of the interactions. In addition, STANDCARB does not have a nitrogen cycling component and therefore it was not possible to model nutrient cycling interactions at the edge, which may be important (T. Redding, T. Hayes, personal communication). In addition, wind-mortality events may be stochastic, e.g., in the form of a blowdown, whereas our modeled increases in mortality were constant through time. An improvement to the modeling strategy employed here would be to invoke a stochastic component to wind-mortality that would be more closely related to actual temporal patterns in wind mortality events.

Even given these limitations, we were able to show that light and wind interacted, leading to emergent behaviors at the stand-scale (based on interactions of processes among cells) and the landscape-scale (based on interactions of processes

between patches). It follows that, based on the current mechanistic understanding of independent effects of light and wind processes as expressed in the STANDCARB model, we may not be able to make accurate predictions of carbon at the stand or landscape scale. Instead, the *interaction* of light and wind processes requires attention. Calculating the independent effects of light and wind processes in an additive approach, may lead to either an overestimate or underestimate of carbon storage depending on the type of interaction, the processes considered, the magnitude of the processes, and the age of the landscape. For example, cell-to-cell interactions were larger for old-growth landscapes than young landscapes. One would expect more variation in old-growth landscapes because of their larger height variability. This suggests that one could ignore cell-to-cell interactions in young stands but not older ones. Also, emergent behaviors in some cases was not significant until very high k values, indicating that they may be minimal in areas with low wind mortality and could be dealt with by models that included both processes.

Interactions at the landscape scale show that patches interact with each other when the k value is high and that this effect exceeds the expected variability in the model. The effect is largest when light and wind are simulated together. However, the effect can be either positive or negative, depending on the landscape being simulated. One reason for this may be the interactions of processes across patches, demonstrated by the patch-to-patch * process test. In the latter test, an additive approach was not sufficient to predict carbon stores when processes interacted in heterogeneous landscapes and when the wind mortality was high. Further, our results indicate that artificial landscapes with different spatial structures resulted in

different levels of emergent behaviors. These emergent behaviors at the landscape scale, due to the interactions of patches, ranged from + 21 % to - 22 %, depending on the type of interaction, the landscape structure, the type of processes considered, and the magnitude of the processes.

Our results indicate that emergent behaviors due to process interactions across patches are important, even though most carbon models do not include these effects. Typically, the assumption is that these edge effects are either insignificant or will "cancel out" over broad-scales. If processes are asymptotic or non-linear across edges, however, edge zones must be considered separately as part of an additive approach to scale carbon stores to a fragmented landscape. We found that emergent behaviors across edges are significant at high k values (i.e., >5), ranging from +12 % to -11 %, but are not significant at lower k values.

Given that our tests for emergent behaviors at the landscape scale largely examined one patch size, it would be helpful if there were a simple way to estimate the magnitude of this effect for a range of patch sizes. Assuming the relative effects of emergent behaviors are a function of the relative width of edge effects relative to patch width, we can extrapolate the effects for other square-shaped patches, assuming a constant edge width. In our simulations, the maximum edge width was approximately 51 m (3 cells into a patch 10 cells wide, where each cell is 17 m). Since the simulated patches were 170 m wide, the edge-affected area represents approximately 30 % of the patch and this resulted in potential errors of ± 20 % based on the emergent behaviors we observed. Typical harvest cuts may be between 20 and 40 ha, much larger than the patches simulated here, with less edge-affected area.

The potential for errors is thus between 5 % and 7 % (**Figure 4.26**). Similarly, around larger patches, such as from natural fires, the potential for error would be from less than 1 % to 4 %. It should be noted, however, that the trend in forest management is to reduce the size of clear-cut patches. As the average cut size for harvests is reduced, the relative amount of edge-affected area would increase suggesting errors due to emergent behaviors might be larger than we observed.

Using an additive approach, it may be possible to adjust values in a fragmented landscape to account for the area affected by edges as described above. Specifically, describing the edge zone as another patch may be all that is necessary to include patch interactions at broader scales. Yet, an additive solution to edges in fragmented landscapes may not be the appropriate solution if the arrangement of patches on the landscape is also important, because an additive solution does not consider topological relationships. Indeed, we found that, when the wind mortality was set very high (8 times the base mortality rate) the level of emergent behavior of one landscape, the aggregated directional (AD), was significantly different than that found in the other landscapes, by almost 28 %. The different response of landscape AD from the other landscapes may be due to the fact that there are proportionately fewer cells that are considered to be edge cells than in the other spatial structures. One would then expect larger differences between the checkerboard (which has the highest edge length) and the other aggregated cuts. However, we did not observe this pattern. Instead, it is more likely that Landscape AD has more interior cells (unaffected by an edge) than the other landscapes. With more interior cells, both dead and live biomass increase and the relative effects of light limitations and wind

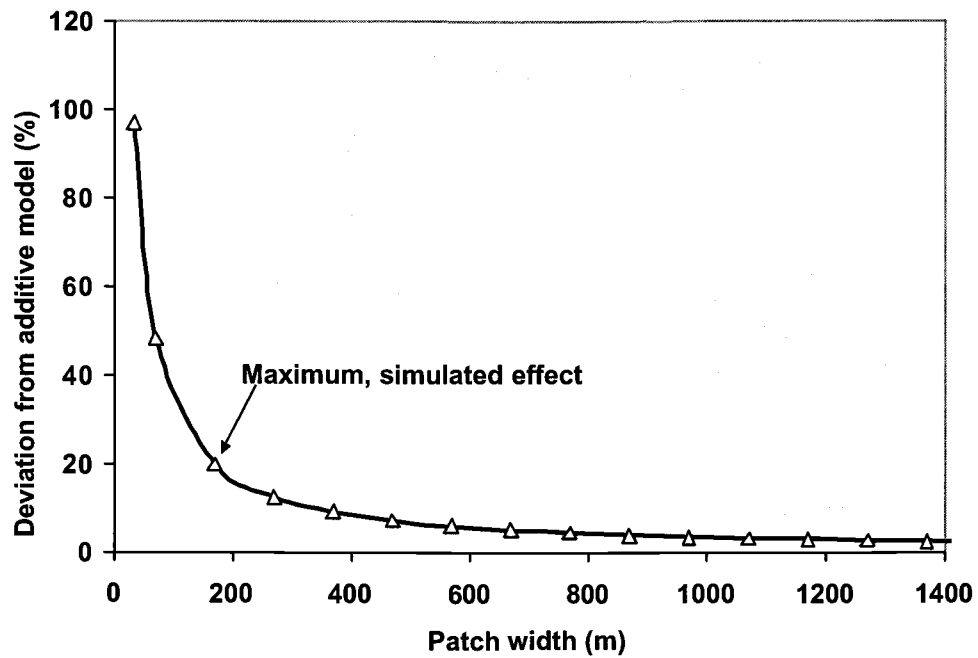


Figure 4.26. Results of a simple mixing model showing the potential errors caused by edge-induced, emergent behaviors for increasing patch widths. The maximum, simulated effect observed here is $\pm 20\%$ at a patch width of 170 m. Calculations assume a constant edge width of 51 m.

mortality are reduced. Elucidation of the role of spatial pattern in influencing these emergent behaviors is needed and a more precise study of landscape pattern indices (Krummel et al. 1987; Li 2000) may be useful in this effort to identify landscapes with differing potential to exhibit emergent behaviors. Our results suggest that the spatial arrangement of age classes was significant in one case (landscape AD, under high k values) but was not significant among other landscape structures. This indicates that more research is needed to elucidate the cause of these emergent behaviors and, especially, to determine the effect of wind mortality at forest edges across a broader range of conditions and environments.

Emergent behaviors have been previously identified in several disciplines. Bella (1997) suggested that organizational systems of a technological society are complex, adapting, and nonlinear; they display emergent behaviors that cannot be reduced to the level of the individual. The decline of Pacific Northwest salmon, Bella (1997) suggests, is partly due to the hesitance to accept and identify these emergent behaviors in the organizational structure that is responsible for their management. In the field of conservation biology, Lidicker (1999) suggests that emergent behavior at habitat edges are of "central importance." In this paper, we suggest that spatial emergent behaviors are also important in the context of ecosystem process modeling. Despite the increasing evidence over the short and long term that horizontal processes across edges are important, and despite the generally recognized notion that assumptions of scale limit prediction, there have been few studies to systematically test the effect of complex, nonlinear processes at multiple scales. Here, we presented a novel, modeling analysis to assess the

importance of emergent behaviors on carbon storage. By using artificial landscapes, and coupling them to an ecosystem process model, we provided various null models for generating predictions about carbon storage in fragmented landscapes (With 1997). While this approach may not lend itself to predictions on real landscapes in a spatially-explicit context, one may still be able to make quantitative predictions about the effect of forest edges on carbon storage, thereby elucidating new methodologies to cope with fragmentation issues at multiple scales. Particularly, the goal of this work is to alert modelers to assumptions of spatial homogeneity, which may or may not hold when complex, nonlinear dynamics are applied in heterogeneous landscapes.

Conclusions

Forest edges are likely to affect landscape processes, although their relative effect on carbon storage has not been evaluated previously at the landscape scale. We asked whether the interactions of processes at broad, spatial scales can be predicted from the interactions of the processes at finer, spatial scales and whether emergent behaviors, if present, cease to be important at broader scales.

In cell-to-cell interactions, light-limitation interactions were more important than edge-induced, wind mortality in changing carbon stores unless the elevated mortality rate was 8 times the base level. Light and wind interactions also affected the degree to which Douglas-fir and western hemlock were able to regenerate in canopy openings, indirectly affecting carbon stores. In patch-to-patch interactions, we observed changes in carbon storage at the boundaries between patches.

We found that spatial interactions at all levels were potentially significant and resulted in emergent behaviors in both homogenous and heterogeneous landscapes. Cell-to-cell interactions are part of most (non-point) model structures and thus these spatial interactions are straightforward to include; were this the only type of spatial interaction then additive scaling to broader scales would be possible. Similarly, if patch-to-patch interactions were the only type of interaction then we might be able to suggest a simple correction for edge zones. However, the fact that we detected emergent behaviors among landscapes with different spatial structures in one instance indicates that the spatial arrangement of patches on the landscape may be important when scaling information to broader scales. An additive correction for edge zones, therefore, may not capture the variability in patch-to-patch interactions in all cases. The potential error of not accounting for these emergent behaviors depends on the relative area of the edge relative to patch size and the level effect of the emergent behaviors. More understanding of how processes interact at the local level may be necessary before predictions of carbon dynamics can be made accurately at broad scales.

Acknowledgments

We are grateful to Julia Jones, Barbara Bond, Dave Turner, and Warren Cohen for providing helpful comments on early drafts of this paper. The work was supported by NASA-LCLUC (Land-Cover, Land-Use Change Program), an H. J. Andrews Long Term Ecological Research Grant (DEB-9632921), a National Science Foundation Fellowship in Landscape Ecology through Oregon State University, and the Richardson Endowment to the College of Forestry, Oregon State University.

References

- Acker, S.A., McKee, A., Harmon, M.E., and Franklin, J.F. 1998. Long-term research on forest dynamics in the Pacific Northwest: a network of permanent forest plots. *In* Forest Biodiversity in North, Central and South America, and the Caribbean: Research and Monitoring, UNESCO and The Parthenon Publishing Group, Paris, pp. 93-106.
- Baker, W.L. 1989. A review of models of landscape change. *Landscape Ecol.* 2: 111-133.
- Bella, D.A. 1997. Organizational systems and the burden of proof. *In* Pacific Salmon and their Ecosystems, D.J. Strouder, P.A. Bisson, R.J. and Naiman (Eds.), Chapman and Hall, New York, pp 617-638.
- Brown, S. 1996. Mitigation potential of carbon dioxide emissions by management of forests in Asia. *Ambio* 25: 273-278.
- Chen, J., Franklin, J.F., and Spies, T. A. 1992. Vegetation responses to edge environments in old-growth Douglas-fir forests. *Ecol. Appl.* 2: 387-396.
- Cohen, W.C., Harmon, M.E., Wallin, D.O., Fiorella, M. 1996. Two decades of carbon flux from forests of the Pacific Northwest. *BioScience* 46: 836-844.
- Desjardins, R.L., MacPherson, J.I., Mahrt, L., Schuepp, P., Pattey, E., Neumann, H., Baldocchi, D., Wofsy, S., Fitzjarrald, D., McCaughey, H., and Joiner, D.W. 1997. Scaling up flux measurements for the boreal forest using aircraft-tower combinations. *J. Geophys. Res.* 102: 29,125 - 29,133.
- Ferreira, L.V. and Laurance, W.F. 1997. Effects of forest fragmentation on mortality and damage of selected trees in Central Amazonia. *Cons. Biol.* 11: 797-801.
- Forman, R.T.T. and Godron, M. 1981. Patches and structural components for a landscape ecology. *BioScience* 31: 733-740.
- Foster, D.R. 1988. Species and stand response to catastrophic wind in central New England, U.S.A. *J. Ecol.* 76: 135-151.
- Foster, D.R. and Boose, E.R. 1992. Patterns of forest damage resulting from catastrophic wind in central New England, USA. *J. Ecol.* 80: 79-98.
- Franklin, J.F. and R.T.T. Forman. 1987. Creating landscape patterns by forest cutting: ecological consequences and principles. *Lands. Ecol.* 1: 5-18.

- Goulden, M.L., Munger, J.W., Fan, S.-M., Daube, B.C., and Wofsy, S.C. 1996. Measurements of carbon sequestration by long-term eddy covariance: methods and a critical evaluation of accuracy. *Global Change Biol.* 2: 169-182.
- Harmon, M.E. and Domingo, J.B. 2001. A Users Guide to STANDCARB version 2.0: A Model to Simulate the Carbon Stores in Forest Stands. Department of Forest Science, Oregon State University, Corvallis, Oregon.
- Harmon, M.E. and Marks, B. In press. Effects of silvicultural treatments on carbon stores in forest stands. *Can. J. For. Res.*
- Houghton, R.A., Skole, D.L., Nobre, C.A., Hackler, J.L., Lawrence, K.T., Chomentowski, W.H. 2000. Annual fluxes of carbon from deforestation and regrowth in the Brazilian Amazon. *Nature* 403: 301-304.
- Kaharabata, S.K., Schuepp, P.H., Ogunjemiyo, S., Shen, S., Leclerc, M.Y., Desjardins, R.L., and MacPherson, J.I. 1997. Footprint considerations in BOREAS. *J. Geophys. Res.* 102: 29,113-29,124.
- King, A.W., Johnson, A.R. and O'Neill, R.V. 1991. Transmutation and functional representation of heterogeneous landscapes. *Lands. Ecol.* 5, 238-253.
- Krummel, J.R., Gardner, R.H., Sugihara, G., O'Neill, R.V., and Coleman, P.R. 1987. Landscape patterns in a disturbed environment. *Oikos* 48: 321-324.
- Laurance, W.F., Laurance, S.G., Ferreira, L.V., Merona, J.M.R., Gascon, C., and Lovejoy, T.E. 1997. Carbon collapse in Amazonian forest fragments. *Science* 278: 1117-1118.
- Laurance, W.F., Ferreira, L.V., Rankin-de-Merona, J.M., and Laurance, S.G. 1998. Rain forest fragmentation and the dynamics of Amazonian tree communities. *Ecol.* 79: 2032-2040.
- Li, B.-L. 2000. Fractal geometry applications in description and analysis of patch patterns and patch dynamics. *Ecol. Model.* 132: 33-50.
- Lidicker Jr., W.Z. 1999. Responses of mammals to habitat edges: an overview. *Lands. Ecol.* 14: 333-343.
- Lovejoy, T.E., Rankin, J.M., Bierregaard Jr., R.O., Brown, K.S., Emmons, L.H., and Van der Voort, M.E. 1984. Ecosystem decay of Amazon forest fragments. *In* Extinctions, Nitecki, M.H. (Ed.), The University of Chicago Press: Chicago and London, pp. 295-326.
- Ranney, J.W., Brunner, M.C., and Levenson, J.B. 1981. The importance of edge in the structure and dynamics of forest islands. *In* Forest Island Dynamics in Man-Dominated Landscapes, Springer Verlag, New York, NY, pp. 67-96.

- Risser, P.G. 1987. Landscape ecology: state of the art. *In* Landscape Heterogeneity and Disturbance, Turner, M.G. (Ed.), Springer-Verlag, New York, New York, pp. 3-13.
- Risser, P.G. 1999. Landscape ecology: does the science only need to change at the margin? *In* Landscape Ecological Analysis: Issues and Applications, Klopatek, J.M., and Gardner, R.H. (Eds.), Springer, New York, New York, pp. 3-10.
- Schultze, E.-D., Wirth, C., Heimann, M. 2000. Managing forests after Kyoto. *Science* 289: 2058-2059.
- Sinton, D.S., Jones, J.A., Ohmann, J.L., and Swanson, F.J. 2000. Windthrow disturbance, forest composition, and structure in the Bull Run Basin, Oregon. *Ecol.* 81: 2539-2556.
- Smithwick, E.A.H. and M.E. Harmon. In press. Potential upper bounds of carbon stores in forests of the Pacific Northwest. *Ecol. Appl.*
- Turner, D.P. and Gregory, M. In review. Spatially-distributed modeling of gross primary production and evapotranspiration over the flux tower footprint over a boreal forest site. *Agric. For. Meteorol.*
- Watson, R., et al. 2000. Land Use, Land-Use Change, and Forestry, Summary for Policymakers, Special Report of Working Group II of the Intergovernmental Panel on Climate Change.
- Wiens, J.A. 1998. Landscape ecology: scaling from mechanisms to management. *In* Perspectives in Ecology: A Glance from the VII International Congress of Ecology, Farina, A. (Ed.), Springer-Verlag, New York, New York, pp. 13-24.
- Williams-Linera, G. 1990. Vegetation structure and environmental conditions of forest edges in Panama. *J. Ecol.* 78: 356-373.
- With, K.A. 1997. The application of neutral landscape models in conservation biology. *Cons. Biol.* 11: 1069-1080.
- Wofsy, S.C., Goulden, M.L., Munger, J.W., Fan, S.-M., Bakwin, P.S., Daube, B.C., Bassow, S.L., and Bazzaz, F.A. 1993. Net exchange of CO₂ in a mid-latitude forest. *Science* 260: 1314-1317.

CHAPTER 5

CONCLUSIONS AND FUTURE DIRECTIONS

Erica A. H. Smithwick

Conclusions

In this research, I evaluated potential carbon (C) storage at the landscape-scale. I summarized field data from 43 old-growth sites across a wide biogeoclimatic gradient in the Pacific Northwest of the United States (PNW) to approximate the upper bounds of C storage in the region. I developed a new model (MAXCARB) to predict potential carbon storage across a region in response to climate and disturbance regimes. In addition, I modified an existing forest process model (STANDCARB) to test general assumptions for scaling ecosystem processes from stands to landscapes. The major conclusions of this research are the following:

- On average, total ecosystem carbon (TEC) in old-growth forest stands in the PNW ranged from 195 Mg C ha⁻¹ in eastern Oregon to 1127 Mg C ha⁻¹ in coastal Oregon. These estimates included all significant C pools (live and dead branches, foliage, stem bark and wood, fine and coarse roots, fine and coarse woody debris, forest floor, rotten wood, herbs, shrubs, and soil to 1 m).
- A simple, area-weighted estimate of TEC storage for the region indicated that the upper bounds of C storage is 671 Mg C ha⁻¹ when soil C is estimated to a depth of 1 m, and 640 Mg C ha⁻¹ when soil C is estimated to a depth of 50 cm.
- TEC estimates in the region were larger than estimates of current C storage from other mature ecosystems throughout the globe, based on a review of the available literature.
- Reported estimates of TEC storage for the PNW are lower than estimates of the upper bounds presented here, indicating that the region has the potential to store a maximum of 338 Mg C ha⁻¹ more C than is currently stored.

Management for potential C sequestration must also account for natural disturbances, economic ramifications, and a myriad of natural resource objectives.

- Functions describing how ecosystem rates changed through forest succession were developed with STANDCARB; these functions were used in MAXCARB to determine fluxes and stores in a landscape for a particular disturbance regime, negating the need to explicitly simulate succession.
- Site-level predictions of MAXCARB compared favorably to observed, old-growth forest data across the PNW gradient, and to simulation results from STANDCARB. MAXCARB predicted broad-scale potential C storage more efficiently than STANDCARB.
- Landscape-average rate constants calculated in the DISTURBANCE Module of MAXCARB could be used in the future to parameterize global models for the effects of disturbances at finer scales.
- Simulation results from STANDCARB indicated that emergent behaviors, resulting from the interaction of ecological processes, were apparent at all levels of scale examined (cell-to-cell and patch-to-patch). However, the magnitude of the emergent behaviors depended on the scale considered as well as the type and severity of the processes. In some cases, emergent behaviors were negligible (i.e., when elevated wind mortality at forest edges was minimal). Emergent behavior at the patch-to-patch level was significant at the highest level of wind mortality simulated but was not significant at lower levels.

- Emergent behaviors were dependent on the spatial arrangement of patches in the landscape but only in one arrangement (landscape AD). The reason for different levels of emergent behaviors caused by different spatial arrangement of patches is not intuitive, implying that future work must evaluate when spatial arrangement is important. Identification of thresholds, defining scales at which spatial heterogeneity is significant, may be important. Spatial indices may prove useful in this effort.
- Old-growth forests exhibited more emergent behaviors than young forests, presumably due to the spatial complexity of the canopy. Thus, an additive model may be appropriate to describe the interaction of processes when emergent behaviors are minimal (the young forest) but increasing complexity of vegetation structure may limit the application of additive approaches in older forests.

Future Directions

Landscape ecology concerns itself with the elucidation of spatial relationships across multiple scales (Levin 1992; O'Neill et al. 1996). For a broad region such as the Pacific Northwest, this conceptual approach can be useful to understand interactions of biogeoclimatic conditions and disturbance on C storage. There exists considerable uncertainty about the regional variability of C cycle processes, particularly the role of land use change and natural disturbances (Schimel et al. 2001). To constrain global predictions of the C cycle, an efficient methodology is needed to

scale information from regional scales to broader scales. In this research, by examining old-growth forest data and developing a novel modeling approach, I presented a methodology by which this could be achieved. I also assessed, heuristically, the degree spatial interactions at a finer scale could limit the application of additive approaches to scaling, i.e., those that assume spatial homogeneity. Taken together, this work uses principles developed in landscape ecology, ecosystem science, and forestry to address uncertainties in the C cycle.

For example, MAXCARB allows the prediction of landscape-average rate-constants as a function of disturbance regimes, which are currently not incorporated into most global ecophysiological models. Yet, MAXCARB is capable of providing rate-constants that could be used by global models to implicitly capture the effects of disturbances.

In addition, global models typically have a coarse resolution and cannot incorporate many finer-scale processes such as the horizontal interactions between patches on a landscape. This has the potential to cause errors at the global scale since horizontal processes, such as across forest edges, may not be implicitly captured by additive approaches to scaling. While emergent behaviors at the stand-scale can be dealt with by some models (such as non-point, ecosystem-scale models), emergent behaviors at the landscape scale due to patch-to-patch interactions would pose larger difficulties since most models do not account for spatial heterogeneity at the landscape scale. The spatial arrangement of patches on the landscape was only significant for one artificial landscape, indicating the possible importance of spatial interactions in

this case. However, under typical levels of light and wind interactions from the literature, spatial interactions were not significant.

Results of the latter study indicate that more research must be pursued to accurately model C storage in fragmented landscapes and to determine in which cases emergent behavior is important. Toward this goal, more information on the effects of horizontal processes across edges is critical. Abiotic patterns across forest edges, such as changes in microclimate conditions, have been studied in both temperate (Chen et al. 1992; Weathers et al. 2001) and tropical systems (Kapos et al. 1993), although the effects of those patterns on biotic processes are less clear. Changes in species and lifeforms at edges may influence carbon and nutrient storage, but the magnitude of these effects, as well as their persistence through succession, are unknown. Moreover, processes across edges may be best represented by non-linear (or bi-modal, or multi-modal) functions indicating that rates controlling these processes may be controlled by the interaction of multiple processes (Lidicker 1999; Tom Hayes, unpublished data). Such complexity will be informed by future field work that identifies underlying processes. Prediction of their effects may require improved models that incorporate spatial complexity.

Further validation and development of MAXCARB would be assisted by further conceptual work to define the landscape-scale responses to disturbance regimes. For example, the landscape age-class distribution can be predicted to follow a negative exponential distribution by assuming a Poisson random variable controls the mean return time of the disturbance. However, there are many other disturbance distributions that may be appropriate to explain observed age-class distributions that

do not follow a negative exponential distribution. Recently, Zhang and others (2001) suggested that a finite mixture of multiple Weibull distributions might better fit empirical tree height data in some uneven-aged management situations. While these distributions (the 'J-shaped', the Weibull) are typically used for silvicultural applications, they also might be used to define the distributions of age-classes across a landscape.

MAXCARB would be improved with more studies defining the age-dependency of ecological rates. These rates are meant to integrate successional dynamics after disturbance events. Proportions of life-forms and species change through succession, potentially affecting rates of ecosystem production (Janisch and Harmon 2002). Yet, little is known about the functional ramifications of these different successional pathways over the long term. Even for a single species, physiological processes may change with age or height (e.g., Yoder et al. 1994). In addition, allocation ratios may change as a function of stand age, concomitant with fertility and climate factors (Klopatek et al. 2002). Yet, there is little work to identify the generality of these ideas across different ecosystems. Determining these age-dependent rates requires more empirical data on successional dynamics after different disturbance events. Once these relationships are known, they can potentially be fit to one of a family of equations (e.g., Chapman-Richards or Michaelis-Menton).

MAXCARB would also be improved by further empirical work defining other ecological processes that control potential C storage. Nitrogen dynamics, for example, were not included in the model at this time since there is little empirical data on nitrogen stores in some ecosystem pools, such as woody detritus. However, after

disturbances, the concentrations of nitrogen and other nutrients may be altered (DeBano and Conrad 1978; Jensen et al. 2001), affecting productivity (Reed et al. 2001) and potentially influencing long-term C storage. Parameters defining tree mortality, growth, and decomposition rates are also likely to be affected by changes in nutrient cycling after disturbances.

Prediction of potential C storage under changing climate conditions, rather than using average climate conditions of the past, will require a more dynamic modeling scenario in which vegetation and disturbance regimes change in response to changing climate. For example, species dispersal may be changed under future climate scenarios, which may alter how steady-state C storage affects disturbance regimes, particularly if different species are more or less capable of surviving. Also, changes in land use should affect future climate predictions. This was not in the scope of the current work and is partly the focus of evolving global dynamic ecosystem models (e.g., Kucharik et al. 2000). Yet, MAXCARB could be used to predict multiple steady-state scenarios that would constrain potential C storage predictions.

The assumption of steady-state conditions in old-growth forests requires further empirical data, including monitoring above- and below-ground mortality and growth rates. Moreover, it would be helpful to monitor a wider range of sites to determine the extent to which stable conditions are persistent across the landscape. Understanding how vegetation responds to different intensities and types of disturbances, across a wide biogeoclimatic gradient, is also important.

The idea that different spatial arrangements of patches on a landscape result in varying degrees of emergent behaviors is a ripe area of research. Different patch

arrangements may determine the degree of shading within the landscape. As part of this process, it would be helpful to have a wider range of artificial structures simulated than the simple structures presented here. Future modeling efforts with STANDCARB should also examine the role of aspect and elevation on light limitations.

Future improvements to STANDCARB include the incorporation of new information on edge effects in temperate forests (T. Hayes and T. Redding, personal communication). Empirical evidence indicates that nonlinear dynamics at forest edges may be common for some processes such as nutrient cycling, respiration, and decomposition. Modification of processes already included in STANDCARB by indices of edge exposure might elucidate other situations in which emergent behaviors are important.

BIBLIOGRAPHY

- Acker, S.A., W.A. McKee, M.E. Harmon, and J.F. Franklin. 1998. Long-term research on forest dynamics in the Pacific Northwest: a network of permanent forest plots. In: *Forest Biodiversity in North, Central, and South America and the Caribbean: Research and Monitoring*, Dallmeier, F. and Comiskey, J.A. (Eds.), The Parthenon Publishing Group, Inc., New York, New York, pp. 93-106.
- Acker, S. A., P.A. Harcombe, M.E. Harmon, and S.E. Greene. In press. Biomass accumulation over the first 150 years in a coastal Oregon spruce-hemlock forest. *Vegetation Science*.
- Amiro, B.D., J.M. Chen, and J. Liu. 2000. Net primary productivity following forest fire for Canadian ecoregions. *Canadian Journal of Forest Research* 30: 939-947.
- Atjay, G.L., P. Ketner, and P. Duvigneaud. 1979. Terrestrial primary production and phytomass. In: *The Global Carbon Cycle*, Bolin, B., Degens, E. T., Kempe, S., and Ketner, P. (Eds.), John Wiley and Sons, New York, New York, pp. 129-182.
- Baird, C. 1999. *Environmental Chemistry*, 2nd Ed. W. H. Freeman and Company, New York, New York, 557 pp.
- Baker, W.L. 1989. A review of models of landscape change. *Landscape Ecology* 2: 111-133.
- Bella, D.A. 1997. Organizational systems and the burden of proof. In *Pacific Salmon and their Ecosystems*, D.J. Strouder, P.A. Bisson, R.J. Naiman, Eds., Chapman and Hall, New York, pp 617-638.
- Bender, M., C. Field, L.O. Hedin, J. Schimel, E. Sundquist, R. Berner, J. Galloway, F. Mackenzie, M. Torn, K.H. Freeman, J. Hedges, C. Mora, R. Stallard, S.C. Wofsy, and W.H. Schlesinger. 2000. *The Changing C Cycle: A Terrestrial Focus*, Report of the Workshop on the Terrestrial C Cycle. The National Science Foundation, Division of Earth Sciences.
- Birdsey, R.A. 1992. Carbon storage and accumulation in United States forest ecosystems. USDA Forest Service Gen. Tech. Rep. WO-59, 51 pp.
- Birdsey, R.A., A.J. Plantinga, and L.S. Heath. 1993. Past and prospective carbon storage in United States forests. *Forest Ecology and Management* 58: 33-40.
- Bonan, G.B. 1989. A computer model of the solar radiation, soil moisture, and soil thermal regimes in boreal. *Ecological Modelling* 45: 275-306.

- Bond, B.J. and J.F., Franklin. 2002. Aging in Pacific Northwest forests: a selection of recent research. *Tree Physiology* 22: 73-76.
- Bond, B.J., B.T. Farnsworth, R.A. Coulombe, and W.E. Winner. 1999. Foliage physiology and biochemistry in response to light gradients in conifers with varying shade tolerance. *Oecologia* 120: 183-192.
- Boone, R.D., P. Sollins, and K. Cromack, Jr. 1988. Stand and soil changes along a mountain hemlock death and regrowth sequence. *Ecology* 69: 714-722.
- Bormann, F.H. and G.E. Likens. 1979. Catastrophic disturbance and the steady state in northern hardwood forest. *American Scientist* 67: 660-669.
- Brown, R.B. and R.B. Parsons. 1972. Soils of the reference stands - Oregon IBP. Internal Report 128. College of Forest Resources, University of Washington, Seattle, 84 pp.
- Brown, S. 1996. Mitigation potential of carbon dioxide emissions by management of forests in Asia. *Ambio* 25: 273-278.
- Brown, S. and A.E. Lugo. 1982. The storage and production of organic matter in tropical forests and their role in the global carbon cycle. *Biotropica* 14: 161-187.
- Brown, S., A.J.R. Gillespie, and A.E. Lugo. 1991. Biomass of tropical forests of south and southeast Asia. *Canadian Journal of Forest Research* 21: 111-117.
- Busing, R.T., E.E.C. Clebsch, and P.S. White. 1993. Biomass and production of southern Appalachian cove forests reexamined. *Canadian Journal of Forest Research* 23: 760-765.
- Cairns, M.A., S. Brown, E.H. Helmer, and G.A. Baumgardner. 1997. Root biomass allocation in the world's upland forests. *Oecologia* 111: 1-11.
- Caspersen, J.P., S.W. Pacala, J.C. Jenkins, G.C. Hurtt, P.R. Moorcroft, and R.A. Birdsey, 2000. Contributions of land-use history to C accumulation in U.S. forests. *Science* 290: 1148-1151.
- Causton, D.R., C.O. Elias, and P. Hadley. 1978. Biometrical studies of plant growth. *Plant, Cell, and Environment* 1: 163-184.
- Ciais P. 1995. A large northern hemisphere terrestrial CO₂ sink indicated by the ¹³C/¹²C ratio of atmospheric CO₂. *Science* 269: 1098-1102.
- Chen, H., M.E. Harmon, and R.P. Griffiths. 2001. Decomposition and nitrogen release from decomposing woody roots in coniferous forests of the Pacific

- Northwest: a chronosequence approach. *Canadian Journal of Forest Research* 31: 246-260.
- Chen, J., J.F. Franklin, and T.A. Spies. 1992. Vegetation responses to edge environments in old-growth Douglas-Fir forests. *Ecological Applications* 2: 387-396.
- Cohen, W.B., M.E. Harmon, D.O. Wallin, and M. Fiorella. 1996. Two decades of carbon flux from forests of the Pacific Northwest. *BioScience* 46: 836-844.
- Cooper, C.F. 1983. Carbon storage in managed forests. *Canadian Journal of Forest Research* 13: 155-166.
- Corti, G., F.C. Ugolini, and A. Agnelli. 1998. Classing the soil skeleton (greater than two millimeters): proposed approach and procedure. *Soil Science Society of America Journal* 62: 1620-1629.
- Cromack Jr., K., R.E. Miller, O.T. Helgerson, R.G. Smith, and H.W. Anderson. 1999. Soil carbon and nutrients in a coastal Oregon Douglas-fir plantation with red alder. *Soil Science Society of America Journal* 63: 232-239.
- Crow, T.R. 1978. Biomass and production in three contiguous forests in northern Wisconsin. *Ecology* 59: 265-273.
- Dai, A. and I.Y. Fung. 1993. Can climate variability contribute to the "missing" CO₂ sink? *Global Biogeochemical Cycles* 7: 599-609.
- Dale, V.H. 1997. The relationship between land-use change and climate change. *Ecological Applications* 7: 753-769.
- Daly, C., R.P. Neilson, and D.L. Phillips. 1994. A statistical-topographic model for mapping climatological precipitation over mountainous terrain. *Journal of Applied Meteorology* 33: 140-158.
- DeBano, L.F. and C.E. Conrad. 1978. The effects of fire on nutrients in a chaparral ecosystem. *Ecology* 59: 489-497.
- DeBell, D.S. and J.F. Franklin. 1987. Old-growth Douglas-fir and western hemlock: a 36-year record of growth and mortality. *Western Journal of Applied Forestry* 2: 111-114.
- Desjardins, R.L., J.I. MacPherson, L. Mahrt, P. Schuepp, E. Pattey, H. Neumann, D. Baldocchi, S. Wofsy, D. Fitzjarrald, H. McCaughey, and D.W. Joiner. 1997. Scaling up flux measurements for the boreal forest using aircraft-tower combinations. *Journal of Geophysical Research* 102: 29,125 - 29,133.

- Dixon, R.H., S. Brown, R.A. Houghton, A.M. Solomon, M.C. Trexler, and J. Wisniewski. 1994. Carbon pools and flux of global forest ecosystems. *Science* 263: 185-190.
- Dodson, R. and D. Marks. 1997. Daily air temperature interpolation at high spatial resolution over a large mountainous region. *Climate Research* 8: 2-20.
- Emmingham, W.H., R.H. Waring. 1977. An index of photosynthesis for comparing forest sites in western Oregon. *Canadian Journal of Forest Research* 7: 165-174.
- Fan S, M. Gloor, J. Mahlman, S. Pacala, J. Sarmiento, T. Takahashi, and P. Tans. 1998. A large terrestrial C sink in North America implied by atmospheric and oceanic C dioxide data and models. *Science* 282: 442-446.
- Fang J, C. Anping, C. Peng, S. Zhao, and L. Ci. 2001. Changes in forest biomass C storage in China between 1949 and 1998. *Science* 292: 2320-2322.
- Fearnside, P.M., and R.I. Barbosa. 1998. Soil carbon changes from conversion of forest to pasture in Brazilian Amazonia. *Forest Ecology and Management* 108: 147-166.
- Ferreira, L.V. and W.F. Laurance. 1997. Effects of forest fragmentation on mortality and damage of selected trees in Central Amazonia. *Conservation Biology* 11: 797-801.
- Forman, R.T.T. and M. Godron. 1981. Patches and structural components for a landscape ecology. *Bioscience* 31: 733-740.
- Foster, D.R. 1988. Species and stand response to catastrophic wind in central New England, U.S.A. *Journal of Ecology* 76: 135-151.
- Foster, D.R. and E.R. Boose. 1992. Patterns of forest damage resulting from catastrophic wind in central New England, USA. *Journal of Ecology* 80: 79-98.
- Franklin, J.F. and D.T. Dyrness. 1988. *Natural Vegetation of Oregon and Washington*, Oregon State University Press, Corvallis, Oregon.
- Franklin, J.F. and R.T.T. Forman. 1987. Creating landscape patterns by forest cutting: Ecological consequences and principles. *Landscape Ecology* 1: 5-18.
- Franklin, J.F., W.H. Moir, M.A. Hemstrom, S.E. Greene, and B.G. Smith. 1988. The forest communities of Mount Rainier National Park. *Scientific Monograph Series Number 19*. US Department of the Interior, National Park Service, Washington, D.C., 194 pp.

- Franklin, J. F., T. A. Spies, R. Van Pelt, A. Carey, D. Thornburgh, D.R. Berg, D. Lindenmayer, M. E. Harmon, W. Keeton, and D. C. Shaw. In press. Disturbances and the structural development of natural forest ecosystems with some implications for silviculture. *Forest Ecology and Management*.
- Fujimori, T., S. Kawanabe, H. Saito, C.C. Grier, and T. Shidei. 1976. Biomass and net primary production in forests of three major vegetation zones of the northwestern United States. *Journal of the Japanese Forestry Society* 58: 360-373.
- Fung, I. 2000. Variable C Sinks. *Science* 290: 1313.
- Gardner, R.H. B.T. Milne, M.G. Turner, and R.V. O'Neill. 1987. Neutral models for the analysis of broad-scale landscape pattern. *Landscape Ecology* 1: 19-28.
- Garrison, G.A., J.M. Skovlin, C.E. Poulton, and A.H. Winward. 1976. Northwest plant names and symbols for ecosystem inventory and analysis, Gen. Tech.Rep. PNW-GTR-46. USDA Forest Service, Pacific Northwest Forest and Range Experiment Station, Portland, Oregon, 263 pp.
- Gaston, G., S. Brown, M. Lorenzini, and K.D. Singh. 1998. State and change in carbon pools in the forests of tropical Africa. *Global Change Biology* 4: 97-114.
- Gholz, H.L. 1980. Structure and productivity of *Juniperus occidentalis* in Central Oregon. *American Midland Naturalist* 103: 251-261.
- Gholz, H.L., F.K. Fitz, and R.H. Waring. 1976. Leaf area differences associated with old-growth forest communities in the western Oregon Cascades. *Canadian Journal of Forest Research* 6: 49-57.
- Goulden, M.L., J.W. Munger, S.-M. Fan, B.C. Daube, and S.C. Wofsy, S.C. 1996. Measurements of carbon sequestration by long-term eddy covariance: methods and a critical evaluation of accuracy. *Global Change Biology* 2: 169-182.
- Gower, S.T., C.C. Grier, D.J. Vogt, and K.A. Vogt. 1987. Allometric relations of deciduous (*Larix occidentalis*) and evergreen conifers (*Pinus contortus* and *Pseudotsuga menziesii*) of the Cascade Mountains in central Washington. *Canadian Journal of Forest Research* 17: 630-634.
- Grier, C.C. 1976. Biomass, productivity and nitrogen-phosphorus cycles in hemlock-spruce stands of the central Oregon coast. In: *Proceedings: Western Hemlock Management Conference*, Atkinson, W.A. and Zasoski,

- R.J. (Eds.), College of Forest Resources, University of Washington, Seattle, Washington, pp. 71-81.
- Grier, C.C. and R.S. Logan. 1977. Old-growth *Pseudotsuga Menziesii* communities of a western Oregon watershed: biomass distribution and production budgets. *Ecological Monographs* 47: 373-400.
- Grier, C.C. and R.H. Waring. 1974. Conifer foliage mass related to sapwood area. *Forest Science* 20: 205-206.
- Grier, C.C., K.A. Vogt, M.R. Keyes, and R.L. Edmonds. 1981. Biomass distribution and above- and below-ground production in young and mature *Abies amabilis* zone ecosystems of the Washington Cascades. *Canadian Journal of Forest Research* 11: 155-167.
- Grigal, D.F. and L.F. Ohmann. 1992. Carbon storage in upland forests of the Lake States. *Soil Science Society of America Journal* 56: 935-943.
- Guild, L.S., J.B. Kauffman, L.J. Ellingson, D.L. Cummings, and E.A. Castro. 1998. Dynamics associated with total aboveground biomass, C, nutrient pools, and biomass burning of primary forest and pasture in Rondonia, Brazil during SCAR-B. *Journal of Geophysical Research* 103: 32,091 - 32,100.
- Hansen, J. M.Sato, R. Ruedy, A. Lacis, and V. Oinas. 2000. Global warming in the twenty-first century: an alternative scenario. *Proceedings of the National Academy of Sciences* 97 (18): 9875-9880.
- Harcombe, P.A. 1986. Stand development in a 130-year-old spruce-hemlock forest based on age structure and 50 years of mortality data. *Forest Ecology and Management* 14: 41-58.
- Harmon, M.E. and J. Sexton. 1996. Guidelines for measurements of woody detritus in forest ecosystems. U.S. LTER Network Office, University of Washington, Seattle, Washington.
- Harmon, Mark E. and J.B. Domingo. 2001. A User's Guide to STANDCARB version 2.0: A Model to Simulate the C stores in Forest Stands. Department of Forest Science, Oregon State University, Corvallis, Oregon.
- Harmon, M.E. and B. Marks. In press. Effects of silvicultural treatments on carbon stores in Douglas-fir/western hemlock Forests in the Pacific Northwest, USA. *Canadian Journal of Forest Research*.
- Harmon, M.E., J.F. Franklin, F.J. Swanson, P. Sollins, S.V. Gregory, J.D. Lattin, N.H. Anderson, S.P. Cline, N.G. Aumen, J.R. Sedell, G.W. Leinkaemper, K. Cromack Jr., and K.W. Cummins. 1986. Ecology of coarse woody

- debris in temperate ecosystems. *Advances in Ecological Research* 15: 133-302.
- Harmon, M.E., W.K. Ferrell, and J.F. Franklin. 1990. Effects on carbon storage of conversion of old-growth forests to young forests. *Science* 247: 699-702.
- Harmon, M.E., J.M. Harmon, W.K. Ferrell, and D. Brooks. 1996. Modeling carbon stores in Oregon and Washington forest products: 1900-1992. *Climatic Change* 33: 521-550.
- Harmon, M.E., K. Bible, M.J. Ryan, H. Chen, and J. Klopatek. In review. Production, respiration, and overall carbon balance in an old-growth *Pseudotsuga/Tsuga* forest ecosystems.
- Havrenek, W.M. and W. Tranquillini. 1995. Physiological processes during winter dormancy and their ecological significance. In: *Ecophysiology of Coniferous Forests*, Smith, W.K. and T.M. Hinckley (Eds.), Academic Press, San Diego, California, pp. 95-124.
- Hibbard, K.A. 1995. Landscape Patterns of C and Nitrogen Dynamics in a Subtropical Savanna: Observations and Models. Ph.D. Dissertation, Texas A&M University.
- Holland, E.A. and S. Brown. 1999. North American C sink: technical comments. *Science* 283: 1815a.
- Houghton, R.A. 1993. Is C accumulating in the northern temperate zone? *Global Biogeochemical Cycles* 7: 611-617.
- Houghton, R.A. 1999. The annual net flux of C to the atmosphere from changes in land use 1850-1990. *Tellus* 51B: 298-313.
- Houghton, R.A., R.D. Boone, J.R. Fruci, J.E. Hobbie, J.M. Melillo, C.A. Palm, B.J. Peterson, G.R. Shaver, and G.M. Woodwell. 1987. The flux of carbon from terrestrial ecosystems to the atmosphere in 1980 due to changes in land use: geographic distribution of the global flux. *Tellus* 39B: 122-139.
- Houghton, R.A., E.A. Davidson, and G.M. Woodwell. 1998. Missing sinks, feedbacks, and understanding the role of terrestrial ecosystems in the global C balance. *Global Biogeochemical Cycles* 12: 25-34.
- Houghton, R.A., J.L. Hackler, K.T. Lawrence. 1999. The U.S. C budget: contributions from land-use change. *Science* 285: 574-578.
- Houghton, R.A., Skole, D.L., Nobre, C.A., Hackler, J.L., Lawrence, K.T., Chomentowski, W.H. 2000. Annual fluxes of carbon from deforestation and regrowth in the Brazilian Amazon. *Nature* 403: 301-304.

- Janisch, J.E. and M.E. Harmon. 2002. Successional changes in live and dead wood stores: Implications for net ecosystem productivity. *Tree Physiology* 22: 77-89.
- Jensen, M.E. and H.R. Haise. 1963. Estimating evapotranspiration from solar radiation. *Journal of Irrigation and Drainage Engineering* 89: 15-41.
- Jensen, M., A. Michelsen and M. Gashaw. 2001. Responses in plant, soil inorganic and microbial nutrient pools to experimental fire, ash and biomass addition in a woodland savanna. *Oecologia* 128: 85-93.
- Johnson, E.A. and S.L. Gutsell. 1994. Fire frequency models, methods and interpretations. *Advances in Ecological Research* 25: 239-287.
- Johnson, E.A. and C.E. Van Wagner. 1985. The theory and use of two fire history models. *Canadian Journal of Forest Research* 15:214-220.
- Jones, H.G. 1992. *Plants and Microclimate: A Quantitative Approach to Environmental Plant Physiology*. Cambridge University Press, Cambridge, 428 pp.
- Kaharabata, S.K., P.H. Schuepp, S. Ogunjemiyo, S. Shen, M.Y. Leclerc, R.L. Desjardins, and J.I. MacPherson. 1997. Footprint considerations in BOREAS. *Journal of Geophysical Research* 102: 29,113 - 29,124.
- Kapos, V., G. Ganade, E. Matsui and R.L. Victoria. 1993. Delta13C as an indicator of edge effects in tropical rainforest reserves. *Journal of Ecology* 81: 425-432.
- Kaufmann, M.R. and C.A. Troendle. 1981. The relationship of leaf area and foliage biomass to sapwood conducting area in four subalpine forest tree species. *Forest Science* 27: 477-482.
- Kauppi, P.E., K. Mielikainen, and K. Kuusela. 1992. Biomass and carbon budget of European forests from 1971-1990. *Science* 256: 70-74.
- Keyes, M.L. and C.C. Grier. 1981. Above- and below-ground net production in 40-year-old Douglas-fir stands on low and high productivity sites. *Canadian Journal of Forest Research* 11: 599-605.
- Kimmins, J.P. and G.J. Krumlik. 1973. Comparison of the biomass distribution and tree form of old virgin forests at medium and high elevations in the mountains of South Coastal British Columbia, Canada. IUFRO Working

Party on the Mensuration of Forest Biomass, paper presented in Vancouver, B.C., August 20-24.

- King, A.W., Johnson, A.R. and O'Neill, R.V. 1991. Transmutation and functional representation of heterogeneous landscapes. *Landscape Ecology* 5: 238-253.
- Klopatek, J.M. 2002. Belowground carbon pools and processes in different age stands of Douglas-fir. *Tree Physiology* 22: 197-204.
- Krankina, O.N. and R.K. Dixon. 1994. Forest management options to conserve and sequester terrestrial carbon in the Russian Federation. *World Research Review* 6: 88-101.
- Krankina, O.N., M.E. Harmon, and J.K. Winjum. 1996. Carbon storage and sequestration in the Russian forest sector. *Ambio* 25: 284-288.
- Krummel, J.R., R.H. Gardner, G. Sugihara, R.V. O'Neill, and P.R. Coleman. 1987. Landscape patterns in a disturbed environment. *Oikos* 48: 321-324.
- Kucharik, C.J., J.A. Foley, C. Delire, V.A. Fisher, M.T. Coe, J.D. Lenters, C. Young-Molling, N. Ramankutty. 2000. Testing the performance of a Dynamic Global Ecosystem Model: water balance, carbon balance, and vegetation structure. *Global Biogeochemical Cycles* 14: 795-825.
- Kurz, W.A. and M.J. Apps. A 70-year retrospective analysis of carbon fluxes in the Canadian forest sector. *Ecological Applications* 9: 526-547.
- Lassen, L.E. and E.A. Okkonen. 1969. Sapwood thickness of Douglas-fir and five other western softwoods. FPL-124, Oregon State University, Corvallis, Oregon.
- Laurance, W.F., L.V. Ferreira, J.M. Rankin-de-Merona, and S.G. Laurance. 1998. Rain forest fragmentation and the dynamics of Amazonian tree communities. *Ecology* 79: 2032-2040.
- Laurance, W.F., S.G. Laurance, L.V. Ferreira, J.M.R. Merona, C. Gascon, and T.E. Lovejoy. 1997. Carbon collapse in Amazonian forest fragments. *Science* 278: 1117-1118.
- Lenihan, J.M., C. Daly, D. Bachelet, R.P. Neilson. 1998. Simulating broad-scale fire severity in a dynamic global vegetation model. *Northwest Science* 72: 91-103.
- Levin, S.A. 1992. The problem of pattern and scale in ecology. *Ecology* 73: 1943-1967.

- Levitus, S. J.I. Antonov, J. Wang, T.L. Delworth, K.W. Dixon, A.J. Baldocchi. 2001. Anthropogenic warming of the earth's climate system. *Science* 292: 267-270.
- Li, B.-L. 2000. Fractal geometry applications in description and analysis of patch patterns and patch dynamics. *Ecological Modelling* 132: 33-50.
- Lidicker Jr., W.Z. 1999. Responses of mammals to habitat edges: an overview. *Landscape Ecology* 14: 333-343.
- Leibowitz, S.G., C. Loehle, B.-L. Lin, and E.M. Preston. 2000. Modeling landscape functions and effects: a network approach. *Ecological Modelling* 132: 77-94.
- Lovejoy, T.E., J.M. Rankin, R.O. Bierregaard Jr., K.S. Brown, L.H. Emmons, M.E. Van der Voort. 1984. Ecosystem decay of Amazon forest fragments. In: *Extinctions*, Nitecki, M.H. (Ed.), The University of Chicago Press: Chicago and London, pp. 295-326.
- Long, J.N. and J. Turner. 1975. Aboveground biomass of understorey and overstorey in an age sequence of four Douglas-fir stands. *Journal of Applied Ecology* 12: 179-188.
- Marshall, J.D. and R.H. Waring. 1986. Comparison of methods of estimated leaf area index in old-growth Douglas-fir. *Ecology* 67: 975-979.
- Matthews, E. 1997. Global litter production, pools, and turnover times: estimates from measurement data and regression models. *Journal of Geophysical Research* 102: 18,771 - 18,800.
- Means, J.E., S.A. Acker, D.J. Harding, J.B. Blair, M.A. Lefsky, W.B. Cohen, M.E. Harmon, and W.A. McKee. 1999. Use of large-footprint scanning airborne lidar to estimate forest stand characteristics in the western Cascades of Oregon. *Remote Sensing of Environment* 67: 298-308.
- Means, J.E., H.A. Hansen, G.J. Koerper, P.B. Alaback, and M.W. Klopsch. 1994. *Software for Computing Plant Biomass - BIOPAK Users Guide*, PNW-GTR-340, U.S.D.A. Forest Service, Pacific Northwest Research Station, Portland, Oregon.
- Means, J.E., P.C. MacMillan, K. and Cromack Jr. 1992. Biomass and nutrient content of Douglas-fir logs and other detrital pools in an old-growth forest, Oregon, U.S.A. *Canadian Journal of Forest Research* 22: 1536-1546.
- Melillo, J.M., J.R. Fruci, R.A. Houghton, B. Moore, and D.L. Skole. 1988. Land-use change in the Soviet Union between 1850 and 1980: causes of a net release of CO₂ to the atmosphere. *Tellus* 40B: 116-128.

- Mencuccini, M. and J. Grace. 1996. Hydraulic conductance, light interception and needle nutrient concentration in Scots pine stands and their relations with net primary productivity. *Tree Physiology* 16: 459-468.
- Moorcroft, P.R., G.C. Hurtt, and S.W. Pacala. 2001. A method for scaling vegetation dynamics: the Ecosystem Demography model (ED). *Ecological Monographs* 71: 557-586.
- Odum, E.P. 1969. The strategy of ecosystem development. *Science* 164: 262-269.
- Olson, J.S. 1963. Energy storage and the balance of producers and decomposers in ecological systems. *Ecology* 44: 322-331.
- Olson, P. 1978. Changes in the global carbon cycle and the biosphere. ORNL/EIS-109. ORNL, 169pp.
- O'Neill, R.V. 1988. Hierarchy theory and global change. In: *Scales and Global Change*, Rosswall, T., Woodmansee, R.G., and Risser P.G. (Eds.), John Wiley & Sons, Ltd., New York, New York, pp. 29-45.
- O'Neill, R.V., C.T. Hunsaker, S.P. Timmins, B.L. Jackson, K.B. Jones, K.H. Riitters, J.D. Wickham. 1996. Scale problems in reporting landscape pattern at the regional scale. *Landscape Ecology* 11: 169-180.
- Pacala, S.W., G.C. Hurtt, D. Baker, P. Peylin, R.A. Houghton, R.A. Birdsey, L.S. Heath, E. Sundquist, R. Stallard, P. Ciais, P.R. Moorcroft, J.P. Casperson, E. Shevliakova, B. Moore, G. Kohlmaier, E.A. Holland, M. Gloor, M.E. Harmon, S.-M. Fan, J. Sarmiento, C.L. Goodale, D. Schimel, and C.B. Field. 2001. Consistent land- and atmosphere-based U.S. C sink estimates. *Science* 292: 2316-2319.
- Parson, E.A. and D.W. Keith. 1998. Fossil fuels without CO₂ emissions. *Science* 282: 1053-1054.
- Peng, C. 2000. From static biogeographical model to dynamic global vegetation model: a global perspective on modeling vegetation dynamics. *Ecological Modelling* 135: 33-54.
- Pierce, L.L. and S.W. Running. 1995. The effects of aggregating sub-grid land surface variation on large-scale estimates of net primary production. *Landscape Ecology* 10: 239-253.
- Pike, L.H., R.A. Rydell, and W.C. Denison. 1977. A 400-year-old Douglas-fir tree and its epiphytes: biomass, surface area, and their distributions. *Canadian Journal of Forest Research* 7: 680-699.

- Potter, C.S., S. Klooster, and V. Brooks. 1999. Interannual variability in terrestrial net primary production: exploration of trends and controls on regional to global scales. *Ecosystems* 2: 36-48.
- Potter, C, V.B. Genovese, S.A. Klooster, M. Bobo, A. Torregrosa. 2001. Biomass burning losses of C estimated from ecosystem modeling and satellite data analysis for the Brazilian Amazon region. *Atmospheric Environment* 35: 1773-1781.
- Prescott, C.E., P. Corbin, and D. Parkinson. 1989. Biomass, productivity, and nutrient-use efficiency of aboveground vegetation in four Rocky Mountain coniferous forests. *Canadian Journal of Forest Research* 19: 309-317.
- Ranney, J.W., M.C. Brunner, and J.B. Levenson. 1981. The importance of edge in the structure and dynamics of forest islands. In: *Forest Island Dynamics in Man-Dominated Landscapes*, Springer-Verlag, New York, New York, pp. 67-96.
- Reed, R.A., M.E. Finley, W.H. Romme, and M.G. Turner. 2001. Aboveground net primary production and leaf-area index in early postfire vegetation in Yellowstone National Park. *Ecosystems* 2: 88-94.
- Remillard, S.M. 1999. Soil Carbon and Nitrogen in Old-Growth Forests in Western Oregon and Washington, M.S. Thesis, Oregon State University, Corvallis.
- Richards, F.J. 1959. A flexible growth function for empirical use. *Journal of Experimental Botany* 10: 290-300.
- Risser, P.G. 1987. Landscape ecology: state of the art. In: *Landscape Heterogeneity and Disturbance*, Turner, M.G. (Ed.), Springer-Verlag, New York, New York, pp. 3-13.
- Risser, P.G. 1999. Landscape ecology: does the science only need to change at the margin? In: *Landscape Ecological Analysis: Issues and Applications*, Klopatek, J.M., and Gardner, R.H. (Eds.), Springer, New York, New York, pp. 3-10.
- Rogers, R. and T.M. Hinckley. 1979. Foliage weight and area related to current sapwood area in oak. *Forest Science* 25: 298-303.
- Romm, J.M. Levine, M. Brown, and E. Petersen. 1998. A Road map for U.S. carbon reductions. *Science* 279: 669-670.
- Running, S.W. and J.C. Coughlan. 1988. A general model of forest ecosystem processes for regional applications I. Hydrologic balance, canopy gas exchange and primary production processes. *Ecological Modelling* 42: 125-154.

- Santantonio, D. and R.K. Hermann. 1985. Standing crop, production, and turnover of fine roots on dry, moderate, and wet sites of mature Douglas-fir in western Oregon. *Annals of Science Forestry* 42: 113-142.
- Santantonio, D., R.K. Hermann, and W.S. Overton. 1977. Root biomass studies in forest ecosystems. *Pedobiologia* 17: 1-31.
- Schimel, D.S., VEMAP Participants, and B.H. Braswell. 1997. Continental scale variability in ecosystem processes: models, data, and the role of disturbance. *Ecological Monographs* 67: 251-271.
- Schimel, D., I.G. Enting, M. Heimann, T.M.L. Wigley, D. Raynaud, D. Alves, U. Siegenthaler. 2000. CO₂ and the Carbon Cycle. In: *The Carbon Cycle*, Wigley, T.M.L. and Schimel, D.S. (Eds.), Cambridge University Press, New York, New York, pp 7-36.
- Schimel, D., J. Melillo, H. Tian, A.D. McGuire, D. Kicklighter, T. Kittel, N. Rosenbloom, S. Runnings, P. Thornton, D. Ojima, W. Parton, R. Kelly, M. Sykes, R. Neilson, B. Rizzo. 2000. Contribution of increasing CO₂ and climate to carbon storage by ecosystems in the United States. *Science* 287: 2004-2006.
- Schimel, D.S., J.I. House, K.A. Hibbard, P. Bousquet, P. Ciais, P. Peylin, B.H. Braswell, M.J. Apps, D. Baker, A. Bondeau, J. Canadell, G. Churkina, W. Cramer, A.S. Denning, C.B. Field, P. Friedlingstein, C. Goodale, M. Heimann, R.A. Houghton, J.M. Melillo, B. Moore III, D. Murdiyarso, I. Noble, S.W. Pacala, I.C. Prentice, M.R. Raupach, P.J. Rayner, R.J. Scholes, W.L. Steffen, C. Wirth. 2001. Recent patterns and mechanisms of carbon exchange by terrestrial ecosystems. *Nature* 414: 169-172.
- Schlesinger, W.H. 1977. Carbon balance in terrestrial detritus. *Annual Review of Ecology and Systematics* 8: 51-81.
- Schultze, E.-D., C. Wirth, and M. Heimann. 2000. Managing forests after Kyoto. *Science* 289: 2058-2059.
- Sedjo, R.A. 1992. Temperate forest ecosystems in the global C cycle. *Ambio* 21: 274-277.
- Shugart, H.H., P.J. Michaels, T.M. Smith, D.A. Weinstein, and E.B. Rastetter. 1988. Simulation models of forest succession. In: *Scales and Global Change*, Rosswall, T., Woodmansee, R.G., and Risser, P.G. (Eds.), John Wiley & Sons, Ltd., New York, New York.
- Sinton, D.S., J.A. Jones, J.L. Ohmann, and F.J. Swanson. 2000. Windthrow disturbance, forest composition, and structure in the Bull Run Basin, Oregon. *Ecology* 81: 2539-2556.

- Snell, J.A.K. and J.K. Brown. 1978. Comparison of tree biomass estimators - DBH and sapwood area. *Forest Science* 24: 455-457.
- Smithwick, E.A.H. and M.E. Harmon. In press. Potential upper bounds of carbon stores in forests of the Pacific Northwest. *Ecological Applications*.
- Sollins, P., C.C. Grier, F.M. McCorison, K. Cromack, Jr., and R. Fogel. 1980. The internal element cycles of an old-growth Douglas-fir ecosystem in western Oregon. *Ecological Monographs* 50: 261-285.
- Turner, D.P., G.J. Koerper, M.E. Harmon, and J.J. Lee. 1995. A Carbon budget for forests of the conterminous United States. *Ecological Applications* 5: 421-436.
- Turner, D.P., W.B. Cohen, and R.E. Kennedy. 2000a. Alternative spatial resolution and estimation of carbon flux over a managed forest landscape in Western Oregon. *Landscape Ecology* 15: 441-452.
- Turner, D.P., S.A. Acker, J.E. Means, and S.L. Garman. 2000b. Assessing alternative allometric algorithms for estimating leaf area of Douglas-fir trees and stands. *Forest Ecology and Management* 126: 61-76.
- Turner, D.P. and M. Gregory. In review. Spatially-distributed modeling of gross primary production and evapotranspiration over the flux tower footprint over a boreal forest site. *Agricultural and Forest Meteorology*.
- Turner, J. and J.N. Long. 1975. Accumulation of organic matter in a series of Douglas-fir stands. *Canadian Journal of Forest Research* 5: 681-690.
- Turner, M.G. 1989. Landscape ecology: The effect of pattern on process. *Annual Review of Ecology and Systematics* 20: 171-97.
- Ugolini, F.C., G. Corti, A. Agnelli, and F. Piccardi. 1996. Mineralogical, physical, and chemical properties of rock fragments in soil. *Soil Science* 161: 521-542.
- U.S. Forest Products Laboratory. 1974. *Wood Handbook: Wood as an Engineering Material*. USDA Agricultural Handbook 72, revised edition.
- Van Wagner, C.E. 1978. Age-class distribution and the forest fire cycle. *Canadian Journal of Forest Research* 8: 220-227.
- Vitousek, P.M. 1991. Can planted forests counteract increasing atmospheric carbon dioxide? *Journal of Environmental Quality* 20: 348-354.

- Vitousek, P.M., T. Fahey, D.W. Johnson, and M.J. Swift. 1988. Element interactions in forest ecosystems: succession, allometry and input-output budgets. *Biogeochemistry* 5: 7-34.
- Wallin, D.O., F.J. Swanson, B. Marks, J.H. Cissel, J. Kertis. 1996. Comparison of managed and pre-settlement landscape dynamics in forests of the Pacific Northwest, USA. *Forest Ecology and Management* 85: 291-309.
- Waring, R.H. and J.F. Franklin. 1979. Evergreen coniferous forests of the Pacific Northwest. *Science* 204: 1380-1386.
- Waring, R.H. and S.W. Running. 1998. *Forest Ecosystems: Analysis at Multiple Scales*, Academic Press, San Diego, California, 370 pp.
- Waring, R.H., H.L. Gholz, C.C. Grier, and M.L. Plummer. 1977. Evaluating stem conducting tissue as an estimator of leaf area in four woody angiosperms. *Canadian Journal of Botany* 55: 1474-1477.
- Waring, R.H., K. Newman, and J. Bell. 1981. Efficiency of tree crowns and stemwood production at different canopy leaf densities. *Forestry* 54: 129-157.
- Waring, R.H., P.E. Schroeder, and R. Oren. 1982. Application of the pipe model theory to predict canopy leaf area. *Canadian Journal of Forest Research* 12: 556-560.
- Watson, R., M.C. Zinyowera, R.H. Moss, D.J. Dokken (Eds.) 1997. *The Regional Impacts of Climate Change: An Assessment of Vulnerability*. Special Report of Working Group II of the International Panel on Climate Change.
- Watson, R. et al. 2000. *Land Use, Land-Use Change, and Forestry, Summary for Policymakers*, Special Report of Working Group II of the Intergovernmental Panel on Climate Change.
- Weathers, K.C., M.L. Cadenasso, S.T.A. Pickett. 2001. Forest edges as nutrient and pollutant concentrators: potential synergisms between fragmentation, forest canopies and the atmosphere. *Conservation Biology* 15: 1506-1514.
- White, A., M.G.R. Cannell, and A.D. Friend. 2000. The high latitude terrestrial carbon sink: a model analysis. *Global Change Biology* 6: 227-245.
- Whitehead, D., D.U.U. Okali, and F.E. Fasehun. 1981. Stomatal response to environmental variables in two tropical forest species during the dry season in Nigeria. *Journal of Applied Ecology* 18: 571-587.

- Whitehead, D., W.R.N. Edwards, and P.G. Jarvis. 1984. Conducting sapwood area, foliage area, and permeability in mature trees of *Picea sitchensis* and *Pinus contorta*. *Canadian Journal of Forest Research* 14: 940-947.
- Whittaker, R.H. 1975. *Communities and Ecosystems*, MacMillan Publishing Co., Inc., New York, New York, 385 pp.
- Whittaker, R.H. and G.E. Likens. 1973. Carbon in the biota. In: *Carbon and the Biosphere*, Woodwell, G. M. and Pecan, E.V. (Eds.), U.S. Atomic Energy Commission Symposium Series 30, National Technical Information Service, Springfield, Virginia, pp. 281-302.
- Wiens, J.A. 1998. Landscape ecology: scaling from mechanisms to management. In: *Perspectives in Ecology: A Glance from the VII International Congress of Ecology*, Farina, A. (Ed.), Springer-Verlag, New York, New York, pp. 13-24.
- Williams-Linera, G. 1990. Vegetation structure and environmental conditions of forest edges in Panama. *Journal of Ecology* 78: 356-373.
- With, K.A. 1997. The application of neutral landscape models in conservation biology. *Conservation Biology* 11: 1069-1080.
- Wofsy, S.C., Goulden, M.L., Munger, J.W., Fan, S.-M., Bakwin, P.S., Daube, B.C., Bassow, S.L., and Bazzaz, F.A. 1993. Net exchange of CO₂ in a mid-latitude forest. *Science* 260: 1314-1317.
- Yoder, B.J., M.G. Ryan, R.H. Waring, A.W. Schoett, M.R. Kaufman. 1994. Evidence of reduced photosynthetic rates in old trees. *Forest Science* 40: 513-527.
- Zhang, L., J.H. Gove, C. Liu, W.B. Leak. 2001. A finite mixture of two Weibull distributions for modeling the diameter distributions of rotated-sigmoid, uneven-aged stands. *Canadian Journal Forest Research* 31: 1654-1659.

APPENDICES

Appendix A. Species names, foliage biomass equations, and global comparison of old-growth forest data from Chapter 2.

Table A.1. Scientific and common names of observed tree species and their abbreviations (Garrison et al. 1976).

Scientific Name	Common Name	Abbreviation
<i>Abies amabilis</i>	Silver fir	ABAM
<i>Abies concolor</i>	White fir	ABCO
<i>Abies grandis</i>	Grand fir	ABGR
<i>Abies lasiocarpa</i>	Subalpine fir	ABLA
<i>Abies procera</i>	Noble fir	ABPR
<i>Acer macrophyllum</i>	Bigleaf maple	ACMA
<i>Alnus rubra</i>	Red alder	ALRU
<i>Arbutus menziesii</i>	Pacific madrone	ARME
<i>Castanopsis chrysophylla</i>	Golden chinkapin	CACH
<i>Calocedrus decurrens</i>	Incense cedar	CADE
<i>Chamaecyparis nootkatensis</i>	Alaska cedar	CHNO
<i>Cornus nutallii</i>	Pacific dogwood	CONU
<i>Pinus contorta</i>	Lodgepole pine	PICO
<i>Pinus lambertiana</i>	Sugar pine	PILA
<i>Pinus monticola</i>	Western white pine	PIMO
<i>Pinus ponderosa</i>	Ponderosa pine	PIPO
<i>Picea sitchensis</i>	Sitka spruce	PISI
<i>Pseudotsuga menzeseii</i>	Douglas-fir	PSME
<i>Quercus garryana</i>	Oregon white oak	QUGA
<i>Rhamnus purshiana</i>	Cascara buckthorn	RHPU
<i>Taxus brevifolia</i>	Pacific yew	TABR
<i>Thuja plicata</i>	Western red cedar	THPL
<i>Tsuga heterophylla</i>	Western hemlock	TSHE
<i>Tsuga merensiana</i>	Mountain hemlock	TSME

Table A.2. Source of equations used to calculate foliage biomass.

Scientific Name ¹	DBH to Sapwood Area	Sapwood Area: Leaf Area	Specific Leaf Area ²
ABAM	see <i>Tsuga heterophylla</i>	Waring et al. 1982	Gholz et al. 1976
ABCO	see <i>Tsuga heterophylla</i>	see <i>Pinus monticola</i>	see <i>Pinus monticola</i>
ABGR	see <i>Tsuga heterophylla</i>	Waring et al. 1982	Gholz et al. 1976
ABLA	see <i>Tsuga heterophylla</i>	Kaufman and Troendle 1981 ^a	Kaufmann and Troendle 1981
ABPR	see <i>Tsuga heterophylla</i>	Grier and Waring 1974 ^b	Gholz et al. 1976
ACMA		Waring et al. 1977	Kaufmann and Troendle 1981 ^c
ALRU		see <i>Acer macrophyllum</i>	Kaufmann and Troendle 1981 ^c
ARME		see <i>Acer macrophyllum</i>	Kaufmann and Troendle 1981 ^c
CACH		Waring et al. 1977	Kaufmann and Troendle 1981 ^c
CADE	see <i>Thuja plicata</i>	see <i>Thuja plicata</i>	see <i>Thuja plicata</i>
CHNO	see <i>Thuja plicata</i>	see <i>Thuja plicata</i>	see <i>Thuja plicata</i>
CONU	see <i>Acer macrophyllum</i>	see <i>Acer macrophyllum</i>	Kaufmann and Troendle 1981 ^c
PICO	from Lassen and Okonen 1969	^d	Bond et al. 1999 ^e
PILA	see <i>Pseudotsuga menzeseii</i>	see <i>Pinus monticola</i>	see <i>Pseudotsuga menzeseii</i>
PIMO	see <i>Pseudotsuga menzeseii</i>	Snell and Brown 1978	see <i>Pinus contorta</i>

Table A.2. (Continued)

Scientific Name ¹	DBH to Sapwood Area	Sapwood Area: Leaf Area	Specific Leaf Area ²
PIPO	S. Acker	Waring et al. 1982	Bond et al. 1999 ^e
PISI	from Lassen and Okonen 1969 ^f	Whitehead et al. 1984	Kaufmann and Troendle 1981
PSME	S. Acker, N. McDowell	Waring et al. 1982	Gholz et al. 1976
QUGA		Rogers and Hinkley 1979 ^g	Kaufmann and Troendle 1981 ^c
RHPU		see <i>Acer macrophyllum</i>	Kaufmann and Troendle 1981 ^c
TABR	see <i>Tsuga heterophylla</i>	see <i>Tsuga heterophylla</i>	Gholz et al. 1976
THPL	S. Acker	Turner et al. 2000b	Gholz et al. 1976
TSHE	S. Acker	Waring et al. 1982	Gholz et al. 1976
TSME	see <i>Tsuga heterophylla</i>	Waring et al. 1982	see <i>Tsuga heterophylla</i>

¹ As given in Table A.1

² Converted to projected area by dividing by 2.3, unless otherwise noted

^a Converted to projected area by dividing by 2.5 in Waring et al. 1982

^b Converted from biomass to leaf area in Waring et al. 1981

^c Originally for aspen, *Populus tremuloides*, divided by 2 to convert from total leaf area to projected leaf area

^d Used LA:SA = 0.16, average from literature (Gower et al. 1987, 0.14, Waring et al. 1982, 0.15, Kaufman and Troendle 1981, 0.18, Whitehead et al. 1981, 0.17)

^e Calculated from LMA (leaf mass per area)

^f Equation originally for *Picea engelmannii*

^g Originally for *Quercus alba*

Table A.3. Comparison with estimates from the literature for vegetation, detritus, and soil carbon stores in ecosystems around the globe. Reported biomass values were converted to carbon by assuming a 2:1 biomass to carbon ratio. Units are Mg C ha⁻¹. Unless stand age is specifically noted, carbon (C) refers to an average value for that ecosystem. When pools were not described in detail, the summary variable, as described by the authors, was included.

Forest Type	Vegetation C Store	Reference	Age	Pools Included^a
Temperate Forest				
<i>Pseudotsuga-Tsuga</i> H.J. Andrews, Oregon Cascades	557	This Study	450	1,2,3,4,5,6,7,8,9
<i>Pseudotsuga-Tsuga</i> H.J. Andrews, Oregon Cascades	435	Grier and Logan 1977	450	1,2,3,4,5,6,7,8,9
<i>Pseudotsuga-Tsuga</i> Middle Santiam, Oregon Cascades	398	Fujimori et al. 1976	>500	1,2, 3, 4,5
<i>Pseudotsuga-Tsuga</i> Blue River, Oregon Cascades	331	Fujimori et al. 1976	90-110	See Above
<i>Pseudotsuga menziesii</i> H.J. Andrews, Oregon Cascades	587	Means et al. 1992	450	Total aboveground live tree C
<i>Tsuga-Picea</i> Cascade Head, Oregon Coast	436	Fujimori et al. 1976	100-120	See Above
<i>Tsuga-Picea</i> Cascade Head, Oregon Coast	598	This Study	150	See Above
<i>Abies-Pseudotsuga</i> Wildcat Mountain, Oregon	440	Fujimori et al. 1976	100-130	See Above
<i>Pinus Ponderosa</i> Eastern Oregon	113	This Study	300-500	See Above
<i>Abies-Pseudotsuga-Thuja</i> Washington Cascades	480	This Study	300-1200	See Above
<i>Abies-Pseudotsuga</i> Goat March RNA, Washington	422	Fujimori et al. 1976	310	See Above
<i>Abies amabilis</i> Washington Cascades	293	Grier et al. 1981	180	1,2,3,4,6,7,8,9,10
<i>Tsuga-Picea</i> Washington Coast	479	This Study	122-250	See Above
Giant Temperate Conifer	312	Vitousek et al. 1988	old growth	1,2,3,4,5
Temperate Evergreen N. Amer., Europe, China, Pacific-developed, N.Africa, Middle East	160	Houghton et al. 1987, Houghton 1999	undisturbed	Above- and below- ground live biomass of trees and ground cover (Average values from references therein)
Temperate Evergreen	175	Whittaker 1975		not specified
Temperate Broadleaf Evergreen	158	Vitousek et al. 1988	mature	1,2,4,8,9 (Average value from references therein)

Table A.3. (Continued)

Forest Type	Vegetation C Store	Reference	Age	Pools Included ^a
Temperate Broadleaved Forest	100	Houghton et al. 1999		See Above
Temperate Broadleaf Deciduous	143	Vitousek et al. 1988		See Above
Temperate Deciduous N. Amer, Europe, China, Pacific-developed	135	Houghton et al. 1987, Houghton 1999		See Above
Temperate Deciduous	150	Whittaker 1975		See Above
Mid Latitudinal Belt	57	Dixon et al. 1994		Above- and Belowground tree living and dead mass (Average value from references therein)
<i>Pseudotsuga menziesii</i> Washington	278	Keyes and Grier 1981	40	1,2,3,4,8,9 High productivity site
<i>Tsuga canadensis</i> or <i>Pinus strobus</i> , Wisconsin	286	Crow 1978	225	Upper bound of estimate
<i>Tsuga mertensianna</i> Waldo Lake, Oregon	158	Boone et al. 1988	>400	Aboveground tree
Cove forests Southern Appalachian, Tennessee	236	Busing et al. 1993		1,2,4,5
Closed-canopy forests Lake States, USA	150	Grigal and Ohmann 1992		Total above-ground, 8
<i>Picea engelmannii</i> - <i>Abies lasiocarpa</i> Southwestern Alberta	102	Prescott et al. 1989	350	1,2,6,7,10
Tropical Forest				
Tropical/Subtropical Closed Forest	247	Vitousek et al. 1988	mature	See Above
Tropics (6 forest categories)	46-183	Brown and Lugo 1982		Weighted by area of forest type
Lowland-moist forest	185	Brown and Lugo 1982		Maximum, not area- weighted
Tropics (3 forest categories)	113-189	Atjay et al. 1979		
Tropics (6 categories)	70-180	Olson 1978		
Tropics (2 categories)	160-200	Whittaker and Likens 1973		
Tropics Rondonia, Brazil	178-200	Guild et al. 1998		1,11,12,15, dicot seedlings, rootmat, palm
Closed Tropical Forests South Asia	25-265	Brown et al. 1991	mature, undisturbed	Mean total aboveground tree C (>10cm dbh)
Low Latitudinal Belt	121	Dixon et al. 1994		See Above
Tropical Rain Forest	225	Whittaker 1975		See Above
Tropical Seasonal Forest	175	Whittaker 1975		See Above

Table A.3. (Continued)

Forest Type	Vegetation C Store	Reference	Age	Pools Included ^a
Lowland Moist Forests Africa	178	Gaston et al. 1998		Above- and belowground, maximum
Tropical Moist Forests West Africa	250			
Tropical Moist Forest China, Pacific-developed, N. Africa, Middle East, Tropical Asia	250	Houghton 1999		See Above
Warm Coniferous Forest Latin America	168	Houghton 1999		See Above
Tropical Equatorial Forest, Latin America	200	Houghton 1999		See Above
Tropical Seasonal Forest Latin America	140	Houghton 1999		See Above
Tropical Seasonal Forest Tropical Asia	150	Houghton 1999		See Above
Closed Forest Sub-Saharan Africa	136	Houghton 1999		See Above
Savanna/Woodland/Grassland				
Tropical/subtropical woodland/savanna	54	Vitousek et al. 1988		See Above
Woodland Tropical, Asia	60	Houghton et al. 1999		See Above
Tropical Woodland Latin America	55	Houghton 1999		See Above
Temperate Grassland, N.Amer., Europe China, N. Africa, Pacific-developed, Middle East	7	Houghton 1999		See Above
Temperate Grassland, USSR	10	Houghton 1999		See Above
Grassland, Latin America	10	Houghton 1999		See Above
Grassland, Tropical Asia	60	Houghton 1999		See Above
Temperate Woodland N.Amer., Pacific-developed	27	Houghton 1999		See Above
Open Forest, Sub-Saharan Africa	30	Houghton 1999		See Above
Woodland and shrubland	30	Whittaker 1975		See Above
Savanna	20	Whittaker 1975		See Above
Temperate Grassland	8	Whittaker 1975		See Above

Table A.3. (Continued)

Forest Type	Vegetation C Store	Reference	Age	Pools Included ^a
Boreal/Northern Latitudes				
Northern/subalpine Conifer	117	Vitousek et al. 1988		See Above
High Latitudinal Belt	64	Dixon et al. 1994		See Above
Boreal Forest	100	Whittaker 1975		See Above
Boreal Forest, N.Amer., Eur., USSR	90	Houghton 1999		See Above
<i>Pinus-Picea-Larix-Abies</i> Boreal Forest (taiga), Russia	48	Krankina et al. 1996		2 (>6 cm dbh)
Tundra and Alpine	3	Whittaker 1975		See Above
Desert/Arid				
Juniper Woodland	21	Gholz 1980	uneven-aged 30-350	1,2, 3, 4,5
Desert and semidesert shrub	4	Whittaker 1975		See Above
Grass Savanna, Africa	6	Gaston et al. 1998		See Above
Desert Scrub, N. Africa, Middle East	6	Houghton 1999		See Above
Desert Scrub, Latin America	12	Houghton 1999		See Above
Detritus				
Forest type	C Store	Reference	Age	Pools Included ^a
Temperate Forest				
<i>Pseudotsuga-Tsuga</i> Oregon Cascades	150	This Study		12,13,14,15,16,17
<i>Pseudotsuga-Tsuga</i> Oregon Cascades	133	Sollins et al. 1980	350-550	12,16
<i>Pseugotsuga menziesii</i> Oregon Cascades	207	Means et al. 1992	450	12,13,15
<i>Tsuga-Picea</i> Oregon Coast	164	This Study		See Above
<i>Pinus ponderosa</i> Eastern Oregon	45	This Study		See Above
<i>Abies-Pseudotsuga-Thuja</i> Washington Cascades	158	This Study		See Above
<i>Tsuga-Picea</i> Washington Coast	146	This Study		See Above
<i>Pseudotsuga-Tsuga</i> Oregon Cascades	133	Grier and Logan 1977		12, 13, 14,15,16,17

Table A.3. (Continued)

Forest type	Detritus C Store	Reference	Age	Pools Included^a
Temperate Forest	118	Schlesinger 1977 ^b		(45 studies)
Temperate Grassland	192	Schlesinger 1977		See Above;
<i>Tsuga mertensianna</i> Waldo Lake, Oregon	72	Boone et al. 1988		17, 12, 13 (their Table 1; Fig. 3) Assumed aboveground biomass = 45% C
<i>Abies amabilis</i> Washington Cascades	195	Grier et al. 1981	180	5,12,13,14,15
<i>Tsuga heterophylla</i> Coastal Washington	106	Grier 1976	121	12
Tropical Forest				
Tropical Forest	104	Schlesinger 1977		(22 studies)
Tropical Montane rain forest	11	Edwards and Grubb 1977		Cited in Harmon et al. 1986
Tropical Savanna/Woodland				
Woodland and Shrubland	69	Schlesinger 1977		(10 studies)
Tropical Savanna	37	Schlesinger 1977		
Boreal/Northern Latitudes				
Boreal Forest	149	Schlesinger 1977		(22 studies)
Tundra and Alpine	216	Schlesinger 1977		(31 studies)
<i>Pinus-Picea-Larix-Abies</i> Boreal forests (taiga), Russia	30	Krankina et al. 1996	mixed	12,13,14,15, slash; average value for all Russian forests
Desert/Arid				
Desert Scrub and Semidesert	56	Schlesinger 1977		(22 studies)
Other				
Swamp and Marsh	343	Schlesinger 1977		(10 studies)
Depth				
Forest Type	SOC	Reference	(when described, cm)	
Temperate Forest				
Oregon Cascades	123	Remillard 1999	100	

Table A.3. (Continued)

Forest Type	SOC	Reference	Depth (when described, cm)
Oregon Cascades	67	Sollins et al. 1980	100
Oregon Cascades	190	Means et al. 1992	100
Oregon Coast	366	Remillard 1999	100
Eastern Oregon	37	Remillard 1999	100
Washington Coast	195	Remillard 1999	100
Washington Cascades	117	Remillard 1999	100
Washington Cascades	137	Grier et al. 1981	60
Oregon Cascades	56	Grier and Logan 1977	100
Mid Latitudinal Belt	96	Dixon et al. 1994	100
Temperate Evergreen N. Amer., Europe, China, Pacific-developed, N. Africa, Middle East	134	Houghton et al. 1987, Houghton 1999	
Temperate Deciduous N. Amer, Europe, China, Pacific-developed	134	Houghton et al. 1987, Houghton 1999	
Temperate Forest, Europe, USA, USSR, Japan, Sweden, Thailand	118	Schlesinger 1977 ^b	20-100 (45 studies)
Temperate Broadleaved Latin America	134	Houghton 1999	
Temperate Grassland N.Amer., Europe, China, USSR N. Africa, Pacific-developed, Middle East	189	Houghton 1999	
Temperate Grassland Japan, USA, USSR	192	Schlesinger 1977	100-228 (19 studies)
North-central USA	106	Grigal and Ohmann 1992	
<i>Tsuga mertensiana</i> Waldo Lake, Oregon	33	Boone et al. 1988	depth to 30cm
Tropical Forest			
Tropical Forest Ecosystems	87	Brown and Lugo 1982	
Tropical Forest Ecosystems	83	Atjay et al. 1979	100
Tropical Forest Ecosystems	138	Olson et al. 1978	
Brazilian Amazonia	86	Fearnside and Barbosa 1998	100
Brazilian Amazonia	228	Fearnside and Barbosa 1998	800
Tropical Forest Brazil, Colombia, Nigeria, Suriname, Thailand	104	Schlesinger 1977	50-178 (22 studies)

Table A.3. (Continued)

Forest Type	SOC	Reference	Depth (when described, cm)
Warm Coniferous Forest Latin America	134	Houghton 1999	
Tropical Equatorial Forest Latin America	98	Houghton 1999	
Tropical Seasonal Forest Latin America	98	Houghton 1999	
Tropical Seasonal Forest Tropical Asia	80	Houghton 1999	
Tropical Moist Forest China, Pacific- developed, N. Africa, Middle East, Tropical Asia	120	Houghton 1999	
Low Latitudinal Belt	123	Dixon et al. 1994	100
Woodlands/Savannas/Grasslands			
Grassland Latin America	42	Houghton 1999	
Grassland Tropical Asia	50	Houghton 1999	
Woodland N.Amer., Pacific-developed, Latin America	69	Houghton 1999	
Open Forest Sub-Saharan Africa	50	Houghton 1999	
Woodland and Shrubland Europe, USA	69	Schlesinger 1977	20-60 (10 studies)
Tropical Savanna Africa, Thailand, Venezuela	37	Schlesinger 1977	20-100 (33 studies)
Woodland, Tropical Asia	50	Houghton 1999	
Closed Forest, Sub-Saharan Africa	100	Houghton 1999	
Boreal Forest			
Boreal Forest N.Amer., Europe, USSR	206	Houghton 1999	
Boreal Forest Canada, Sweden, USA, USSR	149	Schlesinger 1977	61-230 (22 studies)
High Latitudinal Belt	343	Dixon et al. 1994	100
Desert/Arid			
Desert Scrub N. Africa, Middle East, Latin America	58	Houghton 1999	

Table A.3. (Continued)

Forest Type	SOC	Reference	Depth (when described, cm)
Desert Scrub and Semidesert USA, USSR	56	Schlesinger 1977	33-173 (22 studies)
Other			
Tundra and Alpine Canada, Sweden, USA, USSR	216	Schlesinger 1977	35-175 (31 studies)
Swamp and Marsh Canada, England, USA, USSR	686	Schlesinger 1977	60-291 (10 studies)

^a 1=Foliage, 2=Bole, 3=Bark, 4=Live Branches, 5=Dead Branches, 6=Shrubs, 7=Herbs, 8=Coarse Roots, 9=Fine Roots, 10=Epiphytes or Mosses, 11=Grasses, 12=Logs, 13=Snags, 14=Stumps, 15=Forest Floor, 16=Fine Woody Debris, 17=Rotten Wood

^b Schlesinger (1977) includes total detritus to a depth of 50 cm as well as surface litter and soil

Appendix B. Abbreviations used in descriptions of the MAXCARB model.

Table B.1. Abbreviations used in the MAXCARB module equations.

Pools

SW	Sapwood
HW	Heartwood
BR	Branches
FOL	Foliage
CR	Coarse-root
FR	Fine-root
HR	Heart-rot
Dead	Dead pool
<i>Italics</i>	Generalized pool

Fluxes, Rates

Input	Input flux
Output	Output flux

Climate variables

Evap	Evaporation
Min	Minimum
Max	Maximum
Mon	Monthly
Temp	Temperature
Thru_Fall	Throughfall
Pot	Potential
Delta	Change in

Subscripts

LA	Landscape-average
D	Calculated in the DISTURBANCE Module
SS	Calculated in the STEADY-STATE Module
C	Calculated in the CLIMATE Module

Arithmetic terms

exp (x)	e^x
x^y	x^y
Avg	Average

Appendix C. The calculations in the DISTURBANCE Module of MAXCARB.

OVERVIEW

The purpose of the DISTURBANCE Module is to calculate the landscape-average rate-constants used in the STEADY-STATE Module. To accomplish this objective, the DISTURBANCE Module simulates carbon stores through time for an ecoregion's disturbance regime. The simulation has an annual time-step. The user specifies the simulation length.

Generally, landscape-average rates are calculated by summing fluxes and masses over the length of the simulation. Fluxes and masses of carbon pools are calculated with rates. In the DISTURBANCE Module, the rates that describe changes in fluxes and mass of carbon pools are set to vary with age. They can be represented by a set of constants, or dynamic, age-dependent functions that capture age-dependent behavior. The user specifies these rate functions. The development of dynamic age-dependent functions is described in detail in the next section.

At the core of the DISTURBANCE Module are annual calculations of flux and mass, which use these rate functions. The third section of this appendix describes these annual calculations. The fourth section describes how the carbon stores are adjusted when disturbance events occur. The final section describes how the DISTURBANCE module uses the results of the annual calculations to calculate the landscape-average rate constants.

AGE-DEPENDENT FUNCTIONS

The list of age-dependent functions used by the DISTURBANCE Module are listed in the table below.

Table C.1. The age-dependent functions used by the DISTURBANCE Module.

Category	Functions
Production	FOL_mass bole_growth
Live Pool Ratios	BR_bole_ratio CR_bole_ratio FR_FOL_ratio
Bole Formation Rates	HW_formation HR_formation
Respiration Rates	SW_respiration HR_respiration BR_respiration CR_respiration
Turnover Rates	FOL_turnover FR_turnover
Prune Rates	BR_prune CR_prune
Mortality Rates	tree_mortality percent_snags
Input Decay Rates	dead_FOL_input_decay dead_SW_input_decay dead_HW_input_decay dead_BR_input_decay dead_CR_input_decay dead_FR_input_decay
Stable Decay Rates	stable_FOL_decay stable_wood_decay stable_soil_decay
Transfer Rates	dead_FOL_transfer dead_SW_snags_transfer dead_SW_logs_transfer dead_HW_snags_transfer dead_HW_logs_transfer dead_BR_transfer dead_CR_transfer dead_FR_transfer

These age functions have a format similar to formulas used in common spreadsheet applications. There are several built-in functions that the user may use in the definition of an age function. One such built-in function is the "if" function, which can be

used to select between two values based upon a condition:

if(*condition*, *value_T*, *value_F*) = value_T if the condition is true; value_F otherwise.

These conditional statements can be used to develop step-functions. Other built-in functions include a Chapman-Richards function and a Modified Chapman-Richards function, which are named "CR" and "mCR" respectively, and are defined as follows:

$$\text{CR}(b_1, b_2) = (1 - \exp(-b_1 * \text{age}_t)) ^ b_2$$

$$\text{mCR}(b_1, b_2, b_3, b_4) = b_4 - (b_4 - b_3) * \text{CR}(b_1, b_2)$$

where:

b1 = rate of increase
 b2 = lag
 b3 = min, max
 b4 = max, min
 age_t = the current age

The rest of this section describes the specific age functions used to produce the MAXCARB results, and how these functions were created from output from STANDCARB.

Production

FOL Mass

Foliage mass through time is calculated with a modified Chapman-Richards equation.

$$(1) \quad \text{FOL_mass}(\text{age}) = \text{CR}(0.1, 2) * \text{mCR}(0.03, 120, 15, \text{ecoregion:steady_state_foliage})$$

Bole Growth

The bole growth is currently set to 1 since the CLIMATE module accounts for climate effects.

$$(2) \quad \text{bole_growth}(\text{age}) = 1$$

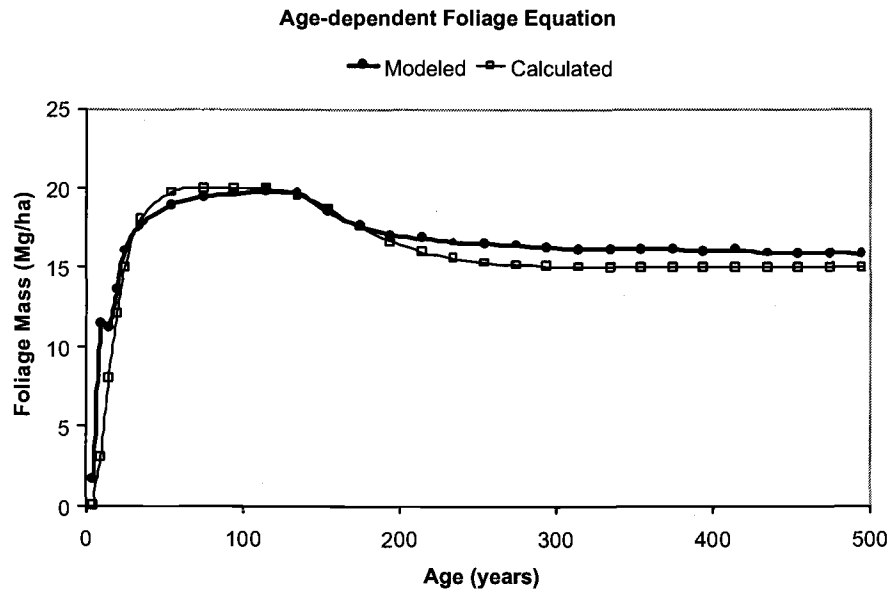


Figure C.1. Foliage mass as a function of age.

Live Pool Ratios

BR-Bole Ratio

Conceptually, in STANDCARB, the branch to bole ratio is equal to the proportion of bole allocation that is allocated to branches. The ratio in STANDCARB is developed from species-specific, allometric equations (Means et al. 1994). In MAXCARB, the branch to bole ratio changes with stand age in the following way:

$$(3) \quad \text{BR_bole_ratio}(\text{age}) = \text{mCR}(0.3, \text{ecoregion:time_close}, 0.12, 1.4)$$

The branch to bole ratio is initially high due to the large proportion of shrubs early in succession. After a period of shrub dominance, the branch to bole ratio reflects an average of Douglas-fir and western hemlock ratios.

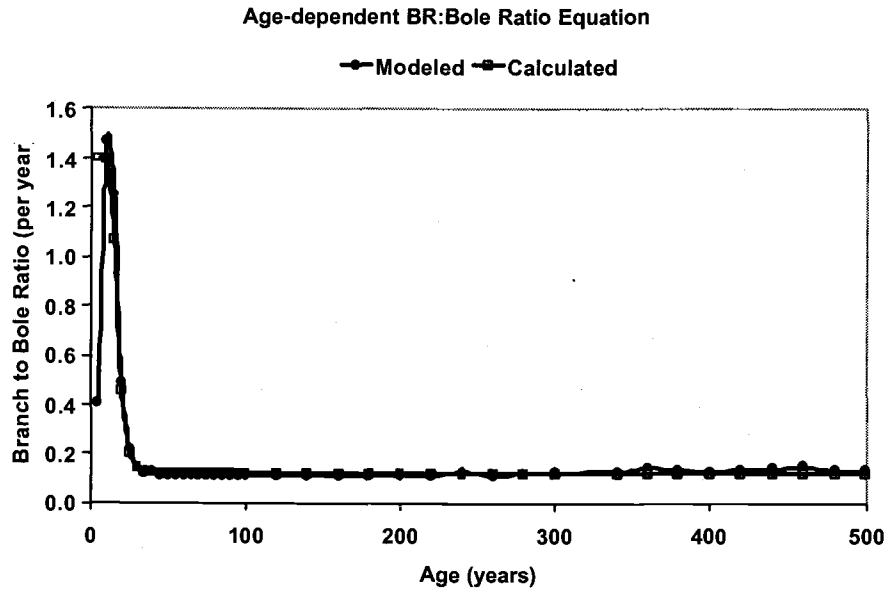


Figure C.2. Branch to bole ratio as a function of age.

CR-Bole Ratio

(4) $CR_bole_ratio(age) = mCR(0.3, 120, 0.6, 1.5)$

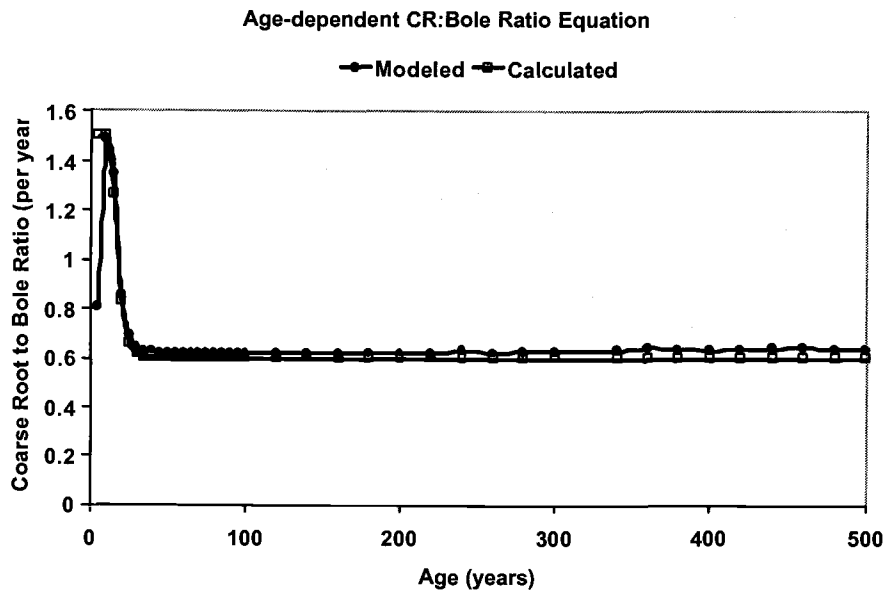


Figure C.3. Coarse root to bole ratio as a function of age.

The coarse-root to bole ratio is initially high due to the large proportion of shrubs early in succession. After a period of shrub dominance, the coarse-root to bole ratio reflects an

average of Douglas-fir and western hemlock ratios.

FR-FOL Ratio

While the two previous ratios are *allocation* ratios, this ratio of fine roots to foliage is function of pool size.

(5) $FR_FOL_ratio (age) = 0.33$

Bole Formation Rates

HW Formation

The rate of heartwood formation as a function of age was developed from parameters in the STANDCARB model. We assumed that heartwood formation decreases from a maximum of 0.059 for Douglas-fir to a minimum of 0.02 for western hemlock as the latter species occupies more of the stand later in succession.

(6) $HW_formation (age) = mCR(0.02, 60, 0.02, 0.059)$

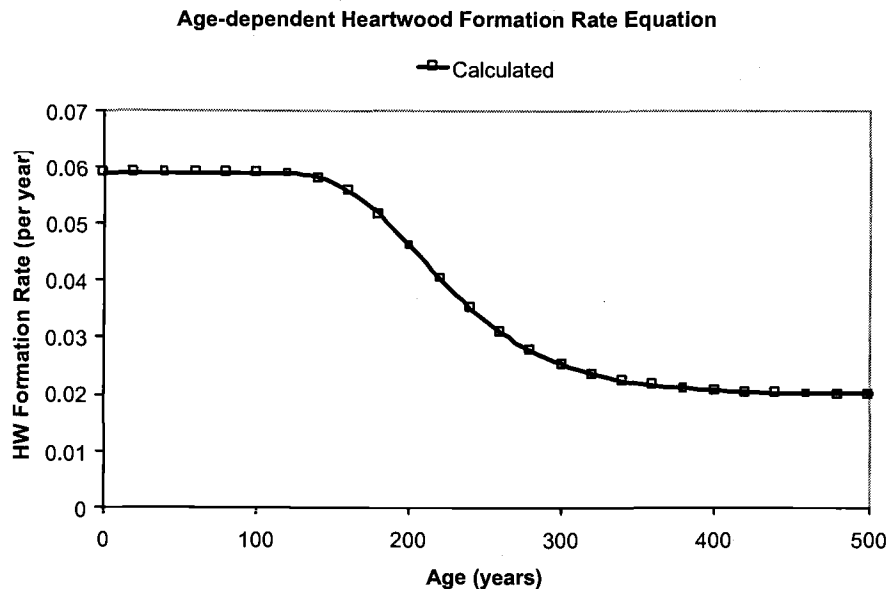


Figure C.4. The rate of heartwood formation as a function of age.

HR Formation

The rate at which heart-rot is formed is assumed to be insignificant for a certain number of years in the early stages of tree growth. This number of years is known as the "heart-rot lag"; it is a function of species in STANDCARB but is an average value for an

ecoregion in MAXCARB, based on the ecoregion's species composition. The rate of heart-rot formation was calculated from parameters in STANDCARB using the rate of heart-rot formation for Douglas-fir until year 500, and then the rate of heart-rot formation for western hemlock after that year. The final equation is a simple step-function:

$$(7) \quad \text{HR_formation (age)} = \text{if} (t < \text{ecoregion:HR_lag}, 0, \text{if} (t < 500, 0.01, 0.02))$$

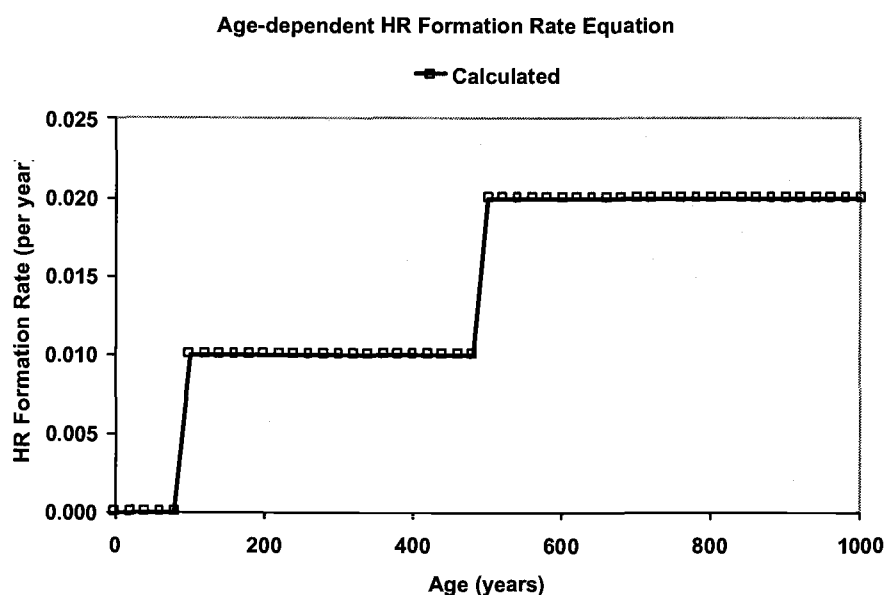


Figure C.5. The rate of heart-rot formation as a function of age.

Respiration Rates

The respiration rates for sapwood, branch and coarse-root pools were developed from the respiration fluxes and pool masses output by the STANDCARB model. Dominance by shrubs and herbs during early successional stages results in higher respiration rates than later successional stages.

SW Respiration

$$(8) \quad \text{SW_respiration (age)} = 0.025 * \text{CR}(0.1, 5)$$

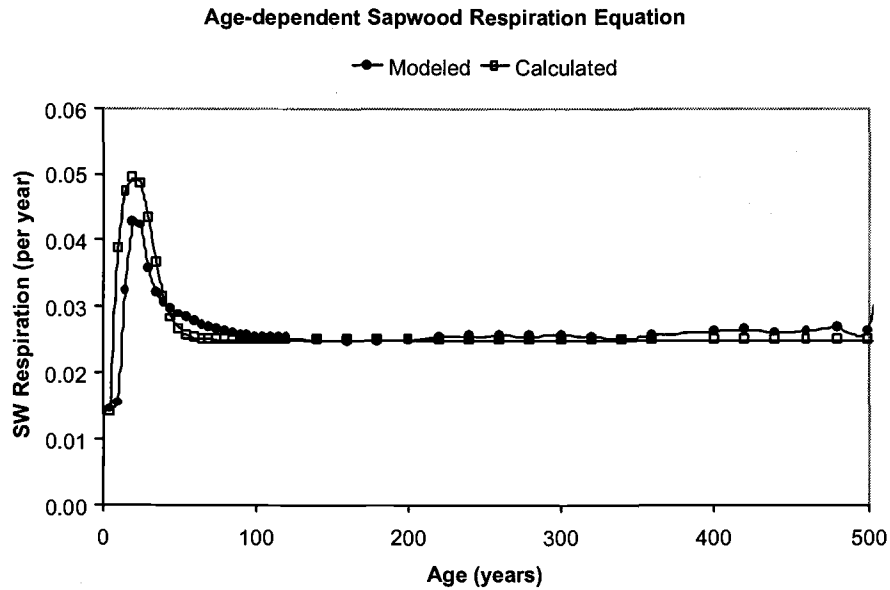


Figure C.6. The rate of sapwood respiration as a function of age.

HR Respiration

The age function for the respiration rate of the heart-rot pool was developed from the STANDCARB parameters for heart-rot respiration.

(9) $HR_respiration (age) = \text{if} (t < \text{ecoregion:HR_lag}, 0, 0.009)$

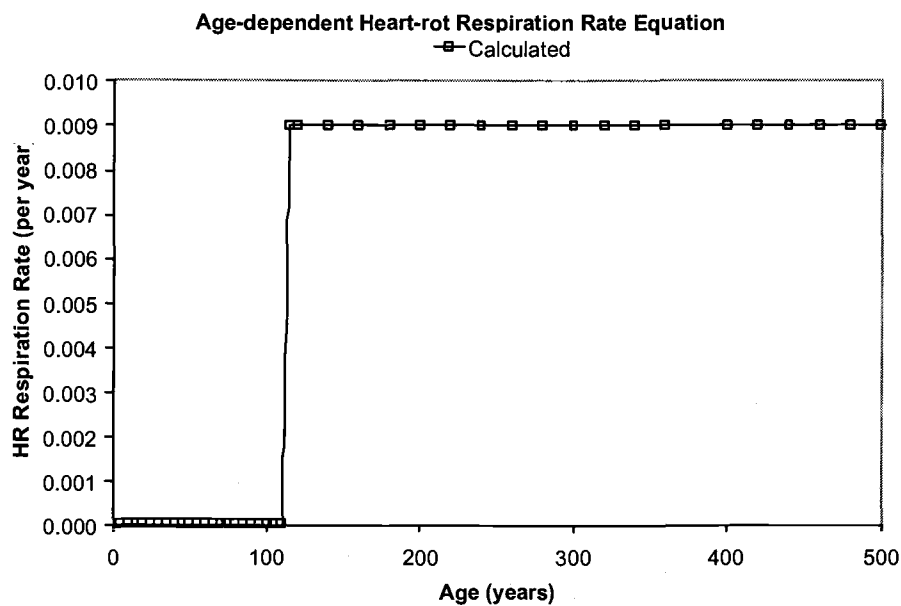


Figure C.7. The rate of heart-rot respiration as a function of age.

BR Respiration

$$(10) \quad \text{BR_respiration}(\text{age}) = \text{CR}(0.2, 2) \\ * \text{mCR}(0.2, \text{ecoregion:time_close}, 0.015, 0.055)$$

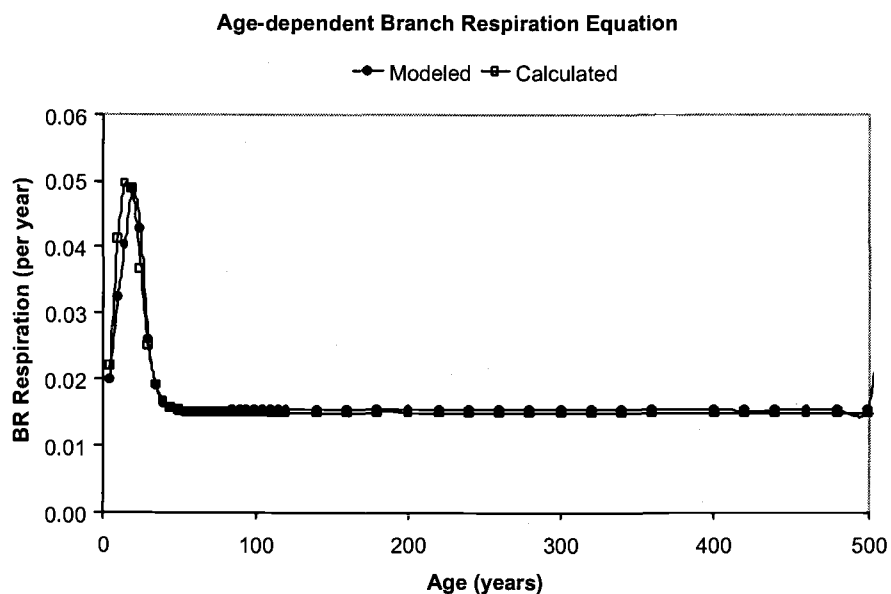


Figure C.8. The rate of branch respiration as a function of age.

CR Respiration

$$(11) \quad \text{CR_respiration}(\text{age}) = \text{CR}(0.18, 4) * \text{mCR}(0.12, 10, 0.015, 0.06)$$

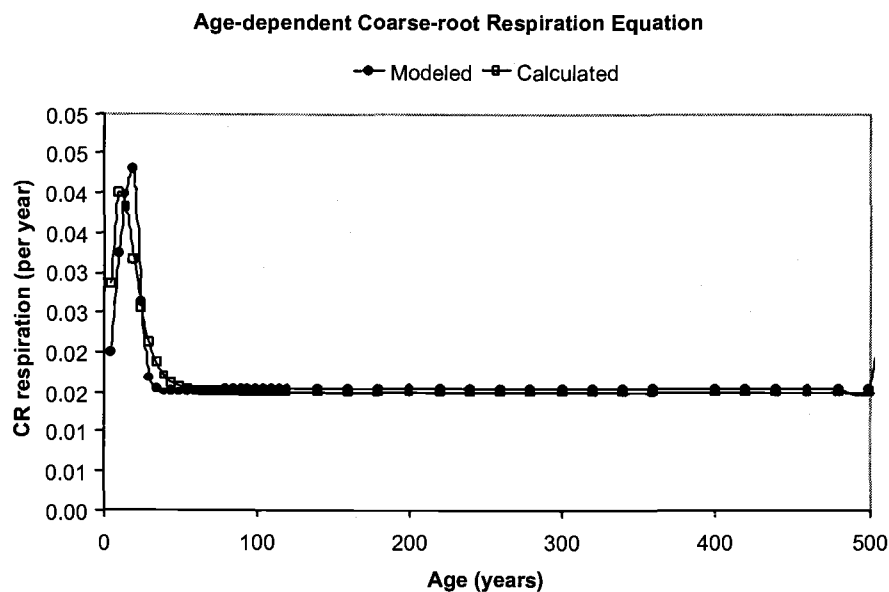


Figure C.9. The rate of coarse root respiration as a function of age.

Turnover Rates

FOL Turnover

The rate of foliage turnover was computed from STANDCARB's output (transfer diagnostics), by dividing the annual turnover input to dead foliage by foliage mass.

$$(12) \quad \text{FOL_turnover (age)} = \text{CR}(0.05, 2) * \text{mCR}(0.1, 10, 0.2, 0.9)$$

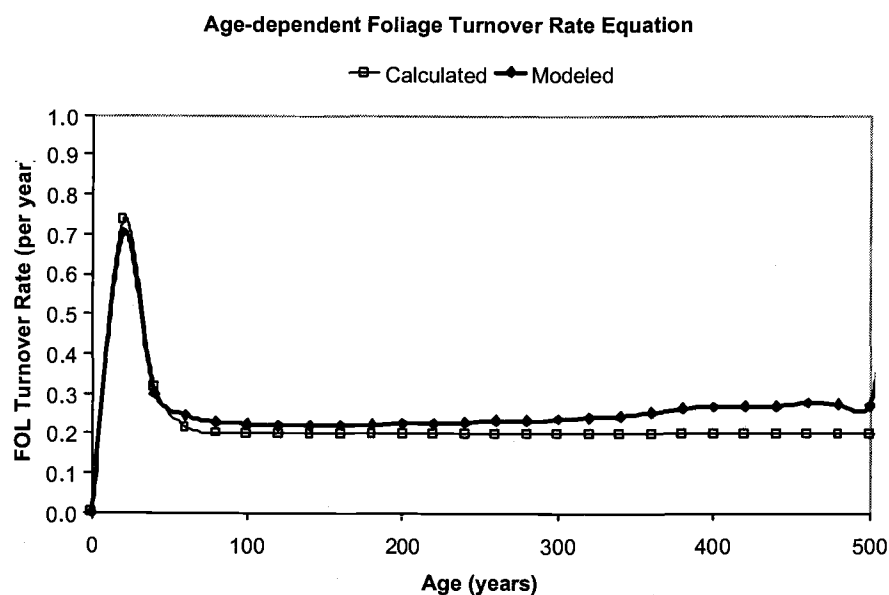


Figure C.10. The rate of foliage turnover as a function of age.

FR Turnover

$$(13) \quad \text{FR_turnover (age)} = (\text{CR}(0.2, 2) * \text{mCR}(0.15, 120, 0.47, 0.5)) \\ * \text{mCR}(0.4, 120, 0.5, 0.45)$$

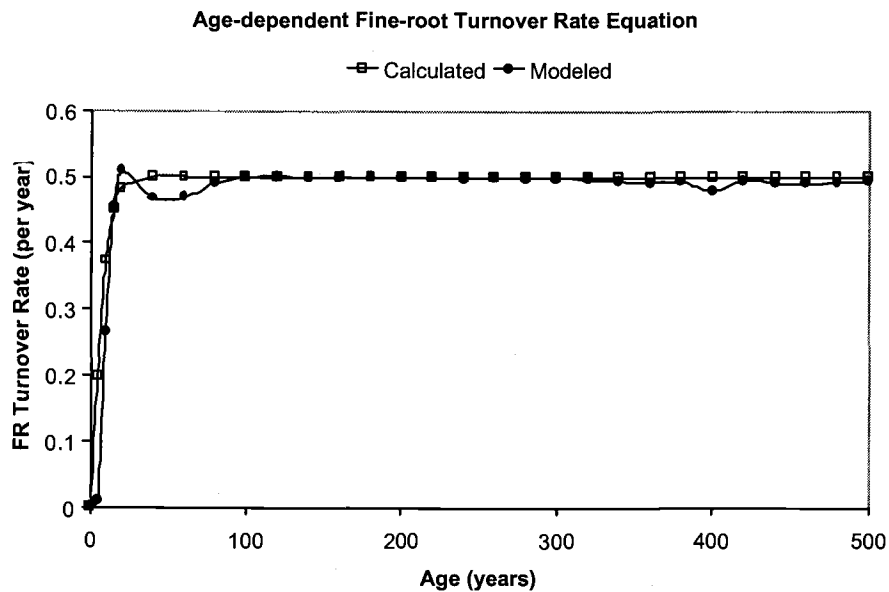


Figure C.11. The rate of fine root turnover as a function of age.

Prune Rates

The rates of pruning for both branch and coarse-root pools were developed from STANDCARB's output (transfer diagnostics), by dividing the mass being transferred from the live pool due to pruning by the mass of its corresponding dead pool.

BR Prune

$$(14) \quad BR_prune (age) = 0.02 * CR(0.3, 5)$$

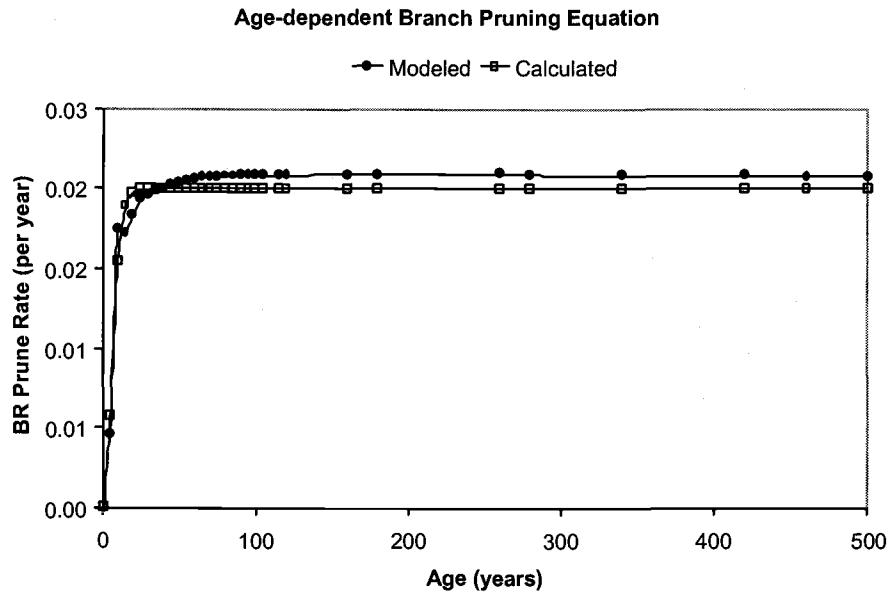


Figure C.12. The rate of branch pruning as a function of age.

CR Prune

(15) $CR_prune(age) = 0.005 * CR(0.3, 5)$

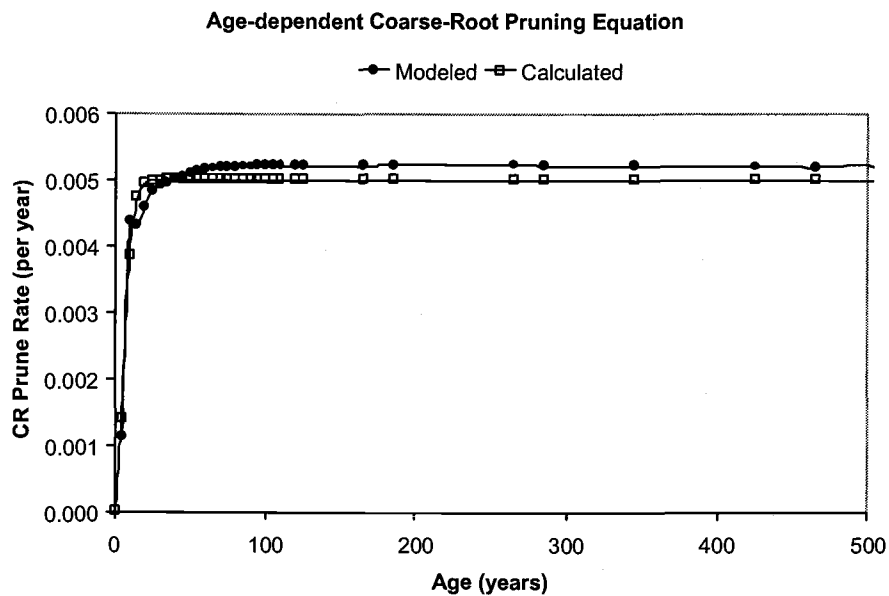


Figure C.13. The rate of coarse root pruning as a function of age.

Mortality Rates

Tree Mortality

The mortality of trees through time is given by the following equation:

$$(16) \quad \text{tree_mortality}(\text{age}) = \text{mCR}(0.2, 120, 0.005, 0.015) * \text{CR}(0.3, 2)$$

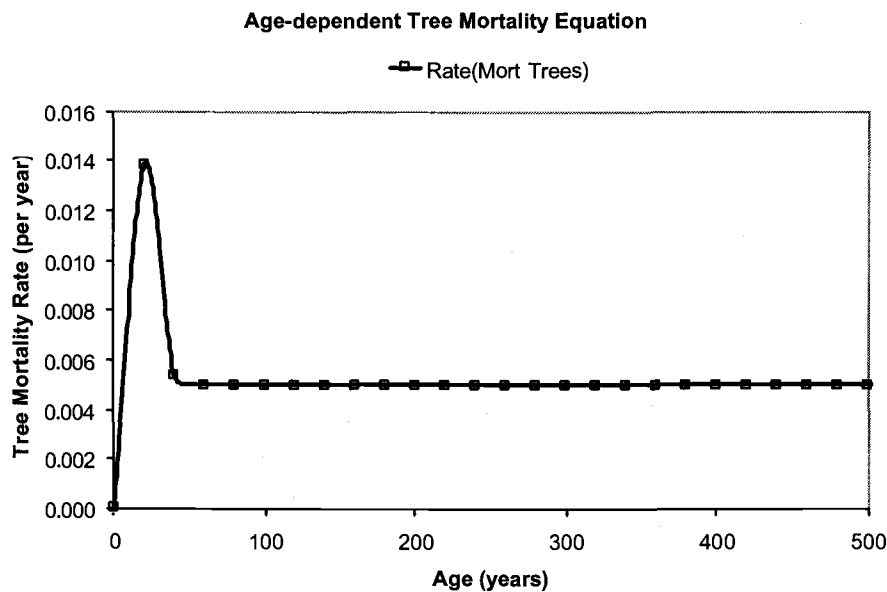


Figure C.14. The mortality rate of trees as a function of age.

This function was developed from the relationship between the maximum mortality rate (when the maximum amount of light is absorbed) and the mortality rate for old-growth forests in STANDCARB. To develop this equation, we assumed a maximum mortality rate of about 0.015 and a minimum, old-growth mortality rate of 0.005. In STANDCARB, maximum mortality rates for tree species in the Pacific Northwest range from approximately 0.008 to 0.018.

Percent Snags

The percent of snags through time is defined with the following equation:

$$(17) \quad \text{percent_snags}(\text{age}) = \text{if}(t < \text{ecoregion:time_close}, \text{snags_open}, \text{snags_closed}).$$

The percent of snags equals that of an open canopy before time close. After time close, the percent of snags equals that of a closed canopy. The user specifies the percent of

snags in open and closed canopies for the ecoregion being simulated.

Input Decay Rates

The decay rates associated with the input to the dead pools were calculated from STANDCARB.

Dead FOL Input Decay

$$(18) \quad \text{dead_FOL_input_decay}(\text{age}) = \text{mCR}(0.3, 120, 0.35, 0.5)$$

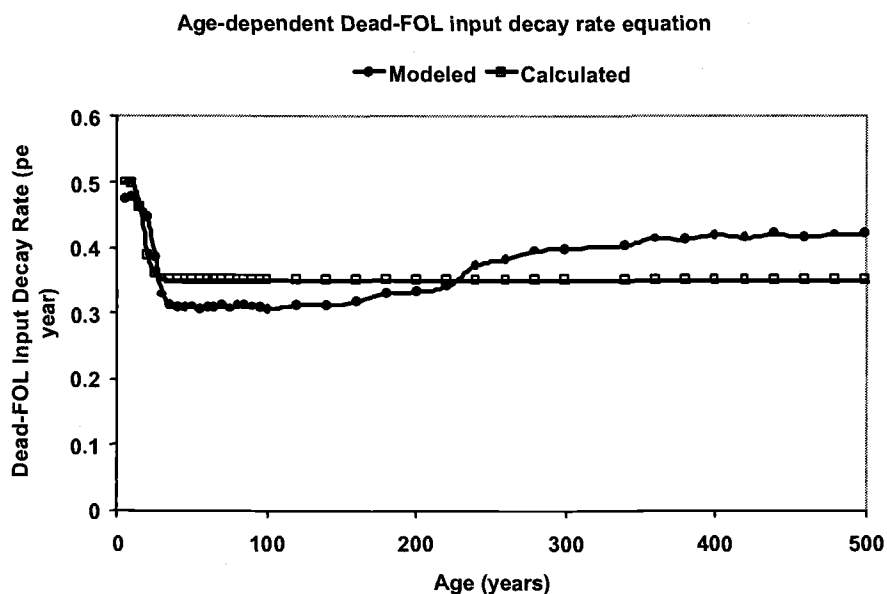


Figure C.15. The decay rate of dead foliage inputs as a function of age.

Dead SW Input Decay

$$(19) \quad \text{dead_SW_input_decay}(\text{age}) = \text{mCR}(0.3, 120, 0.07, 0.01)$$

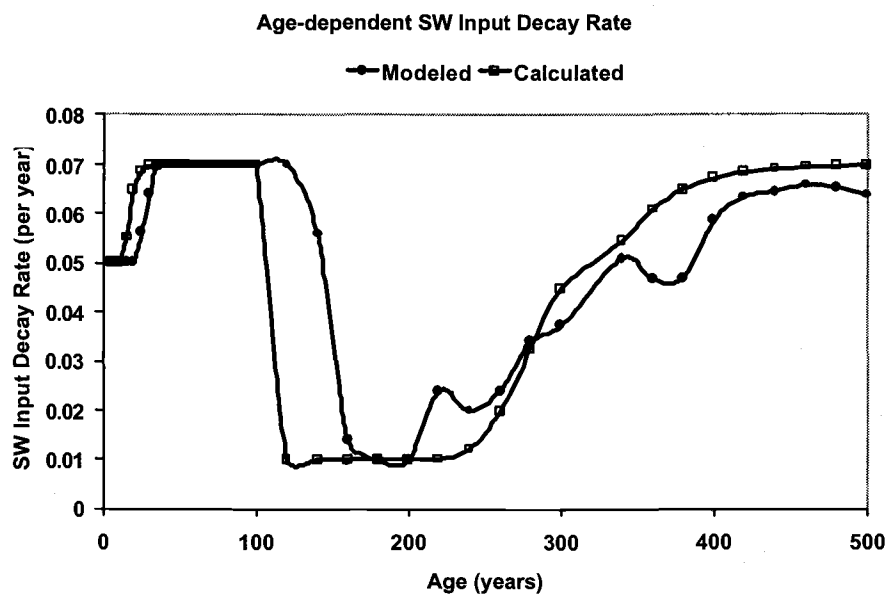


Figure C.16. The decay rate of dead sapwood inputs as a function of age.

Dead HW Input Decay

(20) $\text{dead_HW_input_decay}(\text{age}) = \text{mCR}(0.3, 120, 0.02, 0)$

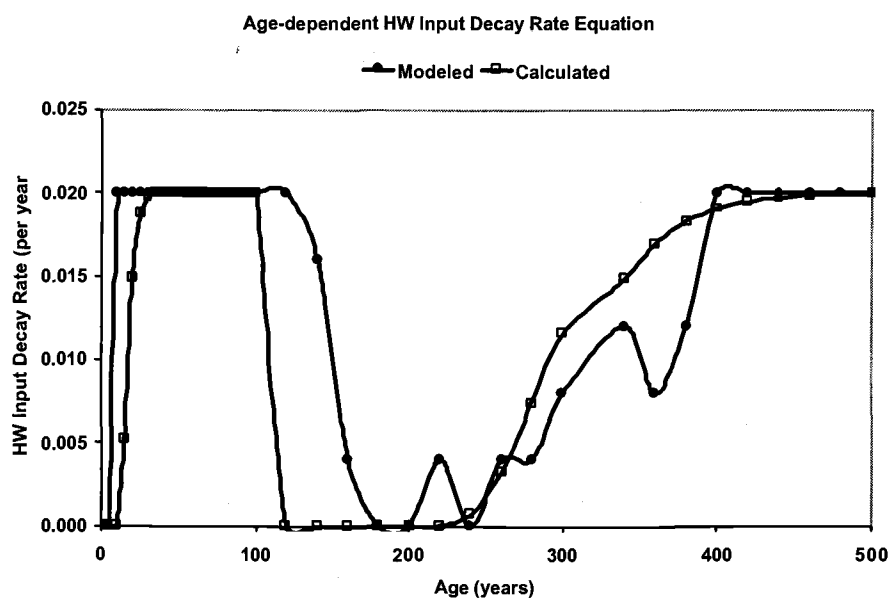


Figure C.17. The decay rate of dead heartwood inputs as a function of age.

Dead BR Input Decay

(21) $\text{dead_BR_input_decay}(\text{age}) = \text{mCR}(0.3, 120, 0.15, 0.1)$

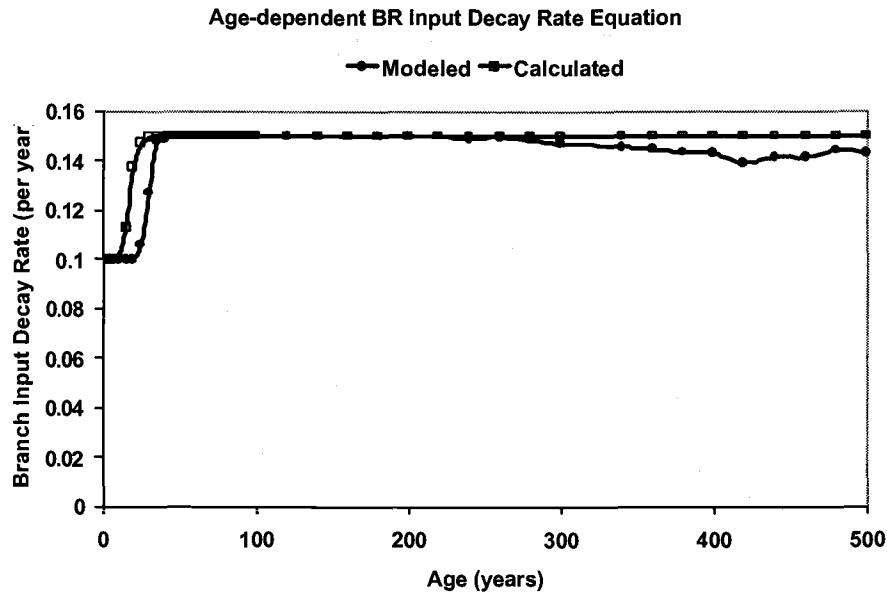


Figure C.18. The decay rate of dead branch inputs as a function of age.

Dead CR Input Decay

$$(22) \quad \text{dead_CR_input_decay}(\text{age}) = \text{mCR}(0.3, 120, 0.15, 0.1)$$

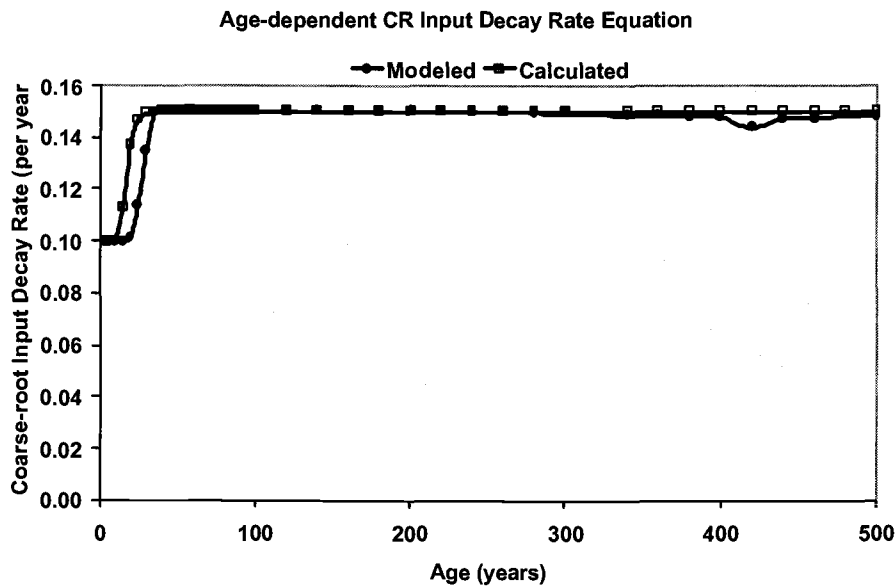


Figure C.19. The decay rate of dead coarse root inputs as a function of age.

Dead FR Input Decay

$$(23) \quad \text{dead_FR_input_decay}(\text{age}) = \text{mCR}(0.3, 120, 0.3, 0.45)$$

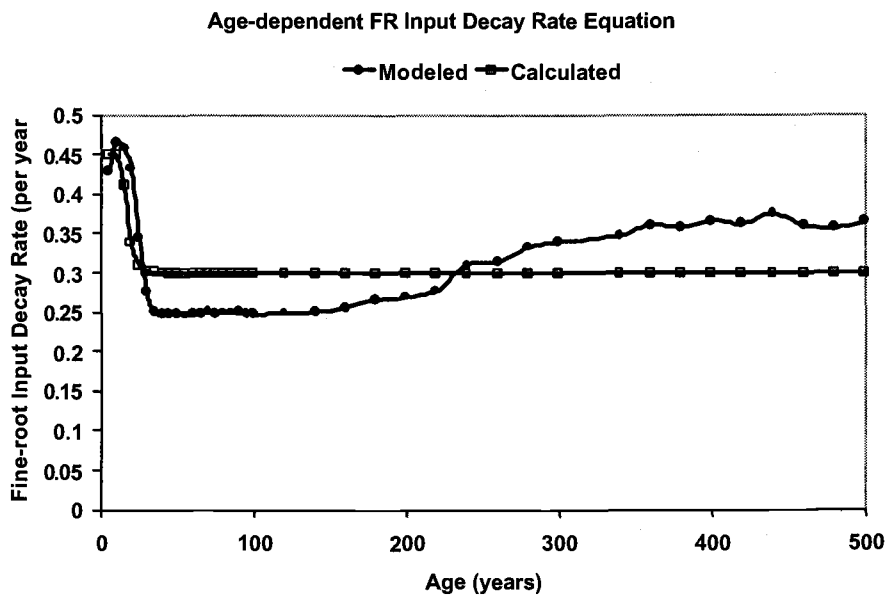


Figure C.20. The decay rate of dead fine root inputs as a function of age.

Stable Decay Rates

These are all constants based on the associated STANDCARB parameters.

Stable FOL Decay

(24) $\text{stable_FOL_decay}(\text{age}) = 0.20$

Stable Wood Decay

(25) $\text{stable_wood_decay}(\text{age}) = 0.05$

Stable Soil Decay

(26) $\text{stable_soil_decay}(\text{age}) = 0.012$

Transfer Rates

The transfer rates for all the dead pools were calculated from the non-cohort version of the STANDCARB model, accounting for time lags under optimum decomposition conditions (Harmon and Domingo, 2001).

Dead FOL Transfer

(27) $\text{dead_FOL_transfer}(\text{age}) = 0.057$

Dead SW Snags Transfer

(28) **dead_SW_snags_transfer (age) = 0.009**

Dead SW Logs Transfer

(29) **dead_SW_logs_transfer (age) = 0.010**

Dead HW Snags Transfer

(30) **dead_HW_snags_transfer (age) = 0.009**

Dead HW Logs Transfer

(31) **dead_HW_logs_transfer (age) = 0.016**

Dead BR Transfer

(32) **dead_BR_transfer (age) = 0.0033**

Dead CR Transfer

(33) **dead_CR_transfer (age) = 0.016**

Dead FR Transfer

(34) **dead_FR_transfer (age) = 0.022**

ANNUAL POOL CALCULATIONS

This section describes the calculations that are performed for each annual time-step in a simulation of the DISTURBANCE Module.

Pool Mass

For each time-step, the mass of each carbon pools is computed, prior to accounting for any disturbance events that occur in the time-step:

$$\mathbf{pool:mass}_{t, \text{ before disturbance}}$$

To determine the pool's mass for the end of a time-step, the pre-disturbance mass is adjusted for all events that occur in that time-step. If no disturbances occur, then

$$(35) \quad \mathbf{pool:mass}_t = \mathbf{pool:mass}_{t, \text{ before disturbance}}$$

If only a harvest event occurs, then

$$(36) \quad \mathbf{pool:mass}_t = \mathbf{pool:mass}_{t, \text{ after harvest}}$$

If only a fire event occurs (with or without a preceding harvest event), then

$$(37) \quad \mathbf{pool:mass}_t = \mathbf{pool:mass}_{t, \text{ after fire}}$$

The calculations related to disturbance events are described at the end of this section.

Foliage & Fine Roots

Foliage mass is calculated directly from the age-dependent function, which describes how foliage mass changes with age. Fine root mass is thus a function of foliage mass and the age-dependent, fine root to foliage ratio.

$$(38) \quad \mathbf{foliage:mass}_{t, \text{ before disturbance}} = \mathbf{FOL_mass}(\mathbf{age}_t)$$

$$(39) \quad \mathbf{fine_roots:mass}_{t, \text{ before disturbance}} = \mathbf{foliage:mass}_{t, \text{ before disturbance}} * \mathbf{FR_FOL_ratio}(\mathbf{age}_t)$$

Transfer Fluxes

Both pools transfer mass to their corresponding dead pools because of turnover and tree mortality.

$$(40) \quad \mathbf{pool:turnover}_t = \mathbf{pool:mass}_{t, \text{ before disturbance}} * \mathbf{pool_turnover}(\mathbf{age}_t)$$

$$(41) \quad \mathbf{pool:mortality_transfer}_t = \mathbf{pool:mass}_{t, \text{ before disturbance}} * \mathbf{tree_mortality}(\mathbf{age}_t)$$

Mass and Fluxes – All Other Pools

Mass

For all pools other than foliage and fine-roots, their masses change during a time-step based on the fluxes into and out of the pools during the time-step.

$$(42) \quad \text{pool:mass}_{t, \text{ before disturbance}} = \text{pool:mass}_{t-1} + \text{pool:input}_t - \text{pool:output}_t$$

Output Fluxes

In general, a pool's output flux consists of a loss to the atmosphere and transfers to other pools.

$$(43) \quad \text{pool:output}_t = \text{pool:loss}_t + \text{pool:transfers}_t$$

A pool may not have any losses; for example, heartwood has no respiration loss. A pool may have no transfers (e.g., stable pools) or multiple transfers (e.g., sapwood, heartwood).

Input Flux

In general, a pool's input flux is the sum of the transfer fluxes from one or more contributing pools.

Live Pools

Respiration Loss

For the sapwood, heart-rot, branch and coarse-root pools, each pool's loss is due to respiration.

$$(44) \quad \text{pool:loss}_t = \text{pool:respiration_loss}_t$$

$$(45) \quad \text{pool:respiration_loss}_t = \text{pool:mass}_{t-1} * \text{pool_respiration}(\text{age}_t)$$

Mortality Transfer

All live pools other than foliage and fine-roots transfer mass to their corresponding dead pools because of tree mortality.

$$(46) \quad \text{pool:mortality_transfer}_t = \text{pool:mass}_{t-1} * \text{tree_mortality}(\text{age}_t)$$

Sapwood

Input Flux

The input flux to the sapwood pool assumes that allocation of mass to sapwood is proportional to foliage mass.

$$(47) \quad \text{sapwood:input}_t = \text{foliage:mass}_t * \text{bole_growth}(\text{age}_t)$$

Transfer Flux

The sapwood pool transfers mass to dead sapwood (Eqn. 46) and heartwood.

$$(48) \quad \text{sapwood:transfers}_t = \text{sapwood:formation_transfer}_t \\ + \text{sapwood:mortality_transfer}_t$$

$$(49) \quad \text{sapwood:formation_transfer}_t = \text{sapwood:mass}_{t-1} * \text{HW_formation}(\text{age}_t)$$

Heartwood

Input Flux

$$(50) \quad \text{heartwood:input}_t = \text{sapwood:formation_transfer}_t$$

Loss Flux

Heartwood has no loss since it does not respire.

$$(51) \quad \text{heartwood:loss}_t = 0$$

Transfer Flux

The heartwood pool transfers mass to dead heartwood (Eqn. 46) and heart-rot.

$$(52) \quad \text{heartwood:transfers}_t = \text{heartwood:formation_transfer}_t \\ + \text{heartwood:mortality_transfer}_t$$

$$(53) \quad \text{heartwood:formation_transfer}_t = \text{heartwood:mass}_{t-1} * \text{HR_formation}(\text{age}_t)$$

Heart-Rot

Input Flux

$$(54) \quad \text{heartrot:input}_t = \text{heartwood:formation_transfer}_t$$

Transfer Flux

Heart-rot transfers mass only to dead heartwood (Eqn. 46).

$$(55) \quad \text{heartrot:transfers}_t = \text{heartrot:mortality_transfer}_t$$

Branch, Coarse Roots

Input Flux

The input fluxes to the branch and coarse-root pool are proportional to the sapwood's input flux.

$$(56) \quad \text{pool:input_flux}_t = \text{sapwood:input}_t * \text{pool_bole_ratio}(\text{age}_t)$$

The rationale is that the allocation to branches and coarse roots is a fixed proportion of the allocation to sapwood.

Transfer Flux

Both pools contribute to their corresponding dead pool because of pruning and tree mortality (Eqn. 46).

$$(57) \quad \text{pool:transfers}_t = \text{pool:pruning_transfer}_t + \text{pool:mortality_transfer}_t$$

$$(58) \quad \text{pool:pruning_transfer}_t = \text{pool:mass}_{t-1} * \text{pool_prune}(\text{age}_t)$$

Detrital Pools

Loss Flux

All detrital pools (dead and stable) lose mass due to decomposition.

$$(59) \quad \text{detrital_pool:loss}_t = \text{detrital_pool:decay_loss}_t$$

Non-composite Dead Pools

A non-composite dead pool is a dead pool that is not composed of other pools. The only composite dead pools are the dead bole pools (dead sapwood and dead heartwood); they each are composed of two pools: snags and logs. These snag and log pools are non-composite pools.

Decay Loss

The decay loss for a non-composite pool is based on the pool's decay rate.

$$(60) \quad \text{dead_pool:decay_loss}_t = \text{dead_pool:mass}_{t-1} * \text{dead_pool:decay_rate}_t$$

Decay Rates – Input & Pool

The input flux to a non-composite pool has an associated decay rate. This input decay rate is used in a simple weighted average to compute the pool's overall decay rate.

$$(61) \quad \text{dead_pool:decay_rate}_t = \text{weighted_average}(\text{dead_pool:input_decay_rate}_t, \\ \text{dead_pool:input}_t, \\ \text{dead_pool:decay_rate}_t, \\ \text{dead_pool:mass}_{t-1})$$

$$(62) \quad \text{weighted_average}(\text{rate}_1, \text{mass}_1, \\ \text{rate}_2, \text{mass}_2) = (\text{rate}_1 * \text{mass}_1 + \text{rate}_2 * \text{mass}_2) \\ / (\text{mass}_1 + \text{mass}_2)$$

Transfer Flux

A non-composite pool transfers mass to a stable pool with the exception of the snag pools, which transfer mass to their corresponding log pools. The transfer flux out of a non-composite pool is based on the pool's transfer rate.

$$(63) \quad \text{dead_pool:transfers}_t = \text{dead_pool:mass}_{t-1} * \text{dead_pool_transfer}(\text{age}_t)$$

Dead Foliage, Dead Fine Roots

Input Flux

The input fluxes to these pools are the transfer fluxes from their corresponding live pools due to turnover (Eqn. 40) and tree mortality (Eqn. 41).

$$(64) \quad \text{dead_pool:input}_t = \text{live_pool:tumover}_t + \text{live_pool:mortality_transfer}_t$$

The decay rate associated with the input flux is just an age function.

$$(65) \quad \text{dead_pool:input_decay_rate}_t = \text{dead_pool_input_decay}(\text{age}_t)$$

Dead Branch, Dead Coarse Roots

Input Flux

The input fluxes to these pools are the transfer fluxes from their corresponding live pools (Eqn. 57).

$$(66) \quad \text{dead_pool:input}_t = \text{live_pool:transfers}_t$$

Like dead foliage and dead fine-roots, the decay rate associated with the input flux is just an age function (see Equation 65).

Dead Bole Pools – Dead Sapwood, Dead Heartwood

Each dead bole pool is composed of two internal pools representing snags and logs.

Input Flux

The input flux to a dead bole pool is the sum of the mortality transfer(s) from its corresponding live pool(s) (Eqn 46).

$$(67) \quad \text{dead_sapwood:input}_t = \text{sapwood:mortality_transfer}_t$$

$$(68) \quad \text{dead_heartwood:input}_t = \text{heartwood:mortality_transfer}_t \\ + \text{heartrot:mortality_transfer}_t$$

Like the other dead pools, the decay rate associated with this input flux is age-dependent (see Equation 65).

The input flux of a dead bole pool is separated into its snag and log pools. The input flux to the log pool includes the transfer flux from the snag pool (Eqn. 63).

$$(69) \quad \text{dead_bole:snags:input}_t = \text{dead_bole:input}_t * \text{percent_snags}(\text{age}_t)$$

$$(70) \quad \text{dead_bole:logs:input}_t = \text{dead_bole:logs:input_from_live}_t \\ + \text{dead_bole:snags:transfers}_t$$

$$(71) \quad \text{dead_bole:logs:input_from_live}_t = \text{dead_bole:input}_t \\ - \text{dead_bole:snags:input}_t$$

The decay rate associated with the snag's input flux is simply the dead bole's input decay rate.

$$(72) \quad \text{dead_bole:snags:input_decay_rate}_t = \text{dead_bole:input_decay_rate}_t$$

However, the decay rate associated with the log's input flux is a weighted average (Eqn. 62) of the decay rates associated with the two components of its input flux.

$$(73) \quad \text{dead_bole:logs:input_decay_rate}_t = \text{weighted_average}(\\ \text{dead_bole:input_decay_rate}_t, \\ \text{dead_bole:logs:input_from_live}_t, \\ \text{dead_bole:snags:decay_rate}_t, \\ \text{dead_bole:snags:transfers}_{t-1})$$

Decay Loss

The decay loss for a dead bole pool is the sum of the decay losses from its snag and log pools.

$$(74) \quad \text{dead_bole:decay_loss}_t = \text{dead_bole:snags:decay_loss}_t \\ + \text{dead_bole:logs:decay_loss}_t$$

Transfer Flux

The transfer flux out of a dead bole pool is simply the transfer flux out of its log

pool.

$$(75) \quad \text{dead_bole:transfers}_t = \text{dead_bole:logs:transfers}_t$$

Stable Pools

Input Flux

The input flux to a stable pool is the sum of the transfer flux(es) from its corresponding dead pool(s) (Eqns. 63 and 75).

$$(76) \quad \text{stable_foliage:input}_t = \text{dead_foliage:transfers}_t$$

$$(77) \quad \text{stable_wood:input}_t = \text{dead_sapwood:transfers}_t \\ + \text{dead_heartwood:transfers}_t \\ + \text{dead_heartrot:transfers}_t$$

$$(78) \quad \text{stable_soil:input}_t = \text{dead_coarse_roots:transfers}_t \\ + \text{dead_fine_roots:transfers}_t$$

Decay Rate

The decay rate for a stable pools is age-dependent.

$$(79) \quad \text{stable_pool:decay_rate}_t = \text{stable_pool_decay}(\text{age}_t)$$

CALCULATIONS FOR A DISTURBANCE EVENT

There are two types of disturbance events simulated by MAXCARB, harvests and fires. In addition, harvests may have fires due to site preparation. Fires are considered to be part of a natural disturbance regime, whereas harvests are considered to be part of a regulated disturbance regime.

In years in which there is a disturbance event, there are additional losses and transfers from the pools other than those described in the previous section. For live pools, mass may be lost to the atmosphere (i.e., combustion), or transferred to its corresponding dead pool after a fire disturbance event. Additionally, if the disturbance event is a harvest, live pool mass may be transferred to the forest products pool. For dead pools, mass may be also lost to the atmosphere after fire (either for a natural fire event, or a site-preparation fire for a harvest event), and there may be an addition of mass to the dead pools from the live pools after harvest or fire. Dead pools do not transfer material to stable pools during disturbance events.

Currently, only catastrophic disturbance events are supported. With a catastrophic disturbance event, each live pool is completely killed, i.e., its mass is 0 after the event.

The effects of natural disturbances in MAXCARB are to increase (1) transfers from live pools to dead pools and (2) losses from all pools due to combustion, i.e., in the case of fire. The effects of regulated harvests in MAXCARB are to increase (1) transfers from live pools to dead and forest products pools and (2) losses through site preparation fires, i.e., in the case of forest harvesting.

Regulated Disturbances (Harvest)

The mass of each pool before a harvest event is always the mass after the annual pool calculations.

$$(80) \quad \text{pool:mass}_{t, \text{ before harvest}} = \text{pool:mass}_{t, \text{ before disturbance}}$$

Live Pools

Since harvest events are catastrophic, all live pools are reduced to zero after the

disturbance event.

$$(81) \quad \text{live_pool:mass}_{t, \text{ after harvest}} = 0$$

Non-bole Pools – Live and Dead

Each live non-bole pool (foliage, branch, coarse roots, fine roots) transfers all its mass that was cut to its corresponding dead pool.

$$(82) \quad \text{live_pool:cut_transfer}_t = \text{live_pool:mass}_{t, \text{ before harvest}}$$

$$(83) \quad \text{dead_pool:mass}_{t, \text{ after harvest}} = \text{dead_pool:mass}_{t, \text{ before harvest}} + \text{live_pool:cut_transfer}_t$$

Bole Pools – Live and Dead

When each live bole pool (sapwood, heartwood, and heart-rot) is cut, a user-specified portion of its mass is taken off site (i.e., harvested).

$$(84) \quad \text{live_bole:harvest_transfer}_t = \text{live_bole:mass}_{t, \text{ before harvest}} * \text{percent_taken}$$

$$(85) \quad \text{live_bole:cut_transfer}_t = \text{live_bole:mass}_{t, \text{ before harvest}} - \text{live_bole:harvest_transfer}_t$$

The portion of the live bole pools cut but not taken is transferred into the log pools of their corresponding dead pools.

$$(86) \quad \text{dead_sapwood:logs:mass}_{t, \text{ after harvest}} = \text{dead_sapwood:logs:mass}_{t, \text{ before harvest}} + \text{sapwood:cut_transfer}_t$$

$$(87) \quad \text{dead_heartwood:logs:mass}_{t, \text{ after harvest}} = \text{dead_heartwood:logs:mass}_{t, \text{ before harvest}} + \text{heartwood:cut_transfer}_t + \text{heartrot:cut_transfer}_t$$

$$(88) \quad \text{dead_bole:snags:mass}_{t, \text{ after harvest}} = \text{dead_bole:snags:mass}_{t, \text{ before harvest}}$$

$$(89) \quad \text{dead_bole:mass}_{t, \text{ after harvest}} = \text{dead_bole:snags:mass}_{t, \text{ after harvest}} + \text{dead_bole:logs:mass}_{t, \text{ after harvest}}$$

Stable Pools

Harvest events do not affect the stable pools in this version of MAXCARB.

Natural Disturbances (Fire)

There are three intensity levels for fire events: low, medium, high. The mass of each pool before a fire event depends upon whether there was a preceding harvest event.

If there's no harvest before the fire, then

$$(90) \quad \text{pool:mass}_{t, \text{ before fire}} = \text{pool:mass}_{t, \text{ before disturbance}}$$

If there is a harvest before the fire (i.e., it's a site-prep fire), then

$$(91) \quad \text{pool:mass}_{t, \text{ before fire}} = \text{pool:mass}_{t, \text{ after harvest}}$$

Live Pools

Since fire events are assumed to be catastrophic, all live pools are reduced to zero after the disturbance event.

$$(92) \quad \text{live_pool:mass}_{t, \text{ after fire}} = 0$$

A portion of each live pool is transferred to its corresponding dead pool; the percentage is specified by the user, and is a function of the fire's intensity.

$$(93) \quad \text{live_pool:burn_transfer}_t = \text{live_pool:mass}_{t, \text{ before fire}} * \%_{\text{transfer_to_dead_pool}}(\text{fire_intensity})$$

The remaining portion is lost to the atmosphere.

$$(94) \quad \text{live_pool:burn_loss}_t = \text{live_pool:mass}_{t, \text{ before fire}} - \text{live_pool:burn_transfer}_t$$

Detrital Pools

All non-composite dead pools and stable pools lose a percentage of their mass to the atmosphere due to combustion. The user specifies the percentage of a pool's mass that *remains* after a fire.

$$(95) \quad \text{detrital_pool:burn_loss}_t = \text{detrital_pool:mass}_{t, \text{ before fire}} * (100\% - \%_{\text{remaining_pool}}(\text{fire_intensity}))$$

Dead Pools

For non-bole dead pools (dead foliage, dead branch, dead coarse roots, and dead fine roots), the pool's mass is adjusted for the burn loss and the transfer from the corresponding live pool.

$$(96) \quad \text{dead_pool:mass}_{t, \text{ after fire}} = \text{dead_pool:mass}_{t, \text{ before fire}} - \text{dead_pool:burn_loss}_t + \text{live_pool:burn_transfer}_t$$

For the dead bole pools, the transfer from the corresponding live pool(s) is added to the snag pool.

$$(97) \quad \text{dead_sapwood:snags:mass}_{t, \text{ after fire}} = \text{dead_sapwood:snags:mass}_{t, \text{ before fire}} - \text{dead_sapwood:snags:burn_loss}_t + \text{sapwood:burn_transfer}_t$$

$$(98) \quad \text{dead_heartwood:snags:mass}_{t, \text{ after fire}} = \text{dead_heartwood:snags:mass}_{t, \text{ before fire}} - \text{dead_heartwood:snags:burn_loss}_t + \text{heartwood:burn_transfer}_t + \text{heartrot:burn_transfer}_t$$

$$(99) \quad \text{dead_bole:logs:mass}_{t, \text{ after fire}} = \text{dead_bole:logs:mass}_{t, \text{ before fire}} - \text{dead_bole:logs:burn_loss}_t$$

$$(100) \quad \text{dead_bole:mass}_{t, \text{ after fire}} = \text{dead_bole:snags:mass}_{t, \text{ after fire}} + \text{dead_bole:logs:mass}_{t, \text{ after fire}}$$

Additionally, decay rates are adjusted based on the decay rate associated with the input from disturbances. Thus:

$$(101) \quad \text{dead_pool:decay_rate}(t, \text{ after event}) = \text{weighted_average} (\text{dead_pool:input_decay_rate}_t, \text{live_pool:[cut or burn]_transfer}_t, \text{dead_pool:decay_rate}_{t, \text{ before event}}, \text{dead_pool:mass}_{t, \text{ before event}})$$

LANDSCAPE-AVERAGE RATE-CONSTANTS

The general equation describing the landscape-average rate-constant is:

$$\text{Rate}_{LA} = \frac{\sum_t^{\text{Time_End}} \text{pool} : \text{flux}_t}{\sum_t^{\text{Time_End}} \text{mass}_t} = \frac{\sum_t^{\text{Time_End}} (\text{pool} : \text{mass}_t * \text{rate}(\text{age})_t)}{\sum_t^{\text{Time_End}} \text{mass}_t}$$

where $\sum_t \text{pool} : \text{flux}_t$ equals the sum of the flux for all years in the simulation, and $\sum_t \text{pool} : \text{mass}(\text{age})$ equals the sum of the mass for all years in the simulation for that pool (equations listed in the table below). Since the rate-constants vary with age, the sum over time of the fluxes based on those rate-constants will be different for different disturbance regimes. Since the fluxes affect the accumulation of mass through time, the sum of a pool's mass will also be different for different disturbance regimes and therefore must be weighted by the mass of the pools, as reflected in the above equation.

Years With No Disturbances

For computing landscape averages, the disturbance-related transfers (cut_transfer, burn_transfer, burn_loss) of the pools are all set to 0 in those years when a disturbance event does not occur. Furthermore, the mass of each pool before a disturbance is simply the mass after the annual pool calculations (Eqns. 80 and 90).

Table C.2. Equations for landscape-average rate-constants in the DISTURBANCE Module.

Rate _{LA}	Equation
FOL_dist_adjustment	$\frac{\text{average}^a (\text{foliage} : \text{mass}_t)}{\text{ecoregion} : \text{steady_state_foliage}}$
BR_bole_ratio CR_bole_ratio	$\frac{\text{sum}^b (\text{pool} : \text{input}_t)}{\text{sum} (\text{sapwood} : \text{input}_t)}$

FR_FOL_ratio	$\frac{\text{sum (fine_roots:mass }_t, \text{ before disturbance)}}{\text{sum (foliage:mass }_t, \text{ before disturbance)}}$
HW_formation	$\frac{\text{sum (sapwood:formation_transfer }_t)}{\text{sum (sapwood:mass }_{t-1})}$
HR_formation	$\frac{\text{sum (heartwood: formation_transfer }_t)}{\text{sum (heartwood:mass }_{t-1})}$
SW_respiration HR_respiration BR_respiration CR_respiration	$\frac{\text{sum (pool:respiration_loss }_t)}{\text{sum (pool:mass }_{t-1})}$
BR_prune CR_prune	$\frac{\text{sum (pool:pruning_transfer }_t)}{\text{sum (pool:mass }_{t-1})}$
FOL_mortality FR_mortality	$\frac{\text{sum (pool: mortality_transfer }_t)}{\text{sum (pool:mass }_t, \text{ before disturbance)}}$
BR_mortality CR_mortality SW_mortality HW_mortality HR_mortality	$\frac{\text{sum (pool: mortality_transfer }_t)}{\text{sum (pool:mass }_{t-1})}$
FOL_turnover FR_turnover	$\frac{\text{sum (pool_turnover }_t)}{\text{sum (pool:mass }_t, \text{ before disturbance)}}$

<p>%_snags</p>	$\frac{\text{sum (dead_sapwood:snags:input }_t \text{)}}{\text{sum (dead_sapwood:input }_t \text{)}}$
<p>dead_FOL_decay dead_SW_snags_decay dead_SW_logs_decay dead_HW_snags_decay dead_HW_logs_decay dead_BR_decay dead_CR_decay dead_FR_decay stable_FOL_decay stable_wood_decay stable_soil_decay</p>	$\frac{\text{sum (pool:decay_loss }_t \text{)}}{\text{sum (pool:mass }_{t-1} \text{)}}$
<p>dead_FOL_transfer dead_SW_snags_transfer dead_SW_logs_transfer dead_HW_snags_transfer dead_HW_logs_transfer dead_BR_transfer dead_CR_transfer dead_FR_transfer</p>	$\frac{\text{sum (pool:transfers }_t \text{)}}{\text{sum (pool:mass }_{t-1} \text{)}}$
<p>SW_burn_loss HW_burn_loss HR_burn_loss BR_burn_loss CR_burn_loss</p> <p>dead_FOL_burn_loss dead_SW_snags_burn_loss dead_SW_logs_burn_loss dead_HW_snags_burn_loss dead_HW_logs_burn_loss dead_BR_burn_loss dead_CR_burn_loss dead_FR_burn_loss</p> <p>stable_FOL_burn_loss stable_wood_burn_loss stable_soil_burn_loss</p>	$\frac{\text{sum (pool:burn_loss }_t \text{)}}{\text{sum (pool:mass }_{t, \text{ before fire}} \text{)}}$

FOL_cut_transfer SW_cut_transfer HW_cut_transfer HR_cut_transfer BR_cut_transfer CR_cut_transfer FR_cut_transfer	$\frac{\text{sum} (\text{pool: cut_transfer}_t)}{\text{sum} (\text{pool:mass}_{t, \text{ before harvest}})}$
FOL_burn_transfer SW_burn_transfer HW_burn_transfer HR_burn_transfer BR_burn_transfer CR_burn_transfer FR_burn_transfer	$\frac{\text{sum} (\text{pool:burn_transfer}_t)}{\text{sum} (\text{pool:mass}_{t, \text{ before fire}})}$
SW_harvest_transfer HW_harvest_transfer HR_harvest_transfer	$\frac{\text{sum} (\text{pool:harvest_transfer}_t)}{\text{sum} (\text{pool:mass}_{t, \text{ before harvest}})}$

^a $\text{average} (\text{pool:attribute}_t) = \text{sum}(\text{pool:attribute}_t) / \# \text{ of years in } T$

^b $\text{sum} (\text{pool:attribute}_t) = ? \text{ pool:attribute}_t \text{ for all } t \text{ in } T$

T = the set of years selected for landscape averages; it is constructed by skipping the first S years. S is specified by the user.

Appendix D. The calculations in the STEADY-STATE Module of MAXCARB.

STEADY-STATE POOL MASS

For every pool except foliage and fine-roots, the pool's landscape-average mass at steady-state (mass area⁻¹) is the pool's input flux (mass area⁻¹ time⁻¹) divided by the pool's landscape-average rate-constant (time⁻¹).

$$(1) \quad \text{pool:mass}_{SS} = \text{pool:input} / \text{pool:rate}_{LA}$$

The pool's landscape-average rate-constant is the sum of the all landscape-average rate-constants that affect the output of mass from the pool for a given disturbance regime.

These rate-constants include the rates of mass loss and transfer due to a disturbance event. They are all calculated in the DISTURBANCE Module, and hence, are denoted by the subscript "D" or "rate,D". Some of these rates are adjusted for climate by multiplying them by climate indices from the CLIMATE Module (denoted by the subscript "c").

LIVE POOLS

Transfer Flux

Each live pool transfers mass to other pools. This transfer flux is based on the pool's transfer rate.

$$(2) \quad \text{pool:transfer} = \text{pool:mass}_{SS} * \text{pool:transfer_rate}$$

Transfer rates for each pool are described in the following sections.

Foliage, Fine-Roots

Steady-State Mass

The masses of the foliage and fine-root pools are solved directly, rather than with Equation (1). The foliage mass is the ecoregion's steady-state foliage mass adjusted for the ecoregion's disturbance regime.

$$(3) \quad \text{foliage:mass}_{SS} = \text{ecoregion:steady_state_foliage} * \text{FOL_dist_adjustment}_D$$

The ecoregion's steady-state foliage mass is based on the ecoregion's light extinction coefficient (the degree to which light is dissipated through a typical vegetation canopy) and its light compensation point (the minimum percentage of light necessary for growth).

$$(4) \quad \text{ecoregion:steady_state_foliage} = -\log(\text{ecoregion:light_comp_point}) / \text{ecoregion:light_ext_coeff}$$

This equation is based on the Beer-Lambert equation, which describes an inverse proportionality between light availability and the amount of leaf area.

The mass of the fine-root pool is a proportion of the foliage mass that is allocated to fine-roots.

$$(5) \quad \text{fine_roots:mass}_{SS} = \text{foliage:mass}_{SS} * \text{fine_roots_foliage_ratio}_D$$

Transfer Rate

For the foliage and fine-root pools, the rate at which each pool transfers mass to its corresponding dead pool is based on the live pool's turnover rate, mortality rate, and transfer rates due to disturbances.

$$(6) \quad \text{pool:transfer_rate} = \text{pool_turnover}_{\text{rate, D}} + \text{pool_mortality}_{\text{rate, D}} + \text{pool_burn_transfer}_{\text{rate, D}} + \text{pool_cut_transfer}_{\text{rate, D}}$$

Sapwood

Input Flux

The input flux to the sapwood pool is assumed to be directly proportional to the foliage mass (Eqn. 3). This proportion is by the ecoregion's bole growth efficiency multiplied by the production index from the CLIMATE Module.

$$(7) \quad \text{sapwood:input} = \text{foliage:mass}_{SS} * (\text{ecoregion:bole_growth_efficiency} * \text{production_index}_C)$$

Rate

The landscape-average rate-constant for the sapwood pool is based on its respiration rate (adjusted for climate), the formation rate of heartwood, its loss rate due to fires, its transfer rate to dead sapwood (Eqn. 13), and its transfer rate to the forest-products pool.

$$(8) \quad \text{sapwood:rate}_{LA} = (\text{SW_respiration}_{rate, D} * \text{sapwood:respiration_index}_C) \\ + \text{HW_formation}_{rate, D} + \text{SW_burn_loss}_{rate, D} \\ + \text{sapwood:transfer_rate} + \text{SW_harvest_transfer}_{rate, D}$$

Heartwood

Input Flux

The input flux to the heartwood pool is the amount of sapwood that forms (i.e., becomes) heartwood.

$$(9) \quad \text{heartwood:input} = \text{sapwood:mass}_{SS} * \text{HW_formation}_{rate, D}$$

Rate

The landscape-average rate-constant for the heartwood pool is based on the formation rate of heart-rot, heartwood's loss rate due to fires, its transfer rate to dead heartwood (Eqn. 13), and its transfer rate to the forest-products pool.

$$(10) \quad \text{heartwood:rate}_{LA} = \text{HR_formation}_{rate, D} + \text{HW_burn_loss}_{rate, D} \\ + \text{heartwood:transfer_rate} + \text{HW_harvest_transfer}_{rate, D}$$

Heart-rot

Input Flux

The input flux to the heart-rot pool is the amount of heartwood that forms (i.e., becomes) heart-rot.

$$(11) \quad \text{heartrot:input} = \text{heartwood:mass}_{SS} * \text{HR_formation}_{rate, D}$$

Rate

The landscape-average rate-constant for the heart-rot pool is based on its respiration rate (adjusted for climate), its loss rate due to fires, its transfer rate to dead heartwood (Eqn. 13), and its transfer rate to the forest-products pool.

$$(12) \quad \text{heartrot:rate}_{LA} = (\text{HR_respiration}_{rate, D} * \text{heartrot:respiration_index}_C) \\ + \text{HR_burn_loss}_{rate, D} + \text{heartrot:transfer_rate} \\ + \text{HR_harvest_transfer}_{rate, D}$$

Live Bole Pools

Transfer Rate

The rate at which a live bole pool transfers mass to its corresponding dead pool is a combination of the live pool's mortality rate and transfer rates due to disturbances.

$$(13) \quad \text{live_bole:transfer_rate} = \text{live_bole_mortality}_{rate, D} \\ + \text{live_bole_burn_transfer}_{rate, D} \\ + \text{live_bole_cut_transfer}_{rate, D}$$

Harvest Transfer Flux

Each live bole pool transfers some of its mass to the forest-products pool based on its individual harvest transfer rate.

$$(14) \quad \text{live_bole:harvest_transfer} = \text{live_bole:mass}_{SS} \\ * \text{live_bole_harvest_transfer}_{rate, D}$$

Branch, Coarse Roots

Input Flux

For the branch and coarse-root pools, the pool's input flux is based on the sapwood's input flux (Eqn. 7).

$$(15) \quad \text{pool:input} = \text{sapwood:input} * \text{pool_bole_ratio}_D$$

Rates

For the branch and coarse-root pools, the rate at which each pool transfers mass to its corresponding dead pool is based on the live pool's pruning rate, mortality rate, and transfer rates due to disturbances.

$$(16) \quad \text{pool:transfer_rate} = \text{pool_prune}_{\text{rate, D}} + \text{pool_mortality}_{\text{rate, D}} \\ + \text{pool_burn_transfer}_{\text{rate, D}} + \text{pool_cut_transfer}_{\text{rate, D}}$$

For each of these pools, its landscape-average rate-constant is based on its respiration rate (adjusted for climate), its loss rate due to fires, and its transfer rate to its dead pool (previous equation).

$$(17) \quad \text{pool:rate}_{LA} = (\text{pool_respiration}_{\text{rate, D}} * \text{pool:respiration_index}_C) \\ + \text{pool_burn_loss}_{\text{rate, D}} + \text{pool:transfer_rate}$$

DEAD POOLS

Transfer Flux

Each dead pool transfers mass to other pools. This transfer flux is calculated in the same way as for live pools (Eqn. 2), and is based on the pool's transfer rate. Transfer rates for each pool are described in the following sections.

Rates – Non-composite Pools

A non-composite dead pool is a dead pool that is not composed of other pools. The only composite dead pools are the dead bole pools (dead sapwood and dead heartwood); they each are composed of two pools: snags and logs. These snag and log pools are non-composite pools.

For each non-composite dead pool, its landscape-average rate-constant is based on its decay and transfer rates adjusted for climate, and its loss rate due to fires.

$$(18) \quad \text{dead_pool:rate}_{LA} = (\text{dead_pool_decay}_{rate, D} + \text{dead_pool_transfer}_{rate, D}) \\ * \text{dead_pool:decay_index}_C \\ + \text{dead_pool_burn_loss}_{rate, D}$$

Dead Foliage, Dead Branch, Dead Roots

Input Flux

For dead foliage, dead branch, dead coarse-roots and dead fine-roots, their input flux is just the transfer flux from its corresponding live pool (Eqn. 2).

$$(19) \quad \text{dead_pool:input} = \text{live_pool:transfer}$$

Dead Bole Pools

Snags and Logs

Each dead bole pool – dead sapwood and dead heartwood – is composed of two internal pools representing snags and logs.

Input Flux

The input flux to each dead bole pool – dead sapwood and dead heartwood – is the transfer flux(es) from its corresponding live bole pool(s) (Eqn. 2).

$$(20) \quad \text{dead_sapwood:input} = \text{sapwood:transfer}$$

$$(21) \quad \text{dead_heartwood:input} = \text{heartwood:transfer} + \text{heartrot:transfer}$$

This input flux is divided between the pool's snag and log pools. The input flux to the log pool also includes the transfer from the snag pool (Eqn. 2).

$$(22) \quad \text{dead_bole:snags:input} = \text{dead_bole:input} * \%_snags_p$$

$$(23) \quad \text{dead_bole:logs:input} = \text{dead_bole:input} * (100\% - \%_snags_p) \\ + \text{dead_bole:snags:transfer}$$

Steady State Mass

The masses of the snag and log pools are each determined using Equation (1); however, the steady-state mass of a dead bole pool is just the sum of the masses of its snag and log pools.

$$(24) \quad \text{dead_bole:mass}_{SS} = \text{dead_bole:snags:mass}_{SS} + \text{dead_bole:logs:mass}_{SS}$$

Rate

Because of the previous equation, a dead bole pool has no landscape-average rate-constant. However, its snag and log pools each have their landscape-average rate-constant determined using Equation (18).

Transfer Flux

The transfer flux from each of the snag and log pools is determined using Equation (2). The transfer flux from a dead bole pool is just the transfer flux from its log pool.

$$(25) \quad \text{dead_bole:transfer} = \text{dead_bole:logs:transfer}$$

STABLE POOLS

Input Flux

The input to a stable pool is the sum of the transfer fluxes from its corresponding dead pools (Eqns. 2 & 25).

$$(26) \quad \text{stable_foliage:input} = \text{dead_foliage:transfer}$$

$$(27) \quad \text{stable_wood:input} = \text{dead_sapwood:transfer} + \text{dead_heartwood:transfer} \\ + \text{dead_branch:transfer}$$

$$(28) \quad \text{stable_soil:input} = \text{dead_coarse_roots:transfer} + \text{dead_fine_roots:transfer}$$

Rate

For each stable pool, its landscape-average rate-constant is based on its decay rate (adjusted for climate) and its loss rate due to fires.

$$(29) \quad \text{stable_pool:rate}_{LA} = (\text{stable_pool_decay}_{\text{rate, D}} * \text{stable_pool:decay_index}_C) \\ + \text{stable_pool_burn_loss}_{\text{rate, D}}$$

FOREST PRODUCTS

Input Flux

The input flux to the forest products pool is based on the sum of the transfer fluxes from the live bole pools (sapwood, heartwood, and heart-rot) due to harvesting (Eqn. 14). These fluxes are modified by a manufacturing efficiency that accounts for the proportion of harvested boles that remain after the manufacturing process. This efficiency is an input parameter specified by the user.

$$(30) \quad \text{forest_products:input} = (\text{sapwood:harvest_transfer} + \\ \text{heartwood:harvest_transfer} + \\ \text{heartrot:harvest_transfer}) \\ * \text{manufacturing_efficiency}$$

Rate

The landscape-average rate-constant for the forest products pool is just the landscape-average decay rate of forest products

$$(31) \quad \text{forest_products:rate}_{LA} = \text{forest_products_decay}$$

This decay rate is an input parameter specified by the user, who may have determined it using another model such as ForProd (Harmon et al. 1996).

Appendix E. The calculations in the CLIMATE Module of MAXCARB.

OVERVIEW

The purpose of the CLIMATE Module is to calculate the effects of climate on processes that ultimately determine a site's carbon storage. Specifically, the CLIMATE Module calculates a set of indices controlling production (production_index), respiration (respiration_index), and decomposition (decay_index), which are then passed to the STEADY STATE Module where they modify rates that are used to calculate steady-state stores:

$$(1) \quad \text{rate}_C \text{ (with climate effects)} = \text{rate} \text{ (without climate effects)} * \text{climate_index}.$$

Together, these climate indices affect steady-state carbon storage by accounting for the temperature and moisture limitations of the site. Temperature and moisture indices are calculated monthly and are multiplied together at the end of each month to describe the overall monthly climate limitation. The resulting monthly indices are averaged for a year and then passed to the STEADY STATE Module.

RESPIRATION INDICES

The respiration index of a pool (*pool:respiration_index*) is calculated as a function of the mean annual temperature of a site (*mean_annual_temp*) and the ecoregion's Q_{10} value for that pool's respiration:

$$(2) \quad \text{pool:respiration_index} = \text{pool:}Q_{10} \wedge ((\text{mean_annual_temp} - 10)/10),$$

where *mean_annual_temp* equals:

$$(3) \quad \text{mean_annual_temp} = (\sum_{\text{month} = \text{Jan}}^{\text{Dec}} \text{temp_24}_{\text{month}}) / 12,$$

where *temp_24_{month}* is specified in the site's climate text file.

PRODUCTION INDICES

Each living pool has a production index which is an annual average of monthly production indices. The annual production index is initially set equal to one in the CLIMATE Module and is reduced by temperature and moisture limitations, which limit the rate of production of living biomass at each site. In addition to indicating the response of production, it also controls transpiration. The annual production index is the average of the monthly production indices.

$$(3) \quad \text{pool:production_index} = \left(\frac{\sum_{\text{month} = \text{Jan}}^{\text{Dec}} \text{pool:production_index}_{\text{month}}}{12} \right)$$

A monthly production index has a temperature-related component and a moisture-related component. For each month the product of these two indices is computed:

$$(4) \quad \text{pool:production_index}_{\text{month}} = \text{pool:temp_prod_index}_{\text{month}} * \text{pool:moist_prod_index}_{\text{month}}$$

Temperature Production Index

The temperature production index ($\text{temp_prod_index}_{\text{month}}$) determines the effect of temperature on net photosynthesis of each layer. The curve used to simulate this relationship is taken from Running and Coughlan (1988) and defines the mean daytime temperature ($\text{temp_day}_{\text{month}}$) response according to a minimum and maximum temperature compensation point ($\text{temp_min}_{\text{ecoregion}}$ and $\text{temp_max}_{\text{ecoregion}}$) as defined for the ecoregion in the ecoregion.prm input file. The daily (24-hour) mean temperature ($\text{temp_24}_{\text{month}}$) is converted to the mean daytime temperature using the mean maximum temperature for the month:

$$(5) \quad \text{temp_day}_{\text{month}} = 0.212 * (\text{temp_max}_{\text{ecoregion}} - \text{temp_24}_{\text{month}}) + \text{temp_24}_{\text{month}}$$

Essentially, $\text{temp_prod_index}_{\text{month}}$ is a relative index of the response of each site to its average monthly daytime temperature. If the mean daytime temperature exceeds either the minimum or maximum temperature compensation points for an ecoregion, then

the temperature production index at that site is set to zero. If the daytime temperature is within those limits then:

$$(6) \quad \text{temp_prod_index}_{\text{month}} = \frac{[(\text{temp_max}_{\text{ecoregion}} - \text{temp_day}_{\text{month}}) * (\text{temp_day}_{\text{month}} - \text{temp_min}_{\text{ecoregion}})]}{[(\text{temp_max}_{\text{ecoregion}} - \text{pool:temp_opt}) * (\text{pool:temp_opt} - \text{temp_min}_{\text{ecoregion}})],}$$

where the optimum temperature (temp_opt) for a pool is the average of the minimum and maximum temperatures:

$$(7) \quad \text{pool:temp_opt} = (\text{temp_max}_{\text{ecoregion}} - \text{temp_min}_{\text{ecoregion}}) / 2.$$

Moisture Production Index

The moisture production index function ($\text{moist_prod_index}_{\text{month}}$) determines the effect of soil moisture on the production of live biomass. The overall effect of water potential on production for each month is:

$$(8) \quad \text{moist_prod_index}_{\text{month}} = \text{water_logging_index}_{\text{month}} * \text{drought_index}_{\text{month}}$$

where the $\text{water_logging_index}_{\text{month}}$ is the reduction due to water logged conditions for that month and $\text{drought_index}_{\text{month}}$ is the reduction due to drought conditions during the month. Currently, we assume there is no effect on production when water logging occurs:

$$(9) \quad \text{water_logging_index}_{\text{month}} = 1$$

However, in a future version we hope to implement a reduction in productivity when the water potential is less than -0.1 MP. This would provide for a more realistic assumption for sites with poor drainage and water logging.

When soil water potential ($\text{stable_soil:water_potential}_{\text{month}}$) is below -0.3 MPa, we assume that productivity decreases exponentially as a function of drought (Emmingham and Waring 1977). The equation describing this response is:

$$(10) \quad \text{drought_index}_{\text{month}} = 1 - (1 - \exp(-5 * \text{stable_soil:water_potential}_{\text{month}}))^9$$

Stable_soil:water_potential_{month} is described below (see Water Potential section).

DECAY INDICES

The monthly decay index (*pool:decay_index*) determines the combined effects of temperature and moisture on the decomposition rate of each detrital pool and the stable soil pool for each month:

$$(11) \quad \text{pool:decay_index} = \left(\frac{\sum_{\text{month} = \text{Jan}}^{\text{Dec}} \text{pool:decay_index}_{\text{month}}}{12} \right)$$

For each detritus pool, or the stable soil pool, the monthly decay index is:

$$\text{pool:decay_index}_{\text{month}} = \text{pool:temp_decay_index}_{\text{month}} * \text{pool:moist_decay_index}_{\text{month}}$$

The temperature decay index (*pool:temp_decay_index_{month}*) and the moisture decay index (*pool:moist_decay_index_{month}*) are described below.

Temperature Decay Index

This function determines the effect of temperature on the decomposition rate of the detrital and soil pools. The monthly temperature decay index for each month and each pool is given by the following equation:

$$(13) \quad \text{pool:temp_decay_index}_{\text{month}} = \text{pool:temp_increase}_{\text{month}} * \text{pool:temp_limit}_{\text{month}}$$

where *pool:temp_increase_{month}* assumes an increase in respiration rate with temperature following a Q_{10} type curve:

$$(14) \quad \text{pool:temp_increase}_{\text{month}} = \text{pool:}Q_{10}^{\left(\frac{\text{temp}_{24\text{month}} - 10}{10} \right)}$$

where the respiration rate of the layer at 10 °C is assumed to be 1.0, and *pool:Q₁₀* is the rate at which respiration increases with a 10 °C increase in temperature and *temp_{24month}* is the temperature of a given month. The Q_{10} for each pool is specified in the decay parameter file (*detrital_pool_parms.txt*).

The second part of the temperature limitation to decomposition reflects the effect of a lethal temperature limit (*pool:temp_limit_{month}*) that arrests decomposer activity. The equation is:

$$(15) \quad pool:temp_limit_{month} = \exp\left[-\left(\frac{temp_24_{month}}{pool:temp_lag}\right)^{\frac{pool:temp_opt + pool:temp_lag}{pool:temp_shape}}\right]$$

where *pool:temp_opt* is the optimum temperature for decomposition of a detritus pool and *pool:temp_lag* and *pool:temp_shape* are parameters that determine the shape of the response curve. These parameters are also found in the *detrital_pool_parms.txt* file.

Moisture Decay Index

We assume that the moisture content of the pools controls decomposition in two ways. The first is by matric potential limitations, which makes water unavailable for decomposers. For most detrital forms, decomposition ceases when the moisture content reaches the fiber saturation point. The second is caused by poor oxygen diffusion, when the moisture content is too high. For most detrital layers this is not a problem. However, coarse wood respiration is often limited by this factor. We model the matric potential and diffusion limitation portions separately. The combined effect of matric and diffusion limitations for each detritus pool or for the stable soil pool for each month is:

$$(16) \quad pool:moist_decay_index_{month} = pool:matric_limit_{month} * pool:diffuse_limit_{month}$$

The equation for the matric potential limitation (*pool:matric_limit_{month}*) of each detrital pool or the stable soil pool for each month is:

$$(17) \quad pool:matric_limit_{month} = (1 - \exp\left[-\frac{pool:increase_rate * (pool:moisture_content_{month} + pool:matric_lag)}{pool:matric_shape}\right])$$

where *pool:matric_shape* is a dimensionless number that determines when the matric limit is reduced to the point that decay can begin to occur. For all detritus pools except the stable soil pool, the moisture content (%) is based on the mass of water divided by the dry mass of the pool at steady state. For the stable soil pool, the moisture content is based on volume of water divided by volume of soil. The *pool:matric_lag* parameter is used to offset the curve to the left or right. The parameters are in the *decay_parms_funcs.txt* file. The *pool:increase_rate* is the parameter determining the point at which the matric limitation ends:

$$(18) \quad pool:increase_rate = 3 / pool:moist_min$$

where the minimum moisture content (*pool:moist_min* (%)) reflects the minimum water necessary for decomposition to occur.

The diffusion limitation (*pool:diffuse_limit_{month}*) is designed to mimic the reduction in decomposition caused when the substrate becomes water saturated. Water saturation causes a reduction in oxygen diffusion, reducing decomposition. This function remains at 1 until the maximum moisture content (without diffusion limitations) is reached. The function decreases to 0 when moisture content exceeds the maximum for decomposition to occur. This function is calculated for each detrital pool for each month:

$$(19) \quad \mathit{pool:diffuse_limit}_{\mathit{month}} = \exp[-(\mathit{pool:moisture_content}_{\mathit{month}} / (\mathit{pool:moist_max} + \mathit{pool:diffuse_lag}))^{\mathit{pool:diffuse_shape}}]$$

where *pool:moist_max* is the maximum moisture content without diffusion limitations, *pool:diffuse_shape* is a dimensionless number that determines the range of moisture contents where diffusion is not limiting, and *pool:diffuse_lag* is a parameter used to shift the point when moisture begins to limit diffusion.

MOISTURE CONTENT

To calculate the effect of water stores in detritus pools on the moisture decay index, values have to be converted to moisture content based on mass:

$$(21) \quad \mathit{pool:moisture_content}_{\mathit{month}} = \mathit{pool:water_mass}_{\mathit{month}} / \mathit{pool:mass}_{\mathit{SS}}$$

where *pool:mass_{SS}* is the mass from the STEADY STATE Module of each detritus pool during the year being considered. The mass of water (*pool:water_mass_{month}*) covering one hectare in one centimeter of depth is 100 Mg. Therefore each 1 cm of water stored in a detrital layer is:

$$(22) \quad \mathit{pool:water_mass}_{\mathit{month}} = \mathit{pool:water}_{\mathit{month}} * 100 \text{ Mg ha}^{-1} \text{ cm}^{-1},$$

where *pool:water_{month}* equals the monthly water store (described in Water Stores section).

The dead fine root moisture content (*dead_fine_roots:moisture_content_{month}*) is assumed to equilibrate rapidly with the surrounding soil and humus. It is therefore assumed to be the same as the *stable_foliage* pool:

$$(23) \quad \text{dead_fine_roots:moisture_content}_{\text{month}} = \text{stable_foliage:moisture_content}_{\text{month}}$$

Dead coarse root moisture content ($\text{dead_coarse_roots:moisture_content}_{\text{month}}$) is controlled by the moisture of the surrounding mineral soil (Chen and Harmon, in prep.). When the soil is saturated we assume that the dead coarse root pool reaches its maximum moisture content. Therefore, if

$$(24) \quad \text{dead_coarse_roots:moisture_content}_{\text{month}} = 100\%,$$

then

$$(25) \quad \text{dead_coarse_roots:moisture_content}_{\text{month}} = \text{dead_coarse_roots:moist_store_max}.$$

When the moisture content of the mineral soil is less than saturated (<100%), we assume the dead coarse roots and mineral soil are in equilibrium. However, since mineral soil moisture content is expressed in volumetric terms and dead coarse roots in mass terms we must convert units. Then,

$$(26) \quad \text{dead_coarse_roots:moisture_content}_{\text{month}} = 2 * \text{stable_soil:moisture_content}_{\text{month}}$$

The moisture content of the soil ($\text{stable_soil:moisture_content}_{\text{month}}$) is calculated on a volumetric basis relative to the maximum water storage ($\text{stable_soil:water_max}$) of the particular site being examined:

$$(27) \quad \text{stable_soil:moisture_content}_{\text{month}} = \frac{\text{stable_soil:water}_{\text{month}}}{\text{stable_soil:water_max}},$$

where $\text{stable_soil:water_max}$ is equal to the maximum amount of water (in cm) a site's soil can hold:

$$(28) \quad \text{stable_soil:water_max} = \text{soil_texture:water_max_per} * \text{soil_depth} * \%_fine_soil,$$

and the percent of fine soil ($\%_fine_soil$) equals the fraction of the soil that is fragments less than 2 mm in diameter:

$$(29) \quad \%_fine_soil = 100\% - \%_rocks.$$

The percent of rocks greater than or equal to 2 mm ($\%_rocks$), the soil depth to 100 cm (soil_depth), and the soil texture (soil_texture) are defined in the site input file. The value

of `soil_texture:water_max_per` is defined in the soil texture input file (`soil_textures.txt`) for a given soil texture.

WATER POTENTIAL

Soil Water Potential

This function converts the volumetric moisture content of soils to water potential (`stable_soil:water_potentialmonth` (MPa)). Water potential does not increase appreciably from zero when the soil is near saturation; thus, the water potential is set to zero when the soil moisture content (`stable_soil:moisture_contentmonth`) is greater to or equal to 90 %. Otherwise, the soil water potential is represented by a reciprocal function modified by an asymptote:

$$(30) \quad \text{stable_soil:water_potential}_{\text{month}} = \text{soil_texture:water_pot_asym} + \frac{\text{soil_texture:water_pot_1}}{\text{stable_soil:moisture_content}_{\text{month}}}$$

where `soil_texture:water_pot_asym` simulates the behavior of coarse textured soils that yield considerable water without changing their water potential. `Soil_texture:water_pot_1` is the fraction of the water stores when the water potential is equal to 1 MPa. When this latter water potential is reached, moisture becomes limiting to transpiration and production. The values of `soil_texture:water_pot_asym` and `soil_texture:water_pot_1` are defined in the soil texture input file (`soil_textures.txt`) for a given soil texture.

WATER STORES

The water stores are computed for all detrital pools except the root pools. A pool's water stores is based on the water entering into and leaving out of the pool.

$$(31) \quad \text{pool:water}_{\text{month}} = \text{pool:water}_{\text{previous month}} + \text{pool:water_in}_{\text{month}} - \text{pool:water_out}_{\text{month}}$$

The site's water balance is estimated by calculating the inputs and outputs of water to and from each pool. Inputs are calculated as a function of intercepted precipitation. Outputs

are calculated as a function of evaporation and transpiration. There is a maximum limit for the pool's water stores, based on its mass:

$$(32) \quad \text{pool:max_water} = \text{pool:mass}_{\text{SS}} * \text{pool:moist_store_max} / 100 \text{ (Mg ha}^{-1} \text{ cm}^{-1}\text{)}$$

For stable soil, there is a small non-zero minimum (0.01) to prevent the water potential from becoming undefined:

$$(33) \quad \text{stable_soil:available_water}_{\text{month}} = \max (0.01, \text{stable_soil:water}_{\text{previous month}} + \text{stable_soil:delta_water}_{\text{month}})$$

where,

$$(34) \quad \text{stable_soil:delta_water}_{\text{month}} = \text{stable_soil:water_in}_{\text{month}} - \text{stable_soil:water_out}_{\text{month}}$$

Runoff is the excess water beyond the soil's maximum capacity:

$$(35) \quad \text{stable_soil:water}_{\text{month}} = \min (\text{stable_soil:available_water}_{\text{month}}, \text{stable_soil:water_max}),$$

where $\text{stable_soil:runoff}_{\text{month}}$ equals 0 if $\text{stable_soil:available_water}_{\text{month}} = \text{stable_soil:water_max}$. Otherwise, $\text{stable_soil:runoff}_{\text{month}}$ is the difference between the available water and the maximum water store for the stable soil pool ($\text{stable_soil:available_water}_{\text{month}} - \text{stable_soil:water_max}$).

The water stores for the month of January are based on December's water stores from the previous iteration of calculating climate indices. However, the masses of the detrital pools are updated between each iteration. Because the dead wood pools and the forest floor pools have their moisture contents based on mass, their December's water stores must first be adjusted for each pool's new mass. For the first iteration for January, the pool's water content for the previous month is assumed to be zero. For all other iterations, the pool's water content of the previous month is equal to the adjusted value for December of the previous iteration.

Currently, the CLIMATE Module can be configured to use one of two methods for adjusting the December's water stores. In the first method, the maximum limit for the pool's water stores is updated for the pool's new mass. If December's water stores exceed this new limit, then the steady-state stores are adjusted down to this limit:

$$(36) \quad \text{pool:water}_{\text{Dec (iteration } i-1 \text{) adjusted}} = \min (\text{pool:max_water}_{\text{iteration } i},$$

$$pool:water_{Dec (iteration i-1)}.$$

In the second method, the water stores for December are adjusted to maintain the same moisture content for the month of December.

$$(37) \quad pool:water_{Dec (iteration i-1) \text{ adjusted}} = \frac{pool:mass_{iteration i} * pool:moisture_content_{Dec, iteration i-1}}{100 \text{ Mg ha}^{-1} \text{ cm}^{-1}}$$

WATER INPUT

For detrital pools, the water input is the amount of precipitation falling through the canopy that the pool intercepts:

$$(38) \quad pool:water_in_{month} = pool:interception_{month}.$$

Thus, the total dead wood pool interception ($dead_wood_interception_{month}$) is equal to the sum of the interception of all dead wood pools:

$$(39) \quad dead_wood_interception_{month} = \sum_{\text{for all dead wood pools}} pool:interception_{month}$$

and the amount of throughfall through the dead pools is equal to the difference between the inputs from the canopy ($canopy_thru_fall_{month}$ defined below) and the interception by the dead wood pools:

$$(40) \quad dead_wood_thru_fall_{month} = canopy_thru_fall_{month} - dead_wood_interception_{month}$$

Similarly, the water input to the forest floor pools (dead and stable foliage pools) is the amount of precipitation falling through the dead wood that the pool intercepts.

$$(41) \quad pool:water_in_{month} = pool:interception_{month}$$

and the total forest floor interception for the month ($forest_floor_interception_{month}$) is the sum of the interception of dead foliage and stable foliage pools:

$$(42) \quad forest_floor_interception_{month} = \sum_{\text{for both forest floor pools}} pool:interception_{month}$$

and the amount of through fall from these pools is the difference between water entering the pool and that which is intercepted:

$$(43) \quad forest_floor_wood_thru_fall_{month} = dead_wood_thru_fall_{month} - forest_floor_interception_{month}$$

For the soil, the water input is the amount of precipitation falling through the forest floor pools.

$$(44) \quad \text{stable_soil:water_in}_{\text{month}} = \text{forest_floor_thru_fall}_{\text{month}}$$

INTERCEPTION

The monthly canopy interception rate ($\text{interception_rate}_{\text{month}}$) is a function of the mean monthly precipitation ($\text{precipitation}_{\text{month}}$) and the mass of foliage at steady state. The interception rate generally decreases with increasing precipitation (Rothacher 1963, Lee 1980, Ward and Robinson 1990.) This relationship is simulated by:

$$(45) \quad \text{interception_rate}_{\text{month}} = \text{canopy_intercept_min} + (1 - \text{canopy_intercept_min}) * \exp(-0.75 * \text{precipitation}_{\text{month}}),$$

where $\text{canopy_intercept_min}$ is the minimum interception (per Mg) of foliage for an ecoregion (set in `ecoregion.txt` input file).

The interception also increases linearly with increasing foliage mass. This simulates the increase in interception observed with stand age and density (Ward and Robinson 1990). The amount of precipitation intercepted by canopy foliage in a given month is:

$$(46) \quad \text{canopy_interception}_{\text{month}} = \text{precipitation}_{\text{month}} * \text{interception_rate}_{\text{month}} * \text{foliage:mass}_{\text{SS}}$$

where $\text{foliage:mass}_{\text{SS}}$ is the mass of foliage from the STEADY STATE Module.

Canopy throughfall ($\text{canopy_thru_fall}_{\text{month}}$) is the fraction of the precipitation that is not intercepted by the canopy and thereby allowed to pass through the canopy each month:

$$(47) \quad \text{canopy_thru_fall}_{\text{month}} = \text{precipitation}_{\text{month}} - \text{canopy_interception}_{\text{month}}$$

Interception by the dead wood pools (snags, logs, dead branches, and stable wood) and forest floor pools (dead and stable foliage) is the difference between the water entering the pool and its potential interception ($\text{pool:pot_interception}_{\text{month}}$)

$$(47) \quad \text{pool:interception}_{\text{month}} = \min(\text{pool:precip_input}_{\text{month}}, \text{pool:pot_interception}_{\text{month}})$$

The detrital pools intercept precipitation in order of the "highest" pool to the "lowest" pool. In other words, the precipitation input to a pool is the precipitation falling through the next higher pool. The order of the pools is the snag pools, followed by all other dead wood pools, and then the forest floor pools:

- | | |
|----------------------------|--------------------------|
| Snag pools: | 1. Dead Sapwood: Snags |
| | 2. Dead Heartwood: Snags |
| Remaining Dead Wood pools: | 3. Dead Sapwood: Logs |
| | 4. Dead Heartwood: Logs |
| | 5. Dead Branch |
| | 6. Stable Wood |
| Forest Floor pools: | 7. Dead Foliage |
| | 8. Stable Foliage |

Precipitation input to the dead sapwood snags pool (*dead_sapwood:snags*:
precip_input_{month}) equals the through fall from the canopy. For all other pools, the input is the amount passing through the next highest pool, where:

$$(48) \quad \mathit{pool}:\mathit{thru_fall}_{\mathit{month}} = \mathit{pool}:\mathit{precip_input}_{\mathit{month}} - \mathit{pool}:\mathit{interception}_{\mathit{month}}$$

A detritus pool's potential interception is the smaller of two potentials: one based on area (*pool:max_pot_intercept_area_{month}*) and another based on storage capacity (*pool:max_pot_intercept_cap_{month}*). The minimum of the two determines how much water is intercepted and stored by the dead wood pools.

$$(49) \quad \mathit{pool}:\mathit{pot_interception}_{\mathit{month}} = \min(\mathit{pool}:\mathit{max_pot_intercept_area}_{\mathit{month}}, \mathit{pool}:\mathit{max_pot_intercept_cap}_{\mathit{month}})$$

The remainder is passed to the dead foliage pools.

The maximum, potential interception based on area is:

$$(50) \quad \mathit{pool}:\mathit{max_pot_intercept_area}_{\mathit{month}} = \mathit{pool}:\mathit{projected_area} * \mathit{pool}:\mathit{precip_input}_{\mathit{month}}$$

The projected area of each dead wood pool (*pool:projected_area* (%)) is calculated from its mass and the area to mass ratio:

$$(51) \quad \mathit{pool}:\mathit{projected_area} = \mathit{pool}:\mathit{mass} * \mathit{pool}:\mathit{area_mass_ratio},$$

where *pool:projected_area* is the projected area of the cell surface area (%) and *pool:area_mass_ratio* is the ratio of the projected area to the mass of the woody detrital

pool (dimensionless). If the pool is a forest floor pool and its mass is >3 Mg/ha, then the projected area equals 100%.

The maximum potential based on the storage capacity

(*pool:max_pot_intercept_cap*_{month}) is equal to the difference between the maximum water stores for that iteration and the mass of water in that pool:

$$(52) \quad \mathit{pool}:\mathit{max_pot_intercept_cap}_{\mathit{month}} = \mathit{pool}:\mathit{max_water}_{\mathit{iteration} \ i} - \mathit{pool}:\mathit{water_mass}_{\mathit{month}}$$

WATER OUTPUT

For detritus and forest floor pools, the water output is the water lost through evaporation:

$$(53) \quad \mathit{pool}:\mathit{water_out}_{\mathit{month}} = \mathit{pool}:\mathit{water_loss}_{\mathit{month}}$$

where the amount of water lost through the evaporative process is the minimum of the pool's available water (*pool:available_water*_{month}) and the maximum water loss for that pool (*pool:max_water_loss*_{month}):

$$(54) \quad \mathit{pool}:\mathit{water_loss}_{\mathit{month}} = \min (\mathit{pool}:\mathit{available_water}_{\mathit{month}}, \mathit{pool}:\mathit{max_water_loss}_{\mathit{month}}),$$

and where

$$(55) \quad \mathit{pool}:\mathit{available_water}_{\mathit{month}} = \mathit{pool}:\mathit{water}_{\mathit{previous\ month}} + \mathit{pool}:\mathit{water_in}_{\mathit{month}}$$

The maximum water loss for the pool equals the water of the previous month (*pool:water*_{previous month}) if the rate at which water is lost (*pool:water_loss_rate*_{month}) is greater than or equal to 1, indicating all the available water is evaporated. If, however, the rate is less than 1, the maximum water loss equals the water of the previous month multiplied by the rate of water loss. The rate of water loss is a function of the monthly evaporative demand and a constant (defined in the *detrital_pool_parms.txt* input file) that defines the rate of drying:

$$(56) \quad \mathit{pool}:\mathit{water_loss_rate}_{\mathit{month}} = \mathit{pool}:\mathit{evap_demand}_{\mathit{month}} * \mathit{pool}:\mathit{drying_constant}$$

The evaporative demand of a pool depends on its position, i.e., whether it is upright as for snags, or on the ground as for detrital pools, since the position modifies the microclimatic

conditions that modify evaporation. If the average daily temperature for the month is less than zero, evaporative demand is assumed to be zero. Otherwise, the evaporative demand equals the average daily temperature for the month multiplied by the radiation input to the pool. The radiation input is a function of the monthly solar radiation and the amount of light received by the pool:

$$(57) \quad \text{position:radiation_input}_{\text{month}} = \text{solar_rad}_{\text{month}} * \text{position:light_in}.$$

The CLIMATE Module can be set to use one of two methods for computing the total evaporation from the detrital pools. In the first method, the detritus evaporation for the month equals the total water loss from all dead wood and forest floor pools. In the second, the detritus evaporation for the month equals a detrital evaporative percent ($\text{detritus_evap_}\%$) multiplied by the total potential evapotranspiration for the month ($\text{total_PET}_{\text{month}}$ see below).

The water output from the soil pool equals the water lost just from transpiration, assuming there is always plant cover or forest floor cover.

$$(58) \quad \text{stable_soil:water_out}_{\text{month}} = \text{transpiration}_{\text{month}}$$

Transpiration

The potential amount of transpiration by plants ($\text{pot_trans}_{\text{month}}$) can be calculated in two ways. In the first, it is equal to the total potential evapotranspiration ($\text{total_PET}_{\text{month}}$) minus water lost by interception from the canopy pools and by evaporation from the detritus pools:

$$(59) \quad \text{pot_trans}_{\text{month}} = \text{total_PET}_{\text{month}} - \text{canopy_interception}_{\text{month}} - \text{detritus_evaporation}_{\text{month}}$$

In the second method for calculating potential transpiration, it is set as a constant percentage of potential evapotranspiration ($\text{total_PET}_{\text{month}}$):

$$(60) \quad \text{pot_trans}_{\text{month}} = \text{pot_trans_}\% * \text{total_PET}_{\text{month}}.$$

$\text{Pot_trans}_{\text{month}}$ is set so it cannot go below zero. If the interception and evaporation terms are larger than $\text{total_PET}_{\text{month}}$ potential transpiration is set to zero.

Potential transpiration yields a monthly potential transpiration loss assuming that leaf mass and soil water stores are at a maximum. The actual transpiration losses each month ($\text{transpiration}_{\text{month}}$) are additionally controlled by the moisture production index of the previous month and the foliage mass:

$$(61) \quad \text{transpiration}_{\text{month}} = \frac{\text{pot_trans}_{\text{month}} * \text{moist_prod_index}_{\text{previous month}}}{\text{foliage_ratio}}$$

where $\text{moist_prod_index}_{\text{previous month}}$ is calculated in the moisture production index function (described above) and foliage_ratio is the ratio of the current foliage to the maximum possible foliage mass:

$$(62) \quad \text{foliage_ratio} = \frac{\text{foliage_mass}_{\text{SS}}}{\text{ecoregion:maximum_foliage}}$$

$\text{Foliage_mass}_{\text{SS}}$ is the landscape-average foliage mass from the STEADY STATE Module and $\text{ecoregion:maximum_foliage}$ is the maximum total foliage mass possible for a given ecoregion. Max_foliage is calculated from the light compensation point and the light extinction coefficient for each ecoregion.

Potential Evapotranspiration

This function calculates the monthly total potential evapotranspiration (PET, in cm) of the site using a modification of the Priestly-Taylor method (Bonan 1989, Jensen 1973, Campbell 1977). Total potential evapotranspiration for a month ($\text{total_PET}_{\text{month}}$) is assumed to be a function of the solar radiation ($\text{solar_rad}_{\text{month}}$), the monthly mean air temperature ($\text{temp_24}_{\text{month}}$), the number of days in a month ($\text{num_days}_{\text{month}}$), two constants, CT and TX, and the latent heat of vaporization ($\text{lat_heat_vapor}_{\text{month}}$).

$$(63) \quad \text{total_PET}_{\text{month}} = \frac{\text{CT} * (\text{temp_24}_{\text{month}} + \text{TX}) * \text{solar_rad}_{\text{month}} * \text{num_days}_{\text{month}}}{\text{lat_heat_vapor}_{\text{month}}}$$

The constants CT and TX are empirically derived and calculated after Jensen and Haise (1963):

$$(64) \quad \text{CT} = 1 / (38 - (2 * \text{elevation} / 305) + 380 / (\text{sat_vap_pres_max} - \text{sat_vap_pres_min}))$$

$$(65) \quad \text{TX} = 2.5 + (0.14 * (\text{sat_vap_pres_max} - \text{sat_vap_pres_min})) + \text{elevation} / 550,$$

where elevation is the elevation (m) of the site, sat_vap_pres_min and sat_vap_pres_max are the saturation vapor pressures (in mbars) for the mean minimum (temp_min) and mean maximum (temp_max) daily temperatures for the warmest month of the year:

$$(66) \quad \text{sat_vap_pres_max} = \text{sat_vap_pres} (\text{temp_max}_{\text{warmest month}})$$

$$(67) \quad \text{sat_vap_pres_min} = \text{sat_vap_pres} (\text{temp_min}_{\text{warmest month}})$$

The vapor saturation pressures are calculated from the appropriate air temperatures using Bosen's (1960) approximation:

$$(68) \quad \text{sat_vap_pres} = 33.8639 * ((0.00738 * T + 0.8072)^8 - 0.000019*(1.8 * T + 48) + 0.001316)$$

The latent heat of vaporization (cal) for each month and is calculated as follows:

$$(69) \quad \text{lat_heat_vapor}_{\text{month}} = 597 - 0.568 * \text{temp_24}_{\text{month}}$$